Applications de la Chimie Quantique à la Spectroscopie : Molécules, Complexes de Van der Waals, Molécules piégées

Natalia Zvereva-Loëte

Applications de la Chimie Quantique à la Spectroscopie : Molécules, Complexes de van der Waals, Molécules piégées

Habilitation à Diriger des Recherches
présentée par
Natalia Zvereva-Loëte

Soutenue le 30 novembre 2009 à Dijon
devant la comission d'examen composée de :

G. Bertrand, professeur, université de Bourgogne, président
B. Bussery-Honvault, directeur de Recherches, université de Franche-Comté, rapporteur
I. Kleiner, directeur de Recherches, université de Paris 7 et 12
L. Manceron, directeur de Recherches, université de Paris 6, rapporteur
R. Marquardt, professeur, université de Strasbourg, rapporteur
P. Senet, professeur, université de Bourgogne

Remerciements

Je tiens avant tout à remercier Jean-Paul Champion et Gilles Bertrand, ancien et actuel directeurs du Laboratoire Interdisciplinaire Institut Carnot de Bourgogne (ICB) pour leur accueil chaleureux au sein de leurs équipes.

J'adresse mes remerciements sincères aux membres de l'équipe de Spéctroscopie Moléculaire et Applications avec lesquels j'ai travaillé régulièrement au cours des six dernières années, Vincent Boudon, Maud Rotger (qui est maintenant professeur à l'Université de Reims) et Christian Wanger, sans oublier Michel Loëte qui m'a particulièrement encouragée tout au long de la rédaction.

Je veux remercier aussi l'équipe d'Adsorption sur les Solides, notamment Jean-Pierre Bellat, Guy Weber et Anthony Ballandras pour leur soutien et leur collaboration efficace dans le domaine du piégeage des molécules dans les zéolithes.

Yulia Kalugina a contribué à mes recherches les plus récentes par son travail de thèse sur le complexe CH_4–N_2, son implication m'a donné l'occasion de développer de riches échanges dans le cadre d'un encadrement de thèse en France.

Ce travail offre l'occasion de faire le bilan d'un cheminement scientifique dont une partie importante s'est déroulée en Russie, au moment de ma thèse puis durant les années passées comme chercheur dans les différents instituts de l'université d'état de Tomsk. Je voudrais mentionner ici les personnes qui ont compté dans cette période, ainsi A. Terpugova, I. Ippolitov, M. Buldakov, V. Artukhov, Yu. Ponomarev, Sh. Nabiev, L. Suchanov, A. Nadezdinskii, D. Stavrovskii, S. Chernin.

La collaboration continue entre l'Institut Carnot de Bourgogne et Tomsk, au travers d'échanges fructueux, notamment avec Yu. Ponomarev, V. Cherepanov, M. Buldakov.

Ce travail est aussi le fruit de collaborations avec J.Demaison, R.Marquardt, C. Adamo, L. Joubert.

Mes remerciements vont enfin aux rapporteurs, qui ont accepté la tâche d'étudier en détail le manuscrit, et à l'ensemble des membres du jury pour leurs commentaires avisés sur l'ensemble de mon travail.

Table des matières

Chapitre 1

Introduction

Le développement de la mécanique quantique a donné lieu à des progrès importants dans le domaine des études des systèmes électroniques et de leur interaction avec le rayonnement. La mécanique quantique a été élaborée à partir de la mécanique ondulatoire de L. de Broglie et de E. Schrödinger. N. Bohr et W. Heisenberg on a en fait l'interprétation à partir d'un ensemble d'axiomes. Elle fournit une description probabiliste des systèmes. Les lois de la mécanique quantique et la seule connaissance de l'espèce chimique permettent de calculer en principe toute observable physique : c'est le domaine de la chimie quantique. Avec l'arrivée massive des ordinateurs se sont développées les simulations quantiques, qui permettent aujourd'hui de mieux explorer et de comprendre les propriétés de la matière.

Les codes de chimie quantique sont basés sur de nombreuses méthodes qui permettent la résolution de l'équation de Schrödinger. Dans la mesure où elles cherchent à n'inclure aucun paramètre empirique ou semi-empirique dans leurs équations, on les désigne par le terme *ab initio*. Elles contiennent néanmoins certaines hypothèses, et introduisent des approches adaptées, en particulier pour résoudre le problème multiélectronique dans de bonnes conditions de temps de calcul et de taille mémoire. Une des méthodes de base pour le calcul *ab initio* est la méthode de Hartee-Fock. Cette approche fournit la fonction d'onde de départ pour de nombreuses méthodes, dites post-Hartee-Fock, prenant en compte la corrélation électronique [1].

Un des codes de calcul *ab initio* le plus connu est GAUSSIAN [2]. Créé à l'origine par John Pople en 1970 [3], il a depuis connu plusieurs versions. Le nom provient du fait que Pople a proposé d'utiliser les orbitales gaussiennes pour accélérer le calcul par rapport aux logiciels utilisant des orbitales de Slater. Il existe maintenant d'autres codes de chimie quantique, tels que MOLPRO [4] ou GAMESS [5], qui permettent de calculer de multiples propriétés des systèmes électroniques. Les méthodes *ab initio* nécessitent d'établir un niveau d'application de la théorie et une base (au sens mathématique du terme, soit un ensemble de fonctions). En fait, des méthodes de différents niveaux et des bases de fonctions variées sont intégrées dans les codes, qui rendent ces logiciels très efficaces.

Les propriétés recherchées par les calculs numériques sont la structure des composés, l'énergie totale, l'énergie d'interaction, les charges, dipôles, moments multipolaires, l'énergie des transitions électroniques, les énergies rovibrationnelles, la réactivité, etc. Les objets des études peuvent être des molécules, des solides, des clusters ou d'autres systèmes. Les propriétés structurales, électroniques ou dynamiques de la matière peuvent être explorées sans connaissance expérimentale *a priori* par les simulations quantiques. Avec les nouvelles générations d'ordinateurs et l'augmentation de la puissance de calcul, il est possible d'envisager des simulations qui n'étaient pas du tout abordables auparavant et d'effectuer de calculs des systèmes de plus en plus grands avec une précision accrue.

Les calculs *ab initio* constituent un support intéressant dans la modélisation des systèmes multiélectroniques, mais également de leurs spectres, qui sont une source prédominante de la connaissance des structures des systèmes moléculaires et de leur concentration. L'analyse des spectres et des processus induits par photoabsorption permettent en effet de comprendre beaucoup de phénomènes à l'échelle moléculaire. Le caractère prédictif des calculs permet de mettre en évidence de nouveaux

systèmes ou bien des systèmes qui sont expérimentalement difficiles à observer. D'autre part, la comparaison des résultats obtenus avec les expériences disponibles permet de valider la pertinence des approches théoriques.

Mon parcours personnel se place dans cette branche de la recherche ; il comporte une série d'**applications de la chimie quantique à la spectroscopie**. Ce rapport d'habilitation présente une synthèse des activités de recherche que j'ai menées après ma thèse de doctorat, au cours des quinze dernières années. Les études actuelles portent sur l'élaboration de modèles pour la description des interactions intramoléculaires, intermoléculaires et l'interaction molécule–rayonnement (états électroniques excités, processus de formation de complexes, processus de photodissociation, de physisorption). Ces recherches sont sous-tendues par des applications à la physique de l'atmosphère, la planétologie et la photoexcitation laser. Les calculs peuvent servir pour l'analyse de spectres des molécules isolées, de molécules qui sont liées par l'interaction de van der Waals, et également pour des molécules piégées.

Le curriculum vitæ et la liste des travaux figurent en fin de document, afin de résumer les différentes collaborations et les responsabilités que j'ai assurées, et la production scientifique. J'y distingue les **livres (L)**, les articles **des revues à comité de lecture (P)**, **les actes de colloques (A)**, **les présentations lors de colloques (C)** et enfin **les séminaires (S)**. Le manuscrit s'appuie sur un certain nombre d'articles-clés qui sont reproduits à chaque fois *in extenso* dans le corps du texte, à la suite de commentaires synthétiques.

Il commence par un exposé général des méthodes utilisées dans les calculs *ab initio* (chapitre 2), qui décrit les hypothèses faisant partie intégrante des codes de calcul, et les techniques numériques associées. Ceci permet de mettre en évidence les différents niveaux de théorie qui sont disponibles pour le chercheur, et positionne les capacités actuelles de nos calculs. Le chapitre (3) fournit une description des forces de van der Waals et des interactions associées. La raison est qu'elles jouent un rôle prépondérant sur la formation et la stabilité des complexes, assemblages de molécules qu'il importe de détecter et de contrôler, dans l'environnement terrestre ou en planétologie.

A la suite de ces deux chapitres de rappels, nous passons aux applications elles-mêmes, qui sont décrites par ordre de complexité croissante des systèmes étudiés. Au début, nous considérons des calculs sur des molécules isolées (chapitre 4). Ensuite, nous passons à la formation de complexes, qui mettent en œuvre plusieurs molécules en interaction, liées par des forces (faibles) de van der Waals, si bien qu'il peut exister un grand nombre de configurations stables, avec des conséquences importantes sur les spectres produits. Trois chapitres sont consacrés aux molécules interagissant en phase gazeuse (chapitres 5, 6 ,7). Les dernières applications portent sur le piégeage des molécules dans les zéolithes, et font donc intervenir un adsorbat solide (chapitre 8).

Le chapitre 4 est consacré à deux exemples de calcul de molécules de structures relativement simples. Il s'agit d'abord de la molécule SO_2F_2, une molécule quasi-sphérique dont j'ai déterminé les constantes rotationnelles, les constantes de distorsion centrifuge et le moment dipolaire en vue d'interpréter son spectre [P21, P23]. J'ai également étudié le champ de force anharmonique et la structure à l'équilibre de la molécule C_2H_3Br [P22], en comparant cette dernière à la structure expérimentale, obtenue à partir des constantes rotationnelles provenant de l'analyse des spectres. Une approche semi-empirique a été appliquée : la structure a été calculée par une méthode de moindres carrés portant sur les moments d'inertie semi-expérimentaux (les constantes d'interaction de rotation-vibration déduites de calculs *ab initio* ont été combinées avec les constantes de rotation expérimentales). Les articles [P21, P22] sont reproduits dans le texte.

Le chapitre 5 regroupe plusieurs études ayant pour but la détection des molécules organiques en phase gazeuse, dans l'atmosphère terrestre. Cette détection est compliquée par la superposition des spectres d'absorption ou par une faible luminescence, ou par l'interférence chimique avec d'autres composés organiques. Il a fallu développer une approche spéciale adaptée à chacune des espèces étudiées. Dans chaque cas, des calculs *ab initio* ont été mis en œuvre. Les premiers travaux ont fait l'objet de ma thèse à l'Université d'État de Tomsk, les suivants étant menés à l'institut de Physique de Sibérie, à l'Université

d'État de Tomsk. Le lecteur se référera aux publications [P1- P3, P5, P6] traitant des aldéhydes et des alcools aliphatiques, qui ont fait l'objet de ma thèse, et à [P8, P9] pour les molécules de TNT et de 3-4 benzopyrène. J'ai retenu les articles [P6, P9] dans le corps du texte.

Dans le prolongement des études précédentes, je me suis intéressée à des configurations mettant en jeu plusieurs molécules. C'est ainsi que j'ai étudié les états électroniques du dimère de l'eau $(H_2O)_2$ [P4], puis la densité de charge des complexes $(H_2O)_n$ [P10] et l'effet spectroscopique des liaisons hydrogène pour les clusters d'eau [P11], l'influence de l'irradiation par rayonnement ultra-violet sur le dimère d'eau à la transition $S_0 \rightarrow S_1$ et la création du modèle décrivant le spectre photodissociatif du dimère [P13]. Ces résultats figurent dans le chapitre 6. Dans ce chapitre figurent également les résultats sur les complexes de l'eau avec H-Cl [P14,P15,P17], HF [P12,P16,P18] et NH_3, PH_3, AsH_3 [P19]. Il s'agit de déterminer les structures, les énergies de transition électronique et les fréquences vibrationnelles par calculs *ab initio*, afin d'interpréter les spectres existants. Les résultats obtenus figurent dans une base de données pour les applications atmosphériques [P20]. L'ensemble de ces travaux sont également détaillés dans les livres [L1,L2,L3]. J'ai en particulier retenu dix articles-clés [P7, P12, P13,P14, P15, P16, P17, P18, P19, P20] qui sont reproduits dans le corps du texte.

Le chapitre 7 décrit un projet que j'ai mis en place entre le groupe de spectroscopie de Dijon et le département de physique de l'Université d'Etat de Tomsk. Il concerne l'étude du dimère CH_4-N_2 pour les applications atmosphériques et astrophysiques (Titan) et s'inscrit dans la logique de l'expérience sur les dimères et les calculs *ab initio* de l' équipe de Tomsk. Il s'agit (dans le cadre de l'ANR CH_4@Titan, qui se propose de mener une étude exhaustive de l'absorption du méthane dans l'atmosphère de Titan par le calcul et l'expérimentation), d'obtenir un modèle fiable du spectre de CH_4-N_2, sur une large gamme de longueurs d'onde. Ce travail n'a démarré que depuis deux ans dans le cadre d'une thèse. Une première publication est présentée dans ce chapitre [P25].

Le dernier chapitre (8) marque lui aussi ma récente évolution, cette fois-ci vers des systèmes qui ne sont plus uniquement gazeux. Je participe à un travail à long terme sur les molécules piégées, et plus particulièrement à l'étude de la molécule C_2H_4 piégée dans des zéolithes. Le travail est mené au sein de l'Institut Carnot de Bourgogne (ICB), avec les équipes SMA (Spectroscopie Moléculaire et Application) et ASP (Adsorption sur solides Poreux) ; il est au centre du GDR COMOVI (GDR CNRS N^0 2997 Spectroscopies Vibrationnelles des Molécules Confinées dans des Solides). Il s'agit d'étudier par calculs *ab initio* les changements de structure de la molécule dans les canaux de la zéolithe et d'interpréter les déplacements en fréquence et les variations en intensité dans le spectre de la molécule piégée. Il faut maintenant caractériser l'adsorbat (solide) en plus de l'adsorbé, ce qui m'ouvre des directions de recherche nouvelles. Il y a par ailleurs des mesures expérimentales disponibles, qui sont réalisées en spectroscopie infrarouge par l'équipe ASP, ce qui permet un dialogue fructueux avec la théorie. Le lecteur consultera la publication [P24], dans le corps du document.

J'ai pour finir rassemblé dans un court chapitre «Conclusions et Perspectives» les principaux résultats originaux obtenus dans ce travail, ainsi qu'un rappel des conditions dans lesquelles ils ont été obtenus. Je donne également des pistes de réflexion, et des propositions pour des études futures, en prenant en compte les progrès prévisibles, d'une part du côté des ordinateurs et des codes, d'autre part en ce qui concerne les techniques expérimentales. Ceci va permettre des comparaisons à plus haut niveau, et des recalages plus fiables, rendant les modèles plus robustes. Tout ceci est nécessaire, dans la mesure où nous aurons à traiter des cas de plus en plus délicats, pour le contrôle, et si possible la maîtrise, des problèmes de pollution, pour les utilisations industrielles, et pour des problèmes de sciences fondamentales.

Chapitre 2

Méthodes *ab initio*

L'information que l'on peut obtenir sur un système constitué d'un ensemble de particules est contenue dans la fonction d'onde du système. A chaque grandeur physique mesurable sur le système, correspond un opérateur, agissant sur les fonctions. Les fonctions propres de l'opérateur hamiltonien $\hat{H}$ [1] associé à l'énergie du système de particules décrivent des états du système. L'énergie du système est définie et égale à la valeur propre du $\hat{H}$. La recherche des fonctions propres de l'opérateur hamiltonien constitue une action fondamentale de la mécanique quantique et consiste à résoudre l'équation qu'on appelle équation de Schrödinger : $\hat{H}\Psi = E\Psi$. On désigne par le terme *ab initio* l'ensemble des méthodes qui permettent de la résoudre, et de déduire les propriétés d'un système physique de façon *non paramétrique*, à partir des équations physiques et mathématiques les plus fondamentales. Seul un petit nombre de problèmes peuvent être résolus mathématiquement de façon explicite en utilisant ces relations. C'est la raison pour laquelle les méthodes *ab initio* contiennent également un certain nombre d'hypothèses et d'approximations afin de rendre possible la résolution des équations pour les systèmes poly-électroniques. En mécanique quantique et en chimie quantique, les méthodes approchées sont basées sur un principe variationnel équivalent à l'équation de Schrödinger.

Dans la plupart des cas, la première étape de la résolution est constitué par la méthode MO LCAO SCF (Molecular Orbital, Linear Combination Atom Orbital Self Consistent Field) : le calcul des orbitales moléculaires (MO) est recherché sous la forme d'une combinaison linéaire des orbitales atomiques (LCAO) correspondant à la symétrie de la molécule et à la valeur minimale de l'énergie électronique. Une autre hypothèse classique est constituée par l'approximation de Born–Oppenheimer, selon laquelle le noyau de la molécule reste stationnaire dans l'ensemble de la chronologie du mouvement des électrons, ce qui conduit à l'indépendance entre la fonction d'onde des électrons et le mouvement du noyau.

Cette partie du manuscrit reprend brièvement les principales équations qui seront utilisées par la suite, et décrit les techniques numériques mises en place.

2.1 Généralités

Equation de Schrödinger. L'équation de Schrödinger non relativiste indépendante du temps s'écrit :

$$\hat{H}\,\Psi(\mathbf{r}\,;\,\mathbf{R}) = E\,\Psi(\mathbf{r}\,;\,\mathbf{R}) \tag{2.1}$$

où $\hat{H}$ est l'hamiltonien indépendant du temps, $\Psi(\mathbf{r}\,;\,\mathbf{R})$ est la fonction d'onde indépendante du temps, $\mathbf{r}$ et $\mathbf{R}$ sont les coordonnées des électrons et des noyaux et E est l'énergie du système.

Son expression variationnelle est basée sur l'existence de la valeur moyenne de l'énergie du système, qui est une fonctionnelle dépendant de Ψ :

$$\overline{E}(\Psi) = \frac{\langle\Psi|H|\Psi\rangle}{\langle\Psi|\Psi\rangle} \tag{2.2}$$

La solution minimise l'énergie du système lorsque la fonctionnelle est stationnaire

$$\delta\overline{E}(\Psi) = 0 \qquad \overline{E}(\Psi) = E \qquad \delta\langle\Psi|\Psi\rangle = 0 \tag{2.3}$$

La recherche de la solution de l'équation de Schrödinger (eq.2.1) est donc équivalente à la recherche des points extrêmes sur la surface de l'énergie (eq.2.2). Pour un problème particulier, il faut maintenant préciser la forme de l'hamiltonien.

L'hamiltonien d'un système moléculaire. L'hamiltonien d'un système de N noyaux et n électrons peut être présenté sous la forme suivante :

$$\hat{H} = \hat{T}_N + \hat{T}_e + \hat{V}_{Ne} + \hat{V}_{NN} + \hat{V}_{ee} \tag{2.4}$$

où $\hat{T}_N$ est l'opérateur associé à l'énergie cinétique des N noyaux et $\hat{T}_e$ l'opérateur de l'énergie cinétique des électrons, tandis que $\hat{V}_{ee}, \hat{V}_{Ne}, \hat{V}_{NN}$ sont les potentiels coulombiens entre les électrons, entre les noyaux et entre les électrons et noyaux respectivement. En unités atomiques, l'hamiltonien $\hat{H}$ s'écrit comme :

$$\hat{H} = -\sum_{A=1}^{N} \frac{\nabla_A}{2M_A} - \sum_{i=1}^{n} \frac{\nabla_i}{2} - \sum_{A=1}^{N}\sum_{i=1}^{n} \frac{Z_A}{r_{Ai}} + \sum_{A=1}^{N}\sum_{B>A}^{N} \frac{Z_A Z_B}{r_{AB}} + \sum_{i=1}^{n}\sum_{j>i}^{n} \frac{1}{r_{ij}} \tag{2.5}$$

où les indices A et B sont associés aux noyaux et les indices i et j sont associés aux électrons, Z_x et M_x sont la charge et la masse d'un noyau x dans le système d'unités choisi (on rappelle que, dans ce système d'unité, la masse d'un électron m_e= 1 u.a. masse, $\hbar = e^2 = 1$ et que $\frac{e^2}{4\pi\varepsilon_0} = 1$).

L'approximation de Born-Oppenheimer. Cette approximation est utilisée lorsqu'il y a plus d'un électron. Elle consiste à considérer que la masse des noyaux est beaucoup plus grande que celle des électrons ($m_p/m_e \sim 1836$). On peut alors découpler le mouvement des électrons de celui des noyaux, en estimant que le mouvement de ceux-ci est beaucoup plus lent que celui des électrons : on les considère comme fixes dans l'étude du mouvement des électrons de la molécule. On traite alors les distances internucléaires comme des paramètres. L'hypothèse a une conséquence immédiate sur le calcul, qu'on appelle hypothèse adiabatique : le mouvement des électrons s'adapte instantanément au mouvement des noyaux. La fonction d'onde décrivant les particules $\Psi_{tot}(\mathbf{r\,;\,R})$ peut s'exprimer sous la forme d'un produit des fonctions d'onde caractérisant les électrons, Ψ_{el} et les noyaux, Ψ_N :

$$\Psi_{tot}(\mathbf{r\,;\,R}) = \Psi_{el}(\mathbf{r\,;\,R})\Psi_N(\mathbf{R}) \tag{2.6}$$

Les solutions $\Psi_{el}(\mathbf{r\,;\,R})$ dépendent de la position des noyaux mais pas de leur vitesse.

$$\hat{H}\Psi_{tot}(\mathbf{r\,;\,R}) = E_{tot}\Psi_{tot}(\mathbf{r\,;\,R}) \tag{2.7}$$

On peut trouver l'énergie électronique en résolvant l'équation suivante :

$$\hat{H_{el}}\Psi_{el}(\mathbf{r\,;\,R}) = E_{el}\Psi_{el}(\mathbf{r\,;\,R}) \tag{2.8}$$

où l'hamiltonien électronique $\hat{H}_{el}$ est l'hamiltonien électronique associé à une géométrie nucléaire fixée et donnée par :

$$\hat{H}_{el} = -\sum_{i=1}^{n} \frac{\nabla_i}{2} - \sum_{A=1}^{N}\sum_{i=1}^{n} \frac{Z_A}{r_{Ai}} + \sum_{i=1}^{n}\sum_{j>i}^{n} \frac{1}{r_{ij}} \tag{2.9}$$

L'énergie totale du système avec des noyaux fixes est la suivante :

$$E_{el}^{tot}(R) = E_{el}(R) + \sum_{A=1}^{N}\sum_{B>A}^{N} \frac{Z_A Z_B}{r_{AB}} \tag{2.10}$$

Pour trouver la fonction d'onde $\Psi_{tot}(\mathbf{r};\mathbf{R})$, il faut résoudre l'équation suivante, où on a introduit l'énergie cinétique nucléaire $\hat{T}_N = -\sum_{A=1}^{N} \frac{\nabla_A}{2M_A}$:

$$(\hat{T}_N + E_{el}^{tot}(R))\Psi_{el}(\mathbf{r};\mathbf{R})\Psi_N(\mathbf{R}) = E_{tot}\Psi_{el}(\mathbf{r};\mathbf{R})\Psi_N(\mathbf{R}) \tag{2.11}$$

Il faut noter que l'approximation de Born-Oppenheimer ne peut pas être adaptée pour les niveaux électroniques dégénerés, en présence des effets Jahn-Teller ou Renner-Teller, lors de collisions rapides et aussi dans le cas de fortes excitations vibrationnelles.

Approximation des particules indépendantes. L'interaction coulombienne entre les électrons rend la résolution de l'équation de Schrödinger des systèmes à plusieurs électrons très difficile. On ne sait pas résoudre analytiquement le problème électronique à n corps sous sa forme la plus générale. On fait donc l'approximation orbitale qui consiste à chercher la fonction d'onde électronique $\Psi_{el}(\mathbf{r};\mathbf{R})$ sous la forme d'un produit de fonctions monoélectroniques Φ_n dépendant chacune des coordonnées d'un seul électron :

$$\Psi_{el}(\mathbf{r};\mathbf{R}) = \Phi_1\Phi_2\Phi_3\ldots\Phi_n = \Psi(1,2,\ldots) \tag{2.12}$$

Le spin électronique est pris en compte en introduisant une fonction de spin qui est développée sur la base des deux fonctions α et β caractérisées par un nombre quantique de spin m_s . Le produit d'une orbitale et d'une fonction de spin constitue une spinorbitale. Cette approximation présente la base de la description traditionnelle de la structure électronique.

Principe d'indiscernabilité et déterminant de Slater. Ce concept prend son sens en mécanique quantique, il postule que les particules de même type sont indiscernables. La probabilité de présence $|\Psi(1,2\ldots)|^2$ ne dépend pas de la permutation de deux particules :

$$|\Psi(1,2\ldots)|^2 = |\Psi(2,1\ldots)|^2 \tag{2.13}$$

La fonction décrivant l'ensemble des particules peut donc être soit symétrique $\Psi(1,2\ldots) = \Psi(2,1\ldots)$, soit antisymétrique $\Psi(1,2\ldots) = -\Psi(2,1\ldots)$. Il y a deux combinaisons linéaires qui peuvent satisfaire le principe d'indiscernabilité :

$$\Psi_S = \Psi(1,2,3\ldots) + \Psi(2,1,3\ldots) + \Psi(3,2,1\ldots) + \ldots \tag{2.14}$$

$$\Psi_A = \Psi(1,2,3\ldots) - \Psi(2,1,3\ldots) - \Psi(3,2,1\ldots) + \Psi(2,3,1\ldots) + \ldots \tag{2.15}$$

L'expression de Ψ_S permet que deux particules soient dans le même état quantique. ll en résulte que chaque état pour une particule peut être peuplé par un nombre quelconque de particules. Ces particules ont un spin nul ou entier ; elles sont appelés bosons, et obéissent à la statistique de Bose-Einstein. L'expression de Ψ_A ne permet pas que deux particules soient dans le même état quantique. Il en résulte que chaque état pour une particule peut être peuplé par une seule particule. Ces particules sont appelées fermions et ont un spin demi-entier. Elles obéissent à la statistique de Fermi-Dirac. Lors de l'échange de deux particules identiques, l'état quantique global d'un ensemble de bosons indiscernables n'est pas modifié alors que l'état d'un ensemble de fermions est changé en son opposé. Les électrons étant des fermions, ils doivent satisfaire le principe de Pauli : la fonction d'onde d'un système polyélectronique doit être antisymétrique par rapport à la permutation des cordonnées d'espace et de spin de deux électrons quelconques. Le *déterminant de Slater* d'ordre N est un déterminant formé sur N spinorbitales $\phi_i(\xi)$ distinctes.

$$\Psi_{el}(\mathbf{r};\mathbf{R}) = \frac{1}{\sqrt{N!}}\begin{vmatrix} \phi_1(\xi_1) & \phi_2(\xi_1) & \ldots & \phi_N(\xi_1) \\ \phi_1(\xi_2) & \phi_2(\xi_2) & \ldots & \phi_N(\xi_2) \\ \vdots & \vdots & \vdots & \vdots \\ \phi_1(\xi_N) & \phi_2(\xi_N) & \ldots & \phi_N(\xi_N) \end{vmatrix} \tag{2.16}$$

où le facteur $1/\sqrt{N!}$ est un facteur de normalisation valable si les spinorbitales sont elles-mêmes normées. De manière très générale, pour un fermion, en notant $\mathbf{r}$ le vecteur position et σ la variable de spin, cette fonction a pour expression :

$$\phi(\xi) = \varphi^{+}(\mathbf{r})\alpha(\sigma) + \varphi^{-}(\mathbf{r})\beta(\sigma) \tag{2.17}$$

Les fonctions d'espace $\varphi^{+}(\mathbf{r})$ et $\varphi^{-}(\mathbf{r})$ sont appelées «orbitales». Dans la plupart des applications, on utilise une version simplifiée de la formule précédente :

$$\phi(\xi) = \varphi(\mathbf{r})\alpha(\sigma) \tag{2.18}$$

$$\bar{\phi}(\xi) = \varphi(\mathbf{r})\beta(\sigma) \tag{2.19}$$

qui permet de distinguer les spinorbitales α et β ayant la même fonction d'espace. La permutation des cordonnées d'espace et de spin de deux électrons correspond à la permutation des deux lignes correspondantes du déterminant. Le déterminant de Slater satisfait le principe d'antisymétrie car il change de signe lorsque l'on permute deux lignes ou deux colonnes. Cette propriété est également valable pour une combinaison linéaire de déterminants. Les déterminants de Slater formés sur des spinorbitales liées par une transformation unitaire sont égaux. Les spinorbitales sont définies à une transformation unitaire près.

2.2 Le champ auto-cohérent. La méthode Hartee-Fock

La méthode de Hartree-Fock est une méthode de résolution approchée de l'équation de Schrödinger d'un système quantique à n fermions utilisant le principe variationnel dans laquelle la fonction d'onde approchée est écrite sous la forme d'un déterminant de Slater. La répulsion coulombienne électron-électron n'est pas spécifiquement prise en compte. Seul son effet moyen est inclus dans le calcul. Pour l'état de base du système avec couche fermée (les orbitales sont doublement occupées) la fonction d'onde s'écrit :

$$\Psi^{HF} = \frac{1}{\sqrt{(2n)!}} \begin{vmatrix} \phi_1(\xi_1) & \phi_2(\xi_1) & \dots & \phi_N(\xi_1) \\ \phi_1(\xi_2) & \phi_2(\xi_2) & \dots & \phi_N(\xi_2) \\ \vdots & \vdots & \vdots & \vdots \\ \phi_1(\xi_N) & \phi_2(\xi_N) & \dots & \phi_N(\xi_N) \end{vmatrix} \tag{2.20}$$

où $\phi_i(\xi_i) = \chi_i \times \alpha$ (ou β) sont les spinorbitales. L'état du système est décrit par ensemble des orbitales qui peuvent être commodément rassemblées dans un vecteur-ligne :

$$\phi = (\phi_1 \phi_2 \dots \phi_n), \tag{2.21}$$

et on peut écrire sans perte de généralité que :

$$\langle \phi_i | \phi_j \rangle = \int \phi_i \, \phi_j \, dV = \delta_{ij}. \tag{2.22}$$

L'ensemble des fonctions $\{\phi_i'\}$ que l'on peut obtenir à partir de $\{\phi_i\}$ sont liÕes par une transformation unitaire :

$$\phi' = \phi U \qquad U^* U = E, \tag{2.23}$$

et la fonction complète se transforme de la façon suivante

$$\Psi' = \Psi \, Det^2(U), \tag{2.24}$$

de sorte que Ψ' présente le même état physique que Ψ. Dans l'équation (2.20) le facteur est choisi de manière à ce que la mise en œuvre des conditions (2.22) rende la fonction Ψ_{HF} normalisée :

$$\langle \Psi_{HF}|\Psi_{HF}\rangle = \int \ldots \int \Psi^*_{HF}\Psi_{HF} dV^1 \ldots dV^{2n} = 1 \tag{2.25}$$

L'énergie totale électronique s'exprime :

$$\langle \Psi_{HF}|H|\Psi_{HF}\rangle = \int \ldots \int \Psi^*_{HF} H \Psi_{HF} dV^1 \ldots dV^{2n} \tag{2.26}$$

L'hamiltonien du système s'écrit comme :

$$H = \sum_{\mu} h_\mu + \sum_{\mu \neq \nu} (1/r_{\mu\nu}) \tag{2.27}$$

où h_μ est le champ nucléaire plus l'opérateur de l'énergie cinétique de l'électron μ et $r_{\mu\nu}$ est la distance entre les électrons μ et ν. En substituant (2.27) dans (2.26) la valeur attendue de l'énergie est convertie en une somme d' intégrales sur les orbitales :

$$\langle \Psi_{HF}|H|\Psi_{HF}\rangle = 2\sum_i h_i + \sum_{ij}(2J_{ij} - K_{ij}), \tag{2.28}$$

où

$$h_i = \langle \phi_i|h|\phi_i\rangle, \tag{2.29}$$

$$J_{ij} = \langle \phi_i|J_j|\phi_i\rangle = \langle \phi_j|J_i|\phi_j\rangle, \tag{2.30}$$

$$K_{ij} = \langle \phi_i|K_j|\phi_i\rangle = \langle \phi_j|K_i|\phi_j\rangle, \tag{2.31}$$

où J_i est un opérateur coulombien défini par :

$$J_i(1)\phi_j(1) = \phi_j(1)\int_{(2)} \phi^*_i(2)\frac{1}{r_{12}}\phi_i(2) d\tau_2 \tag{2.32}$$

et K_i est un opérateur d'échange défini par son action sur une fonction $\phi_i(1)$:

$$K_i(1)\phi_j(1) = \phi_i(1)\int_{(2)} \phi^*_i(2)\frac{1}{r_{12}}\phi_j(2) d\tau_2 \tag{2.33}$$

En appliquant les méthodes de calcul variationnel, la valeur attendue de l'énergie lorsque les conditions (2.22) sont remplies conduit aux équations de Hartee-Fock :

$$\mathbf{F}\phi = \varepsilon\phi \tag{2.34}$$

où $\mathbf{F}$ est l'opérateur de Fock :

$$\mathbf{F} = h + \sum_i (2J_i - K_i) \tag{2.35}$$

et ε est la matrice hermitienne des multiplicateurs de Lagrange qui sont liés avec les conditions (2.22). L'opérateur $\mathbf{F}$ qui est déterminé par l'ensemble ϕ_i devrait être invariant avec l'opérateur qui est déterminé par l'ensemble ϕ'_i obtenu par la transformation (2.23). En conséquence, l'ensemble ϕ'_i satisfait à l'équation :

$$\mathbf{F}\phi' = \varepsilon'\phi' \tag{2.36}$$

où

$$\varepsilon' = \mathbf{U}^*\varepsilon\mathbf{U} \tag{2.37}$$

par conséquent, on peut choisir un ensemble d'orbitales pour lesquelles la matrice ε est diagonale, si bien que toutes les orbitales doivent satisfaire l'égalité :

$$\mathbf{F}\phi_i = \varepsilon_i\phi_i \tag{2.38}$$

Cette équation satisfait au pseudo-problème sur les valeurs propres, puisque l'opérateur **F** est déterminé à partir de (2.38). L'énergie totale peut être exprimée par les énergies orbitales ε_i et les intégrales monoélectroniques h_i :

$$E = \sum_{i=1}^{n} (h_i + \varepsilon_i) \tag{2.39}$$

Les énergies orbitales ont aussi un sens physique direct : leur valeur est approximativement égale à la valeur du potentiel d'ionisation nécessaire à l'enlèvement d'un électron de l'orbitale ϕ_i (théorème de Koopmans [6]). L'opérateur de Fock dépendant de la solution, le problème posé est donc implicite. La méthode de résolution la plus utilisée est la méthode du champ auto-cohérent (Self Consistent Field - SCF). Elle est mise en œuvre au moyen d'un algorithme itératif où l'opérateur de Fock est mis à jour à chaque itération avec les spinorbitales calculées à l'itération précédente. La calcul est arrêté lorsqu'une convergence satisfaisante (sur l'énergie, la fonction d'onde,...) est obtenue.

Fonction d'onde restreinte et non-restreinte. Les développements précédents n'impliquent aucune hypothèse concernant les spinorbitales autre que celle de leur orthogonalité mutuelle. Comme on a vu, chaque spinorbitale ϕ_i (eq.2.17) est composée d'une fonction spatiale $\phi^+(\mathbf{r})$ et d'une fonction de spin (α ($\sigma_i = +1/2$)), ou bien $\phi^-(\mathbf{r})$ et d'une fonction de spin (β ($\sigma_i = -1/2$)). On peut écrire les opérateurs de Fock pour les électrons α et β de la façon suivante :

$$\hat{F}^{\alpha} = \hat{h} + \sum_{j=1}^{n_\alpha} (\hat{J}_j^{\alpha} - \hat{K}_j^{\alpha}) + \sum_{j=1}^{n_\beta} \hat{J}_j^{\beta} \tag{2.40}$$

$$\hat{F}^{\beta} = \hat{h} + \sum_{j=1}^{n_\beta} (\hat{J}_j^{\beta} - \hat{K}_j^{\beta}) + \sum_{j=1}^{n_\alpha} \hat{J}_j^{\alpha} \tag{2.41}$$

Fonction d'onde restreinte (RHF, Restricted Hartee-Fock). On dit que l'on est dans le formalisme Hartee-Fock restreint (RHF) si, pour les systèmes à couches fermées, on impose à chaque orbitale de représenter deux électrons, au moyen des fonctions de spin α et β et des mêmes fonctions d'onde spatiales $\phi^+ = \phi^-$. On écrit l'opérateur de Fock (RHF) à couches complètes :

$$\hat{F}^{RHF} = \hat{h} + \sum_{j=1}^{n/2} (2\hat{J}_j - \hat{K}_j) \tag{2.42}$$

Toute approche théorique dans laquelle on exprime les orbitales moléculaires (MO) sous la forme de combinaisons linéaires d'orbitales atomiques (AO) est désignée par le vocabulaire général de méthode LCAO (Linear Combination of Atomic Orbitals), et constitue l'approche la plus couramment utilisée dans les calculs de chimie quantique : $\phi_i = \sum_k C_{k,i}\chi_k$. En utilisant cette méthode, les équations de Hartee-Fock se transforment. On obtient alors les équations de Roothaan [7] :

$$\sum_{k=1}^{n/2} F_{j,k}C_{k,i} = \varepsilon_i \sum_{k=1}^{n/2} S_{j,k}C_{k,i} \tag{2.43}$$

où $S_{j,k} = \langle \chi_j | \chi_k \rangle$ est l'intégrale de recouvrement entre deux orbitales atomiques. Les coefficients sont optimisés lors de la procédure d'itération assurant l'auto-cohérence, qui porte sur l'opérateur de Fock et l'énergie.

Fonction d'onde non-restreinte (UHF). Dans la mesure où on se limite à l'approximation orbitale, le formalisme de Hartee-Fock restreint ne constitue pas toujours la meilleure approximation. Si la distance interatomique devient infinie, lors de la dissociation par exemple, la fonction d'onde du système tend vers

le produit antisymétrisé des deux orbitales atomiques des atomes qui s'éloignent, c'est-à-dire de deux fonctions d'espace différentes, et non pas vers la fonction biélectronique imposée par le formalisme RHF. On peut noter aussi le cas des systèmes à couches ouvertes, comme les radicaux ou les systèmes dans les états électroniques excités. Le nombre d'électrons de spin α et de spin β n'est pas le même pour les systèmes mentionnées. Dans le cadre du formalisme Hartee-Fock non restreint (UHF), on utilise deux orbitales moléculaires différentes à toutes les distances interatomiques. Le formalisme utilisant des fonctions spatiales différentes $\phi^+ \neq \phi^-$ est proposé par Pople et Nesbet [8] :

$$\sum_{k=1}^{n_\alpha} F_{j,k}^\alpha C_{k,i}^\alpha = \varepsilon_i^\alpha \sum_{k=1}^{n_\alpha} S_{j,k} C_{k,i}^\alpha \tag{2.44}$$

$$\sum_{k=1}^{n_\beta} F_{j,k}^\beta C_{k,i}^\beta = \varepsilon_i^\beta \sum_{k=1}^{n_\beta} S_{j,k} C_{k,i}^\beta \tag{2.45}$$

Ces équations doivent être résolues de manière itérative en même temps car $F_{j,k}^\alpha$ et $F_{j,k}^\beta$ dépendent à la fois de $C_{k,i}^\alpha$ et de $C_{k,i}^\beta$. L'approximation obtenue est meilleure que celle de l'hypothèse RHF dans certains cas, comme on l'a indiqué, mais il y a également un grave défaut qui s'introduit dans la résolution : les fonctions multiélectroniques ne sont plus, en toute rigueur, les fonctions propres des opérateurs $\mathbf{S}^2$ et $\mathbf{S}$, si bien que les états de spin sont mal définis : tous ces défauts résultent de l'approximation orbitale.

Les fonctions de base dans la théorie des orbitales moléculaires. Dans la plupart des calculs *ab initio*, on utilise deux types de fonctions pour exprimer les bases atomiques :
STO, Slater Type Orbital

$$\chi_{n,l,m}^{STO}(\mathbf{r},\theta,\phi) = N_{n,l,m,\xi} Y_{l,m}(\theta,\phi) r^{n-1} e^{-\xi \mathbf{r}} \tag{2.46}$$

où n est un nombre entier appelé nombre quantique principal, $Y_{l,m}$ représente une harmonique sphérique, l est le nombre entier appelé nombre quantique azimutal et m est le nombre quantique magnétique. N est un coefficient de normalisation. Ces orbitales représentent correctement le comportement de l'électron dans les régions les plus touchées par la liaison chimique. L'exposant ξ peut être obtenu au moyen d'un calcul d'optimisation des énergies atomiques ou être écrit sous la forme : $\xi = Z^*/n$ avec la charge effective Z^* déterminée de façon empirique.
GTO, Gaussian Type Orbital

$$\chi_{a,b,c}^{GTO}(\mathbf{r},\theta,\phi) = N_{a,b,c,\alpha} x^a y^b z^c e^{-\alpha \mathbf{r}^2} \tag{2.47}$$

où a,b,c sont des nombres entiers $(l = a+b+c)$. Les fonctions de base sont centrées sur l'atome A : $\mathbf{r_A} = (x_a, y_b, z_A)$. Cette représentation des orbitales atomiques est intéressante, car les fonctions de type GTO réduisent considérablement l'effort de calcul. Une base de fonctions gaussiennes de la forme $e^{-\alpha \mathbf{r}^2}$ présente une propriété très avantageuse : le produit de deux gaussiennes centrées en deux points différents est équivalent à une gaussienne unique. Ainsi, toutes les intégrales de répulsion électronique se ramènent à une somme d'intégrales monocentriques. La précision des résultats dépend évidemment du nombre de gaussiennes utilisées pour développer chaque orbitale.

La limite Hartee-Fock. La précision des calculs basés sur les considérations précédentes dépend de l'étendue de la base ainsi que du choix des fonctions constituant cette base. La valeur de l'énergie qui est obtenue par un calcul variationnel tend une limite (limite de Hartee-Fock), qui approche la valeur exacte par valeurs supérieures, du fait de l'approximation orbitale.

2.3 Méthodes post-Hartee-Fock

Les méthodes dites *post-Hartree-Fock* introduisent une correction prenant en compte la corrélation qui existe entre le mouvement des divers électrons et qui entraîne l'énergie calculée vers une valeur

supérieure à la valeur exacte. Cette différence est connue sous le nom d'énergie de corrélation électronique. On citera par exemple [9]. Parmi les nombreuses propositions existant dans la littérature, on retiendra quelques grandes classes de théories :
- les théories de perturbation (Rayleigh-Schrödinger perturbation theory, RS-PT ; Møller-Plesset, MPn) ;
- la théorie de l'espace actif complet (Complete Active Space, CAS ; Complete Active Space Perturbation Theory, CASPT) ;
- l'interaction de configuration (CI) ;
- les clusters couplés (CC) ;
- le champ multi-configurationnel auto-cohérent (MCSCF) ;
- la configuration d'interaction multi-référence (Multi-reference configuration interaction, MRCI) ;
- la théorie de la fonctionnelle de densité (Density Function Theory, DFT).

On va présenter dans la suite les méthodes suivantes : MP2, CI, CAS, MCSCF, CC et DFT.

2.3.1 Théorie des perturbations

De nombreuses formes ont été proposées pour la mise en œuvre de la théorie de perturbation. La théorie de Møller-Plesset (MP) est équivalente à la théorie de la perturbation de Rayleigh-Schrödinger (RS-PT). Dans la RS-PT, on considère un opérateur hamiltonien non perturbé $\hat{H}_0$ auquel est ajoutée une petite perturbation $\hat{V}$:

$$\hat{H} = \hat{H}_0 + \lambda\hat{V}, \tag{2.48}$$

où λ est un paramètre arbitraire réel compris entre 0 et 1.

Si la perturbation de l'hamiltonien est assez petite, les énergies et les fonctions d'ondes ne seront pas très différentes du problème non perturbé. La théorie de perturbation exprime les solutions du problème perturbé sous la forme de corrections de l'énergie des fonctions d'ondes du problème non perturbé. Si la valeur propre de l'hamiltonien exact $\hat{H}$ est E_i :

$$\hat{H}\Psi_i = E_i\Psi_i \tag{2.49}$$

On peut exprimer la fonction d'onde Ψ_i et l'énergie E_i en série de puissances de λ :

$$E_i = \lambda^0 E_i^{(0)} + \lambda^1 E_i^{(1)} + \lambda^2 E_i^{(2)} + \dots \tag{2.50}$$

$$\Psi_i = \lambda^0 \Psi_i^{(0)} + \lambda^1 \Psi_i^{(1)} + \lambda^2 \Psi_i^{(2)} + \dots \tag{2.51}$$

On appelle $E_i^{(k)}$ et $\Psi_i^{(k)}$ les corrections d'ordre k sur l'énergie et sur la fonction d'onde. Pour des petites perturbations, quelques termes correcteurs sont suffisants pour atteindre la convergence et obtenir l'énergie et la fonction d'onde de façon assez précise. Regardons plus en détail la théorie de perturbation proposée par Møller et Plesset [10] pour des systèmes décrits par des fonctions moléculaires obtenues par la méthode de Hartree-Fock.
La fonction d'onde non-perturbée Ψ_0 pour le système de N électrons s'écrit :

$$\Psi_0 = N^{-1/2}|\phi_1(1), \dots, \phi_(N)|, \tag{2.52}$$

où ϕ_i sont les solutions des équations de Hartee-Fock :

$$\hat{F}_i\phi_i = \varepsilon_i\phi_i \tag{2.53}$$

L'hamiltonien complet s'écrit :

$$\hat{H} = \hat{H}_0 + \lambda V \tag{2.54}$$

Les expressions des corrections obtenues par Møller et Plesset portent sur la fonction d'onde au premier ordre (éq.2.55) et l'énergie au second ordre (éq.2.56) :

$$\Psi^{(1)} = \frac{1}{4}\sum_{i,j}\sum_{a,b} a_{ijab}\Psi\begin{vmatrix} a & b \\ i & j \end{vmatrix} \tag{2.55}$$

$$E^{(2)} = -\frac{1}{4}\sum_{i,j}\sum_{a,b} D^{-1}_{abij}|\langle ab|ij\rangle|^2 \tag{2.56}$$

où $a_{ijab} = -D^{-1}_{ijab}\langle ab|ij\rangle$ et $\Psi\begin{vmatrix} a & b \\ i & j \end{vmatrix}$ est le déterminant doublement excité.

$$D_{abij} = \varepsilon_a + \varepsilon_b - \varepsilon_i - \varepsilon_j \tag{2.57}$$

$$\langle pq|rs\rangle = \iint \phi^*_p(1)\phi^*_q(1)(1/r_{12})[\phi_r(1)\phi_s(2) - \phi_s(1)\phi_r(2)] \tag{2.58}$$

Les indices (i,j) et (a,b) énumèrent les orbitales occupées et virtuelles respectivement. Dans le cas le plus simple (MP2), le déterminant de Hartee-Fock est construit à partir d'une double substitution uniquement $\Psi\begin{vmatrix} a & b \\ i & j \end{vmatrix}$, comme conséquence du théorème de Brillouin [1]. Au contraire, la méthode MP3 inclut des doubles corrections au deuxième ordre (D), et MP4 est la première méthode qui comprend à la fois des corrections simple, triple et quadruple (STQ).

2.3.2 Méthodes d'interaction de configurations

Interaction de Configurations tronquée (CI). Une méthode commune de construction de la fonction d'onde est une méthode basée sur l'expansion des configurations. L'état d'un système peut être décrit exactement par une somme de tous les déterminants de Slater construits sur une base infinie d'orbitales :

$$\Psi_{CI} = C_0\Psi_0 + \sum_{i,a} C^a_i\Phi^a_i + \sum_{i,j>i}\sum_{a,b>a} C^{ab}_{ij}\Phi^{ab}_{ij} + \dots \tag{2.59}$$

où Φ_0 est une fonction de référence de Hartree-Fock et où la fonction complète peut inclure une excitation simple, double et de plus haut degré du déterminant de Slater/CFS (configuration state functions) : $\Phi^a_i, \Phi^{ab}_{ij}, \Phi^{abc}_{ijk}, \dots$, où $(ijk\dots)$ correspondent aux orbitales occupées et $(a,b,c,\dots)$ correspondent aux orbitales virtuelles. Pour trouver l'énergie électronique la plus basse, on optimise par méthode variationnelle les coefficients $C^a_i, C^{ab}_{ij}, \dots$ Si la base est infinie, on parle de l'énergie d'interaction de configuration complète (Full Configuration Interaction, FCI), E_{FCI}. Cette énergie est la meilleure approximation de l'énergie exacte que l'on puisse obtenir dans la base choisie. Mais la diagonalisation complète est très coûteuse pour les systèmes contenant un grand nombre d'électrons. Très souvent, on est obligé de tronquer la base et de ne considérer que les excitations d'ordre inférieur à un certain seuil. Les méthodes CI tronquées les plus utilisées sont celles dans lesquelles on ne garde que les simples et les doubles excitations (SDCI). Les troncatures avec l'inclusion des triples ou des quadruples excitations conduisent à des calculs plus lourds. Les calculs CI tronquée sont toujours variationnels. L'inconvénient majeur de ces méthodes est de ne pas être extensibles aux problèmes de grande taille.

Méthode CAS. On diagonalise l'hamiltonien dans un espace de déterminants appelés CAS (Complete Active Space) dans cette méthode. Toutes les configurations, qui respectent la symétrie et le spin de l'état cherché sont incluses dans cet espace. La partition des orbitales moléculaires se présente de la façon suivante :
- les orbitales inactives : ces orbitales sont toujours doublement occupées ;
- les orbitales actives : leur occupation varie d'une configuration à une autre (0, 1 ou 2 électrons par

orbitale).
- les orbitales virtuelles : ces orbitales ne contiennent jamais d'électron.
Cette méthode de construction de l'espace variationnel a l'avantage d'être extensible. Un grand nombre de déterminants qui apportent une contribution insignifiante à l'énergie sont également compris dans ces calculs. C'est une conséquence du fait que des configurations dont le poids énergétique n'est pas réellement important sont générées lorsqu'on génère les contributions dominantes. On travaille souvent, donc, avec des espaces actifs assez grands dans le cas de cette méthode.

Le champ multi-configurationnel auto-cohérent (Multi-configurational self-consistent field - MCSCF). Le champ multi-configurationnel auto-cohérent (Multi-configurational self-consistent field - MCSCF) utilise une combinaison linéaire de fonctions d'état de configuration (configuration state function CSF) afin d'approximer la fonction d'onde électronique du système. Dans un calcul MCSCF, l'ensemble des coefficients des CSF et les fonctions de base (les orbitales moléculaires) participent au processus d'optimisation afin d'obtenir la fonction d'onde électronique totale avec l'énergie la plus basse. On peut considérer cette méthode comme intermédiaire entre l'interaction de configuration (CI) (la fonction d'onde est étendue mais les orbitales moléculaires ne sont pas modifiées) et la méthode Hartree-Fock (un seul déterminant mais les orbitales moléculaires varient). On peut donc écrire la fonction d'onde MCSCF du système comme une combinaison de déterminants Ψ_i construits à partir d'un ensemble d'orbitales $(\phi_1, \phi_2, \ldots, \phi_m)$, avec $m > n$ (n est un nombre d'électrons du système) :

$$|\Psi_{MCSCF}\rangle = \sum_i C_i \Psi_i \tag{2.60}$$

L'énergie est optimisée à la fois sur les coefficients C_i et sur les fonctions mono-électroniques ϕ_i :

$$E = \frac{\langle \Psi_{MCSCF} | H | \Psi_{MCSCF} \rangle}{\langle \Psi_{MCSCF} | \Psi_{MCSCF} \rangle}, \tag{2.61}$$

$$\partial E / \partial C_i = 0 \qquad \partial \phi_i / \partial C_i = 0. \tag{2.62}$$

Lorsque l'état du système implique fortement plusieurs déterminants de Slater, cette méthode est très pertinente. C'est une généralisation multi-référence de l'approximation de Hartree-Fock.

2.3.3 Cluster Couplés CC

L'équation fondamentale de cette théorie est :

$$|\Psi_{CC}\rangle = \exp(T)|0\rangle \tag{2.63}$$

Où la fonction d'onde est écrite sous une forme exponentielle à partir d'un état de référence $|0\rangle$. La fonction d'onde Hartree-Fock est souvent choisie comme le déterminant de référence $|0\rangle$. T représente un opérateur de clusterisation sous la forme d'une somme d'opérateurs décrivant toutes les excitations possibles du système étudié, qui s'exprime :

$$T = T_1 + T_2 + T_3 + \ldots \tag{2.64}$$

où les T_i sont les opérateurs d'ordre i :

$$T_1 = \sum_{i,\mu} t_i^{\mu} a_{\mu}^{+} a_i \tag{2.65}$$

$$T_2 = \sum_{i,j>i} \sum_{\mu,\nu>\mu} t_{ij}^{\mu\nu} a_{\mu}^{+} a_j a_{\mu}^{+} a_i, \ldots, \tag{2.66}$$

où on fait appel à des opérateurs du formalisme de la seconde quantification, a_{μ}^{+} et a_i, respectivement des opérateurs de création et d'annihilation, et où les opérateurs $t_i^{\mu}, t_{ij}^{\mu\nu}$ sont les poids associés aux

amplitudes des clusters. L'opérateur $\hat{T}$ crée des excitations, c'est-à-dire qu'il enlève des électrons d'orbitales occupées de $|0\rangle$ pour les placer dans des orbitales non occupées. L'exponentielle peut être développée comme :

$$\exp(T) = 1 + T + \frac{T^2}{2!} + \frac{T^3}{3!} + \ldots, \tag{2.67}$$

si bien que la fonction d'onde pour les Clusters Couplés s'écrit :

$$|\Psi_{CC}\rangle = \{1 + (T_1 + T_2 + T_3 + \ldots) + \frac{1}{2!}((T_1 + T_2 + T_3 + \ldots)^2 + \ldots\}|0\rangle \tag{2.68}$$

$$= 1 + (T_1) + (T_2 + \frac{1}{2!}T_1^2) + (T_3 + T_2T_1 + \frac{1}{3!}T_1^3) + (T_4 + T_3T_1 + \frac{1}{2!}T_2^2 + \frac{1}{2!}T_2T_1^2 + \frac{1}{4!}T_1^4) + \ldots\}|0\rangle \tag{2.69}$$

Ce développement est à rapprocher d'un développement de la fonction d'onde issu d'un calcul «Full CI», écrite en normalisation intermédiaire :

$$\Psi_{FCI} = \Psi_0 + \sum_{i,\mu} d_i^\mu \Psi_i^\mu + \sum_{i,j\rangle\, j\,\mu,\nu\rangle\nu} d^{\mu\nu}\Psi_{ij}^{\mu\nu} + \ldots \tag{2.70}$$

$$|\Psi_{FCI}\rangle = |0\rangle + (D_1 + D_2 + D_3 + \ldots)|0\rangle \tag{2.71}$$

où D_I est l'opérateur d'excitation d'ordre I. La normalisation intermédiaire à la fonction $|\Psi_{FCI}\rangle$ n'est pas normée. Par contre

$$\langle\Psi_{FCI}|0\rangle = 1. \tag{2.72}$$

Les termes correspondant au même ordre d'excitation sont égaux :

$$D_1 = T_1, \tag{2.73}$$

$$D_2 = T_2 + \frac{1}{2!}T_1^2, \tag{2.74}$$

$$D_3 = T_3 + T_2T_1 + \frac{1}{3!}T_1^3, \tag{2.75}$$

$$D_4 = T_4 + T_3T_1 + \frac{1}{2!}T_2^2 + \frac{1}{2!}T_2T_1^2 + \frac{1}{4!}T_1^4, etc\ldots \tag{2.76}$$

Indépendamment de la troncature sur l'opérateur T, les méthodes CC sont extensibles. Mais l'énergie ne peut pas être obtenue par le principe variationnel. En projetant l'équation de Schrödinger sur tous les déterminants générés dans le calcul on obtient l'énergie :

$$(H - E_{CC})|\Psi_{CC}\rangle = 0 \tag{2.77}$$

Il en résulte des équations couplées non linéaires, qui ont les amplitudes $t_i^\mu, t_{ij}^{\mu\nu}\ldots$, et l'énergie E_{CC} comme inconnues. Si l'opérateur T est tronqué aux opérateurs de simple et double excitations (méthode CCSD), la fonction d'onde s'écrit :

$$|\Psi_{CCSD}\rangle = \exp(T_1 + T_2)|0\rangle. \tag{2.78}$$

L'équation précedente est projetée sur l'état de référence $\langle 0|$, sur toutes les mono-excitations $\langle\Psi_i^\mu|$ et sur toutes les di-excitations $\langle\Psi_{ij}^{\mu\nu}|$. Cela nous ramène aux équations couplées suivantes :

$$\langle 0|(H - E_{CCSD})|\Psi_{CCSD}\rangle = 0, \tag{2.79}$$

$$\langle\Psi_i^\mu|(H - E_{CCSD})|\Psi_{CCSD}\rangle = 0, \forall i, j, \tag{2.80}$$

$$\langle\Psi_{ij}^{\mu\nu}|(H - E_{CCSD})|\Psi_{CCSD}\rangle = 0, \forall i, j, \mu, \nu, \tag{2.81}$$

Les équations contiennent seulement des opérateurs mono et bi-électroniques et on peut écrire :

$$\langle 0|(H-E_{CCSD})(1+T_1+T_2+\frac{1}{2}T_1^2)|0\rangle = 0, \tag{2.82}$$

$$\langle \Psi_i^\mu|(H-E_{CCSD})(1+T_1+T_2+\frac{1}{2}T_1^2+T_1T_2+\frac{1}{3!}T_1^3)|0\rangle = 0, \forall i,j, \tag{2.83}$$

$$\langle \Psi_{ij}^{\mu\nu}|(H-E_{CCSD})(1+T_1+T_2+\frac{1}{2}T_1^2+T_1T_2+\frac{1}{2}T_2^2+\frac{1}{2}T_1^2T_2+\frac{1}{3!}T_1^3+\frac{1}{4!}T_1^4)|0\rangle = 0, \forall i,j,\mu,\nu, \tag{2.84}$$

Des mono et des di-excitations mais aussi des tri et quadri-excitations entrent en jeu dans ces équations comme un produit de mono- ou de di-excitations. Ce fait est dû à la forme exponentielle de la fonction d'onde, qui rend la méthode CC extensible. On peut résoudre les équations CC de façon itérative à partir d'un jeu initial de coefficients $\{t_i^\mu t_{ij}^{\mu\nu} \ldots\}$.
Dans la méthode CCSD(T), on commence par un calcul CCSD ($T = T_1 + T_2$) et le terme T_3 intervient par un traitement perturbatif MP4. Les méthodes CC convergent plus rapidement que les méthodes CI vers le résultat FCI (CI complet).

2.3.4 Théorie de la fonctionnelle densité

Les méthodes de calcul de la structure électronique des molécules et des solides de cette théorie reposent sur une approche assez différente du type Hartee-Fock (SCF). La théorie de la fonctionnelle de la densité (DFT) décrit un système en considérant la densité $\rho(\mathbf{r})$ comme variable de base. Cela ramène le problème à n électrons dans l'espace de dimension 3, au lieu de l'espace de dimension $3n$ de la fonction d'onde $|\Psi\rangle$. La densité d'un système à n électrons associée à une fonction d'onde $\Psi(\mathbf{r_1},\mathbf{r_2},\ldots,\mathbf{r_n})$ s'écrit :

$$\rho(\mathbf{r}) = \int |\Psi(\mathbf{r_1},\mathbf{r_2},\ldots,\mathbf{r_n})|^2 d\mathbf{r_1},\mathbf{r_2},\ldots,\mathbf{r_n}, \tag{2.85}$$

où ρ est normée à n. Le fondement des méthodes de DFT se trouve dans deux théorèmes de Hohenberg et Kohn [11]. Le premier théorème démontre l'existence d'une fonctionnelle de la densité ρ et le deuxième théorème stipule que le principe variationnel peut être étendu à la densité ρ.
Théorème 1 : Les propriétés de l'état fondamental d'un système électronique dans un potentiel externe $V(\mathbf{r})$ ne dépendent que de la densité électronique totale en chaque point $\rho(\mathbf{r})$. Autrement dit, il existe une fonctionnelle universelle de la densité $F[\rho]$, qui est indépendante de V, de sorte que l'énergie du système s'exprime comme :

$$E[\rho] = F[\rho] + \int \rho(\mathbf{r})V(\mathbf{r})\,d\mathbf{r} \tag{2.86}$$

Théorème 2 : L'énergie de l'état fondamental est le minimum de la fonctionnelle $E[\rho]$:

$$E = \min_{\rho(\mathbf{r})} E[\rho(\mathbf{r})] \tag{2.87}$$

Ces théorèmes ne sont valables que pour l'état fondamental non dégénéré. Sans tenir compte du spin, la fonctionnelle énergie s'écrit sous la forme suivante :

$$E[\rho] = T[\rho] + V_{ee}[\rho] + \int \rho(\mathbf{r})V(\mathbf{r})\,d\mathbf{r} \tag{2.88}$$

où le potentiel externe $V(\mathbf{r})$ est le potentiel créé par les noyaux, $T[\rho]$ est la fonctionnelle d'énergie cinétique et $V_{ee}[\rho]$ la fonctionnelle d'énergie d'interaction électronique. Les théorèmes de Hohenberg et Kohn démontrent l'existence de la fonctionnelle $E[\rho]$ mais n'en donnent pas une forme analytique. Le problème se ramène à la recherche d'une expression approchée. La contribution cinétique T_0

d'un système d'électrons sans interaction et la contribution coulombienne d'un système classique interviennent dans l'expression de la fonctionnelle $E[\rho]$:

$$E[\rho] = T_0[\rho] + \frac{1}{2}\iint \frac{\rho(\mathbf{r})\rho(\mathbf{r}')}{|\mathbf{r}-\mathbf{r}'|}\,d\mathbf{r}\,d\mathbf{r}' + \int \rho(\mathbf{r})V(\mathbf{r})\,d\mathbf{r} + E_{xc}[\rho]. \tag{2.89}$$

La fonctionnelle $E_{xc}[\rho]$ est une fonctionnelle d'échange-corrélation qui intègre les effets d'échange et de corrélation, et également les contributions cinétiques et coulombiennes liées à l'interaction entre les électrons.

$$E_{xc}[\rho] = T[\rho] - T_0[\rho] + V_{ee}[\rho] - \frac{1}{2}\iint \frac{\rho(\mathbf{r})\rho(\mathbf{r}')}{|\mathbf{r}-\mathbf{r}'|}\,d\mathbf{r}\,d\mathbf{r}'. \tag{2.90}$$

L'application du principe variationnel avec le multiplicateur de Lagrange λ donne :

$$\frac{\delta E[\rho]}{\delta\rho(\mathbf{r})} = \frac{\delta T_0}{\delta\rho(\mathbf{r})} + V(\mathbf{r}) + \int \frac{\rho(\mathbf{r}')}{|\mathbf{r}-\mathbf{r}'|}\,d\mathbf{r} + \frac{\delta E_{xc}[\rho]}{\delta\rho(\mathbf{r})} = \lambda. \tag{2.91}$$

La méthode de Kohn et Sham [12] va permettre de résoudre cette équation. L'équation régissant un système d'électrons sans interaction dans un potentiel externe $V^*(\mathbf{r})$ est la suivante :

$$\frac{\delta E[\rho]}{\delta\rho(\mathbf{r})} = \frac{\delta T_0}{\delta\rho(\mathbf{r})} + V^*(\mathbf{r}) = \lambda. \tag{2.92}$$

En comparant les deux équations précédentes :

$$V^*(\mathbf{r}) = V(\mathbf{r}) + \int \frac{\rho(\mathbf{r}')}{|\mathbf{r}-\mathbf{r}'|}\,d\mathbf{r} + \frac{\delta E_{xc}[\rho]}{\delta\rho(\mathbf{r})}. \tag{2.93}$$

La solution de (2.92) est connue et correspond à la densité calculée avec les orbitales déterminées par l'équation suivante :

$$\left(-\frac{1}{2}\nabla_i^2 + V^*(\mathbf{r})\right)\phi_i(\mathbf{r}) = \varepsilon_i\phi_i(\mathbf{r}) \tag{2.94}$$

$$\rho(\mathbf{r}) = \sum_{i=1}^{n} |\phi_i(\mathbf{r})|^2. \tag{2.95}$$

L'équation (2.91) est résolue en remplacant le système d'électrons en interaction par un système fictif d'électrons sans interaction évoluant dans un potentiel externe effectif à une particule $V^*(\mathbf{r})$. Les équations autocohérentes obtenues ont une forme qui rappelle celles de Hartree-Fock. Elles en différent cependant par le fait qu'elles font intervenir la densité électronique totale du système dans les termes d'interaction entre électrons. Les ϕ_i (orbitales de Kohn–Sham) et les ε_i contribuent à déterminer la densité $\rho(\mathbf{r})$.

ll est nécessaire de connaître l'énergie d'échange-corrélation $E_{xc}[\rho]$ pour effectuer des calculs DFT. Cette énergie peut être décomposée comme suit en faisant apparaître des termes d'énergie d'échange et d'énergie de corrélation : $E_{xc}[\rho] = E_x[\rho] + E_c[\rho]$.

Les différents types de fonctionnelles sont connus dans la littérature et de nouveaux développements sont en cours.

Les principales méthodes de la DFT **:**

- LDA (Local Density Approximation) : la fonctionnelle ne dépend que de $\rho(\mathbf{r})$;
- GGA (Generalized Gradient Approximation) : la fonctionnelle dépend de $\rho(\mathbf{r})$ et de son gradient $\nabla\rho(\mathbf{r})$;
- meta-GGA : la fonctionnelle dépend de $\rho(\mathbf{r})$, de son gradient $\nabla\rho(\mathbf{r})$ et du Laplacien de la densité $\nabla^2\rho(\mathbf{r})$;
- DFT hybryde : contient l'échange exact de Hartee-Fock dans la fonctionnelle d'échange.

Les méthodes DFT ne sont pas considérées comme des méthodes *ab initio* pures, car la plupart des

fonctionnelles contiennent des paramètres empiriques ; cependant on rencontre aussi des fonctionnelles purement théoriques [13, 14, 15].

On peut noter que la plupart des méthodes présentées sont incluses dans le logiciel GAUSSIAN [2], MOLPRO [4] et dans plusieurs autres codes de chimie quantique.

2.4 Erreur de base incomplète (Basis Set Incompletness Error, BSIE)

La convergence de l'énergie de corrélation électronique dans les méthodes classiques de calcul de la structure électronique devient de plus en plus lente avec l'expansion de la base de fonctions. Heureusement, lorsqu'on considère les valeurs d'énergie successivement obtenues, la convergence est assez systématique, ce qui permet d'extrapoler vers la limite pour la base complète (complete basis set (CBS) limit). Pour les propriétés comme la structure géométrique, par exemple, le comportement de convergence est beaucoup moins systématique. L'extrapolation des paramètres géometriques est donc assez problématique. En se basant sur l'utilisation de la base «correlation consistened - cc» : «aug-cc-pV(X)Z» [16], plusieurs formules d'extrapolation d'énergie, incluant le nombre cardinal dans ces séries, ont été proposées . L'hypothèse selon laquelle le passage de X à $(X+1)$ rend l'énergie totale plus basse en suivant une progression géométrique est équivalente à une extrapolation sous une forme exponentielle dite de Feller [17] :

$$E_X = E_{CBS} + ae^{-bX} \tag{2.96}$$

Cette forme semble valable pour les énergies d'Hartree-Fock (HF) et les différentes propriétés. Cependant, plusieurs calculs indiquent que l'extrapolation exponentielle sous-estime la limite d'énergie de corrélation [18]. De nombreux auteurs [17, 19, 20, 21] proposent d'utiliser une fonction puissance négative.

$$E_X = E_{CBS} + \alpha(X+\beta)^{-\gamma} \tag{2.97}$$

où γ n'est pas nécessairement un entier.

$$E_X = E_{CBS} + \sum_{k=3}^{k_{max}} \alpha_k (X+\beta_k)^{-k} \tag{2.98}$$

Helgaker [20] a proposé dans l'équation (2.97) $\gamma = 3$ et $\beta = 0$. C'est une forme simple qui permet à l'énergie E_{CBS} d'être estimée à partir des énergies de corrélation de deux bases des séries corrélées cohérentes («cc»). Martin [19] a choisi une expression phénoménologique sous la forme :

$$E_X = E_{CBS} + \frac{a}{(X+1/2)^4} + \frac{b}{(X+A/2)^6} \tag{2.99}$$

On ne sait pas clairement quantifier la précision d'une forme donnée pour une large classe de systèmes moléculaires. Il est par conséquent nécessaire de poursuivre les études dans ce domaine. La difficulté principale réside dans le coût des calculs.

2.5 Le problème vibrationnel

En utilisant l'approximation de Born-Oppenheimer, nous avons montré que la fonction d'onde totale peut être séparée en fonction d'onde électronique et la fonction d'onde nucléaire. Cela nous ramène à l'étude du mouvement de noyaux se déplaçant dans un champ de force dérivant d'un potentiel V_{el} défini au voisinage d'une position d'équilibre stable. L'équation de Schrödinger nucléaire s'écrit :

$$\hat{H}_N \Psi_N(\mathbf{R}) = E_N \Psi_N \tag{2.100}$$

où l'hamiltonien nucléaire $\hat{H}_N$ est une somme de l'énergie cinétique des noyaux $\hat{T}_N$ et du potentiel électronique $\hat{V}_{el}$. Pour N atomes, cette équation comporte 3N degrés de liberté. Si le système multiélectronique est défini dans le référentiel mobile ayant pour origine le centre de masse (G) de la molécule, trois parmi les $3N$ coordonnées décrivent la translation de la molécule. Si on suppose que la quantité de mouvement totale des noyaux dans le repère mobile est nulle, on obtient la condition du centre de masse ou première condition d'Eckart, appelée encore condition d'Eckart translationnelle :

$$\sum_i m_i \mathbf{r}_i = 0 \tag{2.101}$$

Après avoir lié l'origine o du repère mobile à la molécule, il nous reste à lier les axes ox, oy et oz à celle-ci. Ceci peut être fait en exprimant que la molécule n'effectue pas de mouvement de rotation dans le repère mobile, lors qu'elle passe par sa configuration d'équilibre, c'est-à-dire que le moment angulaire par rapport au trièdre mobile est nul, soit :

$$\sum_i m_i (\mathbf{r}_i^{eq} \wedge \mathbf{v}_i) = 0 \tag{2.102}$$

Cela nous ramène à la seconde condition d'Eckart, dite condition d'Eckart rotationnelle. Compte tenu des 6 relations d'Eckart, les vibrations sont caractérisées par $3N-6$ coordonnées de déplacement indépendantes (mais liées par ailleurs à la position relative des noyaux). La rotation est caractérisée par 3 coordonnées (généralement les angles d'Euler) qui définissent l'orientation du repère mobile par rapport au repère fixe. A ceci s'ajoutent 3 coordonnées de translation définissant la position du centre de gravité $G \equiv o$. Dans le cas de molécules linéaires, la rotation est définie uniquement par 2 angles, donc les coordonnées de vibration sont au nombre de $3N-5$. On peut maintenant écrire l'équation de Schrödinger nucléaire sous la forme :

$$(\hat{T}_N + \hat{V})\Psi_{trans}\Psi_{rovib} = E\Psi_{trans}\Psi_{rovib} \tag{2.103}$$

où :

$$\hat{T}_N = \hat{T}_{trans} + \hat{T} = \hat{T}_{trans} + \hat{T}_{vib} + \hat{T}_{rot} + \hat{T}_{rovib} \tag{2.104}$$

Comme il n' y a pas d'interaction entre la translation et les autres mouvements moléculaires, la fonction d'onde peut être écrite comme un produit. T et V ne dépendent que de la position relative des noyaux et sont donc invariants par translation. On peut aisément écrire :

$$(\hat{T} + \hat{V})\Psi_{rovib} = E_{rovib}\Psi_{rovib} \tag{2.105}$$

avec $E_{rovib} = E_N - E_{trans}$ et $\hat{T}_{trans}\Psi_{trans} = E_{trans}\Psi_{trans}$. Ignorer l'énergie de translation revient simplement à faire coïncider les origines des deux trièdres (fixe et mobile). En fait, on considère que les deux trièdres sont entraînés par la molécule. On peut faire l'approximation qu'il n'y a pas de couplage entre la rotation et la vibration si la molécule est considérée comme un rotateur. Cela ramène à :

$$\hat{T}_N = \hat{T}_{rot} + \hat{T}_{vib} \tag{2.106}$$

$$\Psi_{rovib} = \Psi_{rot}(\theta, \phi, \chi)\Psi_{vib}(x_i, y_i, z_i) \tag{2.107}$$

où (θ, ϕ, χ) sont les angles d'Euler qui décrivent la rotation de la molécule dans le référentiel mobile et (x_i, y_i, z_i) sont les coordonnées cartésiennes des atomes définies par rapport à G.
L'énergie rotationnelle pour un niveau vibrationnel donné peut être calculée en résolvant l'équation aux valeurs propres rotationnelles :

$$\hat{H}_{rot}\Psi_{rot} = E_{rot}\Psi_{rot} \tag{2.108}$$

$$\text{avec} \quad \hat{H}_{rot} = \frac{\hat{f}_a^2}{2I_a} + \frac{\hat{f}_b^2}{2I_b} + \frac{\hat{f}_c^2}{2I_c} \tag{2.109}$$

où a, b et c sont les axes d'inertie de la molécule, $\hat{J}_x(x=a,b,c)$ les projections du moment angulaire total sur les axes principaux et I_x les moments principaux d'inertie associés à ces axes et définis par :

$$I_x = \sum_i^N m_i (r_i^x)^2 \tag{2.110}$$

où m_i est la masse de l'atome i et r_i^x sa distance à l'axe d'inertie x. Compte tenu des conditions d'Eckart qui éliminent la translation et rotation dans le trièdre mobile, on peut évaluer l'énergie de déformation de la molécule, qui est, en première approximation, égale à la somme des énergies de $3N-6$ (ou $3N-5$) oscillateurs harmoniques. Le choix des coordonnées est important pour résoudre l'équation vibrationnelle. On peut utiliser les coordonnées cartésiennes (x_i, y_i, z_i) et les coordonnées de la position d'équilibre $(x_i^{eq}, y_i^{eq}, z_i^{eq})$ de chaque atome pour écrire les coordonnées cartésiennes de déplacement pondérées par la masse s_i, telles que :

$$s_1 = \sqrt{m_1}(x_1 - x_1^{eq}), s_2 = \sqrt{m_2}(x_2 - x_2^{eq}), s_3 = \sqrt{m_3}(x_3 - x_3^{eq}), etc. \tag{2.111}$$

Il existe une transformation des coordonnées cartésiennes pondérées telle que l'operateur hamiltonien vibrationnel s'écrive :

$$\hat{H}_{vib} = \hat{T}_{vib} + \hat{V} = \frac{1}{2} \sum_{k=1}^{3N-6} (\dot{Q}_k^2 + \lambda_k Q_k^2) + \dots \tag{2.112}$$

avec :

$$Q_k = \sum_{j=1}^{3N} L_{kj} s_j, k = 1, \dots, 3N-6, \tag{2.113}$$

ou bien avec $l^{-1} = l^+ = L$. Q_k sont les coordonnées normales. L est une matrice de $(3N-6)$ lignes et $3N$ colonnes.

Les termes supplémentaires de ce développement (2.112) sont les termes anharmoniques du potentiel. Dans ce système de coordonnées normales, les vibrations sont indépendantes les unes des autres et les Q_k sont orthogonales. L'équation de Schrödinger vibrationnel dans ce système est :

$$-\frac{\hbar^2}{2} \sum_{i=1}^{3N-6} \frac{\partial^2}{\partial Q_i^2} \Psi_{vib} + \hat{V} \Psi_{vib} = E_{vib} \Psi_{vib} \tag{2.114}$$

On déduit l'énergie potentielle du calcul électronique, à partir d'une des méthode discutées auparavant. Les déplacements des noyaux par rapport à la position d'équilibre sont petits et la fonction de potentiel $\hat{V}$ dans un état électronique donné (généralement l'état électronique de base) peut être développée en série de Taylor :

$$\hat{V} = V_{eq} + \sum_i \left(\frac{\partial V}{\partial Q_i} \right)_{eq} Q_i + \frac{1}{2} \sum_{i,j} \left(\frac{\partial^2 V}{\partial Q_i \partial Q_j} \right)_{eq} Q_i Q_j + \frac{1}{6} \sum_{i,j,k} \left(\frac{\partial^3 V}{\partial Q_i \partial Q_j \partial Q_k} \right)_{eq} Q_i Q_j Q_k + \dots \tag{2.115}$$

ou autrement :

$$\hat{V} = V_{eq} + \sum_i \lambda_i Q_i + \frac{1}{2} \sum_{i,j} \Phi_{ij} Q_i Q_j + \frac{1}{6} \sum_{i,j,k} \Phi_{ijk} Q_i Q_j Q_k + \dots \tag{2.116}$$

où λ_i, Φ_{ij}, Φ_{ijk}, etc. sont les les dérivées, appelées constantes de force. On rappelle que la matrice des dérivées secondes est la matrice Hessienne. Prenons la configuration d'équilibre $V_{eq} = 0$ comme configuration de référence. Dans cette configuration V est minimale si bien que les dérivées du premier ordre sont nulles. Dans l'approximation des petits mouvements, on peut limiter ce développement au terme d'ordre deux (appelé *potentiel harmonique*). L'équation de Schrödinger vibrationnel s'écrit :

$$-\frac{\hbar^2}{2} \sum_{i=1}^{3N-6} \frac{\partial^2}{\partial Q_i^2} \Psi_{vib}^{har} + \frac{1}{2} \sum_i^{3N-6} \Phi_{ii} Q_i^2 \Psi_{vib}^{har} = E_{vib}^{har} \Psi_{vib}^{har} \tag{2.117}$$

C'est l'équation d'un oscillateur harmonique quantique à une dimension. Ces solutions sont bien connues et s'écrivent en fonction d'un nombre quantique vibrationnel v et d'une fréquence harmonique caractéristique ω. Les fonctions propres dépendent des polynômes de Hermite $H_v(z)$. L'énergie de vibration d'un mode normal i (non dégénéré) s'écrit :

$$E^i_{vib} = (v + \frac{1}{2})\hbar\omega_i \tag{2.118}$$

où le nombre quantique vibrationnel v est un entier positif ou nul. La fonction d'onde vibrationnelle s'exprime sous forme du produit des fonctions propres des oscillateurs harmoniques et l'énergie est une somme des énergies associées à chacun des modes normaux de vibration :

$$\Psi^{har}_{vib} = \prod_i^{3N-6} \Psi^i_{vib}(Q_i) \tag{2.119}$$

$$E^{har}_{vib} = \sum_{i=1}^{3N-6} \left(v_i + \frac{1}{2}\right) \hbar\omega_i \tag{2.120}$$

Quand tous les v_i sont nuls, on retrouve l'énergie de l'état vibrationnel fondamental, appelée énergie de point zéro (ZPE). L'énergie totale du système dans son état fondamental est la somme de l'énergie électronique et de la ZPE : $E_{tot} = ZPE + E_{el}$.

Au-delà de l'approximation harmonique Pour calculer le spectre de vibration des molécules polyatomiques ou des systèmes moléculaires, il est préférable de résoudre exactement l'équation de Schrödinger nucléaire. Ceci, cependant, n'est actuellement possible que pour des systèmes relativement petits (4 à 6 atomes). Pour des systèmes plus importants, des approximations doivent être introduites pour rendre le problème accessible par ordinateur.

Théorie des perturbations. Les fréquences anharmoniques peuvent être calculées par l'approche de la théorie des perturbations PT2 en termes des coordonnées normales. L'article de V. Barone [22] décrit la mise en œuvre d'un code entiérement automatisé pour la construction des constantes de force anharmoniques et leur utilisation dans une évaluation de deuxième ordre perturbatif de paramètres rovibrationnels. Ce code est implementé dans GAUSSIAN03 [2]. Un calcul perturbatif donne les relations entre des paramètres moléculaires et les constantes de force. Il utilise la relation linéaire entre les coordonnées normales et les coordonnées cartésiennes de déplacement pondérées par la masse :

$$Q = L^+ M^{1/2} x \tag{2.121}$$

où x est la matrice des coordonnées cartésiennes de déplacement et M est la matrice diagonale de masse atomique, et L la matrice des vecteurs propres de la matrice des constantes de force sur les coordonnées cartésiennes de déplacement pondérées par la masse $M^{-1/2}FM^{-1/2}$. La matrice des dérivées secondes sur les modes normaux s'écrit :

$$\Phi = L^+ M^{-1/2} F M^{-1/2} L \tag{2.122}$$

Les dérivées d'ordre supérieur sont ensuite évaluées par differentiation numérique des matrices hessiennes analytiques, pour de petits incréments de la géométrie de référence à l'équilibre :

$$\Phi_{ijk} = \frac{1}{3}\left(\frac{\Phi_{jk}(\delta Q_i) - \Phi_{jk}(-\delta Q_i)}{2\delta Q_i} + \frac{\Phi_{ki}(\delta Q_k) - \Phi_{ki}(\delta Q_j)}{2\delta Q_j} + \frac{\Phi_{ij}(\delta Q_k) - \Phi_{ij}(-\delta Q_k)}{2\delta Q_k}\right) \tag{2.123}$$

$$\Phi_{ijkk} = \frac{\Phi_{ij}(\delta Q_k) + \Phi_{ij}(-\delta Q_k) - 2\Phi_{ij}(0)}{\delta Q_k^2} \tag{2.124}$$

$$\Phi_{iikk} = \frac{1}{2}\left(\frac{\Phi_{ii}(\delta Q_k) + \Phi_{ii}(-\delta Q_k) - 2\Phi_{ii}(0)}{\delta Q_k^2} + \frac{\Phi_{kk}(\delta Q_i) + \Phi_{kk}(-\delta Q_i) - 2\Phi_{kk}(0)}{\delta Q_i^2}\right) \tag{2.125}$$

L'hamiltonien de vibration est exprimé en unités de nombre d'onde en utilisant des coordonnées normales réduites q :

$$q_i = \gamma^{1/2} Q_i \tag{2.126}$$

où

$$\gamma_i = \frac{\lambda_i^{1/2}}{\hbar} = \frac{2\pi c \omega_i}{\hbar} \tag{2.127}$$

Il faut finalement sommer le terme d'ordre zéro harmonique et les termes définissant la contribution des composantes cubiques et quartique du potentiel pour la théorie du second ordre de perturbation ; la contribution cinétique est également incluse (au travers du moment angulaire de vibration $\mathbf{j}_\alpha$) :

$$\mathbf{H}_{vib} = \mathbf{H}_{vib}^0 + \mathbf{H}_{vib}^1 + \mathbf{H}_{vib}^2 = \frac{1}{2}\sum_r \omega_r (p_r^2 + q_r^2) + \frac{1}{6}\sum_{rst} \phi_{rst} q_r q_s q_t + \frac{1}{24}\sum_{rstu} \phi_{rstu} q_r q_s q_t q_u + \sum_\alpha B_\alpha^e \mathbf{j}_\alpha^2 \tag{2.128}$$

$$\mathbf{j}_\alpha = \sum_{i<j} \zeta_{ij}^\alpha (q_i p_j - q_j p_i) \tag{2.129}$$

où α correspond à l'axe de rotation, B_α^e est une constante de rotation d'équilibre, ζ_{ij}^α est la constante de couplage de Coriolis :

$$\zeta_{ij}^\alpha = \sum_k (L_{ik}^\beta L_{jk}^\gamma - L_{ik}^\gamma L_{jk}^\beta) \tag{2.130}$$

et

$$\phi_{rst} = (\omega_r \omega_s \omega_t)^{-1/2} \Phi_{rst} \tag{2.131}$$

La fonction d'onde de vibration $|v_i\rangle$ est :

$$|v_i\rangle = |v_i^0\rangle + |v_i^1\rangle + |v_i^2\rangle \tag{2.132}$$

La matrice hamiltonienne effective de vibration pour l'ensemble des états $|v_i\rangle$, $|v_j\rangle$ quasi-dégénérés peut être écrite comme :

$$\langle v_i | H_{vib}^{eff} | v_j \rangle = \langle v_i^0 | \mathbf{H}_{vib}^2 | v_j^0 \rangle + \langle v_i^1 | \mathbf{H}_{vib}^1 | v_j^0 \rangle + \langle v_i^0 | \mathbf{H}_{vib}^1 | v_j^1 \rangle \tag{2.133}$$

Les termes diagonaux s'expriment :

$$\langle v_i | \mathbf{H}_{vib}^{eff} | v_i \rangle = \chi_0 + \sum_i \omega_i \left(n_i + \frac{1}{2}\right) + \sum_{i<j} \chi_{ij} \left(n_i + \frac{1}{2}\right)\left(n_j + \frac{1}{2}\right) \tag{2.134}$$

où les constantes d'anharmonicité χ sont de simples fonctions des termes constants, cubiques et quartiques [22]. Il faut noter que cette approche est bien adaptée surtout pour les molécules semi-rigides, et dans les cas où l'énergie potentielle a un minimum profond et pointu à l'équilibre.

«Vibrational Self Consisted Field» (VSCF). Une des méthodes les plus couramment utilisée pour traiter le problème vibrationnel est le champ auto-cohérent de vibration (VSCF) [23, 24]. Pour résoudre l'équation de Schrödinger vibrationnelle à N dimensions pour système à N modes, une hypothèse de séparabilité est utilisée, ce qui réduit le problème à résoudre à N mono-modes :

$$\left[-\frac{1}{2}\frac{\partial}{\partial Q_j^2} + \bar{V}_j^{(n_j)}(Q_j)\right] \Psi_j^{(n_j)} = \varepsilon_n \Psi_j^{(n_j)} \tag{2.135}$$

où $\bar{V}_j^{(n_j)}(Q_j)$ est le potentiel effectif VSCF pour le mode Q :

$$\bar{V}_j^{(n_j)}(Q_j) = \langle \prod_{i\neq j}^{N} \Psi_i^{(n_i)}(Q_i) | V(Q_1 \ldots Q_N) | \prod_{i\neq j}^{N} \Psi_i^{(n_i)}(Q_i) \rangle \tag{2.136}$$

et où $V(Q_1 \ldots Q_N)$ est un potentiel complet du système. L'état vibrationnel total dans cette approximation est $\Psi = \prod_{i\neq j}^{N} \Psi_i^{(n_i)}(Q_i)$. Ces équations sont résolues par une méthode auto-cohérente. L'approche VSCF de l'énergie totale est alors donnée par

$$E_n = \sum_{j=1}^{N} \varepsilon_j^{(n)} - (N-1) \langle \prod_{j=1}^{N} \Psi_j^{(n)}(Q_j) | V(Q_1 \ldots Q_N) | \prod_{j=1}^{N} \Psi_j^{(n)}(Q_j) \rangle \tag{2.137}$$

Les solutions qui résultent de (2.136) sont encore corrigées pour les effets de corrélation entre les modes de vibration à l'aide de la théorie de perturbation du second ordre (CC-VSCF). Le potentiel du système est la somme des termes séparables (mono-modes) et des termes de couplage croisés :

$$V(Q_1, \ldots, Q_N) = \sum_{j}^{N} V^{eff}(Q_j) + \sum_{i}^{N-1} \sum_{j>i}^{N} V_{ij}^{coup}(Q_i, Q_j) \tag{2.138}$$

Les intensités anharmoniques infrarouges sont calculées en utilisant le moment dipolaire *ab initio* :

$$I_i = \frac{8\pi^3 N_A}{3hc} \omega_i |\langle \Psi_i^{(0)}(Q_i) | \vec{\mu}(Q_i) | \Psi_i^{(m)}(Q_i) \rangle|^2 \tag{2.139}$$

où ω_i est une fréquence vibrationnelle VSCF pour le mode normal i et où $\Psi^{(0)}$, $\Psi^{(m)}$ sont des fonctions d'ondes pour l'état de base et pour les états vibrationnels excités. Cette méthode est implémentée dans le code GAMESS [5]. Si les équations VSCF sont résolues en utilisant des méthodes s'appuyant sur une grille [25], la valeur de la fonction d'énergie potentielle est connue uniquement de façon discrète, sur les points de celle-ci. Par conséquent, la nécessité d'une forme analytique pour calculer le potentiel est éliminée. Cette méthode ouvre la voie à des calculs des premiers principes de la spectroscopie de vibration des molécules polyatomiques et, en comparant les résultats avec l'expérience, fournit une méthode pour l'étalonnage des différentes méthodes de calcul des structures électroniques disponibles aujourd'hui. La méthode VSCF *ab initio* a jusqu'ici été appliqué à plusieurs systèmes, y compris aux clusters [25, 26, 27].

Chapitre 3

Théorie des systèmes de van der Waals

Les forces de van der Waals sont sensibles dans de nombreux systèmes. Dans ce manuscrit, elles constituent le phénomène de base qui gouverne l'existence des complexes en phase gazeuse qui seront étudiés aux chapitres 6 et 7, ainsi que le processus de physisorption des molécules dans les zéolithes (chapitre 8).

3.1 Interaction de van der Waals

Une liaison de van der Waals est une interaction électrique de faible intensité entre atomes, molécules, ou entre une molécule et un cristal. Elle a été décrite pour la première fois par Johannes Diderik van der Waals (1837 - 1923), prix Nobel de physique 1910, qui détermina leur effet en modifiant l'équation d'état des gaz parfaits. C'est la physique quantique qui, des années plus tard, a permis de mieux comprendre les actions qu'elle recouvre.

Forces de van der Waals Les systèmes à couche fermée manifestent toujours une énergie d'interaction due aux forces de van der Waals qui peuvent être décomposées en quatre termes principaux [28, 29] :

- le terme *électrostatique* résulte de l'interaction entre moments électriques permanents : charge, dipôle, quadrupôle etc. Ce terme peut être attractif ou répulsif selon l'orientation relative des molécules qui interagissent ;
- le terme *d'induction* résulte de l'interaction entre des moments permanents d'une molécule avec les moments induits par polarisation dans l'autre molécule. Ces interactions découlent du fait qu'une molécule est toujours polarisable si elle se retrouve dans un champ électrique. Ce terme est attractif dans le cas de molécules dans leur état électronique fondamental ;
- le terme de *dispersion* résulte de la polarisabilité électronique mutuelle des partenaires d'interaction. Ce terme est attractif et il a une origine purement quantique ;
- le terme *d'échange* se manifeste à courte distance intermoléculaire et croît rapidement lorsque celle-ci décroît. Ce terme a aussi une origine quantique.

Développement multipolaire de la perturbation. La prise en compte du potentiel d'interaction des deux sous-systèmes peut se faire dans le cadre de la théorie de perturbation. L'énergie d'interaction limitée au deuxième ordre de perturbation peut être décomposée en trois termes. Le terme du premier ordre est une énergie électrostatique :

$$U_e = \langle \Psi_0^A \Psi_0^B | \hat{H}' | \Psi_0^A \Psi_0^B \rangle \tag{3.1}$$

où Ψ_0^A, Ψ_0^B sont les fonctions d'ondes des molécules A, B dans leur état de plus basse énergie et $\hat{H}'$ représente le potentiel d'interaction des deux molécules. Le potentiel d'interaction entre les moments

multipolaires, qui s'exprime à l'aide de leurs valeurs moyennes dans les états électroniques de base de chaque système moléculaire, peut être calculé en fonction de la distance et de l'orientation relative des paires de molécules. Ces calculs s'effectuent pour les distances intermoléculaires où le recouvrement des nuages électroniques de chaque molécule est négligable. En unité électrostatique (e.s.u.), le potentiel correspondant s'écrit dans sa forme générale comme :

$$V_{mult} = (4\pi)^{3/2} \sum_{\substack{l_1,m_1,m_1',\\ l_2,m_2,m_2'}} (-1)^{l_1} \left[\frac{(2l_1+2l_2)!}{(2l_1+1)!(2l_2+1)!}\right]^{1/2} \times \begin{pmatrix} l_1 & l_2 & l_1+l_2 \\ m_1 & m_2 & -m_1-m_2 \end{pmatrix} Y^{(l_1+l_2)}_{m_1+m_2}(\hat{R}) \\ \frac{1}{R^{l_1+l_2+1}} \times D^{(l_1)}_{m_1' m_1}(\Omega_1)\, {}^1Q^{(l_1)}_{m_1'}\, {}^2Q^{(l_2)}_{m_2'} D^{(l_2)}_{m_2' m_2}(\Omega_2), \tag{3.2}$$

où :
- on trouve ici un symbole $3J$;
- $\hat{R}$ représente l'orientation du vecteur joignant les centres des masses des deux molécules par rapport à un repère fixe ;
- $D^{(l_i)}_{m_i' m_i}(\Omega_i)(i = 1,2)$ est un élément de matrice de rotation faisant passer du repère dont le centre est au centre de masse de la molécule i et dont les axes coïncident avec ceux du repère fixe à un repère lié à la molécule i ;
- ${}^iQ^{(l_i)}_{m_i'}$ (i = 1,2) est une composante sphérique du moment multipolaire d'ordre l_i.

Les noms et des symboles des premiers opérateurs multipolaires sont suivants :

q :	Charge	l = 0
μ :	Dipôle	l = 1
Θ :	Quadrupôle	l = 2
Ω :	Octupôle	l = 3
Φ :	Hexadépôle	l = 4

L'énergie électrostatique se décompose en :
- un terme charge-charge qui varie avec la distance R entre les deux systèmes comme R^{-1} ;
- un terme charge-dipôle qui varie comme R^{-2} ;
- un terme dipôle-dipôle et charge-quadrupôle qui varie comme R^{-3} ;
- un terme quadrupôle- quadrupôle, dipôle-octupôle et charge-hexadécapôle qui varie comme R^{-5} ;
- etc...

L'effet d'induction. Les interactions d'induction constituent une partie des termes d'ordre deux de la théorie des perturbations sur les états électroniques des molécules.

$$U_i = -\sum_{i\neq 0} \frac{|\langle \Psi_i^A \Psi_0^B | \hat{H}' | \Psi_0^A \Psi_0^B \rangle|^2}{E_i^A - E_0^A} - \sum_{j\neq 0} \frac{|\langle \Psi_0^A \Psi_j^B | \hat{H}' | \Psi_0^A \Psi_0^B \rangle|^2}{E_j^B - E_0^B} \tag{3.3}$$

La première contribution U_i^A est une variation d'énergie du système par suite de la polarisation de la molécule A sous l'influence de la molécule B non perturbée, la seconde contribution U_i^B représente l'équivalent relatif à la molécule B. Il est possible d'évaluer ces deux contributions individuellement grâce à relation (3.1). On obtient l'expression en terme d'élements de tenseurs qui représentent les grandeurs appelées polarisabilités dipolaires $\alpha^B_{\alpha\beta}$, mixte dipôle-quadrupôle $A^B_{\alpha\beta\gamma}$ et quadrupôle $C^B_{\alpha\beta\gamma\delta}$ respectivement [1]. Ces polarisabilités caractérisent l'aparition de moments induits correspondants dans la molécule sous l'influence d'un champ électrique externe. L'expression du potentiel U comporte des termes qui varient comme R^{-6}, R^{-8}, R^{-10}, etc. Le terme d'induction est toujours négatif.

Forces de London ou forces de dispersion. Ces interactions ont une origine purement quantique. Elles sont décrites par le terme d'ordre deux de la théorie des perturbations ne contenant pas de moments

multipolaires permanents. Le terme correspondant est obtenu à partir des états biexcités :

$$U_d = -\sum_{i\neq 0}\sum_{j\neq 0} \frac{|\langle \Psi_i^A \Psi_j^B | \hat{H}' | \Psi_0^A \Psi_0^B \rangle|^2}{E^A - E_0^A + E_j^B - E_0^B} \tag{3.4}$$

On trouve dans l'interaction de dispersion isotrope des termes :
- en $-C_6/R^6$, traduisant une interaction de type dipôle–dipôle ;
- en $-C_8/R^8$, traduisant une interaction de type dipôle–quadrupôle ;
- en $-C_{10}/R^{10}$, traduisant une interaction de type quadrupôle–quadrupôle,
où les multipôles sont les moments instantanés (ou dynamiques) des molécules. Dans le cas de certaines molécules (toupies sphériques, par exemple [30]), ces interactions ont aussi une partie anisotrope dépendant des hyperpolarisabilités de chaque molécule.

Forces de répulsion. Aux forces d'attraction, il convient d'ajouter des forces de répulsion qui prédominent à très courte distance, dès que les orbitales moléculaires tendent à s'interpénétrer. Ces forces correspondent à l'anisotropie des nuages électroniques des molécules, mais aussi à leur recouvrement et aux effets d'échanges électroniques entre les molécules. En combinant la contribution répulsive avec les termes d'attraction, le potentiel d'énergie résultant possède un minimum. Une des représentations très connue de ce potentiel est le potentiel de Lennard-Jones :

$$V = 4\varepsilon \left[\left(\frac{\sigma}{R}\right)^{12} - \left(\frac{\sigma}{R}\right)^{6} \right] \tag{3.5}$$

où $4\varepsilon\sigma^6$ correspond au coefficient C_6 déjà mentionné, et où le terme répulsif est en R^{-12}. L'énergie de répulsion peut être également exprimée sous une forme expontielle, de type Be^{-bR}.

Interactions de transfert de charge. Une molécule possédant un faible potentiel d'ionisation peut former avec une autre molécule de grande affinité électronique, un complexe donneur-accepteur. La formation d'un tel complexe se manifeste par une bande de transfert de charge dans le spectre d'absorption électronique.

Liaison hydrogène. La liaison *hydrogène* résulte d'une interaction locale où prédomine le terme électrostatique, et, dans une moindre mesure, le transfert de charge. Comme le proton de l'atome d'hydrogène est partagé entre les molécules liées, cette liaison est partiellement covalente. La liaison par pont hydrogène (ou liaison hydrogène (H)) est un cas particulier des liaisons intermoléculaires de Van der Waals, qui contribue à la cohésion des liquides ou des gaz. Les liaisons H sont très importantes pour les assemblages macromoléculaires (repliement des polypeptides, structure quaternaire, association des 2 brins du DNA). Une autre illustration est celle de l'eau solide (glace).

L'origine de la liaison hydrogène est essentiellement électrostatique et de type dipôle–dipôle induit. Un hydrogène attaché à un atome fortement électronégatif va porter une fraction de charge positive qui polarisera fortement une autre molécule possédant un doublet non liant. L'interaction forte entre dipôle et dipôle induit entraînera leur alignement et une grande proximité des atomes considérés par rapport aux interactions typiques de van der Waals. La liaison hydrogène est donc dirigée et de force supérieure aux liaisons de van der Waals. Pour que cette liaison s'établisse, il faut être en présence d'un donneur de liaison hydrogène et d'un accepteur :
- le donneur est formé d'un composé à pH acide, c'est-à-dire un hétéroatome (azote, oxygène, fluor) porteur d'un atome hydrogène (comme dans les amines, alcools, thiols) ;
- l'accepteur est composé d'un hétéroatome (uniquement azote, oxygène ou fluor) porteur de doublets libres. Lorsqu'une liaison hydrogène s'établit, les deux hétéroatomes se trouvent à une distance d'environ 0,2 nm.

3.2 Spécificité des complexes de van der Waals

Les complexes de van der Waals faiblement liés représentent une catégorie spéciale de molécules non-rigides. Un complexe moléculaire faiblement lié en phase gazeuse (ou dans un jet moléculaire) se forme entre deux (ou plusieurs) monomères neutres, atomiques ou moléculaires. Ces complexes ne peuvent pas être caractérisés par une seule structure d'équilibre autour de laquelle les atomes effectuent des mouvements de faible amplitude. La spécificité de ces complexes tient dans le fait qu'ils ont plusieurs minima d'énergie avec des structures d'équilibre équivalentes. Ces structures sont reliés entre elles par les mouvements de grande amplitude de chaque monomère, ce qui rend la structure des spectres de ces monomères plus complexe. La complexité du spectre est due également à des mouvements de grande amplitude des protons identiques réalisés par effet tunnel pour les molécules possédant certaines symétries (NH_3 par exemple), Il devient difficile dans ce cas d'effectuer l'attribution du spectre. Le groupe Complet de Permutation-Inversion Nucleaire (CNPI) s'applique pour résoudre ce problème [31, 32]. Longuet-Higgins ont montré [32] que pour un grand nombre de noyaux identiques, on ne conserve pas toutes les opérations de permutation : le sous-groupe correspondant est le groupe de symétrie moléculaire. Des études théoriques sur les processus de réarrangements moléculaires par effet tunnel sont nécessaires pour la détermination du groupe de symétrie moléculaire, ainsi que des calculs *ab initio* [31]. On peut noter les travaux consacrés aux calculs des états de vibration-rotation-tunnel (VRT) de complexes de van der Waals [33, 34, 35]. Dans les complexes de van der Waals, il existe une hiérarchie dans le domaine des mouvements du noyau. Dans les molécules chimiquement stables qui constituent le complexe, les atomes vibrent rapidement. Les mouvements des molécules dans le complexe sont gouvernés par les forces de van der Waals, qui sont faibles, ou par la liaison hydrogène, qui n'est que légèrement plus forte. Ils sont donc plus lents ; les basses fréquences qui n'ont pas été observées pour les monomères vont apparaître dans ce cas. Cette situation permet d'appliquer une approche de type Born-Oppenheimer, dans laquelle on sépare les vibrations intramoléculaires et les vibrations intermoléculaires. Ces dernières ont généralement de grandes amplitudes et, comme il y a souvent plusieurs minima dans la surface équipotentielle avec des barrières basses, les vibrations intermoléculaires ressemblent plus à des rotations entravées ou des mouvements de tunnel. Dans pratiquement tous les cas, il existe un couplage fort entre les différents degrés de liberté intermoléculaires.

Il faut noter cependant que, parfois, les molécules stables qui constituent le complexe sont flexibles. Dans ce cas, certains des modes intramoléculaires présentent eux-mêmes des fréquences basses et de grandes amplitudes, et ces modes de vibration sont fortement couplés avec les modes intermoléculaires ou modes de van der Waals. En conséquence, les méthodes reposant sur les modèles de l'oscillateur harmonique et le rotateur rigide avec corrections de perturbations, qui sont utilisés pour étudier les spectres des molécules presque rigides, ne sont pas vraiment adaptées pour les modes intermoléculaires des complexes de van der Waals. Pour la description des mouvement intermoléculaires, on utilise souvent les coordonnées curvilignes, tandis que pour les mouvements intramoléculaires il est de coutume d'utiliser les coordonnées normales (harmoniques). Un choix naturel des coordonnées de van der Waals dans un dimère est donné par la distance R entre les centres de masse des monomères et les angles d'Euler qui définissent l'orientation des trièdres d'Eckart sur les monomères. Ces angles d'Euler peuvent être définis par rapport à un trièdre de laboratoire (trièdre fixe) ou par rapport à un trièdre qui est installé dans le dimère (trièdre mobile). Ce dernier présente des avantages si on essaie de séparer les vibrations intermoléculaires du dimère de toutes les rotations. Mais, bien évidemment, il est possible de faire un autre choix de coordonnées en fonction du problème que l'on veut résoudre. La nature des complexes de van der Waals étant gouvernée par une surface potentielle difficile à caractériser, leur étude au moyen des méthodes *ab initio* nécessite l'utilisation de théories de haut niveau.

Il est intéressant de noter que les dimères de van der Waals sont souvent quasiment des toupies symétriques allongées («prolate» en anglais, $I_x = I_y > I_z$) en raison de la grande distance R de la liaison de van der Waals.

Dans le cas des complexes formés de trois molécules ou plus, les complexes sont plus rigides, si bien

que leur étude avec les méthodes standards peut donner des résultats assez raisonnables, surtout quand on traite les modes intramoléculaires.

3.2.1 Généralités sur la détermination de potentiels *ab initio*

L'utilisation dans les calculs de méthodes prenant en compte la corrélation électronique avec de grandes bases de fonctions bien équilibrées peut fournir des calculs de potentiels très précis pour les dimères. Ces calculs se divisent en deux types : les calculs basés sur l'approche «supermolécule» et les calculs basés sur l'approche de «Symmetry Adapted Perturbation Theory» (SAPT) [36, 37, 38, 39]. Pour les grands complexes, les calculs *ab initio* de haut niveau ne sont généralement pas pratiqués.

Approche «supermolécule». Le moyen le plus simple pour déterminer l'énergie d'interaction – moyen que j'utilise dans mes calculs – est fourni par l'approche de type «supermolécule». Pour deux sous-systèmes en interaction A et B, l'énergie d'interaction non corrigée E^{AB} du complexe est une différence :

$$\Delta E(R) = E^{AB}(AB,R) - E^{AB}(AB,\infty) = E^{AB}(AB,R) - E^{A}(A) - E^{B}(B) \tag{3.6}$$

Dans cette équation, R est une distance de séparation AB, les lettres en parenthèses sont liées à la base finie dans les calculs, et le système pour lequel l'énergie est calculée est donné en exposant. Cependant, cette méthode présente certains désavantages. On effectue en effet une différence entre deux grands nombres, et le résultat cherché est plus faible de 4 ou 5 ordres de grandeur que les valeurs des nombres à soustraire. La description précise de la surface d'énergie potentielle nécessite donc l'utilisation d'une théorie de haut niveau, et un nombre de points à calculer assez élevé. Les calculs sont alors assez coûteux, ce qui exige de faire un certain compromis entre le niveau de calculs et le nombre de points. Les calculs d'énergies d'interaction sont susceptibles de produire des erreurs de superposition de base s'ils sont effectués à partir de bases finies. Lors du calcul de l'énergie du complexe, on utilise une base plus étendue que lors du calcul de l'énergie des monomères A et B, ce qui se répercute sur l'énergie.

Erreur de superposition de base (Basis Set Superposition Error, BSSE). Une méthode de correction connue est l'approche par rééquilibrage : la méthode de correction dite du contrepoids, (CP - Counterpoise), proposée initialement par Boys et Bernardi [40], consiste à calculer la BSSE en ré-effectuant tous les calculs en utilisant les bases mélangées. L'énergie d'interaction s'écrit :

$$\Delta E^{BSSE}(R) = E^{AB}(AB,R) - (E^{AB}(A,R) + E^{AB}(B,R)) \tag{3.7}$$

où $E^{AB}(A,R)$ et $E^{AB}(B,R)$ sont les énergies des molécules A et B calculées avec la base utilisée pour le calcul du complexe AB. En effet, le calcul pour l'énergie de la molécule A est fait en présence des fonctions de base de la molécule B pour la même géométrie que dans le dimère AB (les noyaux de B ne sont pas présents dans le calcul). De cette façon, la base pour la molécule A est étendue par les fonctions de base de l'autre monomère. Cette méthode donne une bonne estimation de l'énergie d'interaction.

Approche «SAPT». L'énergie d'interaction peut être obtenue également à partir de la théorie perturbative. Dans cette approche, on obtient séparément les différentes contributions à l'énergie totale d'interaction, ce qui constitue son principal avantage [41] :

$$E_{int} = E^1_{pol} + E^1_{ech} + E^2_{pol} + E^2_{ech} + \dots \tag{3.8}$$

où E^1_{pol} est l'énergie électrostatique classique calculée prenant en compte l'effet de pénétration (chevauchement de charge), E^2_{pol} est la somme de l'énergie d'induction et de dispersion. $E^2_{pol} + E^2_{ech}$ est rigoureusement amorti par les effets de chevauchement de charge, et E^n_{ech}, $n = 1,2$ sont les contributions d'échange, qui peuvent physiquement s'interpréter comme l'effet de résonance du tunnel des électrons entre des systèmes interagissants. Cette méthode perturbative permet d'éviter l'erreur du type BSSE du fait qu'on calcule uniquement les fonctions d'onde des monomères. Mais il faut noter que la convergence de l'énergie totale d'interaction peut être assez lente [34].

3.2.2 Problème rovibrationnel

En s'appuyant sur le potentiel *ab initio* on peut résoudre le problème rovibrationnel pour les complexes. Notons qu'il y a six méthodes couramment utilisées pour résoudre l'équation de Schrödinger pour les complexes faiblement liés : la méthode variationnelle, la méthode variationnelle discrète (DVM), la méthode de collocation, la méthode de liaison forte, la méthode variationnelle de Monte-Carlo et la méthode de diffusion quantique de Monte-Carlo. On trouve dans la littérature une description de ces méthodes, par exemple dans [42].

Chapitre 4

Calculs *ab initio* pour la spectroscopie de vibration-rotation

Publications : P21, P22, P23

Ce chapitre présente les possibilités des calculs *ab initio* pour l'évaluation de constantes rovibrationnelles. Leur connaissance est nécessaire pour caractériser la structure moléculaire et calculer les spectres rovibrationnels. Deux molécules ont été traitées : SO_2F_2 qui offre l'occasion de considérer une molécule quasi-sphérique, et le bromure de vinyle.

4.1 Etude de la molécule SO_2F_2

4.1.1 Présentation du calcul

Ce travail a été effectué à Dijon, en relation avec les thèmes de recherche du groupe de spectroscopie moléculaire, qui étudie les spectres rovibrationnels à haute résolution. Le calcul des constantes rovibrationnelles pour les molécules quasi-sphériques (c'est-à-dire avec un paramètre de sphéricité $\gamma\frac{2(C-B)}{(C+B)}$ proche de zéro) peuvent être dérivées de celles des toupies sphériques. Il s'agit d'étudier des molécules dont le groupe de symétrie dérive des groupes tétraédrique, T_d et octaédrique, O_h. La molécule SO_2F_2 dérive de l'ion SO_4^{2-}. Depuis longtemps, le laboratoire de Dijon est spécialisé dans l'étude des toupies sphériques ; le développement de nouveaux modèles dérivés des modèles de toupies sphériques est déjà en cours. Il s'agit de modèles globaux capables de tenir compte de tous les types d'interaction possibles entre les bandes vibrationnelles. La validation de ces modèles peut être faite en confrontant leurs résultats à ceux qui sont obtenus avec une autre approche, comme le formalisme de Watson, ou encore en introduisant le calcul *ab initio*.

4.1.2 Résultats des calculs *ab initio*

Les calculs *ab initio* sont effectués à l'aide du code GAUSSIAN98 [43], en utilisant les méthodes `B3LYP/cc-pVDZ` et `B3LYP/6-31++G(3df,2pd)`. On obtient les constantes rotationnelles B_x, B_y et B_z, qui sont ensuite utilisées pour calculer les constantes de distorsion centrifuge. Le programme INFRA de Breiding et Thiel a été utilisé pour calculer ces constantes en employant la transformation suivante obtenue par des calculs *ab initio*.

$$s_{i\alpha} = \sum_{k=1}^{3N-6} l_{i\alpha k} Q_k \tag{4.1}$$

où $s_{i\alpha}$ sont les coordonnées cartésiennes pondérées par la masse et Q_k les coordonnées normales. L'enchaînement des codes GAUSSIAN et INFRA a donc permis d'obtenir :

– les nombres d'ondes λ_k, valeurs propres de la matrice GF [44] ;
– les moments d'inerties I_{xx} ;
– la matrice de transformation l ;
– les dérivées premières du tenseur d'inertie

$$a_k^{\alpha\alpha} = 2\sum_i m_i^{1/2}(a_{i\beta}l_{i\beta,k} + a_{i\gamma}l_{i\gamma,k}) \tag{4.2}$$

$$a_k^{\alpha\beta} = -\sum_i m_i^{1/2}(a_{i\alpha}l_{i\beta,k} + a_{i\beta}l_{i\alpha,k}), \alpha \neq \beta, a^{\beta\alpha} = a^{\alpha\beta}, \tag{4.3}$$

où $a_{i\alpha}$, $a_{i\beta}$ et $a_{i\gamma}$ sont les coordonnées des atomes à l'équilibre ;
– les constantes de distorsion centrifuge quartiques :

$$\tau_{\alpha\beta\gamma\delta} = -\frac{1}{2}\sum_k \frac{a_k^{\alpha\beta}a_k^{\delta\gamma}}{\lambda_k I_{\alpha\alpha}I_{\beta\beta}I_{\gamma\gamma}I_{\delta\delta}} \tag{4.4}$$

– les constantes de distorsion quartiques $\tilde{T}$ (Hamiltonien de Watson, réduction S) [44].

Tous les résultats sont en bon accord et montrent l'efficacité des calculs *ab initio* dans ce type de situation.

4.2 Etude de la molécule de bromure de vynile

4.2.1 Motivation

Ce sujet a été traité en collaboration avec J. Demaison de l'Université de Lille, qui réalise avec son groupe des études systématiques portant sur différentes molécules. Il utilise la spectroscopie micro-onde pour obtenir les constantes spectroscopiques. Lorsque les constantes de rotation sont connues, il est possible de calculer la structure moléculaire à l'équilibre. Cependant :
- il faut déterminer toutes les constantes d'interaction de vibration-rotation pour chaque isotopomère ;
- le système d'équations normales de l'ajustement par moindres carrés est souvent mal conditionné, si bien que la structure calculée est très sensible à de petites erreurs dans les données.
On peut améliorer le conditionnement en utilisant des données d'origines différentes. Les calculs *ab initio* constituent *a priori* une source intéressante de données supplémentaires permettant de corriger les constantes de rotation expérimentales. La méthode la plus intéressante à utiliser est la méthode du champ de force anharmonique *ab initio* (quadratique et cubique). Il est également très important d'établir avec quelle précision on obtient les constantes de forces.

4.2.2 Résultats des calculs

Les constantes de force quadratiques, cubiques et quartiques semi-diagonales sont calculées pour divers isotopomères en utilisant GAUSSIAN03. Les nombres d'ondes harmoniques, les corrections anharmoniques et les centres de bandes vibrationnelles sont calculés (la déviation médiane absolue est de 13 cm^{-1}) en utilisant la méthode `MP2/SDB-CC-pVTZ` et l'approximation *frozen core* (Stuttgart-Dresden-Bonn relativistic effective core potential, [45]).
Trois méthodes ont été utilisées pour déterminer la structure à l'équilibre du bromure de vynile :
– calculs *ab initio* ;
– approche semi-empirique : la structure a été calculée par une méthode de moindres carrés portant sur les moments d'inertie semi-expérimentaux (les constantes d'interaction de rotation-vibration déduites de calculs *ab initio* ont été combinées avec les constantes de rotation expérimentales) ;
– approche empirique, avec le calcul des structures r_m.

En conclusion, on observe que les diverses structures montrent un bon accord de r_m avec les calculs *ab initio* et les structures semi-expérimentales ; ces dernières sont un peu plus précises que les autres. Enfin, la structure du bromure de vynile est très proche de celle du chlorure de vynile.

4.3 Articles-clés : P21, P22

Available online at www.sciencedirect.com
SCIENCE DIRECT®
Journal of Molecular Structure 780–781 (2006) 124–133
Journal of MOLECULAR STRUCTURE
www.elsevier.com/locate/molstruc

The SO_2F_2 quasi-spherical top: Correspondence between tensorial and Watson's formalisms

V. Boudon*, M. Rotger, N. Zvereva-Loëte, M. Loëte

Laboratoire de Physique de l'Université de Bourgogne—UMR CNRS 5027, 9, av. Alain Savary, B.P. 47870, F-21078 Dijon Cedex, France

Received 13 April 2005; revised 3 May 2005; accepted 3 May 2005
Available online 26 August 2005

Abstract

The SO_2F_2 quasi-spherical top molecule with C_{2v} symmetry is considered as a distorted spherical top deriving from the SO_4^{2-} tetrahedral ion. We present here a detailed correspondence between the tensorial formalism using the $T_d \supset C_{2v}$ reorientation and the usual Hamiltonian of Watson. We have also performed ab initio calculations in order to determine the centrifugal distorsion constants in the vibrational ground state.

Keywords: Quasi-spherical tops; Asymmetric top molecules; Tensorial formalism; Reductions; Ab initio calculations.

1. Introduction

Sulfuryl fluoride (SO_2F_2) is a C_{2v} asymmetric top, which is very close to tetrahedral symmetry. Its three rotational constants are close to each other, leading to a very small value of the sphericity parameter: $\gamma = 2(C-B)/(C+B) \simeq -0.0032$. Such a molecule can thus be regarded as a distorted spherical top, for instance as deriving from the tetrahedral sulfate ion, SO_4^{2-}. Technically, this means that we can work in the $O(3) \supset T_d \supset C_{2v}$ group chain.

In a previous paper [1], we have developed a tensorial formalism adapted to this problem and we have applied it to the microwave absorption spectrum of SO_2F_2 in its ground vibrational state in Ref. [2]. The analysis was realized thanks to a set of programs called C_{2v} TDS [3] implementing this formalism and that is freely available at the URL http://www.u-bourgogne.fr/LPUB/shTDS.html

In the present paper, we investigate in detail the relations between this tensorial formalism and the usual approach of Watson for asymmetric tops [4].

After reviewing the basic principles of both approaches, we first consider the purely rotational Hamiltonians and thus establish exact correspondence formulas for the vibrational ground state parameters. We then outline how the same kind of correspondence can be performed for excited vibrational states by considering the case of the $\nu_3/\nu_7/\nu_9$ bending triad. The relation between eigenstate labels in both formalisms is also detailed.

Moreover, we present some ab initio calculations that allowed us to estimate the centrifugal distorsion constants.

Finally, some numerical applications are given.

2. Basic principles

The formalism that we use for quasi-spherical top molecules with C_{2v} symmetry has already been described in previous papers [1–3], so we only outline here the points that are essential for the present purpose.

We consider an XY_2Z_2 molecule with C_{2v} symmetry (like SO_2F_2) as deriving from an XY_4 species (like SO_4^{2-}), just as illustrated in Fig. 1. In other words, we work in the $O(3) \supset T_d \supset C_{2v}$ group chain.

The basic idea is thus to start from the tetrahedral formalism used for molecules like methane, for instance [5,6], for which the $|J, M\rangle$ standard basis of $O(3)$ is symmetrized (oriented) into the T_d point group thanks to a G

* Corresponding author. Fax: +33 3 80 39 59 71.
E-mail address: vincent.boudon@u-bourgogne.fr (V. Boudon).

0022-2860/$ - see front matter © 2005 Elsevier B.V. All rights reserved.
doi:10.1016/j.molstruc.2005.05.056

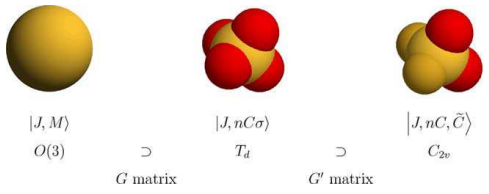

Fig. 1. Orientation in the group chain.

matrix [7]:

$$|J, nC\sigma\rangle = \sum_M G^M_{nC\sigma} |J, M\rangle, \tag{1}$$

where $C = A_1$, A_2, E, F_1 or F_2 is a T_d irreducible representation (irrep) and n is a multiplicity index used to number identical irreps within a J block.

This T_d basis is then symmetrized again (reoriented) into the C_{2v} subgroup thanks to another matrix called G' [1]:

$$|J, nC, \tilde{C}\rangle = \sum_\sigma {}^{(C)}G^{I\sigma}_{\tilde{C}} |J, nC\sigma\rangle, \tag{2}$$

where $\tilde{C} = a_1, a_2, b_1$ or b_2 is a C_{2v} irrep (we use lower case letters to avoid confusion with T_d irreps). Since all C_{2v} irreps are non-degenerate, the component label is not necessary and is thus omitted in this article.

The same kind of relations holds for tensor operators:

$$T^{(J,nC)}_\sigma = \sum_M {}^{(J)}G^{nC\sigma}_M T^{(J)}_M, \tag{3}$$

and

$$T^{(J,nC,\tilde{C})} = \sum_\sigma {}^{(C)}G^{I\sigma}_{\tilde{C}} T^{(J,nC)}_\sigma. \tag{4}$$

3. Rotational Hamiltonian

We now consider the comparison between Watson's Hamiltonian and the tensorial form in the vibrational ground state.

3.1. Watson's Hamiltonian

Let us consider the usual untransformed Watson's Hamiltonian (or Watsonian) expanded up to degree 6 in its standard form [4]:

$$\begin{aligned} H_{\text{Watson}} &= B_{200}J^2 + B_{020}J_Z^2 + T_{400}(J^2)^2 + T_{220}J^2J_Z^2 \\ &\quad + T_{040}J_Z^4 + \Phi_{600}(J^2)^3 + \Phi_{420}(J^2)^2J_Z^2 + \Phi_{240}J^2J_Z^4 \\ &\quad + \Phi_{060}J_Z^2 + \frac{1}{2}[B_{002} + T_{202}J^2 + T_{022}J_Z^2 + \Phi_{402}(J^2)^2 \\ &\quad + \Phi_{222}J^2J_Z^2 + \Phi_{042}J_Z^4, \mathcal{J}_+^2 + \mathcal{J}_-^2]_+ \\ &\quad + \frac{1}{2}[T_{004} + \Phi_{204}J^2 + \Phi_{024}J_Z^2, \mathcal{J}_+^4 + \mathcal{J}_-^4]_+ \\ &\quad + \Phi_{006}(\mathcal{J}_+^6 + \mathcal{J}_-^6), \end{aligned} \tag{5}$$

where $[\ldots,\ldots]_+$ terms represent anti-commutators:

$$[A, B]_+ = AB + BA, \tag{6}$$

and

$$\mathcal{J}_\pm = J_X \pm \mathrm{i}J_Y. \tag{7}$$

We use here an $(OXYZ)$ molecule-fixed frame (with capital letters). The reason for this notation will be explained in Section 3.3 below.

We work in the I^r representation ($B_X = B$, $B_Y = C$ and $B_Z = A$) and we have for the rotational constants:

$$B_{200} = \frac{B+C}{2}, \quad B_{020} = \frac{2A-B-C}{2} \quad \text{and} \quad B_{002} = \frac{B-C}{4}. \tag{8}$$

3.2. Tensorial Hamiltonian

The tensorial rotational Hamiltonian that we use is built as a sum of symmetrized tensors which are themselves constructed just as in the work of Moret–Bailly [8,9]. Thus, we symbolically call this Hamiltonian $H_{\text{Moret–Bailly}}$ and write it as:

$$H_{\text{Moret–Bailly}} = \sum_{\Omega,K,n,\Gamma} t^{\Omega(K,n\Gamma)} \beta R^{\Omega(K,n\Gamma,a_1)}, \tag{9}$$

where

$$\beta = \left(-\frac{\sqrt{3}}{4}\right)^{\Omega/2} \tag{10}$$

is a numerical factor used to let the scalar terms ($\Gamma = A_1$) match the usual form for spherical tops (so that $t^{2(0,A_1)} = B_0$ for a tetrahedral molecule, for instance). We will detail later the construction of $R^{\Omega(K,n\Gamma,a_1)}$ operators.

Up to degree $\Omega = 6$ and using (4) we get, in terms of T_d components of the operators:

$$\begin{aligned} H_{\text{Moret–Bailly}} &= -t_1 \frac{\sqrt{3}}{4} R^{2(0,A_1)} + t_2 R_1^{2(2,E)} + t_3 R_z^{2(2,F_2)} \\ &\quad + t_4 \frac{3}{16} R^{4(0,A_1)} + t_5 R_1^{4(2,E)} + t_6 R_z^{4(2,F_2)} \\ &\quad + t_7 R^{4(4,A_1)} + t_8 R_1^{4(4,E)} + t_9 R_z^{4(4,F_2)} \\ &\quad - t_{10} \frac{3\sqrt{3}}{64} R^{6(0,A_1)} + t_{11} R_1^{6(2,E)} \\ &\quad + t_{12} R_z^{6(2,F_2)} + t_{13} R^{6(4,A_1)} + t_{14} R_1^{6(4,E)} \\ &\quad + t_{15} R_z^{6(4,F_2)} + t_{16} R^{6(6,A_1)} + t_{17} R_1^{6(6,E)} \\ &\quad + t_{18} R_z^{6(6,0F_2)} + t_{19} R_z^{6(6,1F_2)}, \end{aligned} \tag{11}$$

where the notation for the parameters has been simplified for the present purpose.

Let us call (*Oxyz*) the molecule-fixed frame used in this case. In other words, the rotational operators $R^{\Omega(K,n\Gamma,a_1)}$ are functions of the J_x, J_y and J_z components. We show in the next paragraph why (*OXYZ*) and (*Oxyz*) are different.

3.3. Frame axes

If we consider only the zeroth order terms (i.e. terms with degree 2) for both Hamiltonians, we get:

$$H^0_{\text{Watson}} = (B_{200} + 2B_{002})J_X^2 + (B_{200} - 2B_{002})J_Y^2 + (B_{020} + B_{200})J_Z^2 \tag{12}$$

and

$$H^0_{\text{Moret–Bailly}} = \left(t_1 - 2\sqrt{\frac{2}{3}}t_2\right)J_x^2 + \left(t_1 - 2\sqrt{\frac{2}{3}}t_2\right)J_y^2 + \left(t_1 + 4\sqrt{\frac{2}{3}}t_2\right)J_z^2 + 2\sqrt{2}t_3(J_xJ_y + J_yJ_x) \tag{13}$$

We immediately see that $H^0_{\text{Moret–Bailly}}$ contains a cross-term $[J_x, J_y]_+$. The reason for this is quite obvious. This Hamiltonian is built starting from that of a tetrahedral molecule for which the molecule-fixed frame (*Oxyz*) is as shown in Fig. 2. This is not the principal axes frame of a C_{2v} molecule. On the other hand, (*OXYZ*) is such a principal axes frame.

Both frames are linked through a $\pi/4$ rotation around the $Z{=}z$ axis and this gives, in terms of angular momentum components:

$$\begin{cases} J_X = \dfrac{1}{\sqrt{2}}(J_x + J_y), \\ J_Y = -\dfrac{1}{\sqrt{2}}(J_x - J_y), \\ J_Z = J_z, \end{cases} \quad \text{or} \quad \begin{cases} J_x = \dfrac{1}{\sqrt{2}}(J_X - J_Y), \\ J_y = \dfrac{1}{\sqrt{2}}(J_X + J_Y), \\ J_z = J_Z. \end{cases} \tag{14}$$

It is easy to verify that expressing $H^0_{\text{Moret–Bailly}}$ in terms of J_X, J_Y and J_Z eliminates the cross term.

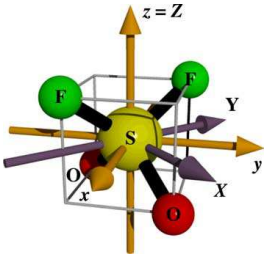

Fig. 2. Frame axes for SO_2F_2.

3.4. Correspondence formulas

In order to compare, the two rotational Hamiltonians defined above, we first need to expand $H_{\text{Moret–Bailly}}$ in a suitable way.

The oriented rotational operators in (9) are constructed by applying successively the G and G' transformations to $O(3)$ tensors $R_M^{\Omega(K)}$, using Eq. (3) and (4):

$$R^{\Omega(K,n\Gamma,a_1)} = \sum_\gamma {}^{(\Gamma)}G'^{\gamma}_{a_1} R^{\Omega(K,n\Gamma)}_\gamma = \sum_M \sum_\gamma {}^{(\Gamma)}G'^{\gamma(K)}_{a_1} G^M_{n\gamma\Gamma} R^{\Omega(K)}_M \tag{15}$$

For the present example, which is limited to $\Omega \leq 6$, the multiplicity index n only appears for $K{=}6$ and $\Gamma{=}F_2$. In this case, the G coefficients are imaginary non-rational numbers. We have:

$$\begin{cases} {}^{(6)}G^{-6}_{0F_2z} = -a\mathrm{i}, \\ {}^{(6)}G^{-2}_{0F_2z} = +b\mathrm{i}, \\ {}^{(6)}G^{2}_{0F_2z} = -b\mathrm{i}, \\ {}^{(6)}G^{6}_{0F_2z} = +a\mathrm{i}, \end{cases} \text{and} \quad \begin{cases} {}^{(6)}G^{-6}_{1F_2z} = -b\mathrm{i}, \\ {}^{(6)}G^{-2}_{1F_2z} = -a\mathrm{i}, \\ {}^{(6)}G^{2}_{1F_2z} = +a\mathrm{i}, \\ {}^{(6)}G^{6}_{1F_2z} = +b\mathrm{i}, \end{cases} \tag{16}$$

with

$$a = \frac{3\sqrt{55}}{4\sqrt{1684 + 79\sqrt{421}}}, \text{ and } b = -\frac{79 + 4\sqrt{421}}{4\sqrt{1684 + 79\sqrt{421}}}. \tag{17}$$

The $O(3)$ components are constructed as defined by Moret–Bailly [8,9] and using the recursion procedure of Zhilinskiĭ [10]:

$$R^{\Omega(K)}_M = (R^{2(0)}_0)^{((\Omega-K)/2)} R^{K(K)}_M, \tag{18}$$

and

$$R^{K(K)}_M = (R^{K-1(K-1)} \otimes R^{1(1)})^{(K)}_M, \tag{19}$$

with

$$R^{2(0)}_0 = -\frac{4}{\sqrt{3}}J^2, \tag{20}$$

and

$$R^{1(1)}_M = 2J^{(1)}_M. \tag{21}$$

The elementary operators $J^{(1)}_M$ are:

$$J^{(1)}_0 = J_z \text{ and } J^{(1)}_{\pm 1} = \mp\frac{1}{\sqrt{2}}J_\pm = \mp\frac{1}{\sqrt{2}}(J_x \pm iJ_y), \tag{22}$$

due to the values of the ${}^{(1)}G^M_{F_1\sigma}$ coefficients [7] (the **J** vector having F_1 symmetry in the T_d group).

However, in order to get expanded expressions in a standard form that makes the comparison with H_{Watson} easier, we can use the work of Buckmaster et al. [11] and remark that their T_{KM} operators are directly proportional to

our $R_M^{K(K)}$. More precisely, we have:

$$R_M^{K(K)} = 2^K T_{\mathrm{KM}} \tag{23}$$

Thus, using expressions given in Ref. [11], it is easy to obtain expressions in terms of elementary angular momentum operators in the general form

$$R_M^{Q(K)} = \sum_{k,l,m} C_{klm} (J^2)^{k/2} (J_z^2)^{l/2} ((J_+^2)^{m/2} \pm (J_-^2)^{m/2}), \tag{24}$$

where k, l and m are even integers. H_{Watson} is expressed in the same manner using transformation (14).

It is then possible to solve the equation $H_{\mathrm{Moret\text{–}Bailly}} = H_{\mathrm{Watson}}$ truncated at degree $Q=6$ using Maple symbolic calculation software [12]. We used Maple's &* operator as the non-commutative multiplication. We get:

$$B_{002} = -\sqrt{2}t_3 - \frac{20\sqrt{14}}{7}t_9 - \frac{816b\sqrt{55}}{11}t_{18} - \frac{816a\sqrt{55}}{11}t_{19} + \cdots \tag{25}$$

$$B_{020} = 2\sqrt{6}t_2 + \frac{10\sqrt{30}}{3}t_7 - \frac{50\sqrt{42}}{21}t_8 - \frac{56\sqrt{462}}{11}t_{16} + \frac{392\sqrt{66}}{11}t_{17} + \cdots \tag{26}$$

$$B_{200} = t_1 - \frac{2\sqrt{6}}{3}t_2 - \frac{4}{5}t_7 + \frac{4\sqrt{42}}{7}t_8 + \frac{80\sqrt{462}}{77}t_{16} - \frac{80\sqrt{66}}{11}t_{17} + \cdots \tag{27}$$

$$T_{400} = t_4 + \frac{8\sqrt{2}}{3}t_5 + \frac{2\sqrt{30}}{5}t_7 - \frac{2\sqrt{42}}{7}t_8 + \frac{16\sqrt{10}}{5}t_{13} - \frac{16\sqrt{14}}{7}t_{14} - \frac{160\sqrt{462}}{231}t_{16} + \frac{160\sqrt{66}}{33}t_{17} + \cdots \tag{28}$$

$$T_{220} = -8\sqrt{2}t_5 - 4\sqrt{30}t_7 + \frac{20\sqrt{42}}{7}t_8 - \frac{40\sqrt{10}}{3}t_{13} + \frac{200\sqrt{14}}{21}t_{14} + \frac{100\sqrt{462}}{11}t_{16} - \frac{700\sqrt{66}}{11}t_{17} + \cdots \tag{29}$$

$$T_{040} = \frac{14\sqrt{30}}{3}t_7 - \frac{10\sqrt{42}}{3}t_8 - \frac{140\sqrt{462}}{11}t_{16} + \frac{980\sqrt{66}}{11}t_{17} + \cdots \tag{30}$$

$$T_{202} = \frac{4\sqrt{6}}{3}t_6 + \frac{4\sqrt{14}}{7}t_9 - \frac{80\sqrt{42}}{21}t_{15} - \frac{80b\sqrt{55}}{11}t_{18} - \frac{80a\sqrt{55}}{11}t_{19} + \ldots \tag{31}$$

$$T_{004} = -\frac{\sqrt{30}}{3}t_7 - \frac{\sqrt{42}}{3}t_8 + \frac{76\sqrt{462}}{11}t_{16} + \frac{76\sqrt{66}}{11}t_{17} + \cdots \tag{32}$$

$$T_{022} = -4\sqrt{14}t_9 + \frac{984b\sqrt{55}}{11}t_{18} + \frac{984a\sqrt{55}}{11}t_{19} + \cdots \tag{33}$$

$$\Phi_{600} = t_{10} - \frac{32\sqrt{6}}{9}t_{11} - \frac{8\sqrt{10}}{5}t_{13} + \frac{8\sqrt{14}}{7}t_{14} + \frac{20\sqrt{462}}{231}t_{16} - \frac{20\sqrt{66}}{33}t_{17} + \cdots \tag{34}$$

$$\Phi_{420} = \frac{32\sqrt{6}}{3}t_{11} + 16\sqrt{10}t_{13} - \frac{80\sqrt{14}}{7}t_{14} - \frac{20\sqrt{462}}{11}t_{16} + \frac{140\sqrt{66}}{11}t_{17} + \cdots \tag{35}$$

$$\Phi_{240} = -\frac{56\sqrt{10}}{3}t_{13} + \frac{40\sqrt{14}}{3}t_{14} + \frac{60\sqrt{462}}{11}t_{16} - \frac{420\sqrt{66}}{11}t_{17} + \cdots \tag{36}$$

$$\Phi_{240} = -4\sqrt{462}t_{16} + 28\sqrt{66}t_{17} + \cdots \tag{37}$$

$$\Phi_{402} = -\frac{16\sqrt{2}}{3}t_{12} - \frac{16\sqrt{42}}{21}t_{15} - \frac{8b\sqrt{55}}{11}t_{18} - \frac{8a\sqrt{55}}{11}t_{19} + \cdots \tag{38}$$

$$\Phi_{222} = \frac{16\sqrt{42}}{3}t_{15} + \frac{144b\sqrt{55}}{11}t_{18} + \frac{144a\sqrt{55}}{11}t_{19} + \cdots \tag{39}$$

$$\Phi_{042} = -24b\sqrt{55}t_{18} - 24a\sqrt{55}t_{19} + \cdots \tag{40}$$

$$\Phi_{204} = \frac{4\sqrt{10}}{3}t_{13} + \frac{4\sqrt{14}}{3}t_{14} + \frac{2\sqrt{462}}{11}t_{16} + \frac{2\sqrt{66}}{11}t_{17} + \cdots \tag{41}$$

$$\Phi_{024} = -2\sqrt{462}t_{16} - 2\sqrt{66}t_{17} + \cdots \tag{42}$$

$$\Phi_{006} = 8at_{18} - 8bt_{19} + \cdots \tag{43}$$

with a and b given by Eq. (17). Inverse formulas are found in the same way:

$$t_1 = B_{200} + \frac{1}{3}B_{020} - \frac{1}{15}T_{040} + \frac{1}{21}\Phi_{060} + \cdots \tag{44}$$

$$t_2 = \frac{\sqrt{6}}{12}B_{020} - \frac{5\sqrt{6}}{84}T_{040} + \frac{\sqrt{6}}{12}\Phi_{060} + \cdots \tag{45}$$

$$t_3 = -\frac{\sqrt{2}}{2}B_{002} - \frac{5\sqrt{2}}{14}T_{022} + \frac{3\sqrt{2}}{14}\Phi_{042} + \cdots \tag{46}$$

$$t_4 = T_{400} + \frac{1}{3}T_{220} + \frac{1}{5}T_{040} - \frac{1}{15}\Phi_{240} - \frac{1}{7}\Phi_{060} + \cdots \tag{47}$$

$$t_5 = -\frac{\sqrt{2}}{16}T_{220} - \frac{3\sqrt{2}}{56}T_{040} + \frac{5\sqrt{2}}{112}\Phi_{240} + \frac{5\sqrt{2}}{56}\Phi_{060} + \cdots \quad (48)$$

$$t_6 = \frac{\sqrt{6}}{8}T_{202} + \frac{\sqrt{6}}{56}T_{022} + \frac{5\sqrt{6}}{56}\Phi_{222} + \frac{13\sqrt{6}}{168}\Phi_{042} + \ldots \quad (49)$$

$$t_7 = \frac{\sqrt{30}}{240}T_{040} - \frac{\sqrt{30}}{24}T_{004} - \frac{7\sqrt{30}}{528}\Phi_{060} - \frac{19\sqrt{30}}{132}\Phi_{024} + \cdots 1 \quad (50)$$

$$t_8 = -\frac{\sqrt{42}}{336}T_{040} - \frac{\sqrt{42}}{24}T_{004} + \frac{5\sqrt{42}}{528}\Phi_{060} - \frac{19\sqrt{42}}{132}\Phi_{024} + \ldots \quad (51)$$

$$t_9 = -\frac{\sqrt{14}}{56}T_{022} - \frac{41\sqrt{14}}{616}\Phi_{042} + \cdots \quad (52)$$

$$t_{10} = \Phi_{600} + \frac{1}{3}\Phi_{420} + \frac{1}{5}\Phi_{240} + \frac{1}{7}\Phi_{060} + \cdots \quad (53)$$

$$t_{11} = \frac{\sqrt{6}}{64}\Phi_{420} + \frac{3\sqrt{6}}{224}\Phi_{240} + \frac{5\sqrt{6}}{448}\Phi_{060} + \cdots \quad (54)$$

$$t_{12} = -\frac{3\sqrt{2}}{32}\Phi_{402} - \frac{3\sqrt{2}}{224}\Phi_{222} - \frac{\sqrt{2}}{224}\Phi_{042} + \cdots \quad (55)$$

$$t_{13} = -\frac{\sqrt{10}}{320}\Phi_{240} + \frac{\sqrt{10}}{32}\Phi_{204} - \frac{3\sqrt{10}}{704}\Phi_{060} + \frac{\sqrt{10}}{352}\Phi_{024} + \cdots \quad (56)$$

$$t_{14} = \frac{\sqrt{14}}{448}\Phi_{240} + \frac{\sqrt{14}}{32}\Phi_{204} + \frac{15\sqrt{14}}{4928}\Phi_{060} + \frac{\sqrt{14}}{352}\Phi_{024} + \cdots \quad (57)$$

$$t_{15} = \frac{\sqrt{42}}{224}\Phi_{222} + \frac{3\sqrt{42}}{1232}\Phi_{042} + \cdots \quad (58)$$

$$t_{16} = -\frac{\sqrt{462}}{14784}\Phi_{060} - \frac{\sqrt{462}}{1056}\Phi_{024} + \cdots \quad (59)$$

$$t_{17} = \frac{\sqrt{66}}{2112}\Phi_{060} - \frac{\sqrt{66}}{1056}\Phi_{024} + \cdots \quad (60)$$

$$t_{18} = -\frac{b\sqrt{55}}{660}\Phi_{042} + \frac{a}{4}\Phi_{006} + \cdots \quad (61)$$

$$t_{19} = -\frac{a\sqrt{55}}{660}\Phi_{042} - \frac{b}{4}\Phi_{006} + \cdots \quad (62)$$

However, one should keep in mind that the above relations are only developments. This is due to the fact that Moret–Bailly's $R_M^{K(K)}$ (or Buckmaster's T_{KM}) rotational operators contain terms with different degrees in J_z, J_+ or J_-. Ω is only the maximum degree. For instance,

$$R_0^{4(4)} = 4\sqrt{70}\left(J_z^4 + \frac{5}{7}J_z^2 - \frac{6}{7}J_z^2J^2 - \frac{6}{35}J^2 + \frac{3}{35}J^4\right), \quad (63)$$

which contains three terms with degree 4 and 2 terms of degree 2. Thus, adding operators with higher Ω values will add new terms in the development of lower order Watsonian parameters.

With this stated, Eqs. (25)–(43) and (44)–(62) represent an exact correspondence for a truncation at order $\Omega = 6$.

3.5. Reductions

All what we discussed above concerns, the exact untransformed rotational Hamiltonian. However, Watson has shown that there exists some indeterminacy in this Hamiltonian in the sense that the number of parameters can be reduced through a contact transformation [4,13]. It is easy to show the following equivalences for the two well-known reductions defined by Watson:

- For *A*-reduction:

$$\begin{cases} \tilde{T}_{004} = 0, \\ \tilde{\Phi}_{204} = 0, \\ \tilde{\Phi}_{024} = 0, \\ \tilde{\Phi}_{006} = 0, \end{cases} \Leftrightarrow \begin{cases} \tilde{t}_8 = -\sqrt{\frac{5}{7}}\tilde{t}_7, \\ \tilde{t}_{14} = -\sqrt{\frac{5}{7}}\tilde{t}_{13}, \\ \tilde{t}_{17} = -\sqrt{7}\tilde{t}_{16}, \\ \tilde{t}_{19} = -\frac{3\sqrt{55}}{79 + 4\sqrt{421}}\tilde{t}_{18}. \end{cases} \quad (64)$$

- For *S*-reduction:

$$\begin{cases} \tilde{T}_{022} = 0, \\ \tilde{\Phi}_{222} = 0, \\ \tilde{\Phi}_{042} = 0, \\ \tilde{\Phi}_{024} = 0, \end{cases} \Leftrightarrow \begin{cases} \tilde{t}_9 = 0, \\ \tilde{t}_{15} = 0, \\ \tilde{t}_{17} = -\sqrt{7}\tilde{t}_{16}, \\ \tilde{t}_{19} = \frac{79 + 4\sqrt{421}}{3\sqrt{55}}\tilde{t}_{18}. \end{cases} \quad (65)$$

As usual, we use tildes (˜) to denote parameters of the transformed Hamiltonian.

The so-called 6-reduction used by Sarka et al. [14] is identical to the *S*-reduction with the exception that $\tilde{T}_{022}$ (and thus $\tilde{t}_9$ in our case) is not fixed to zero.

4. Rovibrational Hamiltonian for the bending triad

Correspondence between both formalisms can also be established for excited vibrational states. We examplify this below in the case of the bending triad of SO_2F_2. The vibrational structure of this molecule can be correlated to that of the SO_4^{2-} tetrahedral ion as shown in Fig. 3. The $\nu_3(a_1)/\nu_7(b_1)/\nu_9(b_2)$ triad derives from the $\nu_4(F_2)$ fundamental[1] of SO_4^{2-}.

4.1. Band parameters

An important difference between our approach and the usual one is that we use the so-called vibrational extrapolation technique. Details about this can be found in Refs. [5,6]. In short, it means that the effective Hamiltonian for a given polyad contains all the operators (and thus all the parameters) from the lower polyads. Terms specific to the polyad under consideration are (at least in principle) small corrections.

In the case of the bending triad, this can be written as:

$$\tilde{H}^{\langle\text{Triad}\rangle} = \tilde{H}^{\langle\text{Triad}\rangle}_{\{\text{GS}\}} + \tilde{H}^{\langle\text{Triad}\rangle}_{\{\text{Triad}\}} = \tilde{H}_{\text{Moret–Bailly}} + \sum_{\Omega,K,n,\Gamma,\Gamma',\tilde{\Gamma}} \beta' \tilde{t}^{\Omega(K,\Gamma,\tilde{\Gamma})\Gamma'}_{\{4\}\{4\}} (R^{\Omega(K,n\Gamma,\tilde{\Gamma})} \otimes {}^{\varepsilon}V^{F_2F_2(\Gamma',\tilde{\Gamma})}_{\{4\}\{4\}})^{(a_1)}, \tag{66}$$

where $\varepsilon=(-1)^{\Omega}$ and $\beta'=\sqrt{3}(-\sqrt{3}/4)^{\Omega/2}$. $\tilde{H}_{\text{Moret–Bailly}}$ is the ground-state purely rotational contribution defined previously, which has been reduced in the sense of Watson (see Section 3.5). The ${}^{\varepsilon}V^{\{4\}\{4\}}_{F_2F_2(\Gamma',\tilde{\Gamma})}$ are vibrational operators constructed through recursive couplings of the $a^{+(F_2)}_{4\sigma}$ and $a^{(F_2)}_{4\sigma}$ ($\sigma=x$, y or z) elementary creation and anihilation operators of the $\nu_4(F_2)$ normal mode of the 'parent' tetrahedral molecule [1,5,6].

It should be noticed that in Eq. (66) the rotational and vibrational operators are first symmetrized in the group chain and then coupled together in the C_{2v} group. This approach is similar to that defined by Champion [5] for tetrahedral molecules and differs from the original work of Moret–Bailly [16] in which the couplings were realized in the $O(3)$ group, the symmetrization being performed afterwards on the coupled operators.

The whole Hamiltonian above has also been implicitly reduced since interactions with other polyads have been eliminated through some contact transformations.

The Watsonian form for excited vibrational states can be found for instance in Ref. [4].

As we will show it later, parameters with $\tilde{\Gamma}=a_2, b_1$ or b_2 correspond to Coriolis interactions.

The procedure used to compare the rovibrational Watsonian and tensorial Hamiltonian can be summarized as follows:

[1] We can notice on Fig. 3 that the ν_7 and ν_9 band labels have been inverted compared to Ref. [15]. This fact will be explained in a forthcoming paper dedicated to the detailed analysis of the bending triad using the present tensorial formalism.

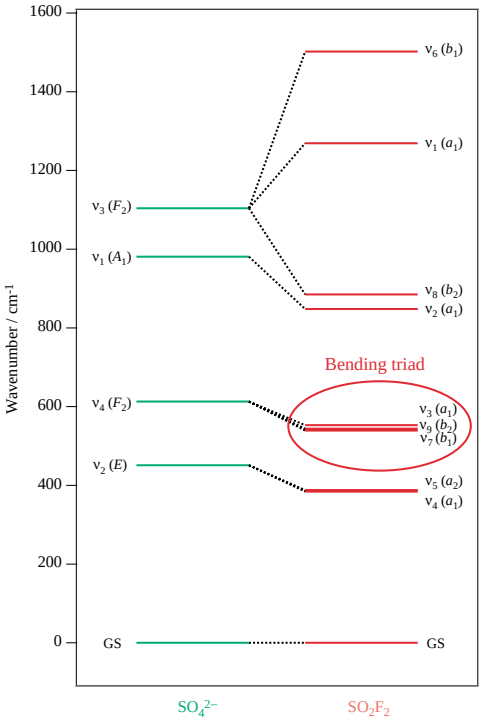

Fig. 3. Correlation between the vibrational levels of SO_4^{2-} and SO_2F_2.

Rotational operators for both Hamiltonains are expressed in terms of J^2, J_z^2, J_+^2 and J_-^2 as described before. Then, we take the matrix elements in the vibrational basis, that is:

- For the Watsonian: $\{|\nu_3=1, a_1>\rangle, |\nu_7=1, b_1\rangle, |\nu_9=1, b_2\rangle\}$.
- For the tensorial Hamiltonian: $\{|\nu_4=1, F_2, \tilde{\Gamma}\rangle, \tilde{\Gamma}=a_1, b_1, \text{ or } b_2\}$.

We now present the results of this comparison.

Let us first consider non-Coriolis parameters, that is parameters with $\tilde{\Gamma}=a_1$. In this case, for each $\Omega(K, n\Gamma)$ we have always a triplet of parameters $\tilde{t}^{\Omega(K,n\Gamma,a_1)\Gamma'}_{\{4\}\{4\}} = t^{A_1}, t^E$ or t^{F_2} that can be related to parameters specific to each band ν_3, ν_7 or ν_9 through:

$$t^{A_1} = \gamma\frac{t^3+t^7+t^9}{3}, t^E = \gamma\frac{t^7+t^9-2t^3}{3}, t^{F_2} = \gamma\frac{t^9-t^7}{\sqrt{2}}, \tag{67}$$

where $\gamma=\sqrt{3}$ if $\Gamma'=E$ or F_2 and 1 otherwise.

The $t^i = \tilde{t}^{\Omega(K,n\Gamma,a_1)i}_{\{4\}\{4\}}$ ($i=3, 7$ or 9) parameters can then obtained from those of the Watson Hamlitonian through

$$\tilde{t}^{\Omega(K,n\Gamma,a_1)i}_{\{4\}\{4\}} = f(\Delta\tilde{B}^i_{klm}, \Delta\tilde{T}^i_{klm}, \Delta\tilde{\Phi}^i_{klm}), \tag{68}$$

where f represents the same set of relations that we have established between ground-state parameters and $\Delta\tilde{T}^i_{klm} = \tilde{T}^i_{klm} - \tilde{T}^0_{klm}$, etc. are differences between ν_i (i=3, 7 or 9) and ground-state parameters. The use of 'Δ' parameters here results from the vibrational extrapolation.

For purely vibrational parameters (band centers), we have:

$$\tilde{t}^{A_1} = \frac{\nu_3+\nu_7+\nu_9}{3}, t^E = \frac{\nu_7+\nu_9-2\nu_3}{3}, t^{F_2} = \frac{\nu_9-\nu_7}{\sqrt{2}}. \quad (69)$$

Here is another example concerning rotational constants:

$$t^{2(0A_1,a_1)A_1}_{\{4\}\{4\}} = \frac{1}{3}\left(\frac{\Delta A_3+\Delta B_3+\Delta C_3}{3} + \frac{\Delta A_7+\Delta B_7+\Delta C_7}{3} + \frac{\Delta A_9+\Delta B_9+\Delta C_9}{3}\right). \quad (70)$$

4.2. Coriolis interaction parameters

The correspondence for Coriolis interaction parameters can be found in the same way. For first-order Coriolis interactions within the bending triad, we get:

$$\tilde{t}^{1(1,F_1,a_2)F_1}_{\{4\}\{4\}} = \sqrt{\frac{3}{2}} Z^a_{7,9}, \quad (71)$$

$$\tilde{t}^{1(1,F_1,b_1)F_1}_{\{4\}\{4\}} = \sqrt{\frac{3}{2}} Z^b_{3,9}, \quad (72)$$

$$\tilde{t}^{1(1,F_1,b_2)F_1}_{\{4\}\{4\}} = \sqrt{\frac{3}{2}} Z^c_{3,7}, \quad (73)$$

where

$$Z^\alpha_{i,j} = \frac{1}{\sqrt{2}}\xi^\alpha_{i,j} = B_\alpha \frac{\omega_j+\omega_j}{\sqrt{\omega_i\omega_j}}\zeta^\alpha_{i,j}, \quad (74)$$

and B_X=B, B_Y=C, B_Z=A as before (I^r representation). The $\zeta^\alpha_{i,j}$ are the usual Coriolis parameters [4].

Here is an example of a second-order Coriolis interaction:

$$(R^{2(2,E,a_2)} \otimes {}^+V^{F_2F_2(E,a_2)}_{\{4\}\{4\}})^{(a_1)} = -2(J_x^2 - J_y^2)(N_x - N_y) \quad (75)$$

N_x and N_y being the usual number operators for harmonic oscillators:

$$N_x = a^{+(F_2)}_{4x} a^{(F_2)}_{4x} \quad \text{and} \quad N_y = a^{+(F_2)}_{4y} a^{(F_2)}_{4y} \ . \quad (76)$$

We can deduce that

$$t^{2(2,E,a_2)E}_{\{4\}\{4\}} = \eta^a_{7,9}, \quad (77)$$

$\eta^a_{7,9}$ being the usual notation [4] for second-order Coriolis parameters.

5. Dipole moment parameters

In our approach, intensities of microwave or infrared absorption transitions are calculated using a tensorial development of the dipole moment operator, as described in Ref. [1]. If we consider only the zeroth order dipole moment parameters for the ground vibrational state and for the bending triad, then the correspondence between the tensorial and the usual formalisms is trivial. In the molecule-fixed frame, only the ${}^+V^{A_1A_1(A_1,a_1)}_{\{0\}\{0\}} = \mu_0$ (permanent dipole moment), ${}^+V^{A_1F_2(F_2,a_1)}_{\{0\}\{4\}} = \mu_3$, ${}^+V^{A_1F_2(F_2,b_1)}_{\{0\}\{4\}} = \mu_7$ and ${}^+V^{A_1F_2(F_2,b_2)}_{\{0\}\{4\}} = \mu_9$ are implied and there is thus a direct one-to-one correspondence between the parameters.

6. State labels

Matrix elements of the tensorial Hamiltonian are calculated using the Wigner–Eckart theorem and the various coupling relations given in Ref. [1] in a coupled rovibrational basis set:

$$|\{v_i\}C_v\tilde{C}_v, JnC_r\tilde{C}_r, \tilde{C}\rangle = |[\Psi^{(\{v_i\}C_v,\tilde{C}_v)}_v \otimes \Psi^{(J,nC_r,\tilde{C}_r)}_r]^{(\tilde{C})}\rangle, \quad (78)$$

where $\Psi^{(\{v_i\}C_v,\tilde{C}_v)}_v$ (resp.$\Psi^{(J,nC_r,\tilde{C}_r)}_r$) are tetrahedral vibrational (resp. rotational) wavefunctions which are symmetrized in the C_{2v} group. The $\{v_i\}$ represent the set of quantum numbers for the parent tetrahedral molecule. C_v and C_r are T_d irreps which constitute intermediate 'tetrahedral quantum numbers'. In fact, all what has been presented up to now is, strictly speaking, valid for any XY_2Z_2 molecule with C_{2v} symmetry. But it is clear that this approach mainly makes sense in the quasi-tetrahedral case, i.e. when the basis (78) turns out to be 'close' to the final eigenbasis defined below.

The Hamiltonian eigenfunctions obtained after diagonalization are denoted

$$|J, \tilde{C}, \alpha\rangle, \quad (79)$$

where α is a running index that numbers eigenstates with the same C_{2v} symmetry $\tilde{C}$ within a given J block, in increasing energy order.

On the other hand, the usual state labeling for an asymmetric top [4] is:

$$|\tilde{C}_v\rangle|J, K_aK_c\rangle. \quad (80)$$

The overall symmetry $\tilde{C}$ of each eigenstate can be deduced from the vibrational symmetry $\tilde{C}_v$ and the parities of K_a and K_c (e=even, o=odd) as shown in Table 1.

In order to get a full correspondence between eigenstates in both formalisms, we need to relate α to K_aK_c, which is a more complex problem. This can be done easily for the ground vibrational state, or for any isolated vibrational state. In this case, it is well-known that the (K_a, K_c) labels of the eigenstates sorted in increasing energy order make the

Table 1
Overall symmetry ($\tilde{C}$) of rovibrational levels

K_aK_c	Symmetry ($\tilde{C}_v$) of vibrational state			
	a_1	a_2	b_1	b_2
ee	a_1	a_2	b_1	b_2
eo	a_2	a_1	b_2	b_1
oo	b_1	b_2	a_1	a_2
oe	b_2	b_1	a_2	a_1

following sequence:

$$\begin{aligned}(K_a,K_c) = \quad & (0,J)\\ & (1,J)\\ & (1,J-1)\\ & (2,J-1)\\ & \vdots\\ & (J-1,2)\\ & (J-1,1)\\ & (J,1)\\ & (J,0)\end{aligned} \tag{81}$$

Thus (see Table 1), the parity labels always alternate in a sequence like: …, *eo*, *oo*, *oe*, *ee*,… If we define:

$$\eta = K_a - K_c + J, \tag{82}$$

then it is straightforward to show that:

$$\alpha = [\eta/4] + 1 \tag{83}$$

where $[\cdots]$ is the integer part.

This problem is much more complex for a polyad in which the rotational states pertaining to different vibrational states overlap, since α numbers states globally over the whole polyad. We do not treat such a case here.

7. Numerical applications

In this section, we give some numerical applications to illustrate the correspondence formulas derived above. We also make some ab initio calculations for the rotational and centrifugal distorsion constants that we give here for comparison.

7.1. Ab initio calculation of centrifugal distorsion constants

Ab initio calculations were carried out with the GAUSSIAN 98 program [17] at B3LYP level of theory [18]. The density functional theory with hybrid functional B3LYP (Beckes three parameter functional employing the Lee, Yand, and Parr correlation functional) is able to give reliable harmonic force fields [19]. Dunnings correlation consistent cc-pVDZ basis set [20] and split-valence basis set with polarization and diffuse functions 6-311++G(3*df*,2*pd*) [21] stored internally in the GAUSSIAN 98 were employed.

From this calculation, we get the ground state rotational constants B_X, B_Y and B_Z as well as the data necessary to obtain the centrifugal distorsion constants. In order to get these, we employed the INFRA program from Breidung and Thiel [22]. In short, this program uses the l transformation (obtained from the GAUSSIAN 98 output) that relates the mass-weighted Cartesian coordinates $s_{i\alpha}$ ($\alpha = X$, Y or Z) to the normal coordinates Q_k:

$$s_{i\alpha} = \sum_{k=1}^{3N-6} l_{i\alpha,k} Q_k \tag{84}$$

INFRA can calculate the τ constants [4]:

$$\tau_{\alpha\beta\gamma\delta} = -\frac{1}{2}\sum_k \frac{a_k^{\alpha\beta} a_k^{\delta\gamma}}{\lambda_k I_{\alpha\alpha} I_{\beta\beta} I_{\gamma\gamma} I_{\delta\delta}}, \tag{85}$$

where the $I_{\alpha\alpha}$, etc. are the moments of inertia, the λ_k are the eigenvalues of the GF matrix [4] and

$$a_k^{\alpha\alpha} = 2\sum_i m_i^{1/2}(a_{i\beta} l_{i\beta,k} + a_{i\gamma} l_{i\gamma,k}), \tag{86}$$

$$a_k^{\alpha\beta} = -\sum_i m_i^{1/2}(a_{i\alpha} l_{i\beta,k} + a_{i\beta} l_{i\alpha,k}), \quad \alpha \neq \beta, \tag{87}$$

$$a_k^{\beta\alpha} = a_k^{\alpha\beta}, \tag{88}$$

are the first derivatives of the inertia tensor, the $a_{i\alpha}$, etc. being the atom coordinates at equilibrium obtained from Gaussian.

We can then obtain the centrifugal distorsion constants through the relations [4]:

$$\begin{aligned}\tilde{T}_{400} = {} & \frac{1}{32}(3\tau_{XXXX} + 3\tau_{YYYY} + 2\tau_{XXYY} + 4\tau_{XYXY})\\ & -\frac{1}{2}(B_X - B_Y)S_{XYZ},\end{aligned} \tag{89}$$

$$\begin{aligned}\tilde{T}_{220} = {} & \frac{1}{4}(\tau_{ZZXX} + \tau_{YYZZ} + 2\tau_{ZXZX} + 2\tau_{ZYZY}) - \frac{1}{16}\\ & \times(3\tau_{XXXX} + 3\tau_{YYYY} + 2\tau_{XXYY} + 4\tau_{XYXY})\\ & + 3(B_X - B_Y)S_{XYZ},\end{aligned} \tag{90}$$

$$\begin{aligned}\tilde{T}_{040} = {} & \frac{1}{4}(\tau_{ZZZZ} - \tau_{ZZXX} - \tau_{YYZZ} - 2\tau_{ZXZX} - 2\tau_{ZYZY})\\ & + \frac{1}{32}(3\tau_{XXXX} + 3\tau_{YYYY} + 2\tau_{XXYY} + 4\tau_{XYXY})\\ & - \frac{5}{2}(B_X - B_Y)S_{XYZ},\end{aligned} \tag{91}$$

$$\tilde{T}_{202} = \frac{1}{16}(\tau_{XXXX} - \tau_{YYYY}), \tag{92}$$

Table 2
Ground state parameters for SO_2F_2 up to order 6

Parameter		Value (MHz)[a]	'Calculated' (MHz)[b]	Ab initio (MHz)
A	$(\tilde{B}_Z)$	$5.134877(346)\times10^{+3}$	$5.134877\times10^{+3}$	$5.049\times10^{+3}$
B	$(\tilde{B}_X)$	$5.073077(242)\times10^{+3}$	$5.073077\times10^{+3}$	$4.977\times10^{+3}$
C	$(\tilde{B}_Y)$	$5.057058(244)\times10^{+3}$	$5.057057\times10^{+3}$	$4.963\times10^{+3}$
D_J	$(-\tilde{T}_{400})$	$1.478752(59)\times10^{-3}$	1.478545×10^{-3}	1.55×10^{-3}
D_{JK}	$(-\tilde{T}_{220})$	$-1.530067(56)\times10^{-3}$	-1.529706×10^{-3}	-1.79×10^{-3}
D_K	$(-\tilde{T}_{040})$	$1.851209(229)\times10^{-3}$	1.850947×10^{-3}	2.12×10^{-3}
d_1	$(\tilde{T}_{202})$	$-29.553(30)\times10^{-6}$	-29.680×10^{-6}	-27.5×10^{-6}
d_2	$(\tilde{T}_{004})$	$136.998(13)\times10^{-6}$	137.032×10^{-6}	157×10^{-6}
H_J	$(\tilde{\Phi}_{600})$	$436.93(3.83)\times10^{-12}$	424.04×10^{-12}	–
H_{JK}	$(\tilde{\Phi}_{420})$	$23.68(10.19)\times10^{-12}$	35.47×10^{-12}	–
H_{KJ}	$(\tilde{\Phi}_{240})$	$1.555(18)\times10^{-9}$	1.561×10^{-9}	–
H_K	$(\tilde{\Phi}_{060})$	$-1.602(50)\times10^{-9}$	-1.617×10^{-9}	–
h_1	$(\tilde{\Phi}_{402})$	$451.91(3.14)\times10^{-12}$	462.31×10^{-12}	–
h_2	$(\tilde{\Phi}_{204})$	$91.50(3.06)\times10^{-12}$	112.70×10^{-12}	–
h_3	$(\tilde{\Phi}_{006})$	$-586.06(1.84)\times10^{-12}$	-608.04×10^{-12}	–

[a] From fit of the Watsonian in *S*-reduction.
[b] From fit of the tensorial Hamiltonian and after parameter transformation.

$$\tilde{T}_{022} = \frac{1}{8}(\tau_{ZZXX} - \tau_{YYZZ}) - \frac{1}{16}(\tau_{XXXX} - \tau_{YYYY}) + \frac{1}{4} \times (\tau_{ZXZX} - \tau_{YZYZ}) + (B_X + B_Y - 2B_Z)S_{XYZ}, \quad (93)$$

$$\tilde{T}_{004} = \frac{1}{64}(\tau_{XXXX} + \tau_{YYYY}) - \frac{1}{32}(\tau_{XXYY} + 2\tau_{XYXY}) + \frac{1}{4}(B_X - B_Y)S_{XYZ}, \quad (94)$$

where S_{XYZ} is the contact transformation parameter. Its value is fixed by the choice of reduction. In the next section, we give the numerical results in the case of the *S*-reduction, i.e. for$\tilde{T}_{022} = 0$, which are in good agreement with the experimental values.

7.2. Ground state parameters

Table 2 gives the ground state parameters of SO_2F_2 resulting from the fit of microwave experimental data of Ref. [2] using (i) the Watsonian in *S*-reduction [23] and (ii) the tensorial Hamiltonian with the equivalent (65) of the *S*-reduction as well as the parameter translation formulas (25)–(43). Both models were limited to degree 6. The agreement is quite good, considering that the formulas are truncated developments. We also give the values of the rotational and centrifugal distorsion constants obtained through ab initio calculations as described above.

7.3. Coriolis interactions

Using the ab initio values of the Coriolis parameters for the bending triad given in Ref. [15], we obtain thanks to Eqs. (71)–(73):

$$\tilde{t}^{1(1,F_1,a_2)F_1}_{\{4\}\{4\}} \simeq 0.03429\ \mathrm{cm}^{-1}, \quad (95)$$

$$\tilde{t}^{1(1,F_1,b_1)F_1}_{\{4\}\{4\}} \simeq 0.07067\ \mathrm{cm}^{-1}, \quad (96)$$

$$\tilde{t}^{1(1,F_1,b_2)F_1}_{\{4\}\{4\}} \simeq 0.10912\ \mathrm{cm}^{-1}. \quad (97)$$

8. Conclusion

We have established a detailed correspondence between tensorial and Watson's formalisms in the case of an XY_2Z_2 quasi-spherical top molecules with C_{2v} symmetry. We have presented some numerical applications as well as some ab initio calculations in the case of SO_2F_2. In a future paper, we will give a detailed application of this in the case of the analysis of the $\nu_3/\nu_7/\nu_9$ bending triad of this molecule.

The same kind of procedures that we have used here to establish the correspondences can be applied in a similar way for other types of molecules for which a tensorial approach also exists. This is for instance the case of the $O(3)\supset D_{2\,h}$ formalism adapted to X_2Y_4 molecules with $D_{2\,h}$ symmetry like ethylene (C_2H_4) [24,25].

Acknowledgements

Support from the Région Bourgogne for the computer equipment of the Laboratoire de Physique de l'Université de Bourgogne is gratefully acknowledged. We also wish to thank to SpecMo network of the CNRS.

References

[1] M. Rotger, V. Boudon, M. Loëte, J. Mol. Spectrosc. 216 (2002) 297–307.

[2] M. Rotger, V. Boudon, M. Loëte, L. Margulès, J. Demaison, H. Mäder, G. Winnewisser, H.S.P. Müller, J. Mol. Spectrosc. 222 (2003) 172–179.
[3] C. Wenger, M. Rotger, V. Boudon, J. Quant. Spectrosc. Radiat. Transf. 93 (2005) 429–446.
[4] D. Papoušek, M. Aliev, Molecular Vibrational-Rotational Spectra, Elsevier, New York, 1982.
[5] J.-P. Champion, M. Loëte, G. Pierre, Spherical top spectra in: K.N. Rao, A. Weber (Eds.), Spectroscopy of the Earth's Atmosphere and Interstellar Medium, Academic Press, San Diego, 1992, pp. 339–422.
[6] V. Boudon, J.-P. Champion, T. Gabard, M. Loëte, F. Michelot, G. Pierre, M. Rotger, C. Wenger, M. Rey, J. Mol. Spectrosc. 228 (2004) 620–634.
[7] M. Rey, V. Boudon, C. Wenger, G. Pierre, B. Sartakov, J. Mol. Spectrosc. 219 (2003) 313–325.
[8] J. Moret-Bailly, Cah. Phys. 15 (1961) 237–316.
[9] J. Moret-Bailly, J. Mol. Spectrosc. 15 (3) (1965) 344–354.
[10] B.I. Zhilinskii, Opt. Spectrosc. 51 (3) (1981) 262–263.
[11] H.A. Buckmaster, R. Chatterjee, Y.H. Shing, Phys. Stat. Sol. A 13 (9) (1972) 9–50.
[12] http://www.maplesoft.com.
[13] J.K.G. Watson, Aspects of quartic and sextic centrifugal effects on rotational energy levels in: J. Durig (Ed.), Vibrational Spetra and Structure vol. 6 (1977), pp. 1–89.
[14] K. Sarka, J. Demaison, L. Margulès, I. Merke, N. Heineking, H. Bürger, H. Rulland, J. Mol. Spectrosc. 200 (2000) 55–64.
[15] H. Bürger, J. Demaison, F. Hegelund, L. Margulès, I. Merke, J. Mol. Struct. 612 (2002) 133–141.
[16] J. Moret-Bailly, Cah. Phys. 112 (1959) 476–494.
[17] M.J. Frisch, G.W. Trucks, H.B. Schlegel, G.E. Scuseria, M.A. Robb, J.R. Cheeseman, V.G. Zakrzewski, J.A. Montgomery, R.E. Stratmann, J.C. Burant, S. Dapprich, J.M. Millam, A.D. Daniels, K.N. Kudin, M.C. Strain, O. Farkas, J. Tomasi, V. Barone, M. Cossi, R. Cammi, B. Mennucci, C. Pomelli, C. Adamo, S. Clifford, J. Ochterski, G.A. Petersson, P.Y. Ayala, Q. Cui, K. Morokuma, D.K. Malick, A.D. Rabuck, K. Raghavachari, J.B. Foresman, J. Cioslowski, J.V. Ortiz, B.B. Stefanov, G. Liu, A. Liashenko, P. Piskorz, I. Komaromi, R. Gomperts, R.L. Martin, D.J. Fox, T. Keith, M.A. Al-Laham, C.Y. Peng, A. Nanayakkara, C. Gonzalez, M. Challacombe, P.M.W. Gill, B.G. Johnson, W. Chen, M.W. Wong, J.L. Andres, M. Head-Gordon, E.S. Replogle, J.A. Pople, Gaussian 98 (Revision A.1), Gaussian, Inc., Pittsburgh PA (1998).
[18] A.D. Becke, J. Chem. Phys. 98 (1993) 5648–5652.
[19] M.W. Won, Chem. Phys. Lett. 256 (1996) 391–399.
[20] D.E. Woon, T.H.D. Dunning Jr., J. Chem. Phys. 98 (1993) 1358–1371.
[21] K. Raghavachari, J.A. Pople, E.S. Replogle, M. Head-Gordon, J. Phys. Chem. 94 (1990) 5579–5586.
[22] J. Breidung, W. Thiel, Private communication (2000).
[23] J. Demaison, Private communication (2004).
[24] B. Sartakov, J. Oomens, J. Reuss, A. Fayt, J. Mol. Spectrosc. 185 (1997) 31–47.
[25] W. Raballand, M. Rotger, V. Boudon, M. Loëte, J. Mol. Spectrosc. 217 (2003) 239–248.

Available online at www.sciencedirect.com
SCIENCE DIRECT®
Journal of Molecular Spectroscopy 236 (2006) 248–254
Journal of MOLECULAR SPECTROSCOPY
www.elsevier.com/locate/jms

Ab initio anharmonic force field and equilibrium structure of vinyl bromide

N. Zvereva-Loëte [a,1], J. Demaison [a,*], H.D. Rudolph [b]

[a] Laboratoire de Physique des Lasers, Atomes, et Molécules, UMR CNRS 8523, Université de Lille I, F-59655 Villeneuve d'Ascq Cédex, France
[b] Department of Chemistry, University of Ulm, D-89069 Ulm, Germany

Received 4 January 2006; in revised form 3 February 2006
Available online 20 March 2006

Dedicated to Professor Reint Eujen on the occasion of his 60th birthday.

Abstract

The quadratic, cubic, and semi-diagonal quartic force field of vinyl bromide has been calculated at the MP2 level of theory employing a basis set of triple-ζ quality including a relativistic pseudopotential on bromine. A semi-experimental equilibrium structure has been derived from experimental ground state rotational constants and rovibrational interaction parameters calculated from the ab initio force field. This structure is in excellent agreement with the ab initio structure calculated at the CCSD(T) level of theory using a basis set of quadruple-ζ quality and an offset correction. The experimental mass-dependent r_m structures are also determined and their accuracy is discussed.

Keywords: Anharmonic force field; Ab initio; Equilibrium structure; Vinyl bromide; Microwave; Infrared

1. Introduction

Vinyl bromide or bromoethene, $H_2C{=}CHBr$, is a colorless gas which is used in manufacturing bromopolymers. It is mainly used as a flame retardant in acrylic fibers. It is a recognized carcinogen and liver toxicant.

Its low resolution infrared spectrum was recorded a long time ago [1] and all fundamental vibrations were assigned. The CH stretching was also studied in order to determine the lengths, force constants, and dissociation energies for the CH bonds [2]. The ν_6 band region near 1258 cm^{-1} was investigated under high resolution with a diode laser [3]. The r_z structure was determined by electron diffraction [4] but the derived parameters are not precise because the system of normal equations was very ill-conditioned.

The rotational spectrum was first assigned by Cornwell [5] and it was later extensively studied in Louvain-la-Neuve (see for instance [6,7]). In 1990, Hayashi et al. [8] measured the microwave spectra of 16 isotopologues and determined for each species two diagonal quartic centrifugal distortion and bromine quadrupole coupling constants. They also derived the substitution (r_s) structure. However, the *b*-coordinates of bromine and H_{trans} atoms are so small that the solutions of the Kraitchman equations are not reliable. Furthermore, it is known that the r_s structure is not always accurate, particularly when CH bonds are present [9]. Finally, it has to be noted that vinyl bromide pumped by CO_2 lasers produces some powerful submillimeter continuous emissions [10].

Coffey et al. [11] calculated an ab initio structure which was empirically corrected to obtain r_0 (effective) values. Although their calculations permit to compare the structures of the different vinyl halides, they are not accurate enough to estimate the equilibrium structure: the methods used do not fully take account of the electron correlation,

* Corresponding author. Fax: +33 3 20 33 70 20.
E-mail address: jean.demaison@univ-lille1.fr (J. Demaison).
[1] Present address: Institute of Atmospheric Optics 1, Akademicheskii Avenue, Tomsk 634055 Tomsk, Russia.

0022-2852/$ - see front matter © 2006 Elsevier Inc. All rights reserved.
doi:10.1016/j.jms.2006.02.003

the basis sets are too small, the core correlation and the relativistic effects are neglected.

However, ab initio calculations at the coupled cluster level of theory with a basis set of quadruple zeta quality can give reliable results provided the calculated structure is corrected by an offset derived from structurally similar molecules whose equilibrium structure is already accurately known [12]. It has also been found that the correlation consistent triple zeta valence basis set with the Stuttgart–Dresden–Bonn relativistic effective core potential (SDB-cc-pVTZ) [13] employing the second-order Møller–Plesset perturbation theory (MP2) [14] gives reliable results, particularly for the force field. In other words, the MP2/SDB-cc-pVTZ method can be used to calculate the rotation–vibration interaction constants, and thus, to determine the equilibrium rotational constants from the experimental ground state rotational constants. It is then possible to calculate an equilibrium structure called semi-experimental structure [15,16]. Finally, as shown in the case of vinyl chloride [17], the mass-dependent r_m methods [18] can deliver rather accurate results provided that the number and variety of isotopologues is large enough, which seems to be the case for vinyl bromide. In conclusion, three independent methods may be used to determine the equilibrium structure of vinyl bromide.

In the first part of this paper, the ab initio structure is calculated. In the second part, the ab initio anharmonic force field is given, its accuracy is assessed and the semi-experimental equilibrium structure is deduced. In the third part, the empirical r_m structures are calculated. Finally, in the last part, the different structures are compared between themselves and to those of other vinyl halides.

2. Ab initio structure

The structure has been calculated with the coupled cluster method with single and double excitations [19] augmented by a perturbational estimate of the connected triple excitations [CCSD(T)] [20]. The well known Dunning's correlation consistent polarized valence basis set, cc-pVQZ [21] was employed. The frozen core approximation (fc) was used in these calculations. All calculations were performed with the MOLPRO2000 [22,23] program. The results are reported in Table 1. The coupled cluster T_1 diagnostic [24] which is 0.0108 indicates that non-dynamical electron correlation is not important and that the CCSD(T) results should be reliable. The calculated bond lengths are not true equilibrium values because they are affected by a (mainly) systematic deviation, but it is possible to correct them using an empirical correction (offset) obtained from molecules whose equilibrium structure is assumed to be accurately known. For the C—H bond length, this is a good method because the corresponding offset is fairly constant [12]:

$$r[\mathrm{CCSD(T)/cc\text{-}pVQZ}] - r_e = 0.0015(2)\ \text{Å}$$

For the C=C bond length, the value of the offset was derived from ethylene and vinyl chloride [17], its value is 0.0029 Å. This value should be reliable too because the C=C bond length remains fairly constant. Finally, for the C—Br bond length, the offset was estimated to be 0.0096 Å using CH_3Br, BrCN, HC≡CBr, and FC≡CBr [12]. Of course, the large value of the offset indicates that it might be less accurate. The estimated equilibrium structure is given in Table 1.

3. Ab initio anharmonic force field and semi-experimental structure

The ab initio force field was calculated at the MP2 level of theory using the Gaussian 03 program [25]. The SDB-cc-pVTZ basis set [13,26] was used in the frozen core approximation. The molecular geometry was first calculated. Then, the force fields of the different isotopologues, were evaluated at this geometry up to semi-diagonal quartic terms.

The harmonic frequencies ω_i, anharmonic corrections $\omega_i - v_i$, and vibrational band centers v_i for $CH_2{=}CH^{79}Br$ are given in Table 2. The agreement between the calculated and the experimental vibrational frequencies v_i is rather good, the median of absolute deviations being only 13 cm^{-1} (1.25%). This is comparable, even slightly better, to the results found for vinyl chloride [17]. Likewise, the deviations are mainly systematic and the largest ones are for the CH bond stretches.

It is tempting to compare the ab initio and experimental rotation–vibration interactions constants (α-constants) but the latter ones are only known for two modes : $v_9 = 1$ [7] and $v_6 = 1$ [3], the latter one being furthermore perturbed. Thus, this comparison is not very meaningful, it is nevertheless made in Table 3. What can be said is that the results are of comparable quality to those found for vinyl chloride [17]. Actually, the equilibrium inertial defect is a much better indicator of the quality of the cubic force field. It will be discussed below.

The theoretical rotation–vibration interaction constants deduced from the ab initio force field were combined with the known experimental ground state rotational constants [8] to yield the semi-experimental equilibrium rotational constants of Table 4. We have only used the constants of [8] because mixing sets of rotational constants is a questionable practice: a small incompatibility of the sets would affect the accuracy of the structure determination whereas the error practically compensates if all lines are measured and analyzed in the same way. The equilibrium inertial defect, Δ_e, is also given in this table. It is about two orders of magnitude smaller than the ground state inertial defect, Δ_0, indicating that the equilibrium rotational constants are rather accurate. However, it is not exactly zero as it should be. This is probably mainly due to the limited accuracy of the computed rotation–vibration interaction constants. The equilibrium structure was calculated from a weighted least-squares fit of the semi-experimental moments of

Table 1
Structure of vinyl bromide (bond lengths in Å, bond angles in degrees)

Method	Basis	C_1═C_2	C_1—Br	C_1—H_g[a]	C_2—H_c[a]	C_2—H_t[a]	∠(CCBr)	∠(CCH_g)	∠(CCH_c)	∠(CCH_t)
r_z [4]		1.346(8)	1.880(7)	1.077(10)	1.090(15)	1.07(4)	122.8(3)	123.1(10)	120.4(7)	120(6)
r_s [8]		1.332(1)	1.884(1)	1.080(1)	1.088(1)	1.080(ass)	122.58(15)	123.67(15)	121.28(20)	119.47(25)
CCSD(T)[b]	VQZ	1.3295	1.8927	1.0797	1.0809	1.0822	122.78	124.06	122.12	119.26
MP2[c]	SDB-VTZ	1.3289	1.8786	1.0788	1.0791	1.0805	123.07	123.53	121.98	119.15
Estimate I[d]		1.3266	1.8831	1.0782	1.0794	1.0807	122.78	124.06	122.12	119.26
Semi-experimental		1.3256(3)	1.8835(2)	1.0780(1)	1.0794(1)	1.0804(3)	122.62(1)	124.34(3)	122.03(2)	119.28(4)
r_e vinyl chloride [17]		1.3262(3)		1.0783(1)	1.0796(1)	1.0796(2)	122.75(1)	123.91(1)[e]	121.77(2)	119.28(2)

[a] g, geminal; c, *cis* to chlorine; t, *trans* to chlorine.
[b] Frozen core approximation.
[c] The ab initio force field refers to this geometry.
[d] CCSD(T)/cc-pVQZ—offset correction (for the bond lengths), see text.
[e] ∠(CCCl).

Table 2
Harmonic frequencies ω_i, anharmonic corrections $\omega_i - v_i$, and vibrational band centers v_i for CH_2═$CH^{79}Br$ (in cm^{-1}) calculated at the MP2/SDB-cc-pVTZ level of theory, see text

Mode	Description	ω_i	$\omega_i - v_i$	v_i (calc.)	v_i (obs.)[a]	o − c[b]
$\nu_1(a')$	CH stretch	3298.0	139.8	3158.2	3112	−46
$\nu_2(a')$	CH2 antisym. stretch	3251.3	140.2	3111.1	3087	−24
$\nu_3(a')$	CH2 sym. stretch	3192.2	129.6	3062.6	3027	−36
$\nu_4(a')$	C═C stretch	1649.1	42.0	1607.1	1602	−5
$\nu_5(a')$	CH2 bend	1414.9	34.8	1380.1	1373	−7
$\nu_6(a')$	CH rock.	1291.1	24.6	1266.5	1258	−8
$\nu_7(a')$	CH_2 rock	1024.9	15.6	1009.3	1005	−4
$\nu_8(a')$	CBr stretch	639.1	9.2	629.9	612	−18
$\nu_9(a')$	C═CBr def.	348.2	0.7	347.5	344	−3
$\nu_{10}(a'')$	CH wag.	990.1	23.4	966.8	941	−26
$\nu_{11}(a'')$	CH_2 wag.	921.9	20.1	901.8	901	−1
$\nu_{12}(a'')$	Twist	605.9	7.4	598.6	582	−17

[a] Ref. [1].
[b] Observed minus calculated vibrational frequency v_i.

Table 3
Experimental and ab initio rotation–vibration interaction constants (MHz) for vinyl chloride[a] and vinyl bromide

	$v_6 = 1$				$v_9 = 1$			
	CH_2═$CH^{35}Cl$		CH_2═$CH^{79}Br$		CH_2═$CH^{35}Cl$		CH_2═$CH^{79}Br$	
	obs.	calc.	obs.[b]	calc.	obs.	calc.	obs.[c]	calc.
α^B	−10.5	−13.4	−4.4	−6.7	2.6	0.5	2.5	1.6
α^C	0.3	−0.1	0.18	2.5	7.5	6.2	5.2	4.4

[a] Ref. [17].
[b] Ref. [3].
[c] Ref. [7].

inertia and is given in Table 1. It is in excellent agreement with the ab initio structure of the previous section.

The average value of the equilibrium inertial defect is $\bar{\Delta}_e = 0.001843$ uÅ^2. It will allow us to estimate the approximate error of the calculated atomic coordinates. If we let

$$\begin{aligned}\bar{\Delta}_e &= \overline{\mathrm{err}}(I_c - I_a - I_b)\\ &\approx [\overline{\mathrm{err}}(I_a)^2 + \overline{\mathrm{err}}(I_b)^2 + \overline{\mathrm{err}}(I_c)^2]^{1/2}\\ &\approx \sqrt{3}\cdot\overline{\mathrm{err}}(I)\end{aligned} \quad (1)$$

We then have approximately for the average error of the inertial moments,

$$\overline{\mathrm{err}}(I) = 0.00106 \text{ uÅ}^2 \quad (2)$$

An equally weighted structural fit of the 48 inertial moments with this error applied to all moments gives $\sigma = 0.899$, which is of magnitude unity and indicates that an essentially correct value of average error of the inertial moments has been used when choosing

Table 4
Semi-experimental equilibrium rotational constants (MHz) for vinyl bromide[a]

Species	A_e		B_e		C_e		Δ_e	Δ_0
	Obs.	o − c	Obs.	o − c	Obs.	o − c		
$H_2C{=}CH^{79}Br$	54677.52	−0.13	4181.39	−0.05	3884.40	−0.02	−0.0021	0.1172
$H_2{}^{13}C{=}CH^{79}Br$	54091.54	0. 01	4019.71	−0.00	3741.69	0.04	−0.0015	0.1179
$H_2C{=}{}^{13}CH^{79}Br$	53106.49	1.00	4132.75	0.02	3834.40	0.06	−0.0014	0.1206
$D_2C{=}CH^{79}Br$	45419.99	−0.33	3733.20	0.00	3449.69	0.03	−0.0014	0.1214
$HD_cC{=}CH^{79}Br$	45505.28	−0.75	4037.55	−0.03	3708.54	−0.01	−0.0011	0.1277
$HD_tC{=}CH^{79}Br$	54659.52	−0.05	3851.70	−0.04	3598.19	−0.00	−0.0013	0.1123
$H_2C{=}CD^{79}Br$	42980.04	−0.78	4122.40	−0.07	3761.71	0.04	−0.0035	0.1267
$D_2C{=}CD^{79}Br$	36692.23	1.89	3691.96	−0.01	3354.48	0.05	−0.0020	0.1309
								0.0000
$H_2C{=}CH^{81}Br$	54663.85	−0.18	4156.95	−0.04	3863.23	0.02	−0.0019	0.1170
$H_2{}^{13}C{=}CH^{81}Br$	54077.62	0.01	3995.54	0.00	3720.68	0.04	−0.0015	0.1179
$H_2C{=}{}^{13}CH^{81}Br$	53092.37	0.91	4107.95	0.01	3812.98	0.06	−0.0016	0.1205
$D_2C{=}CH^{81}Br$	45409.74	−0.42	3710.43	−0.00	3430.19	0.03	−0.0014	0.1215
$HD_cC{=}H^{81}Br$	45493.98	−1.22	4013.31	−0.05	3688.01	−0.01	−0.0015	0.1274
$HD_tC = CH^{81}Br$	54646.12	−0.17	3828.81	−0.05	3578.15	0.00	−0.0016	0.1120
$H_2C = CD^{81}Br$	42968.31	−2.27	4097.61	−0.06	3740.97	0.04	−0.0038	0.1266
$D_2C = CD^{81}Br$	36683.97	2.00	3668.87	−0.01	3335.33	0.05	−0.0016	0.1311

[a] o − c, residuals of rotational constants from weighted least squares-fit of semi-experimental equilibrium moments of inertia to yield the structural parameters of Table 1, last row.

$\overline{\text{err}}(\text{I}) = 0.0011$ uÅ^2 for the fit. In the principal axis system (PAS), the inertial moment is e.g.,

$$I_a = \sum_i m_i(b_i^2 + c_i^2) \tag{3}$$

In a non-PAS (which is sufficiently parallel to the PAS) we have

$$I_a = \sum_i m_i[(b_i - b_{\text{com}})^2 + (c_i - c_{\text{com}})^2] \tag{4}$$

where com = center of mass.

Had we instead used Eq. (3) which is incorrect in this non-PAS system

$$I'_a = \sum_i m_i(b_i^2 + c_i^2) \tag{5}$$

the error is

$$\begin{aligned}\overline{\text{err}}(I_a) &= I_a - I'_a \\ &= \sum_i m_i[-2b_i b_{\text{com}} + b_{\text{com}}^2 - 2c_i c_{\text{com}} + c_{\text{com}}^2]\end{aligned} \tag{6}$$

Since

$$\sum_i m_i b_i = M b_{\text{com}} \tag{7}$$

likewise for c_i where M is the molecular mass, we have

$$\overline{\text{err}}(I_a) = M(b_{\text{com}}^2 + c_{\text{com}}^2) \tag{8}$$

If we identify $\overline{\text{err}}(I_a)$ with $\overline{\text{err}}(I)$ and b_{com} as well as c_{com} with the average coordinate error, $\overline{\text{err}}(\text{coord})$, we obtain

$$\overline{\text{err}}(\text{coord}) = \sqrt{\overline{\text{err}}(I)/2M} \tag{9}$$

with $M = 106$ u for vinyl bromide and $\overline{\text{err}}(I) = 0.00106$ uÅ^2, we have at last, though very approximately

$$\overline{\text{err}}(\text{coord}) \approx 0.002 \text{ Å} \tag{10}$$

This value is in agreement with our previous experience and is a better estimator of the error than the standard deviations obtained from the least squares fit, which is usually much too small.

4. Experimental structures

For the "effective" r_0-structure and the more recent r_m-structure models which include approximate mass-dependent rovibrational contributions, the experimental ground state rotational constants of 16 isotopologues listed in [8] were used as input to a program for iterated, weighted and correlated least-squares fitting the 3×16 inertial moments to obtain the nine independent structural parameters of the planar molecule plus up to six optional rovibrational parameters (program Ru211a, author H.D. Rudolph, unpublished). Besides the mass-dependent models [18] $r_m^{(1)}$ and $r_m^{(2)}$ also the $r_m^{(1L)}$ and $r_m^{(2L)}$ models have been applied which include an additional "Laurie-correction" for $H \rightarrow D$ substitution. While the r_0 and all r_m fitting methods operate as stated above (which requires that *all* independent structural parameters must either be fitted or constrained to given or assumed values), the r_s-*fit* model [27] is a true derivate of Kraitchman's original equations (which permit the location of individual substituted positions) and in its *fit*-extension allows the inclusion of multiply substituted species, eventually using least-squares fitting. Also typical for a structure based on Kraitchman's equations, the center-of-mass conditions are not inherent but can be introduced as additional conditions.

The least-squares program sections use true derivatives for all elements of the coefficient or design matrix ∂(inertial

moment)/∂(parameter), recalculated in each iteration cycle, instead of difference quotients. This obviates the necessity of choosing adequate step widths and allows the iterations to continue till the parameter changes from cycle to cycle are no larger than the truncation error of the arithmetic used.

After initial fits with weights derived from the experimental errors of the rotational constants, the residuals of the rotational constants were generally found to be significantly larger than the experimental errors themselves (obviously due to shortcomings of the model). Instead of simply switching to unity-weighting which is often recommended in such cases, we have tried to take notice of the fact that the relative experimental errors of the rotational constants A, B, and C are primarily a consequence of the transition types that could be observed in the investigation. The relation of the errors may influence the result in a way that should be retained. Therefore, we have used for *all* experimental models and also for the semi-experimental equilibrium model the uncorrelated average experimental errors of [8], (in MHz) $\overline{\mathrm{err}}(A) = 0.311$, $\overline{\mathrm{err}}(B) = 0.018$, $\overline{\mathrm{err}}(C) = 0.018$ as the basis for computing the weights. Vinyl bromide being a near-prolate rotator ($\kappa = -0.988$), $\overline{\mathrm{err}}(A)$ is by far the largest error. The (dimensionless) standard deviation of the fit σ represents the factor by which the errors $\overline{\mathrm{err}}$ are effectively increased by the imperfections of the model before the standard errors of the structure parameters are computed by the program. In Table 5, we have collected the results of relevant calculations in terms of bonding and rovib parameters and in Table 6 in terms of the principal axis coordinates of the parent molecule $H_2C{=}CH^{79}Br$. We have listed only those structures that deserve further discussion.

Comparing the "effective" r_0-structure with the simplest of the mass-dependent models, $r_m^{(1)}$, the great progress achieved by the introduction of only three additional rovib-parameters c_a, c_b, c_c [18, Eq. 31] for the entire set of isotopologues, is demonstrated by the sharp decrease of σ; the smaller standard errors of the parameters and their greater nearness to the quantum-chemically obtained values. However, the three parameters r(C_1, Br), c_a, c_b are found to be rather highly correlated which is revealed also by the respective variance-decomposition proportions (not shown), and results in somewhat higher errors of these parameters. Nonetheless, the structural parameters are sufficiently well defined. Eventually, the $r_m^{(1)}$ model was disclosed as the experimental model that is to be preferred over other purely experimental methods.

The $r_m^{(1L)}$ model corrects for the bond shortening upon $H \rightarrow D$ substitution by defining different "effective" bond lengths [18] $r^{eff}(H) = r_m + \delta_H \cdot \mu(H)$ and $r^{eff}(D) = r_m + \delta_H \cdot \mu(D)$, respectively, with mass-dependent factors $\mu(H)$ and $\mu(D)$ and with parameters r_m and δ_H to be adjusted by the least-squares fit. In principle, the pair of parameters

Table 5
Structure of vinyl bromide by experimental methods (bond lengths in Å, bond angles in degrees)

Model	r_0	$r_m^{(1)}$	$r_m^{(1L)}$	$r_m^{(2)}$	r_s-fit + com	Semi-exp.[a]	Ab initio[b]
Number observ.	48	48	48	48	33	48	CCSD(T)/cc-pVQZ-offset
Deg. freedom	39	36	35	33	21	39	
Std. dev. fit σ	87.07	7.065	5.957	6.768	5.355	2.796	
$r(C_1,C_2)$	1.3306(81)	1.3275(8)	1.3289(8)	1.3277(9)	1.3301(21)	1.3256(3)	1.3266
$r(C_1,Br)$	1.8891(66)	1.8817(14)	1.8833(13)	1.8817(15)	1.8854(11)	1.8835(2)	1.8831
$r(C_1,H_g$[c])	1.0777(22)	1.0775(2)	1.0733(11)[d]	1.0767(5)	1.0793(18)	1.0780(1)	1.0782
$r(C_2,H_c$[c])	1.0856(33)	1.0850(3)	1.0810(10)[d]	1.0856(6)	1.0888(17)	1.0794(1)	1.0794
$r(C_2,H_t$[c])	1.0831(85)	1.0815(8)	1.0746(19)[d]	1.0796(16)	1.0791(31)	1.0804(3)	1.0807
$\angle C_2,C_1,Br$	122.52(24)	122.73(5)	122.69(4)	122.76(5)	122.62(16)	122.62(1)	122.78
$\angle C_2,C_1,H_g$	124.16(85)	123.77(9)	123.89(8)	124.04(21)	123.85(12)	124.34(3)	124.06
$\angle C_1,C_2,H_c$	121.29(62)	121.21(6)	121.20(5)	120.98(15)	121.26(11)	122.03(2)	122.12
$\angle C_1,C_2,H_t$	118.74(99)	119.20(11)	119.21(10)	119.19(16)	119.59(50)	119.28(3)	119.26
δ_H[d]			0.0161(41)				
r.m.s. diff. (r)	0.0041	0.0026	(0.0016)[e]	0.0030	0.0053	0.0005	
r.m.s. diff. ($\angle$)	0.51	0.16	0.47	0.57	0.46	0.17	
$c(a)$[f]		0.025(4)	−0.005(8)	0.027(4)			
$c(b)$		0.050(11)	0.031(11)	0.032(15)			
$c(c)$		0.066(11)	0.038(12)	0.041(16)			
$d(a)$				−0.001(4)			
$d(b)$				0.129(94)			
$d(c)$				0.180(100)			

[a] Structure from semi-experimental rotational constants, see last but one row of Table 1.
[b] For comparison: quantum chemical structure, see estimate *I* of Table 1.
[c] g, geminal; c, *cis* to chlorine; t, *trans* to chlorine.
[d] For model $r_m^{(1L)}$ the hydrogen bond lengths in this table are the values r_m in $r^{eff} = r_m + \delta_H \cdot \mu$, [18] Eq. (31).
[e] Excluding the r(C,H) bond lengths = r_m, see Footnote d.
[f] Rovib parameters c and d, [18] Eq. (31).

Table 6
Principal axis coordinates (in Å) of experimental and quantum-chemical structures of vinyl bromide

Model		r_0	$r_m^{(1)}$	$r_m^{(1L)}$	$r_m^{(2)}$	r_s − fit + com	Semi-exp.[a]	Ab initio[b]
C_1	*a*	−1.1992(63)	−1.1940(11)	−1.1948(10)	−1.1940(11)	−1.1961(8)	−1.1955(2)	−1.1950
	b	0.5302(11)	0.5274(5)	0.5282(4)	0.5273(5)	0.5297(18)	0.5280(0)	0.5270
C_2	*a*	−2.2170(40)	−2.2123(11)	−2.2138(10)	−2.2129(11)	−2.2156(4)	−2.2109(1)	−2.2131
	b	−0.3269(18)	−0.3243(4)	−0.3249(3)	−0.3240(4)	−0.3247(16)	−0.3243(1)	−0.3235
Br	*a*	0.6036(3)	0.6020(7)	0.6025(3)	0.6019(4)	0.6029(2)	0.6021(0)	0.6024
	b	−0.0343(3)	−0.0342(0)	−0.0343(0)	−0.0343(1)	−0.0344(10)	−0.0344(0)	−0.0344
H_g[c]	*a*	−1.3107(85)	−1.3093(9)	−1.3097(8)[d]	−1.3035(40)	−1.3111(6)	−1.3020(3)	−1.3043
	b	1.6021(19)	1.5987(5)	1.6115(33)[d]	1.5984(5)	1.6029(5)	1.6008(1)	1.5997
H_c[c]	*a*	−2.0507(55)	−2.0481(9)	−2.0471(8) [d]	−2.0449(26)	−2.0507(4)	−2.0610(2)	−2.0673
	b	−1.3997(24)	−1.3968(5)	−1.4093(32)[d]	−1.3965(5)	−1.4010(6)	−1.3932(1)	−1.3930
H_t[c]	*a*	−3.2271(36)	−3.2227(9)	−3.2331(27)[d]	−3.2213(14)	−3.2267(2)	−3.2215(1)	−3.2230
	b	0.0641(175)	0.0613(16)	0.0635(15)[d]	0.0617(27)	0.0522(77)	0.0579(6)	0.0613

For footnotes see Table 5.

Note that the coordinates b(Br) and $b(H_t)$ are below the limit(conventionally taken as ≈0.15 Å) below which a reliable coordinate value is believed to be no longer determinable from experimental inertial moments. However, this limit depends on the atomic mass involved: for the different methods displayed in the Table, the large scatter of the coordinate values $b(H_t)$ and their formal(i.e., by the lsq treatment generated) errors is clearly visible, whereas b(Br) is practically constant over the width of the Table.

r_m and δ_H must be allowed to be different for any of the three different hydrogen positions g, c, and t. However, we had to restrict the fit to three different r_m but one common δ_H to avoid convergence to irrational results due to extremely high correlations. The results have been collected in Table 7. A check showed that for any of the hydrogen positions c and t the bond lengths r^{eff}(H) and r^{eff}(D) are, within the number of digits given, independent of the presence of H or D in the neighboring position. Neither the effective bond lengths r^{eff} nor the r_m for the three different hydrogen positions can be directly compared with the equilibrium bond lengths r_e of the ab initio estimate of Table 1 and Table 5. They have hence been skipped when calculating the r.m.s. bond length differences (as a sort of quality indicator) between the values in the particular column, here $r_m^{(1L)}$, and the column with the quantum chemical results of Table 5. The value $\delta_H = 0.0161(41)$ u$^{1/2}$Å is not much larger than 0.010 u$^{1/2}$Å, the value expected (in rather wide limits) in [18]. The "Laurie correction" $r^{eff}(H) - r^{eff}(D) = 0.0047(24)$ Å is not far from the conventionally assumed value 0.003 Å. However, since a reliable relation between r^{eff}, r_m, and r_e has not yet been established, and also from a comparison with the ab initio equilibrium values, the present $r_m^{(1L)}$ structure is hardly an improvement over the $r_m^{(1)}$ structure.

Table 7
Vinyl bromide, hydrogen bond lengths of model $r_m^{(1L)}$. Three separately fitted values r_m for model $r_m^{(1L)}$ in Tables 5 and 6 for positions g, c, and t, but one *common* δ_H fitted to enable a realistic lsq convergence

Lengths in Å	Hydrogen positions		
	g	c	t
r_m	1.0733(11)	1.0810(10)	1.0746(19)
δ_H		0.0161(41)	
r_m^{eff}(H)	1.0894(30)	1.0971(31)	1.0908(24)
r_m^{eff}(D)	1.0848(18)	1.0925(19)	1.0861(14)
diff. H—D	0.0047(25)	0.0047(26)	0.0047(20)

The $r_m^{(2)}$ model adds three further rovib parameters d_a, d_b, and d_c for the approximate reproduction of the rovib contributions. However, the resulting structure and rovib parameters parameter have larger errors, and neither the standard deviation of the fit σ nor the r.m.s. deviations from the ab initio equilibrium values indicate any significant improvement over the $r_m^{(1)}$ structure.

We have also checked but not listed in Table 5 the results for the $r_m^{(2L)}$ model. The errors are larger than for the $r_m^{(1L)}$ model. The Laurie parameter $\delta_H = 0.0329(48)$ u$^{1/2}$Å is more than three times larger than the generally accepted value and hence hardly credible.

The standard deviation σ of a r_s-*fit* model cannot compared with that of a r_0 or r_m model owing to the very different statement of the least-squares problem. Also, for a planar molecule the formal number of observations is smaller, since for any isotopologue only two data, the planar inertial moments P_a and P_b are used as input. Table 5 displays only the results of the application of the r_s-*fit*+com model, where the three non-trivial center-of-mass conditions have been used as constraints, the first com-moments for *a* and *b* and the second com-moment for (*a*,*b*). This expedient results only in minute changes of the structure parameters but reduces for many of them the errors. However, Table 5 shows that the r_s-*fit* model deserves no preference over the r_m models.

Table 6 makes evident the same, yet unexplained feature which had already been observed in the earlier study on vinyl chloride [17]: the (negative) principal-axis-coordinate $a(H_c)$ is in *all* experimental determinations by up to 0.02 Å larger than the ab initio estimate (and the semi-experimental equilibrium value). Both, $a(H_c)$ and $b(H_c)$ are large coordinates, the small-coordinate argument for lacking accuracy is hence not applicable. The discrepancy is transferred to the bond parameters $r(C_2,H_c)$ and $\angle(C_1,C_2,H_c)$ of Table 5. If, for the $r_m^{(1)}$ column in Table 5, $r(C_2,H_c)$ were

skipped when calculating the difference indicator r.m.s.diff(r) this value would reduce from 0.0026 to 0.0010 Å, which would represent a very good agreement between the purely experimental $r_m^{(1)}$-structure and the quantum-chemically obtained structure in Table 5.

5. Comparison of the different structures

McKean [2] was able to determine the isolated stretching frequencies of the three CH bonds which are (in cm^{-1}): $\nu(CH_t) = 3057.0 < \nu(CH_c) = 3074.1 < \nu(CH_g) = 3084.7$, the accuracy being about $\pm 3\ cm^{-1}$. These values give (in Å): $r(CH_t) = 1.0816 > r(CH_c)$ 1.0803 $> r(CH_g)$ 1.0796 [28]. They are in excellent agreement with the ab initio results and confirm their accuracy. For the other parameters, Table 5 shows that the $r_m^{(1)}$ structure is in good agreement with both the ab initio structure and the semi-experimental structure. The conclusion is that the derived structures are accurate, the semi-experimental structure being probably the most accurate one. It has been shown that the accuracy of the coordinates is about 0.002 Å. A reasonable estimate of the accuracy for the bond angles is 0.1°–0.2°.

The structure of vinyl chloride [17] is also reported at the bottom of Table 1. It is found extremely close to that of vinyl bromide. It has also to be noted that the r(C=C) bond length is significantly shorter in both vinyl chloride and vinyl bromide than in ethylene, r_eC=C) = 1.3307(3) Å [29]. On the other hand, the r_e(C—H_t) bond lengths are very close to the value of ethylene, r_e(C—H) = 1.0809(3) Å.

Acknowledgments

N.Z.L. thanks the University of Lille I for a fellowship and H.D.R. thanks the Fonds der Chemischen Industrie, Frankfurt/Main for support.

References

[1] C.W. Gullikson, J.R. Nielsen, J. Mol. Spectrosc. 1 (1957) 158–178.
[2] D.C. McKean, Spectrochim. Acta 31A (1975) 1167–1186.
[3] A.P. Charmet, P. Stoppa, A. Baldacci, S. Giorgianni, S. Ghersetti, J. Mol. Struct. 612 (2002) 213–221.
[4] P.A. Huisman, F.C. Mijlhoff, J. Mol. Struct. 57 (1979) 83–93.
[5] C.D. Cornwell, J. Chem. Phys. 18 (1950) 1118–1119.
[6] D. de Kerckhove Varent, Ann. Soc. Sci. Brux. 83 (1969) 120–144.
[7] J. Maroor, M. de Hemptinne, Bull. Acad. R. Belgium 58 (1972) 956–970.
[8] M. Hayashi, C. Ikeda, T. Inagusa, J. Mol. Spectrosc. 139 (1990) 299–312.
[9] J. Demaison, H.D. Rudolph, J. Mol. Spectrosc. 215 (2002) 78–84.
[10] A. Moretti, A. Bertolini, G. Carelli, M. Nannizzi, J.C.S. Moraes, IEEE J. Quantum Elect. 37 (2001) 489–493.
[11] D. Coffey, B.J. Smith, L. Radom, J. Chem. Phys. 98 (1993) 3952–3959.
[12] J. Demaison, L. Margulès, J.E. Boggs, Struct. Chem. 14 (2003) 159–174.
[13] J.M.L. Martin, A. Sundermann, J. Chem. Phys. 114 (2001) 3408–3420.
[14] C. Møller, M.S. Plesset, Phys. Rev. 46 (1934) 618–622.
[15] F. Pawłowski, P. Jørgensen, J. Olsen, F. Hegelund, T. Helgaker, J. Gauss, K.L. Bak, J.F. Stanton, J. Chem. Phys. 116 (2002) 6482–6496.
[16] P. Groner, R.D. Warren, J. Mol. Struct. 599 (2001) 323–335.
[17] J. Demaison, H. Møllendal, A. Perrin, J. Orphal, F. Kwabia Tchana, H.D. Rudolph, F. Willaert, J. Mol. Spectrosc. 232 (2005) 174–185.
[18] J.K.G. Watson, A. Roytburg, W. Ulrich, J. Mol. Spectrosc. 196 (1999) 102–129.
[19] G.D. Purvis III, R.J. Bartlett, J. Chem. Phys. 76 (1982) 1910–1918.
[20] K. Raghavachari, G.W. Trucks, J.A. Pople, M. Head-Gordon, Chem. Phys. Lett. 157 (1989) 479–483.
[21] T.H. Dunning Jr., J. Chem. Phys. 90 (1989) 1007–1023; A.K. Wilson, D.E. Woon, K.A. Peterson, T.H. Dunning Jr., J. Chem. Phys. 110 (1999) 7667–7676.
[22] MOLPRO 2000 is a package of ab initio programs written by H.-J. Werner and P.J. Knowles, with contributions from R.D. Amos, A. Bernhardsson, A. Berning, P. Celani, D.L. Cooper, M.J.O. Deegan, A.J. Dobbyn, F. Eckert, C. Hampel, G. Hetzer, T. Korona, R. Lindh, A.W. Lloyd, S.J. McNicholas, F.R. Manby, W. Meyer, M.E. Mura, A. Nicklass, P. Palmieri, R. Pitzer, G. Rauhut, M. Schütz, H. Stoll, A.J. Stone, R. Tarroni, and T. Thorsteinsson.
[23] P.J. Knowles, C. Hampel, H.-J. Werner, J. Chem. Phys. 112 (2000) 3106–3107.
[24] T.J. Lee, P.R. Taylor, Int. J. Quantum Chem. Symp. 23 (1989) 199–207.
[25] M.J. Frisch, G.W. Trucks, H.B. Schlegel, G.E. Scuseria, M.A. Robb, J.R. Cheeseman, J.A. Montgomery, Jr., T. Vreven, K.N. Kudin, J.C. Burant, J.M. Millam, S.S. Iyengar, J. Tomasi, V. Barone, B. Mennucci, M. Cossi, G. Scalmani, N. Rega, G.A. Petersson, H. Nakatsuji, M. Hada, M. Ehara, K. Toyota, R. Fukuda, J. Hasegawa, M. Ishida, T. Nakajima, Y. Honda, O. Kitao, H. Nakai, M. Klene, X. Li, J.E. Knox, H.P. Hratchian, J.B. Cross, C. Adamo, J. Jaramillo, R. Gomperts, R.E. Stratmann, O. Yazyev, A.J. Austin, R. Cammi, C. Pomelli, J.W. Ochterski, P.Y. Ayala, K. Morokuma, G.A. Voth, P. Salvador, J.J. Dannenberg, V.G. Zakrzewski, S. Dapprich, A.D. Daniels, M.C. Strain, O. Farkas, D.K. Malick, A.D. Rabuck, K. Raghavachari, J.B. Foresman, J.V. Ortiz, Q. Cui, A.G. Baboul, S. Clifford, J. Cioslowski, B.B. Stefanov, G. Liu, A. Liashenko, P. Piskorz, I. Komaromi, R.L. Martin, D.J. Fox, T. Keith, M.A. Al-Laham, C.Y. Peng, A. Nanayakkara, M. Challacombe, P.M.W. Gill, B. Johnson, W. Chen, M.W. Wong, C. Gonzalez, and J.A. Pople, Gaussian, Inc., Pittsburgh PA, 2003. Revision B.04.
[26] Basis sets were obtained from the Extensible Computational Chemistry Environment Basis Set Database, Version 02/25/04, as developed and distributed by the Molecular Science Computing Facility, Environmental and Molecular Sciences Laboratory which is part of the Pacific Northwest Laboratory, P.O. Box 999, Richland, Washington 99352, USA, and funded by the U.S. Department of Energy. The Pacific Northwest Laboratory is a multi-program laboratory operated by Battelle Memorial Institute for the U.S. Department of Energy under contract DE-AC06-76RLO 1830. Contact Karen Schuchardt for further information.
[27] V. Typke, J. Mol. Spectrosc. 69 (1978) 173–178.
[28] J. Demaison, G. Wlodarczak, Struct. Chem. 5 (1994) 57–66.
[29] J.M.L. Martin, P.R. Taylor, Chem. Phys. Lett. 248 (1996) 336–344.

Chapitre 5

Détection de molécules organiques d'intérêt atmosphérique en phase gazeuse

Publications : P6, P8, P9 *Proceedings : A1*

5.1 Introduction

La présence dans l'environnement de matières toxiques d'origine anthropique, telles que le trinitrotoluène (TNT), les aldéhydes, le benzopyrène, présente un danger écologique ; la détection de ces produits demande donc une attention particulière. Toutes les molécules citées présentent des difficultés particulières pour leur détection. Les aldéhydes se caractérisent par la superposition des spectres d'absorption, le TNT par une faible luminescence. Pour la molécule benzopyrène (BP), il y a un problème d'interférence chimique avec d'autres composés organiques, si bien que l'analyse des processus photophysiques dont elle est le siège est très importante. En conséquence, l'utilisation des méthodes traditionnelles de détection (absorption différentielle, fluorescence) est inadaptée ; il faut développer une approche spéciale adaptée à chacune des molécules. Le travail effectué se place dans le cadre de la mécanique quantique et inclut des éléments de physique statistique. Il comporte les étapes suivantes :

- étude des processus de photodissociation correspondant à l'excitation des états électroniques inférieurs des aldéhydes, du TNT et du benzopyrène, afin de détecter ces molécules en phase gazeuse ;
- analyse par la mécanique quantique des molécules ci-dessus permettant de développer une approche théorique en vue de leur détection par la méthode de photofragmentation.

5.2 Principaux résultats obtenus

L'étude des processus photophysiques de base de l'excitation des états électroniques des aldéhydes, du TNT et du benzopyrène a permis de déterminer les constantes de vitesse de photodissociation. La formule de l'approximation RRKM [46] a été appliquée :

$$K(E) = cL \left[\prod_{i=1}^{s} \nu_i \right] / \left[\prod_{i=1}^{s} \nu'_i \right] \left[\frac{E - \Delta S_1^{\neq}}{E} \right]^{s-1} \tag{5.1}$$

Les mécanismes de la photodissociation d'une molécule de trinitrotoluène (TNT) dans les états électroniques excités comporte la possibilité de séparation du groupe NO_2 et de l'oxygène O de la molécule par rayonnement infrarouge IR et par rayonnement ultraviolet UV.

Dans le cas des processus photophysiques présents dans le benzopyrène, il est montré que la solution la plus efficace au problème de diagnostic du 3,4-benzopyrène consiste à utiliser la spectroscopie de masse par laser pour réaliser une photoionisation sélective des molécules.

L'efficacité de la détection en phase gazeuse des molécules possédant le groupe commun chromophore, donc des spectres d'absorption superposés, ainsi que des molécules qui ont une faible luminescence, est déterminée par la possibilité de photofragmentation sous l'effet d'une irradiation de longueur d'onde donnée et par la détection de celle-ci par la méthode de fluorescence induite par laser. Les longueurs d'onde de l'irradiation UV permettant la détection de la photofragmentation ont été définies dans l'étude, ce qui constitue un résultat original.

Il faut noter pour finir que le travail sur les aldéhydes a fait le sujet de ma thèse de doctorat [47].

5.3 Articles-clés : P6, P9

658 Atmos. Oceanic Opt. /December 1994/ Vol.7, No. 9 V.Ya. Artyukhov et al.

FORMALDEHYDE AND ACETALDEHYDE PHOTODISSOCIATION IN THE EXCITED STATE S_2

V.Ya. Artyukhov, N.A. Zvereva, I.I. Ippolitov, and A.F. Terpugova

V.D. Kuznetsov Siberian Physicotechnical Institute
at the State University, Tomsk
Received April 1, 1994

The subject of this theoretical study was the low excited singlet state S_1 of formaldehyde and acetaldehyde and their radical dissociation. Investigation into the dissociation from the S_1 state was carried out using ab initio method. The activation barriers were determined for formaldehyde and acetaldehyde with correction made for energy of zeroth vibrations to be 66.9 *and* 56.5 kcal/mole *, respectively. The analysis of mechnisms of dissociation from S_1 and S_2 excited singlet states was done based on calculated constans of photodissociation and intercombination conversion rates as well as the pecular features of the potential surfaces of these aldehydes. A possibility of using the spectroscopy of photofragments for identification of the aldehydes in their mixtures was studied. Based on calculated constants of the dissociation rate K_d and Frank–Condon factors the signal of fluorescence* $CHO(^2\ddot{I}) \rightarrow CHO(^2A') + h\nu$ *was estimated as a function of the photolytic wavelength.*

INTRODUCTION

Aldehydes play an important role in photochemistry of atmospheric pollution. On the one hand, they are present in anthropogenic discharges into the atmosphere, on the other hand, they are products of a number of phototechnical reactions. The aldehyde photodissociation processes are the substantial source of radical and molecular products of disintegration. Formaldehyde H_2CO and acetaldehyde CH_3CHO being the simplest aldehydes occupy, from this viewpoint, the great attention of scientists.[1–3,16–17]

Authors of Ref. 1 have theoretically analyzed the process of formaldehyde dissociation on the potential surface S_0 in details. According to Ref. 1 the formaldehyde dissociation into molecular products follows the scheme

$$H_2CO\,(S_0) + h\nu \rightarrow H_2CO\,(S_1) \rightsquigarrow H_2CO^*\,(S_0) \rightarrow H_2 + CO\,. \qquad (1)$$

The process (1) proceeds through energy barrier on S_0 surface with the height founded to be $\Delta S_0^{\rceil} = 87$ kcal/mole (3.79 eV, 30 537 cm^{-1}). The energy of zeroth vibrations is included into presented value.

The experimental value of activation barrier $\Delta S_0^{\rceil} =$ $= (78 – 81)$ kcal/mole together with that calculated with allowance for zeroth vibrational energy $\Delta S_0^{\rceil} = 81.4$ kcal/mole, which are in good agreement with each other, are presented in Ref. 16.

The process of disintegration into radical products follows the scheme:

$$H_2CO\,(S_0) + h\nu \rightarrow H_2CO\,(S_1) \rightsquigarrow H_2CO^*(T_1) \rightarrow H + HCO\,(^2A_1) \qquad (2)$$

The height of barrier $\Delta T_1^{\rceil} = 96.7$ kcal/mole (4.21 eV, 33 942 cm^{-1}) for this reaction is presented in Ref. 1, where the possibility of radical dissociation from S_0 state without transient states formation (87.5 kcal/mole, 3.79 eV, 30 600 cm^{-1}) and intramolecular reconstruction into hydroxycarbene (89 kcal/mole, 3.85 eV, 31 000 cm^{-1}) is noted.

Reference 17 gives the experimental value of activation barrier $\Delta T_1^{\rceil} = (90 – 93)$ kcal/mole. The dissociative mechanism of formaldehyde triplet is considered in this paper. The rate of intercombination conversion was previously considered to be small in comparison with $S_1 \rightsquigarrow S_0$ relaxation (or radical course of reaction on S_0 surface) and, consequently, the T_1 mechanism was out of importance. The study[17] demonsrated that barrier for T_1 was the result of superposition of three electronic states, namely, $(n \rightarrow \pi^*)$, $(\pi \rightarrow \pi^*)$, and $[n(\sigma) \rightarrow \sigma^*]$. This superposition was described in terms of two- and three-dimentional triplet states. Changing molecular geometry leads to reduction of symmetry, causes interaction of three states, and gives rise to new superpositions of low triplet states.

The similar calculations for acetaldehyde CH_3CHO were performed in Ref. 2. The values were found $\Delta S_0^{\rceil} = 84.4$ kcal/mole (3.67 eV, 29 624 cm^{-1}) for the barrier of molecular dissociation into CH_4 and CO and $\Delta T_1^{\rceil} = 89.1$ kcal/mole (3.88 eV, 31 274 cm^{-1}) for that of radical dissociation into CH_3 and HCO ($^2A_1$).

1. ALDEHYDE PHOTODISSOCIATION AT EXCITED S_1 STATE

The estimations presented above allow the processes of disintegration of H_2CO and CH_3CHO at excited S_1 state to be forecasted. It should be noted that when zeroth vibrational state of S_1 (80.6 kcal/mole, 3.51 eV, 28 290 cm^{-1} for formaldehyde and 82.5 kcal/mole, 3.59 eV, 28 597 cm^{-1} for acetaldehyde) being excited, the disintegration is unlikely because for acetaldehyde the barrier for any one of the reaction schemes exceeds the value given above, and for formaldehyde $\Delta S_0^{\rceil} = (78 – 81)$ kcal/mole, $\Delta S_1 = 80.6$ kcal/mole, and $\Delta T_1^{\rceil}$ is greater than ΔS_1.

As upper vibrational levels are excited, the following processes are bound to start subsequently: disintegration into radicals from S_0 state, intramolecular reconstruction, and disintegration into radicals from T_1 state.

The existing experimental data[4–8] confirm this sequence as a whole. However, there is unambiguous evidence that the dissociation process can proceed rather effectively from the states with energies less than the barrier, i.e., due to tunneling.[4,6]

The processes discussed above proceed after original act, the optical excitation of one rovibronic level of S_1 state, and subsequent radiationless transfer of excitation energy into S_0 and T_1 states via the mechanisms of internal and intercombination conversion.

We attempted to evaluate the possibility of radiationless energy transfer for S_1 and T_1 electronic states using INDO/CL semiempirical theory.[14] The obtained values of intercombination conversion constants in molecular geometry changing at $S_0 \rightarrow T_1$ and $S_0 \rightarrow S_1$ transitions are as follows:

formaldehyde $K_{S_1T_1} = 2.2 \cdot 10^6$, $K_{S_1T_1^{\rceil}} = 6.5 \cdot 10^6$,

acetaldehyde $K_{S_1T_1} = 2.7 \cdot 10^8$, $K_{S_1T_1^{\rceil}} = 6.1 \cdot 10^8$.

These constants equal zero at equilibrium geometry S_0.

Because semiempirical approach is the base for these results, they cannot be considered as accurate enough. But they give the qualitative pattern of geometry effect on the spin-orbital interaction. It

is clear that the geometry change, or molecular symmetry reduction, leads to intercombination conversion constant increasing several orders of magnitude. Consequently, when exciting S_1 state, the dissociative mechanism on T_1 surface play an important part.

The reaction of radical disintegration seems to be preferential from the viewpoint of optical methods development for diagnostics of particular aldehydes in their mixture, because the formyl radical HCO ($^2A_1$) can be succesfully detected using method of laser–induced fluorescence.[8]

2. ALDEHYDE PHOTODISSOCIATION AT EXCITED S_2 STATE

The formyl radical formation in the first excited state of HCO ($^2\Pi$) allows the passive detection of fluorescence followed by radiative disintegration of this state. According to Refs. 1 and 2 the energy of products of radical disintegration H(^2S) + HCO($^2\Pi$) is 113.5 kcal/mole (4.93 eV, 39 838 cm^{-1}) for formaldehyde and 102 kcal/mole (4.43 eV, 35 801 cm^{-1}) for acetaldehyde $CH_3(^2A''_2)$ + HCO($^2\Pi$).

Using these values as the base, the barriers for the reactions with HCO($^2\Pi$) should be searched for on the S_1 surfaces. We calculated the sections of potential surfaces $H_2CO(S_1)$ and $CH_3CHO(S_1)$ along the reaction coordinate, the bond lengths $R_{C–H}$ for formaldehyde and $R_{C–C}$ for acetaldehyde were chosen as those. The calculations were carried out using MONSTERGAUSS program with 6–31G* basis, which describes the peculiarities of potential surfaces adequately. Fragment optimization was not carried out when $R_{C–H}$ and $R_{C–C}$ varying. Figures 1 and 2 show the curves obtained in such a way for H_2CO and CH_3CHO, respectively. As seen from these figures there exist transient states at $R_{C–H}$ = 1.8Ð for formaldehyde and $R_{C–C}$ = 2.2Ð for acetaldehyde. The height of activation barrier $\Delta S_1^{\neq}$ for H_2CO is 71 kcal/mole without regard for zeroth vibrations and 66.9 kcal/mole with regard to zeroth vibrations. For CH_3CHO these values are 65.5 kcal/mole and 56.5 kcal/mole, respectively. The numerical results given above are presented in Figs. 3 (H_2CO) and 4(CH_3CHO) in diagram form. As seen from diagrams, at excitation of S_1 state and subsequent $S_2 \rightsquigarrow S_1$ conversion, the disintegration channel with formation of CHO($^2\Pi$) and subsequent reaction of radiative disintegration is energetically allowed

$$\mathrm{CHO}\ (^2\Pi) \rightarrow \tilde{\mathrm{N}}\mathrm{IO}\ (^2A') + h\nu\ . \qquad (3)$$

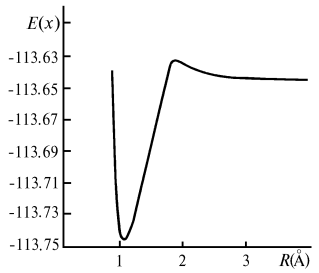

FIG. 1. Formaldehyde potential function in S_1 electronic state when stretching the C–H bond

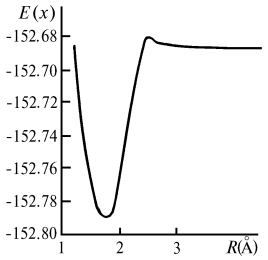

FIG. 2. Acetaldehyde potential function in S_1 electronic state when stretching the C–C bond

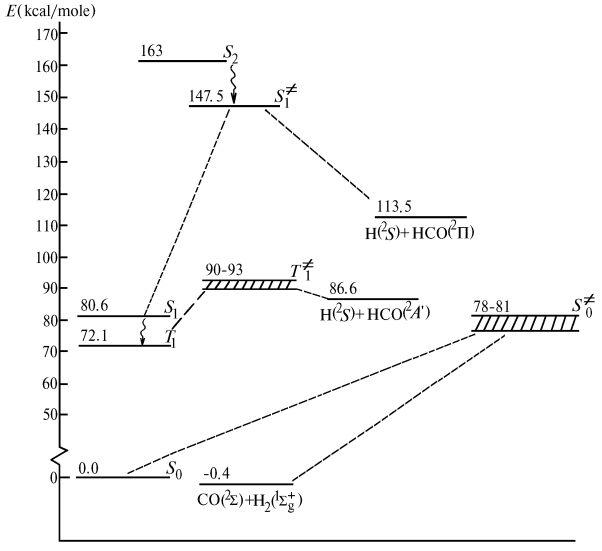

FIG. 3. Diagram of formaldehyde energy levels and dissociation barriers

660 Atmos. Oceanic Opt. /December 1994/ Vol. 7, No. 9 V.Ya. Artyukhov et al.

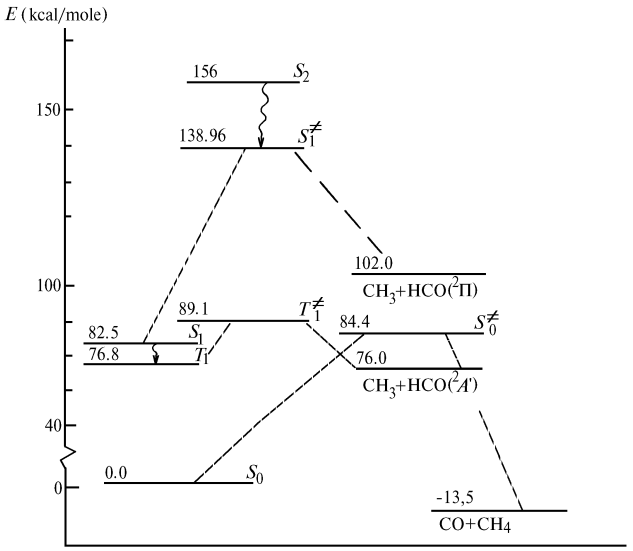

FIG. 4. Diagram of acetaldehyde energy levels and dissociation barriers

Let us consider now the situation, when the admixtures of formaldehyde and acetaldehyde to be detected are in analyzed gaseous mixture. Let us take into account the circuimstance: the S_2 state of formaldehyde lies somewhat above S_2 state of acetaldehyde (163 kcal/mole and 156 kcal/mole, see Ref. 9). Then the excitation of zeroth vibrational level of acetaldehyde ($\lambda \mid 182$ nm) and subsequent internal conversion $S_2 \rightsquigarrow S_1$ can lead to formation of overexcited with respect to barrier $\Delta S_1^{\rceil}$ molecules and their subsequent dissociation via the channel with radicals $HCO(^2\Pi)$ formation. The latter can undergo the radiative disintegration following the reaction (3), and the fluorescence signal can be detected on frequency ν'. In this case the formaldehyde molecules will be excited due to transitions into upper vibrational levels of S_1 state. However, the probability of such transitions is small in accordance with Frank–Condon principle. If the photolytic wavelength decreases to $\lambda \cong 175$ nm, then the new process starts, the excitation of S_2 state of formaldehyde. In doing so the detected signal at frequency ν' should abruptly increase. The degree of this increase can be evaluated by calculation of dissociation rate for H_2CO and CH_3CHO in the frame of semiclassical approximation of RRKM theory[10]

$$K(E) = c\,\mathrm{L}\left(\prod_{i=1}^{s}\nu_i\right)\Big/\left(\prod_{i=1}^{s}\nu_i'\right)\left(\frac{E-\Delta S_1^{\rceil}}{E}\right)^{s-1}, \qquad (4)$$

where ν_i and ν_i' are the vibrational frequencies of a molecule and activated complex in the S_1 state; E is the excitation energy counted off from zeroth vibrational level of S_1 state; s is the number of vibrational degrees of freedom; and, c is the speed of light. The data on vibrational frequencies were borrowed from Ref. 1 for H_2CO and from Ref. 11 for CH_3CHO when calculating. The obtained results for $K(E)$ are presented in Fig. 5. Let us denote the rates of radiative excitation of S_2 state as W^{f} and W^{a} for formaldehyde and acetaldehyde, respectively, and the rates of disintegration of S_2 state with formation of CHO ($^2\Pi$) as K^{f} and K^{a}. Now the degree of change of fluorescent signal at frequency ν' is proportional to the ratio

$$\frac{W^{\mathrm{a}}(175)\,K^{\mathrm{a}}(175) + W^{\mathrm{f}}(175)\,K^{\mathrm{f}}(175)}{W^{\mathrm{a}}(182)\,K^{\mathrm{a}}(182) + W^{\mathrm{f}}(182)\,K^{\mathrm{f}}(182)}. \qquad (5)$$

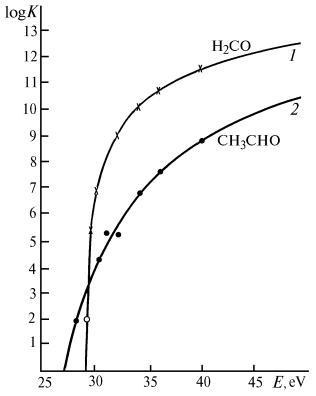

FIG. 5. Constant of photodissociation RCOH + hν → R + COH rate vs. excitation energy for formaldehyde (1) and acetaldehyde (2)

Then, as follows from Figs. 3, 4, and 5

$K^{\mathrm{a}}(175) \sim 5\cdot10^{7}\ \mathrm{s}^{-1}$, $K^{\mathrm{f}}(175) \sim 5\cdot10^{10}\ \mathrm{s}^{-1}$,
$K^{\mathrm{a}}(182) \sim 10^{6}\ \mathrm{s}^{-1}$, $K^{\mathrm{f}}(182) \sim 10^{9}\ \mathrm{s}^{-1}$.

The rate of radiative transition between two rovibronic states is known to be proportional to Frank–Condon factor F. To evaluate the latter one, we use the approximate equation:[12]

$$F_{0 \to n} = | < 0 | n > |^2 = y^n (n!)^{-1} \exp(-y), \quad (6)$$

where n is the number of vibrational levels at upper electronic state; $y = \mu\omega\Delta^2/2\hbar$; ω is vibrational frequency of oscillator; μ is reduced mass; and, $\Delta = R_0 - R_0'$ is the change of equilibrium position 0–0 of transition between S_0 and S_2 states of acetaldehyde (λ = 182 nm). The value of Δ (change of length of C–C bond at transition) is only 0.024 a.u. (see Ref. 13), consequently $F^{a}_{0\to0}(182) \approx 1$.

For formaldehyde this wavelength falls into region of excited vibrational levels of S_1 state. For antisymmetric vibrations of C–H bonds the frequency changes from 2843.4 cm^{-1} in S_0 state to 2968 cm^{-1} in S_1 state. Consequently, the radiation 182 nm in wavelength will excite the vibration with quantum number $n \approx 9$ in formaldehyde. If one takes into account that C–H bond lengths at $S_0 \to S_1$ transition change by $\Delta \approx 0.01$ a.u., then it follows from Eq. 6 that $F^{f}_{0\to9}(182) \approx 0$. If now the 0→0 transition between S_0 and S_2 states of formaldehyde (λ = 175 nm) is excited, then $F^{f}_{0\to0}(182) \approx 1$. In acetaldehyde this wavelength excites the C–C bond vibration with 1055 cm^{-1} frequency[13] and vibrational quantum number $n \approx 2$. For this transition $F^{a}_{0\to2}(175) \approx 2.25\cdot10^{-6} \sim 0$. Then Eq. (5) takes the form

$$\frac{f^{f}}{f^{a}} \frac{K^{f}(175)}{K^{a}(182)} \approx 5 \cdot 10^4 f^{f}/f^{a} = 5\cdot10^4 \cdot 0.889 / 0.427 = 1.145\cdot5\cdot10^4,$$

where f^{f} and f^{a} are the oscillator strengths of electronic transitions $S_0 \to S_2$ for formaldehyde and acetaldehyde. The marked difference in fluorescence signals for two discussed values of photolytic wavelength allows the concentration of each aldehyde to be determined using the expressions, which relate the fluorescence signal power with the concentration of the molecules in S_0 state[15].

ACKNOWLEDGEMENT

This work was partially supported by personal Grant of Special Foundation for Financian Support of Young Gifted Scientist, Russia.

REFERERENCES

1. J.D. Goddard and H.F. Schaefer, J. Chem. Phys. **70**, No. 11, 5117–5134 (1979).
2. J.S. Yadav and J.D. Goddard, J. Chem. Phys. **84**, No. 5, 2682–2690 (1986).
3. N.A. Zvereva, I.I. Ippolitov, and A.F. Terpugova, Izv. Vyssh. Uchebn. Zaved., Ser. Fizika, No. 3, 121–122 (1993).
4. H.L. Dai, R.W. Field, and J.L. Kinsey, J. Chem. Phys. **82**, No. 3, 1606–1607 (1985).
5. C. Cheng, P. Ho, C.B. Moore, and M.B. Zughul, J. Phys. Chem. **88**, No. 2, 296–300 (1984).
6. A. Horowitz and J.G. Calvert, Int. J. Chem. Kinet., No. 10, 713–720 (1978).
7. F. Stoeckel, M. Schuh, N. Goldstein, and G.N. Atkinson, Chem. Phys. **95**, No. 1, 135–144 (1985).
8. B.M. Stone, M. Noble, and F. Lee, Chem. Phys. Lett. **118**, No. 1, 83–87 (1985).
9. O.V. Sverdlova, *Electronic Spectra in Physical Chemistry* (Khimiya, Leningrad, 1973), 248 pp.
10. P.I. Robinson and K.A. Holbrook, *Unimolecular Reactions* (Wiley, New York, 1972).
11. N.A. Zvereva, I.I. Ippolitov, and A.F. Terpugova, Atm. Opt. **4**, No. 1, 55–59 (1991).
12. G.V. Mayer and V.I. Danilova, *Quantum Chemistry, Molecular Structure and Photonics* (State University, Tomsk, 1984), 218 pp.
13. J.S. Crighton and S. Bell, J. Mol. Spectrosc. **112**, No. 2, 285–303 (1985).
14. V.Ya. Artyukhov and A.I. Galeeva, Izv. Vyssh. Uchebn. Zaved., Ser. Fizika, No. 11, 96–100 (1986).
15. N.A. Zvereva, I.I. Ippolitov, and A.F. Terpugova, Izv. Vyssh. Uchebn. Zaved., Ser. Fizika, No. 9, 86–87 (1992).
16. G.E. Scuseria and H.F. Schaefer III, J. Chem. Phys. **90**, No. 7, 3629–3636 (1989).
17. B.F. Yates, Y. Yamaguchi, and H.F. Shaefer III, J. Chem. Phys. **93**, No. 12, 8798–8807 (1990).

Erratum :

Il y a quelques erreurs de reproduction dans cette version de l'article. Il faut lire successivement :

– *En page 659, ligne 28 : «transient states at R_{C-H}=1.8 Å for formaldehyde»*
– *Formule (3)*

$$CHO(^2\Pi) \rightarrow CHO(^2A') + h\nu'$$

– *Formule (4)*

$$K(E) = cL\left(\prod_{i=1}^{s}\nu_i\right) / \left(\prod_{i=1}^{s}\nu_i'\right)\left(\frac{E-\Delta S_1^{\neq}}{E}\right)^{s-1}$$

V.Ya.Artyukhov et al. Vol. 11, No. 5 /May 1998/ Atmos. Oceanic Opt. 387

STUDY OF THE PHOTOPHYSICAL PROCESSES IN THE MOLECULE OF 3,4-BENZPYRENE IN CONNECTION WITH THE PROBLEM OF ITS DETECTION IN THE ENVIRONMENT

V.Ya. Artyukhov, V.A. Bratashov, A.G. Zavodovskii, N.A. Zvereva, and I.I. Ippolitov

V.D. Kuznetsov Siberian Physical-Technical Institute, Tomsk
Received December 1, 1997

The analysis of photophysical processes in the 3,4-benzpyrene molecule has been done. Different approaches to solution of the problem on detecting 3,4-benzpyrene are considered and a new one is being proposed.

INTRODUCTION

The 3,4-benzpyrene (benz-(a)-pyrene) belongs to the type of polycyclic aromatic compounds (PAC). It is a byproduct of the processes in the manufacture of asphalt concrete, in metallurgy, oil-processing, and oil-chemistry, and represents cancerigenic substance assigned to the first class of hazardous substances. The maximum permissible concentration of the 3,4-benzpyrene (BP) in the populated areas is extremely low: 10^{-15} g/cm^3, or $2.4 \cdot 10^6$ cm^{-3}, Ref. 1. It is known that at 0°C 100% of BP in air is in the aerosol phase, whereas at 19°C 1% BP is in the gas phase, and 99% in the aerosol one. Hence, the necessity arises of sampling sufficiently large volumes of air on suitable filters as well as of extracting precipitated substance by benzene or *n*-hexane, concentrating the obtained solution to use it in subseCuent analysis.

Standard analytical approaches[2] use two spectroscopic methods, namely the fluorescent and, more rarely, the absorption one. The problem of selectivity to BP arises when employing one or other of these methods, since, besides the BP, a great number of other organic compounds (like heterocyclic and oxygen-containing compounds, olefins, and paraffins) pass into the solution at extraction of samples from filters. So, the problem of chemical interference of compounds may arise in the analysis. In standard approaches the chromatographic separation of the extract is used to overcome these difficulties that make the process too complicated and laborious.

The aim of our research is to analyze the photophysical processes in the BP molecule, in order to be able to formulate approaches to its detection in air, enabling one to increase the analysis selectivity and to simplify it.

CALCULATED RESULTS OF AND THEIR DISCUSSION

The structure of the BP molecule and numbering of its atoms is presented on Fig. 1. It was the plane geometry that was calculated according to the crystallographic data.[3] The electronic energy levels of the molecule have been calculated by the method of partial ignorance of the differential overlap (PIDO) of the levels and using the parametrization enabling one to correctly calculate the excited states of different nature and multiplicity in molecules of complex aromatic and heterocyclic compounds, Refs. 4–6. The rate constants of the radiative decay of excited states as well as internal and intercombination conversion in the system of singlet and triplet levels were calculated using approaches outlined in Refs. 5–7. All in all, 300 single excited configurations have been taken into account in calculations of the excited electronic states, with 9 occupied and 5 vacant molecular orbitals of π-type. The calculated results are given in Tables I–IV.

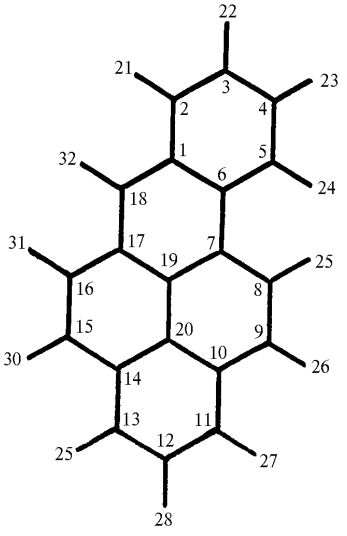

FIG. 1. Structure and numbering of the atoms of 3,4-benzpyrene molecule.

0235-6880/98/05 387-06 $02.00

388 Atmos. Oceanic Opt. /May 1998/ Vol. 11, No. 5 V.Ya.Artyukhov et al.

In Tables I and III the calculated $S_0 \to S_n$ and $S_0 \to T_n$ spectra are presented in a comparison with the experimental data. It follows from these results, that the first two electronic transitions are connected with π-electron excitation. According to the symmetry classification of the wave functions, Ref. 8, Ψ^- function corresponds to S_1 state whereas Ψ^+ to the S_2 state. Since the ground-state wave function is of the Ψ^- type, the $S_0 \to S_1$ transition is forbidden ($k_r = 3.6 \cdot 10^6$ s^{-1}), whereas $S_0 \to S_2$ transition is allowed ($k_r = 3.5 \cdot 10^8$ s^{-1}). These states strongly interact through the mechanism of internal conversion $k_{ic}(S_2 \to S_1) \approx 10^{13}$ s^{-1}. It is just because of this strong interaction (intensity borrowing) that the $S_0 \to S_1$ electronic transition becomes allowed and is experimentally observed in Ref. 9: $\varepsilon(S_0 \to S_1) = 6000$ l/(mole·cm), $\varepsilon(S_0 \to S_2) = 12000$ l/(mole·cm). The estimates of rate constants of internal conversion in systems of singlet and triplet electronic states are given in Tables II and IV. It is obvious from these results that internal conversion between the states of different molecular-orbital nature ($\pi\pi^* \Leftrightarrow \pi\sigma^*$) is a forbidden photoprocess. The rate constant value follows from the symmetry selection rule for the transitions between the states of one and the same molecular-orbital nature (transitions $\Psi^- \Leftrightarrow \Psi^-$ and $\Psi^+ \Leftrightarrow \Psi^+$ are forbidden).

*TABLE I. Calculated and experimental, Ref. 9, characteristics of the singlet electronic transitions in the 3,4-benzpyrene molecule: energy (*nm, cm^{-1}*) rate constant of radiative decay (*s^{-1}*), extinction coefficient (*l/(mole·cm)*).*

	$S_0 \to S_1$ ππ*	$S_0 \to S_2$ ππ*	$S_0 \to S_3$ ππ*	$S_0 \to S_4$ ππ*	$S_0 \to S_5$ πσ*	$S_0 \to S_6$ πσ*
#	396.8	391.0	315,8	296.8	296.6	286.6
	25202	25576	31665	33688	33721	34776
	$3.6 \cdot 10^6$	$3.5 \cdot 10^8$	$4.7 \cdot 10^6$	$2.9 \cdot 10^7$	$1.3 \cdot 10^4$	$2.9 \cdot 10^8$
##	402.0	388.0				
	24820	25745				
	ε = 6000	ε = 12000				

Calculation
Experiment

*TABLE II. Calculated rate constants of the internal conversion $S_i \to S_j$ in 3,4-benzpyrene molecule (*s^{-1}*).*

	$S_1(\pi\pi^*)$	$S_2(\pi\pi^*)$	$S_3(\pi\pi^*)$	$S_4(\pi\pi^*)$	$S_5(\pi\pi^*)$	$S_6(\pi\pi^*)$
S_0	$4.1 \cdot 10^4$	$2.0 \cdot 10^6$	$5.4 \cdot 10^4$	$1.6 \cdot 10^4$	$1.4 \cdot 10^{-7}$	$1.3 \cdot 10^4$
$S_1(\pi\pi^*)$		$9{,}6 \cdot 10^{12}$	$8.5 \cdot 10^9$	$1.2 \cdot 10^9$	$1.1 \cdot 10^0$	$4.2 \cdot 10^9$
$S_2(\pi\pi^*)$			$5.0 \cdot 10^{10}$	$5.5 \cdot 10^9$	$9.5 \cdot 10^0$	$3.1 \cdot 10^9$
$S_3(\pi\pi^*)$				$3.0 \cdot 10^{11}$	$2.5 \cdot 10^2$	$4.9 \cdot 10^{11}$
$S_4(\pi\pi^*)$					$1.1 \cdot 10^5$	$5.6 \cdot 10^{12}$
$S_5(\pi\pi^*)$						$9.6 \cdot 10^3$

The diagram of the energy levels and the main photophysical processes for low states of 3,4-benzpyrene molecule, modeled using results of Cuantum-chemical calculations, is presented in Fig. 2. It is seen from Fig. 2 and Table I that regions of maximum absorption correspond to molecule 3,4-benzpyrene excitation to S_2 (λ = 391 nm) and S_6 (λ = 287.6 nm) states. The internal conversion into S_1 ($k_{ic} \approx 10^{13}$ s^{-1}) state is the main channel of the S_2 state decay. Radiative decay and intercombination conversion of the T-state have significantly lower rate ($\approx 10^8$ s^{-1}). On excitation of the molecule to S_6 state with the energy of $\approx$ 34800 cm^{-1}, several photophysical processes are possible: radiative decay with the rate constant $k_r = 2.9 \cdot 10^8$ s^{-1}, internal conversion $k_{ic}(S_6 \to S_4) = 5.6 \cdot 10^{12}$ s^{-1}, and intercombination conversion into the close by energy triplet states, T_8 to T_{12}. The latter constant can be evaluated as a total $k_{icc}(S_6 \to T) = 5.6 \cdot 10^9$ s^{-1}. It is seen from the ratio among the rate constants of different photoprocesses that the internal conversion is again the main channel of the S_6 state decay. This process of the decay will be the main one for all excited singlet states, except for the S_1 state. As follows from calculations two competitive mechanisms are responsible for the S_1 state decay: the radiative decay with the rate constant $k_r = 3.6 \cdot 10^6$ s^{-1}, and the intercombination conversion into the triplet states $T_2 \to T_4$ $k_{icc}(S_1 \to T) = 5 \cdot 10^7$ s^{-1}. In this case the calculated Cuantum yield of fluorescence is $\varphi = 0.07$. In the experiment the Cuantum yield of the fluorescence may be several times as large because of the above mentioned vibronic interaction between the S_1 and S_2 states with the radiative transition $S_2 \to S_0$ being allowed.

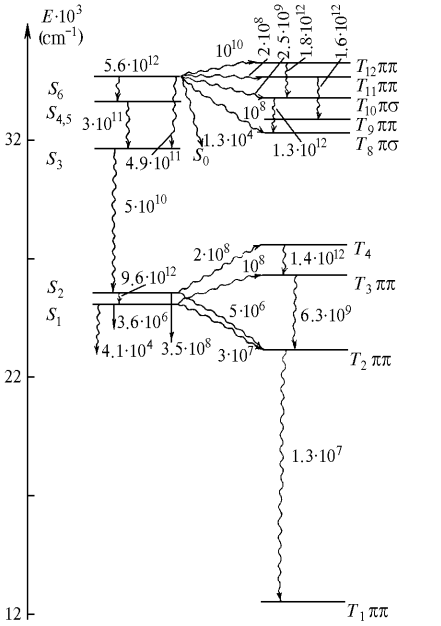

FIG. 2 Scheme of the energy levels and the main photophysical processes for low electronic states of 3,4-benzpyrene molecule.

TABLE III. Calculated and experimental energies (nm, cm^{-1}) *of* $S_0 \rightarrow T_n$ *electronic transitions in 3,4-benzpyrene molecule.*

	$S_0 \rightarrow T_1$ $\pi\pi^*$	$S_0 \rightarrow T_2$ $\pi\pi^*$	$S_0 \rightarrow T_3$ $\pi\pi^*$	$S_0 \rightarrow T_4$ $\pi\pi^*$	$S_0 \rightarrow T_5$ $\pi\sigma^*$	$S_0 \rightarrow T_6$ $\pi\pi^*$	$S_0 \rightarrow T_7$ $\pi\pi^*$	$S_0 \rightarrow T_8$ $\pi\sigma^*$	$S_0 \rightarrow T_9$ $\pi\pi^*$	$S_0 \rightarrow T_{10}$ $\pi\sigma^*$	$S_0 \rightarrow T_{11}$ $\pi\pi^*$	$S_0 \rightarrow T_{12}$ $\pi\sigma^*$	$S_0 \rightarrow T_{13}$ $\pi\sigma^*$	$S_0 \rightarrow T_{14}$ $\pi\pi^*$	$S_0 \rightarrow T_{15}$ $\pi\sigma^*$
Calculation	729.8 12613	431.0 23203	378.1 26446	360.9 27709	356.1 28086	349.9 28577	334.7 29874	308.6 32405	302.7 330037	295.0 33902	287.0 34849	282.5 35402	276.7 36136	272.3 36720	268.7 37219
Experiment	14600	–	–	–	–	–	–	–	–	–	–	–	–	–	–

TABLE IV. Calculated rate constants of the internal conversion $T_i \rightarrow T_j$ *in 3,4-benzpyrene molecule* (s^{-1}).

	$T_2(\pi\pi^*)$	$T_3(\pi\pi^*)$	$T_4(\pi\pi^*)$	$T_5(\pi\sigma^*)$	$T_6(\pi\pi^*)$	$T_7(\pi\pi^*)$	$T_8(\pi\sigma^*)$	$T_9(\pi\pi^*)$	$T_{10}(\pi\sigma^*)$	$T_{11}(\pi\pi^*)$	$T_{12}(\pi\sigma^*)$	$T_{13}(\pi\sigma^*)$	$T_{14}(\pi\pi^*)$	$T_{15}(\pi\sigma^*)$
$T_1(\pi\pi^*)$	$1.3\cdot10^{7}$	$8.5\cdot10^{6}$	$1.8\cdot10^{7}$	$2.6\cdot10^{-5}$	$4.4\cdot10^{7}$	$5.7\cdot10^{5}$	$7.1\cdot10^{-6}$	$2.8\cdot10^{5}$	$2.2\cdot10^{-5}$	$3.5\cdot10^{5}$	$1.7\cdot10^{-5}$	$1.9\cdot10^{-5}$	$9.8\cdot10^{5}$	$3.0\cdot10^{-5}$
$T_2(\pi\pi^*)$		$6.3\cdot10^{9}$	$4.7\cdot10^{10}$	$8.4\cdot10^{-2}$	$9.5\cdot10^{10}$	$2.6\cdot10^{8}$	$3.6\cdot10^{-3}$	$1.3\cdot10^{8}$	$8.6\cdot10^{-3}$	$1.6\cdot10^{8}$	$5.4\cdot10^{-3}$	$3.0\cdot10^{-3}$	$2.1\cdot10^{8}$	$1.5\cdot10^{-2}$
$T_3(\pi\pi^*)$			$1.4\cdot10^{12}$	$5.7\cdot10^{1}$	$1.1\cdot10^{12}$	$8.4\cdot10^{9}$	$1.6\cdot10^{-1}$	$2.8\cdot10^{8}$	$2.2\cdot10^{-1}$	$1.1\cdot10^{9}$	$9.3\cdot10^{-2}$	$1.4\cdot10^{-1}$	$3.2\cdot10^{9}$	$6.7\cdot10^{-1}$
$T_4(\pi\pi^*)$				$4.0\cdot10^{1}$	$1.4\cdot10^{13}$	$2.6\cdot10^{11}$	$1.3\cdot10^{-1}$	$3.0\cdot10^{10}$	$4.0\cdot10^{-1}$	$1.3\cdot10^{10}$	$2.2\cdot10^{-1}$	$7.3\cdot10^{-2}$	$3.2\cdot10^{9}$	$8.8\cdot10^{-1}$
$T_5(\pi\sigma^*)$					$9.7\cdot10^{1}$	$5.5\cdot10^{0}$	$5.1\cdot10^{10}$	$2.4\cdot10^{-1}$	$1.5\cdot10^{10}$	$2.2\cdot10^{-1}$	$5.2\cdot10^{9}$	$4.6\cdot10^{9}$	$3.1\cdot10^{-1}$	$1.2\cdot10^{9}$
$T_6(\pi\pi^*)$						$5.6\cdot10^{12}$	$1.2\cdot10^{0}$	$2.2\cdot10^{11}$	$7.6\cdot10^{-1}$	$3.8\cdot10^{10}$	$5.6\cdot10^{-1}$	$5.6\cdot10^{-1}$	$4.6\cdot10^{9}$	$3.8\cdot10^{0}$
$T_7(\pi\pi^*)$							$9.2\cdot10^{-1}$	$5.6\cdot10^{9}$	$4.8\cdot10^{-1}$	$9.7\cdot10^{9}$	$2.1\cdot10^{-1}$	$2.7\cdot10^{-1}$	$9.9\cdot10^{9}$	$4.9\cdot10^{-1}$
$T_8(\pi\sigma^*)$								$3.5\cdot10^{1}$	$1.3\cdot10^{12}$	$2.2\cdot10^{1}$	$2.0\cdot10^{11}$	$9.2\cdot10^{10}$	$3.0\cdot10^{0}$	$2.9\cdot10^{10}$
$T_9(\pi\pi^*)$									$1.2\cdot10^{2}$	$7.6\cdot10^{11}$	$1.3\cdot10^{1}$	$6.1\cdot10^{0}$	$3.1\cdot10^{11}$	$1.7\cdot10^{1}$
$T_{10}(\pi\sigma^*)$										$4.0\cdot10^{2}$	$1.8\cdot10^{12}$	$4.9\cdot10^{11}$	$1.8\cdot10^{1}$	$5.6\cdot10^{10}$
$T_{11}(\pi\pi^*)$											$4.5\cdot10^{2}$	$1.8\cdot10^{2}$	$2.1\cdot10^{12}$	$3.2\cdot10^{2}$
$T_{12}(\pi\sigma^*)$												$2.9\cdot10^{12}$	$2.0\cdot10^{2}$	$3.7\cdot10^{11}$
$T_{13}(\pi\sigma^*)$													$1.3\cdot10^{3}$	$4.5\cdot10^{11}$
$T_{14}(\pi\pi^*)$														$1.1\cdot10^{4}$

390 Atmos. Oceanic Opt. /May 1998/ Vol. 11, No. 5 V.Ya.Artyukhov et al.

Let us return to the S_6 state. The energy of this state roughly corresponds to the dissociation energy of the C–H bond in aromatic molecules (≈ 35000 cm$^{-1} \approx 4.4$ eV), that is, the energy of the hydrogen atom separation in the ground state of the molecule. With the rate constant $k_{ic}(S_6 \to S_0) \approx 1.3 \cdot 10^4$ s^{-1}, the quantum yield of this process approximately equals to 10^{-9}.

Assuming that the break of the C–H bond is preceded by its weakening, an attempt has been done to find an excited electronic state in which essential weakening of the bond takes place. The bond strength was evaluated from the population (that is from electronic density value between A and B atoms[10]):

$$P_{AB} = 2 \sum_{i=1}^{\max} \sum_{\substack{\mu \in A \\ \nu \in B}} c_{i\mu}^{A} \, c_{i\nu}^{B} \, S_{\mu\nu} ,$$

where $c_{i\mu}^{A}$, $c_{i\nu}^{B}$ are the coefficients of molecular orbital expansion over the atomic orbitals; $S_{\mu\nu}$ is the integral of the atomic orbitals overlap. Coefficients $c_{i\mu}^{A}$ and $c_{i\nu}^{B}$ correspond to non-orthogonal basis of the atomic orbitals (AO).

The search for the states with minimum P_{CH} value has been performed using special computer code to determine stability of the C–H bond. The results are given in Tables V and VI. The P_{CH} values in the ground state of the molecule are given in the second column of these tables, for a comparison. Data from Tables V and VI indicate that the C–H bond population variations are insignificant even in highly excited S_i and T_i states.

TABLE V. Minimum values of P_{CH} in singlet states.

Bond C–H	Number of the state / P_{CH} value							
2–21	0	227	271	291	297	295	300	252
	0.887	0.719	0.721	0.729	0.732	0.734	0.739	0.740
3–22	0	300	298	295	291	271	282	145
	0.889	0.613	0.614	0.616	0.618	0.623	0.623	0.626
4–23	0	300	22	295	298	291	282	145
	0.890	0.607	0.624	0.627	0.631	0.635	0.642	0.651
5–24	0	290	232	289	138	15	164	292
	0.895	0.708	0.715	0.744	0.748	0.749	0.749	0.760
8–25	0	232	290	15	289	35	138	111
	0.892	0.652	0.656	0.685	0.689	0.708	0.709	0.719
9–26	0	232	290	239	289	250	15	241
	0.886	0.777	0.777	0.779	0.788	0.789	0.792	0.792
11–27	0	291	300	295	298	282	297	145
	0.887	0.696	0.709	0.715	0.717	0.723	0.723	0.724
12–28	0	295	300	298	291	282	22	145
	0.888	0.655	0.657	0.660	0.660	0.666	0.669	0.669
13–29	0	288	293	13	285	148	213	119
	0.887	0.717	0.743	0.749	0.754	0.771	0.776	0.779
15–30	0	288	293	13	285	148	213	208
	0.885	0.661	0.698	0.704	0.731	0.736	0.737	0.742
16–31	0	288	293	13	285	148	213	208
	0.885	0.693	0.701	0.708	0.729	0.740	0.748	0.749
18–32	0	10	239	273	290	61	232	235
	0.883	0.740	0.771	0.772	0.779	0.779	0.784	0.785

The above picture of photophysical processes well agrees with the peculiarities of experimentally measured absorption and fluorescence spectra of 3,4-benzpyrene molecule presented in Figs. 3 and 4, Ref. 9. The fluorescence peak at $\lambda = 402$ nm in Fig. 3 corresponds to the radiative transition $S_1 \to S_0$. Similar peak in the absorption spectrum (Fig. 4) corresponds to $S_0 \to S_1$ transition. The structure at $\lambda < 400$ nm represents the vibronic spectrum connected with $S_0 \to S_2$ transition. The maximum cross-section value in this region, at λ<388.6nm, corresponds to pure electronic transition 0→0.

TABLE VI. Minimum values of P_{CH} in triplet states.

Bond C–H	Number of the state / P_{CH} value							
2–21	0	297	274	228	382	292	300	296
	0.887	0.730	0.734	0.736	0.736	0.736	0.736	0.739
3–22	0	274	296	300	298	292	103	284
	0.889	0.596	0.609	0.613	0.615	0.618	0.623	0.625
4–23	0	296	300	103	292	274	298	284
	0.890	0.607	0.609	0.610	0.630	0.632	0.636	0.643
5–24	0	290	234	155	289	97	95	36
	0.895	0.711	0.721	0.729	0.742	0.745	0.754	0.754
8–25	0	234	290	95	289	155	20	97
	0.892	0.663	0.666	0.685	0.686	0.693	0.703	0.704

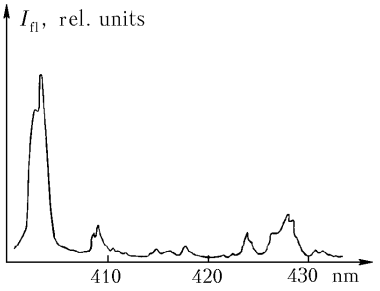

FIG. 3. Fluorescence spectrum of the 3,4-benzpyrene molecule in n-octane at 77 K, Ref. 9.

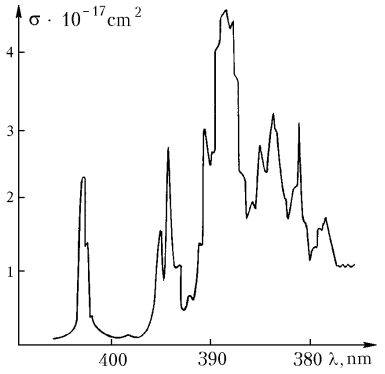

FIG. 4. Absorption spectrum of the 3,4-benzpyrene molecule in n-octane at 77 K, Ref. 9.

It follows from Fig. 4 that $\lambda_0 < 388.6$ nm with $\sigma(\lambda_0) = 4.6 \cdot 10^{-17}$ cm^2, and $\lambda_1 = 400$ nm with $\sigma(\lambda_1) \approx 0$ are the optimal pair of wavelengths for the differential absorption (DA) method. Since at atmospheric temperatures the 3,4-benzpyrene is practically all in the aerosol phase, the attempt to measure its content directly by DA method is an illusive goal.

Pumping of 100 m^3 of air through the filter, yields about 10^{-7} g of 3,4-benzpyrene (at the level of maximum permissible concentration) collected on it. As a result of its subsequent extraction into a solvent and concentration of the solution to 1 cm^3-volume sample, the concentrations of $\approx 10^{-7}$ g/cm^3 or $N = 2.4 \cdot 10^{13}$ cm^{-3} may be obtained. For measurement path of 1 cm length at the above indicated wavelengths and cross-sections, $N_{min} = 2.2 \cdot 10^{13}$ cm^{-3}, that means that the DA method is applicable in this case. However, the problem of influence of other impurities coming into the solution from the filter remains open.

It seems likely (the experimental check is necessary) that this problem can be solved by modification of standard approaches,[2] that use the influence of induced fluorescence. In these approaches a sample, after chromatic separation of fractions, is illuminated by the UV radiation. The fluorescence signal recorded at 402.4 nm wavelength, corresponding to pure electronic transition $S_1 \rightarrow S_0$, is then used for quantitatively estimating the 3,4-benzpyrene concentration.

In different approaches different wavelengths of exciting radiation are used: 254, 338, and 367.4 nm. Based on the above results regarding the mechanisms of the photophysical processes occurring in the molecule, one may state that wide spread of the wavelengths does not influence significantly the final result. In all cases the fluorescence occurs from the S_1 state, provided that the influence of hindering impurities is eliminated by pre-separation of the fractions. The view of the 3,4-benzpyrene absorption spectrum, presented in Fig. 4, and peculiarities of the photophysical processes considered make up the basis for modifying the standard techniques in the way we propose here. Excitation of the extract, which was not previously subjected to separation into fractions, should be alternately done at 338.6 and 400 nm wavelengths. The radiation at the first one efficiently excites the 3,4-benzpyrene fluorescence at 402.4 nm wavelength while the radiation at the second one practically does not produce any fluorescence. Taking into account that both these wavelengths are close one can assume that the excitation of the noise response from impurities at 402.4 nm wavelength occurs with the same efficiency and one may arrive at a conclusion that use of analytical signal $I_{BP}^{402.4} = I_{BP}^{402.4}(388.6 \text{ nm}) - I_{BP}^{402.4}(400 \text{ nm})$ in standard approaches (without chromatographic separation of fractions) can provide for the same precision of analysis while making it less laborious.

The most efficient, in our opinion, solution to the problem of 3,4-benzpyrene diagnostics, that excludes the necessity of using complicated physicochemical methods, characteristic of standard approaches, could be the use of mass-spectroscopy methods in combination with the selective laser photoionization of this molecule. Addressing to Fig. 2, let us note that after the S_2 state excitation, practically all molecules convert into the S_1 state due to nonradiative internal conversion mechanism. As mentioned above, only about 10% of molecules in this state decay through the radiative channel. The remaining 90% will convert into the triplet states due to the nonradiative mechanism of the intercombination conversion and will be accumulated in the T_1 state since the link of the latter with S_0 state is weak $k(T_1 \rightarrow S_0) < 1$ s^{-1}. The experimental value of the T_1 level position is 14670 cm^{-1}, whereas the lowest 3,4-benzpyrene ionization potential is of 57416 cm^{-1}, Ref. 12. Hence, the light quantum of the energy of 42546 cm^{-1} (5.3 eV, 235 nm) is needed to excite the molecule from T_1 state into an ionized state. Thus, using two-photon excitation (λ_1 =388 nm, λ_2 = 235 nm) one can achieve the selective character of molecule ionization. The third degree of the selection is performed in time-of-light-travel type mass-spectrometer while recording current pulses corresponding to arrival, at the detector, of ions with mass number $M = 252$. The sensitivity of the method discussed is very high, according to modern estimations, it comprises of $5 \cdot 10^{-18}$ g, Ref. 13. The possibility of using supersonic gas jets in the ionization volume is the additional attractive feature of this method. In this case the deep freezing of the vibrational degrees of freedom takes place, comparable with that when using liquid helium in the Schpol'skii spectra analysis. As a result, the selectivity of analysis can be significantly increased in the process of laser-induced ionization, the latter may be being performed in this case due to the two-photon mechanism using only one laser and intermediate levels S_2 or S_6.

REFERENCES

1. N.G. Rybalskii, O.A. Zhaketov, and A.E. Ulianova, *Ecological Aspects of Inventions Expertise. Reference Book of Expert and Inventor* (BNIIPI, Moscow, 1989), Pt. 1, 448 pp.

2. *Manual on the Atmospheric Pollution Control*, (State Committee of USSR on Hydrometeorology, Ministerstvo Zdravookhraneniya SSSR, Moscow, 1991), Guiding document RP 52.04.186-89, 693 pp.

3. A.I. Kitaigorodskii, P.M. Zorkii, and V.K. Bel'skii, *Structure of Organic Substance. Data of Structural Analyses*, 1929–1970 (Moscow, 1980), 648 pp.

4. V.Ya. Artyukhov and A.I. Galeeva, Izv. Vyssh. Uchebn. Zaved. SSSR, Ser. Fizika, No. 11, 96–100 (1986).

5. V.Ya. Artyukhov, A.I. Galeeva, G.V. Maier, and V.V. Ponomarev, Opt. Spektrosk. **82**, No. 4, 563–566 (1997).

6. G.V. Maier, V.Ya. Artyukhov, and A.V. Karypov, Opt. Spektrosk. **66**, No. 4, 823–826 (1989).

7. G.V. Maier, *Photophysical Processes and Generating Ability of Aromatic Molecules* (Tomsk, 1992), 265 pp.
8. R. Pariser, J. Chem. Phys. **24**, No. 2, 250–268 (1956).
9. T.N. Bolotnikova, N.V. Dubinina, V.A. Zhukov, N.M. Surin, and A.F. Utkina, Zh. Prikl. Spektrosk. **42**, No. 3, 493–496 (1985).
10. R.S.Mulliken, J.Chem. Phys.**23**, No.10, 1833 (1955).
11. R.I. Nurmukhametov, *Absorption and Luminescence of Aromatic Compounds* (Khimiya, Moscow, 1971), 216 pp.
12. F. Brogli and E. Heilbronner, Angew. Chem. Intern. Edit. **11**, 538 (1972).
13. *Analytical Reference* (Informpribor, Moscow, 1989), 27 pp.

Chapitre 6

Détection de complexes d'intérêt atmosphérique en phase gazeuse

Publications : P7, P10, P11, P12, P13, P14, P15, P16, P18, P18, P19,P20

Proceedings : A2, A3, A4, A5, A6, A7, A8

Livres : L2, L3

6.1 Introduction

Les halogénures sont des molécules chimiquement actives et toxiques, qui interagissent facilement avec l'eau (à basse altitude, celle-ci peut en contenir de 0,02 à 4% en masse), et qui contribuent à la formation dans l'atmosphère de complexes moléculaires dont l'activité optique est assez grande. Ces complexes peuvent être à l'origine de pertes supplémentaires par rayonnement dans l'atmosphère. En phase gazeuse, ils subissent des mouvements de grande amplitude, qui provoquent la transformation des spectres des molécules constituant le complexe (le déplacement spectral en ce qui concerne les molécules libres peut atteindre quelques dizaines de cm^{-1}) et l'apparition de nouvelles bandes à basse fréquence des modes intermoléculaires. Les facteurs indiqués créent donc de sérieuses difficultés pour effectuer la détection des complexes moléculaires dans l'atmosphère et rendent délicat l'usage de la technique moderne du sondage laser à distance.

Les clusters formés par les molécules d'eau, HCl et HF, ont une importance fondamentale. En effet, bien que les dimères assurent un bon point de départ pour la compréhension de la formation de composés complexes, on sait que les changements de propriété des systèmes condensés en phase liquide à partir des dimères sont non additifs. Les études concernant la formation de petits clusters d'eau insérant de forts électrolytes est donc d'une importance considérable. Les clusters présentent un intérêt du point de vue des processus de nucléation, et pour la formation des aérosols. Pour renseigner utilement les études atmosphériques, il faut examiner des systèmes qui prennent effectivement en considération dans l'atmosphère des complexes de taille raisonnable, contenant une assez grande proportion d'eau.

Les clusters formés par l'eau avec l'acide chlorhydrique HCl sont aussi l'objet de l'étude à cause de leur rôle dans le cycle d'épuisement de la couche d'ozone : le radical du chlore est un catalyseur de la réaction de conversion de l'ozone en oxygène [48]. Le radical peut se former à partir de HCl, absorbé sur les surfaces hexagonales des clusters de glace qui apparaissent dans les nuages polaires stratosphériques [49, 50]. Les calculs selon la méthode de Monte-Carlo [51] ont montré que la dissociation ionique a bien lieu à la surface des cristaux de glace.

L'examen [5-9] des résultats du contrôle à distance des rejets accidentels dans le cycle du combustible

nucléaire [48, 49, 50, 52, 53], ainsi que parmi les industries utilisant des gaz contenant des composés volatiles, tels que les fluorures [54] a montré que les corps les plus toxiques et les plus chimiquement actifs sont UF_6, SiF_4, ainsi que les interhalogènes comme XF_3 et XF_5 (X=Cl, Br). De plus, pratiquement à tous les stades de l'hydrolyse de ces combinaisons dans les conditions de l'atmosphère réelle, se formera HF, l'un des composants d'origine anthropique le plus écologiquement dangereux à l'état de traces. Bien que les paramètres de la molécule HF soient assez bien connus [55], et qu'on puisse les trouver dans pratiquement toutes les bases de données spectroscopiques, l'utilisation de ces données pour le contrôle laser rapide de l'atmospère n'est pas toujours rationnelle. Cela est lié au fait que l'interaction de HF et H_2O conduit à la formation d'un complexe stable, structuralement non rigide, de formule totale $(HF)_n(H_2O)_m$ $(n+m \geqslant 2)$, dont le spectre rovibrationnel peut se distinguer considérablement des spectres correspondants de HF et H_2O.

Ni les conditions d'apparition des complexes mentionnés de façon stable dans les conditions atmosphériques, ni les caractéristiques de leurs spectres d'absorption, sur la base desquels peuvent être proposées de nouvelles méthodes efficaces de diagnostic, ne sont étudiées à l'heure actuelle. L'étude de la formation des complexes de l'eau à partir des liaisons hydrogéniques présente un intérêt essentiel pour plusieurs raisons. D'une part, la connaissance de leurs caractéristiques est nécessaire à la compréhension de la structure et des propriétés de l'eau liquide. D'autre part, on sait qu'ils apportent une contribution considérable dans le processus de rayonnement dans l'atmosphère terrestre. Dans la plupart des travaux accomplis dans cette direction, on examine l'influence des dimères de l'eau sur l'absorption par la vapeur d'eau dans le domaine infrarouge du spectre. Mais la question de l'influence des complexes de l'eau sur les caractéristiques de l'absorption par la vapeur d'eau de la radiation ultraviolette est insuffisamment étudiée.

Le but du travail a été de développer une approche dans le cadre de la mécanique quantique incluant des éléments de physique statistique permettant la détection des complexes d'origine anthropique ; ceci concerne donc l'étude du problème de la formation, de la stabilité et de l'activité optique des complexes non rigides moléculaires avec la participation des molécules de l'eau et de HX (X=F, Cl), ainsi que le développement du modèle décrivant les spectres photodissociatifs des dimères. L'étude comporte les étapes suivantes :

1. étude du problème de la formation, de la stabilité et de l'activité optique des complexes formés entre les molécules d'eau et les molécules HF et HCl ;

2. étude de l'influence de l'irradiation par rayonnement ultra-violet sur les complexes de l'eau à la transition $S_0 \rightarrow S_1$, et création du modèle décrivant les spectres photodissociatifs des dimères ;

3. analyse et interprétation des spectres expérimentaux infrarouges des complexes $(H_2O)_n(HF)_m$.

6.2 Méthodes utilisées et principaux résultats obtenus

Le travail a été réalisé en utilisant plusieurs méthodes *ab initio* : dans un premier temps, la méthode Hartee-Fock-Rootan pour les couches fermées, et la méthode restreinte de Hartee-Fock, spécialisée pour les systèmes qui présentent des couches ouvertes pour leurs différents états électroniques. On a utilisé également des approches prenant en compte la corrélation électronique : méthode d'interaction directe de configuration (CI) et méthode de multiconfiguration (MC SCF). L'étude de la structure des complexes moléculaires est fondée sur l'obtention des points stationnaires de la surface de l'énergie potentielle (SEP), compte tenu de la corrélation électronique et de l'erreur liée à la superposition des bases. Pour déterminer les structures géométriques optimales, on a utilisé des méthodes numériques de recherche de points stationnaires : méthodes du gradient, ou encore méthodes fondées sur le calcul des dérivées secondes de l'énergie potentielle.

On définit les configurations d'équilibre pour $[(H_2O)_n(HF)_m]$ avec n=m=2,3, et pour $[(H_2O)_n\,(HCl)_m]$ avec n :m = 1 :2, 2 :2, 3 :3, à la suite de quoi on calcule les fréquences vibrationnelles et on définit le déplacement de ces fréquences par rapport à celles des molécules libres. L'influence de l'irradiation

UV sur les complexes de l'eau avec HF et HCl est établie. Lors de l'excitation, la transition dans l'état électronique de basse énergie est localisée sur les liaisons O-H d'une des molécules d'eau, ce qui assure la préservation du caractère dissociatif de la bande d'absorption comme dans la molécule d'eau isolée, avec cependant un déplacement vers le domaine des ondes courtes. Les sections de l'absorption des spectres de photodissociation des molécules liées par une faible liaison hydrogène, telles que $(H_2O)_2$ et $H_2O\ldots HCl$, pour une excitation électronique modérée (énergie de vibration de la molécule $\leqslant 15$ % de l'énergie de dissociation D_0), sont bien décrites par un modèle fondé sur l'utilisation des fonctions d'Airy (qui représentent la solution de l'équation de Schrö dinger dans un champ homogène)

$$\Psi_{v,E}(x) = N_{v,E} \int_0^\infty \cos\left(z^3/3 + \tilde{\nu}\beta^{-2/3} z - 2\beta^{1/3}\,(x/\rho)\,z\right)\,dz \tag{6.1}$$

où $\beta = \rho^3 mF\hbar^2/4$ et $\tilde{\nu} = (E(R_0) - E)/\hbar\Omega$, et où $N_{\tilde{\nu},E}$ est une constante de normalisation pour le potentiel homogène dont les paramètres sont définis par le calcul *ab initio*.

Les modèles développés sont en bon accord avec les données expérimentales disponibles. Les résultats numériques coïncident également avec ceux qui ont été obtenus par d'autres auteurs pour les complexes examinés. Il faut retenir du travail les résultats originaux suivants :
– on a montré l'applicabilité du potentiel homogène et des fonctions d'Airy pour la description des spectres de photodissociation des dimères ;
– on a révélé les caractéristiques principales des spectres IR et UV des complexes formés de molécules d'eau et des molécules chimiquement actives HF et HCl, ainsi que leurs configurations optimales.

6.3 Perspectives pour le complexe $H_2O - HF$

Des études concernant la surface de potentiel du dimère H_2O-HF et l'interprétation des spectres IR expérimentaux du mélange H_2O et HF sont en cours. Pour ce complexe :

1. une série de calculs *ab initio* CCSD(T)/aug-cc-pVTZ ont été effectués avec le programme MOLPRO (avec 9021 points autour de l'équilibre) afin de déterminer la surface d'énergie potentielle complète H_2O-HF dans les coordonnées polysphériques symétrisées compte tenu des permutations des atomes H ;
2. l'analyse des spectres IR expérimentaux du mélange H_2O et HF, donc du complexe, sur la base de calculs *ab initio* du dimère et des complexes (avec un nombre des monomères variant jusqu'au trois) est en cours, de même que le calcul des bandes rovibrationnelles.

Les calculs de la structure électronique du dimère H_2O–HF étant réalisés, il reste à caractériser la surface de potentiel, et la structure du spectre d'absorption. La structure du spectre d'absorption de la bande ν_1 (H-F stretching) (3600 - 3800 cm^{-1}) résulte de la superposition de la bande fondamentale et des bandes chaudes issues des modes de basses fréquences (intermoléculaires) du complexe. Les maxima du spectre d'absorption correspondent aux têtes de branches P des bandes parallèles. Les premiers résultats (Fig.6.1) montrent un bon accord général dans la zone 3300–3900 cm^{-1}, mais il reste des différences entre expérience et simulation aux environs de 3200 cm^{-1}, zone dans laquelle le calcul prévoit une absorption qui n'est pas présente dans l'expérience. L'interprétation doit donc faire appel à de nouvelles hypothèses.

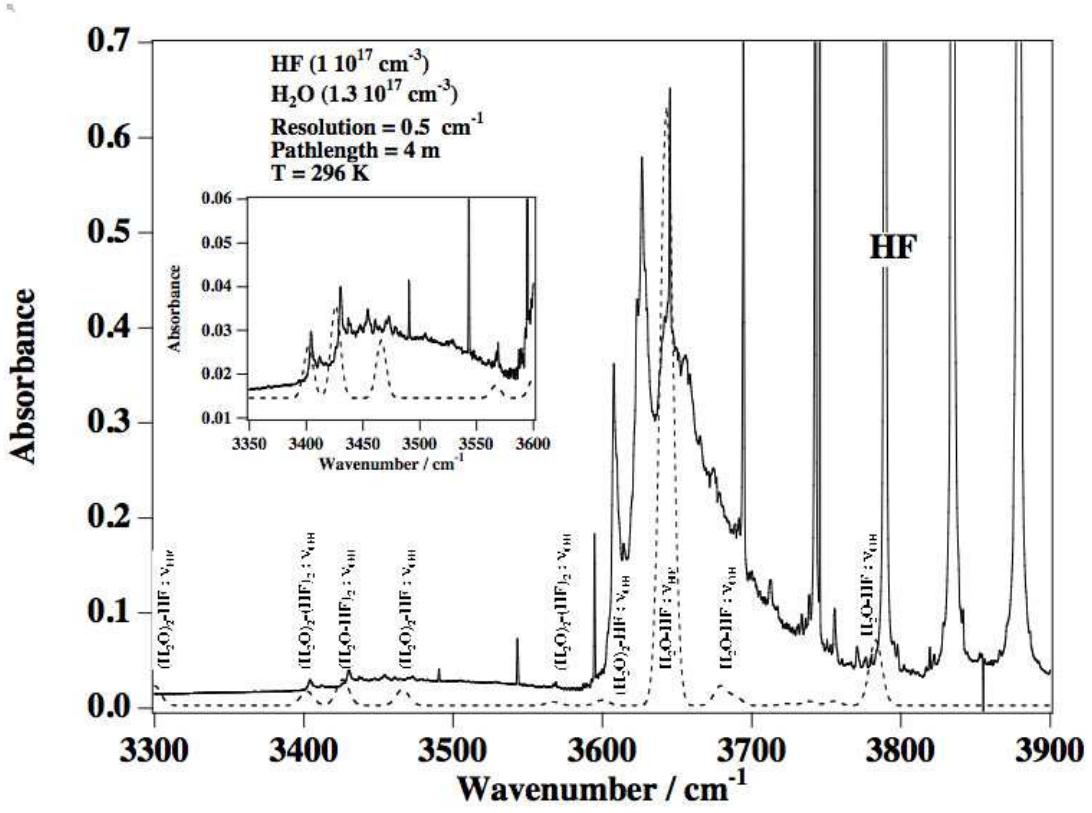

FIG. 6.1 – H_2O–HF : IR spectre expérimental (–) et calculé (. . .)

6.4 Articles-clés : P7, P12, P13,P14, P15, P16, P17, P18, P19, P20

M.A. Buldakov et al. Vol. 8, No. 11 /November 1995/ Atmos. Oceanic Opt. 927

PHOTODISSOCIATION OF WATER VAPOR BY UV LASER RADIATION

M.A. Buldakov, N.A. Zvereva, I.I. Ippolitov, and A.F. Terpugova

V.D. Kuznetsov Siberian Physicotechnical Institute
at the State University, Tomsk
Received May 18, 1995

The energy of low electronic states of monomer and dimer water complexes, H_2O *and* $(H_2O)_2$*, has been calculated. It is shown that* KrF*—laser—induced photoabsorption of water vapor may be accounted for by the transitions from hot rovibrational levels to quasicontinuum of* H_2O *states, whereas the fluorescence may be explained by the recombination of the products of monomer water complex disintegration.*

Water vapor fluorescence induced by Kr—F laser radiation has been studied within 250—280 nm (Ref. 1) and 250—400 nm (Refs. 2, 3) spectral ranges. In Refs. 2 and 3 it has been concluded that

1) fluorescence is observed under excitation mode, linear relative to the laser radiant exitance up to 10^7 W/cm^2;

2) there are regions in the fluorescence spectrum with essentially different decay time.

To interpret the observed fluorescence properly, it is necessary to obtain the energy states between which the radiative transitions take place connected with light absorption. The absorption spectra of water vapor in 250 – 350 nm spectral range has been studied in Refs. 4—7. As has been found, the maximum of absorption band lies at λ = 270 nm ($K = 3 \cdot 10^{-5}$ cm^{-1}), whereas the bottom corresponds to λ = 320 nm, and the band itself is continual without evident structure. It was concluded that the observed spectra are connected with the novel electronic state of H_2O.

To verify this hypothesis, we have calculated the ground and low electronic states of H_2O and $(H_2O)_2$. For each electronic state the energy has been optimized. The calculations have been made with the MONSTERGAUSS program package.

The key idea in studying the spectroscopic properties of water is the Rydberg character of excited electronic states. The electronic configuration of water ground state can be presented as

$$(1a_1)^2\ (2a_1)^2\ (1b_2)^2\ (3a_1)^2\ (1b_1)^2 - \tilde{X}^1A_1\ .$$

Ten excited singlet states result from the electron transition from $1b_1$ orbital to $3s$, $3p$, $4s$, or $3d$ Rydberg orbitals. Some states result from the transition from $3a_1$ orbital. In this paper we consider only low electronic states. In calculations we use the expanded basis including $3s$ and $4s$ orbitals for oxygen atom O, (5211/311), and hydrogen atom H, (211). The calculations have been made for the following transitions: $(1b_1 \to 3sa_1)^1B_1$ and $(1b_1 \to 3pb_2)^1A_2$.

The MKSSP method (49 electronic configurations) has been used to calculate the excited states.

To study the low electronic states in detail, the H_2O potential surfaces have been calculated with geometry optimization. Due to the transition from $\tilde{X}^1A_1$ state to the singlet state A^1B_1 ($1b_1 \to 3sa_1$), the H_2O molecule becomes linear with R_{OH} = 1.2288Å and α = 180° that corresponds to the intermediate state from which photodissociation into H and OH occurs. This stationary point of the potential surface lies in the region of nonequilibrium configurations, and any displacement from the region brings in the valley of the disintegration products. The energy corresponding to this stationary point is — 75.32147 a.u.

In the transition $\tilde{X}^1A_1 \to {}^1A_2$ ($1b_1 \to 3bp_2$) the molecular geometry is near—linear: α = 179.7939°, R_{OH_1} = 3.2722Å and R_{OH_2} = 1.0284Å. The total energy E equals to 75.4037313 a.u. This state corresponds most likely to the complex with hydrogen bond H ... OH. The calculational results for H_2O are shown in Fig. 1.

The total energy of the ground state $\tilde{X}^1A_1$ has been found to be —75.5494 a.u., whereas energy of the vertical transitions into state ${}^1B_1$ and ${}^1A_2$ is —75.26131 and —75.16918 a.u., respectively that corresponds to 7.8 and 10.3 eV, i.e. there is no energy values less than 7 eV for vertical transitions from zero—point vibrational level.

It is not possible, in the present state of the art of both theoretical and computational methods of quantum chemistry, to confirm the hypothesis about the existence of H_2O states intermediate between $\tilde{X}^1A_1$ and A^1B_1. Interpretation of the experimental data obtained is needed to be made within the framework of the present concept concerning the structure of H_2O energy levels. Let us now turn our attention to the diagram presented in Fig.2.

The energy of one quantum of radiation at λ = 248.5 nm (4.99 eV, 40257 cm^{-1}) is not enough for

0235-6880/95/11 927-03 $02.00

928 Atmos. Oceanic Opt. /November 1995/ Vol. 8, No. 11 M.A. Buldakov et al.

H_2O molecule to dissociate into H + OH, if considered are only transitions from zero–point vibrational level 000. However, this quantum energy is practically sufficient for H_2O to dissociate into $O+H_2$ (D_0 = 5 eV), especially when the finite spectral width of KrF laser radiation (~100 cm^{-1}) is taken into account. The energy of 5 eV corresponds to the wavelength λ = 247 nm, consequently, the absorption of radiation with λ > 247 nm is connected with the excitation of rovibrational levels of the ground state of quasicontinuum near the dissociation boundary.

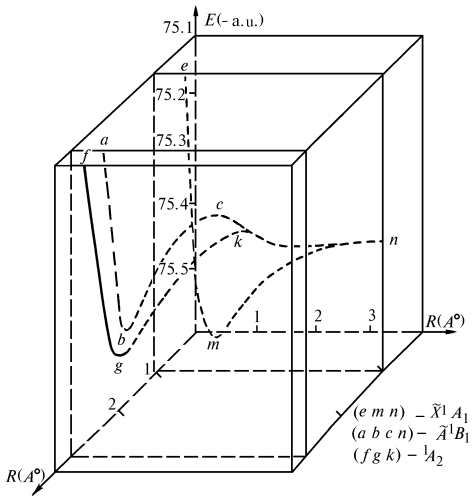

FIG. 1. Potential curves for low electronic states of water monomer H_2O.

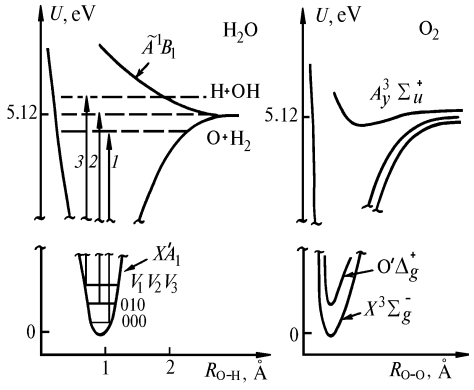

FIG. 2. Diagram of potential curves for H_2O *and* O_2.

The energy deficit, needed for dissociation to follow the reaction H + OH, amounts to 968 cm^{-1}. Then the transitions, induced by radiation with λ = 248.5 nm, from, for example, virbrational level 010 (1647.59 cm^{-1}) will lead to formation of OH (X^2o) radicals. With excitation of water vapor by radiation at λ = 248.5 nm and taking into account the Boltzmann distribution over the energy levels, the following processes will occur:

$$H_2O + h\nu \xrightarrow{248.5\ nm} H_2O^* \rightarrow \begin{cases} H_2O + M \\ O + H_2 \\ O + OH \\ H_2O + h\nu' \end{cases}$$

and, consequently, H_2O, H_2O^*, O, and OH can take part in the succeeding fluorescence. It is naturally to suppose that luminescence of excited molecule, H_2O^*, and recombination luminescence appearing in association $O + OH \rightarrow H_2O$ and $O + H_2 \rightarrow H_2O$ are responsible for the fluorescence. This supposition is confirmed by the fact that in pure water vapor the fluorescence can be quenched effectively by molecular oxygen. To explain qualitatively the existence of the fluorescence continuous spectrum recorded,[4–7] the following assumption should be made.

Excitation of H_2O molecules in the quasicontinuum of states lying below the dissociation threshold is low–efficient due to small values of the Frank–Condon factor. The rate of excitation of continuous states lying above the dissociation threshold may be essentially greater due to borrowing intensities from $^1B_1$ state. Then every radiative transition in absorption will be connected with the continuous spectrum of states, whereas the decay of absorption coefficient in the longwave wing of the band will be due to the Boltzmann distribution of energy levels of the ground electronic state.

It should be noted in conclusion that the absorption and the fluorescence observed in experiment are not connected with water vapor dimer, $(H_2O)_2$. The computations we have made in Ref. 8 have shown that only unplane structure (see Fig. 3) has bound ground and S_1 and T_1 excited states with bond energy of 5.5, 2, and 4.4 kcal/mole, respectively. In this case, as compared to the monomer, a shift in absorption takes place to the blue region by the value within 0.65–0.69 eV.

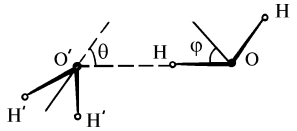

FIG. 3. Geometry of the dimer $(H_2O)_2$ *in the equilibrium configuration corresponding to the global energy minimum.*

REFERENCES

1. I.I. Ippolitov, V.M. Klimkin, and V.M. Mitchenkov, Khimiya Vysokikh Energii **22**, No. 1, 58–61 (1988).
2. V.M. Klimkin and V.N. Fedorishchev, Opt.Atm. **1**, No. 7, 72–76 (1988).
3. I.I. Ippolitov, V.M. Klimkin, and V.M. Mitchenkov, in: *Abstracts of Reports at All–Union Symposium on the Photochemical Processes in the Earth's Atmosphere* (1987), pp. 16–17.
4. V.M. Klimkin and V.N. Fedorishchev, Atm. Opt. **2**, No. 2, 174–175 (1989).
5. V.M. Klimkin, S.F. Luk'yanenko, I.N. Potapkin, and V.N. Fedorishchev, Atm.Opt. **2**, No. 3, 258–259 (1989).
6. S.F. Luk'yanenko, T.I. Novokovskaya, and I.N. Potapkin, Atm. Opt. **2**, No. 7, 579–582 (1989).
7. S.F. Luk'yanenko, T.I. Novokovskaya, and I.N. Potapkin, Atm. Opt. **3**, No. 11, 1080–1082 (1990).
8. M.A. Buldakov, N.A. Zvereva, I.I. Ippolitov, and A.F. Terpugova, Izv. Vyssh. Uchebn. Zaved. Fizika **36**, No. 3, 11–15 (1993).

810 Atmos. Oceanic Opt. /September 1999/ Vol. 12, No. 9 N.A. Zvereva et al.

Energies of the $S_0 \rightarrow S_1$ vertical transitions of low electronic states of optically active hydrogen bonding complexes

N.A. Zvereva, Sh.Sh. Nabiev, and Yu.N. Ponomarev

Tomsk State University
Republican Research Center "Kurchatov Institute," Moscow
Institute of Atmospheric Optics,
Siberian Branch of the Russian Academy of Sciences, Tomsk

Received June 22, 1999

Energies of the $S_0 \rightarrow S_1$ vertical transitions were calculated for hydrogen bonding complexes which can be formed in the atmosphere from interactions of water molecules with each other and with other hydrogen-containing molecules (for example, HF). An excitation energy is localized in the OH bond of one water molecule, what leads to preservation of the Rydberg character of the $S_0 \rightarrow S_1$ transition and the photodissociation type of the absorption band. Interaction of molecules in a complex results in broadening of the absorption bands of $(H_2O)_n$, $n = 2 - 6$, and $(H_2O...HF)_n$, $n = 1 - 4$, and their shift to the blue region with respect to the corresponding bands of the water monomer. It was determined that this shift for $(H_2O)_n$, $n = 2 - 6$, complexes is from 5566 cm^{-1} (water dimer) to 7259 cm^{-1} (water cluster), while for $(H_2O...HF)_n$ (olygomer structure $n = 1, 3, 4$) it is from 6211 cm^{-1} ($n = 1$) to 7582 cm^{-1} ($n = 4$) and 8550 cm^{-1} (cyclic structure $n = 2$).

1. Introduction

Hydrogen bonding complexes can be formed in the atmosphere as H_2O molecules interact with each other or other hydrogen-containing molecules, such as, for instance, HF, which are among most ecologically dangerous components emitted by industrial enterprises.

Molecular complexes $(H_2O)_n$ are of interest for analysis of processes of optical radiation extinction in the atmosphere and clouds. In particular, the contribution of such optically active complexes in the experimentally observed anomalous extinction of optical radiation by clouds[1] is yet to be rigorously treated.

Complexes of the $(H_2O)_n(HF)_m$ type can appear and exist in plumes of industrial enterprises, while the HF molecules are formed practically at all stages of interaction of uranium hexafluoride and products of its hydrolysis in emissions of nuclear fuel cycle enterprises. The HF molecules interacting with the atmospheric water vapor can form the stable gas-phase $HF...H_2O$ complex (hydrate), as well as the weakly bound nonrigid $(HF)_n...(H_2O)_n$ complexes of donor–acceptor type with several types of large-amplitude motions.[2–4] The absorption bands of such complexes can be used for remote analysis of the composition and volume of emissions from nuclear fuel cycle or other enterprises emitting chemically active fluoride compounds into the atmosphere.

Complexes of $(H_2O)_n$, $(HF)_m$, and $(H_2O)_n(HF)_m$ types are also interesting from the viewpoint of fundamental spectroscopy. The detailed study of the structural nonrigidity effects (especially, for molecules and molecular complexes with several types of large-amplitude motions) stimulates development of a new field in spectroscopy of molecules and weakly bound complexes and provides for obtaining new data for further development and revision of some concepts of molecular and chemical physics, theory of reactivity, thermodynamics, formation of complexes, and others.[4]

2. Technique and calculated results

The systems under consideration in this work are water clusters $(H_2O)_n$, where $n = 2 - 6$, and $(HF...H_2O)_n$ complexes with $1 \le n \le 4$. The excited electronic states S_1 of such complexes result from exciting an electron from the double occupied molecular orbital t_n to the first empty virtual orbital t_v (at combining with the appropriate spin function). These orbitals define a nature of the excited electronic state and the type of the electronic transition. In this case the complex is considered as a supermolecule. The nature of the resulting electronic term of a transition can be judged from the electronic density redistribution and cross section of the potential energy surface of the excited electronic state. The energy of the $S_0 \rightarrow S_1$ vertical transition was calculated as a difference of the total energies $E(S_0)$ and $E(S_1)$ determined by two methods: the self-consistent field (SCF) method and the restricted Hartree–Fock (RHF) method for open shells.[5–8]

An optimum geometry of each complex was determined by the BFGS (Broyden–Fletcher–Goldfarb–Shano) method[9] using the 6–31G* basis and the MONSTERGAUSS software package.[10]

0235-6880/99/09 810-04 $02.00

3. Results and discussion

The obtained values of the excitation energy ε for the $S_0 \rightarrow S_1$ transitions of the $(H_2O)_n$ and $(H_2O...HF)_n$ complexes are given in Table 1. The excitation energy of the complexes under consideration is localized in one of the bonds of the component water molecules. This follows from the analysis of the electron density redistribution. Stretching of the OH-bond of the water molecule, in which the excitation is localized, indicates the dissociative nature of the $E(S_1)$ electronic term.

The photodissociative nature of the $\tilde{A}^1B_1$ state governing the first band of the water monomer ($\lambda \sim 165$ nm):

$$H_2O(\tilde{X}^1A_1) + h\nu \rightarrow H_2O(\tilde{A}^1B_1) \rightarrow$$

$$\rightarrow H(^2S) + OH(X^2\Pi),$$

is well known.[14]

Table 1. Energies ε of the $S_0 \rightarrow S_1$ vertical transitions of the $(H_2O)_n$ and $(H_2O...HF)_n$ complexes (RHF, 4-31G)

n	ε, $(H_2O)_n$, eV	n	ε, $(H_2O...HF)_n$, eV
1	7.8 (monomer)		
2	8.35 (dimer)	1	8.57 (dimer)
3	8.4 (cycl.)		
4	8.7 (cycl.)	2	8.86 (cycl.)
5	8.63 (cycl.)	3	8.64 (olygomer)
6	8.51 (cycl.)	4	8.74 (olygomer)

In the complexes considered in this paper the Rydberg nature of the S_1 electronic state is preserved; the type of the $S_0 \rightarrow S_1$ electronic transition can be defined as $\pi \rightarrow \sigma^*$.

Table 2 presents some physical and chemical properties of the $H_2O...HF$ complex and the energies of the $S_0 \rightarrow S_1$ electronic transition of the HF and H_2O monomers (with the zero-point energy correction) in comparison with the results of Refs. 11–14.

Table 2. Physical and chemical properties of the $H_2O...HF$ complex and the energies ε for the HF and H_2O monomers

R_{OF}, Å	D_e, kcal/mol	Bond angle (H..OF), deg.	ε, HF, eV	ε, H_2O, eV
2.71 (Ref. 11)	9.29 (Ref. 11)	–	~10.4 (Ref. 14)	7.4 (Ref. 14)
2.72 (Ref. 12)	9.1 (Ref. 12)	–	–	–
2.65 (Ref. 13)	10.2 (Ref. 13)	4.5 (Ref. 13)	–	–
2.72*	9.55*	3.7*	~10*	7.6*

*Our calculation.

The data of this table are indicative of a close agreement between the results obtained and the experimental and calculated results of other authors.[11–14]

The maximum of the absorption band corresponding to the $S_0 \rightarrow S_1$ electronic transition in the considered complexes shifts toward higher frequencies with respect to the absorption band of the water monomer (Fig. 1). This fact is indicative of weakening of the hydrogen bond.[15]

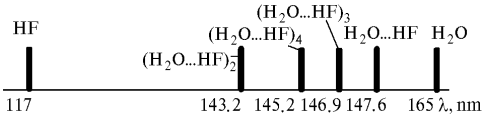

Fig. 1. Relative positions of the maxima of the absorption bands in the $(H_2O...HF)_n$ complexes.

Actually, the calculated binding energies D_e for the water dimer[16] and $H_2O...HF$ dimer in the S_1 electronic state amount to 2 kcal/mol and 1.6 kcal/mol, respectively. The binding energies D_0 of the S_0 ground state of the $(H_2O)_2$ and $H_2O...HF$ dimers are 5.5 kcal/mol and 9.55 kcal/mol. According to Pimentel,[15] the shift of a purely electronic transition depends on the difference between the binding energies of the ground and excited states (D_e^0 and D_e^*): $\Delta\nu = \nu_{complex} - \nu_{monomer} = D_e^0 - D_e^*$. The shift of the maximum of the absorption band depends not only on the difference between D_e^0 and D_e^*, but also on the Frank–Condon energies ω_e, because as the system absorbs a frequency ν, it transits into a certain point at the upper potential surface, which corresponds to the nonequilibrium value ω_e of the potential energy. For the water dimer $\omega_e = 12.5$ kcal/mol, for $H_2O...HF$ $\omega_e = 3.77$ kcal/mol, and correspondingly for the $(H_2O)_2$ dimer $\Delta\nu_e = 0.65$ eV and $\Delta\nu_{max} = D_e^0 - D_e^* + \omega_e = 0.69$ eV, while for the $(H_2O...HF)_2$ dimer we have $\Delta\nu_e = 0.77$ eV and $\Delta\nu_{max} = 0.5$ eV. The frequency shift Δν falls in the 0.65 – 0.69 eV interval for the water dimer and in the 0.5 – 0.77 eV interval for the $H_2O...HF$ dimer. For the $(H_2O...HF)_n$ complexes ($n = 1 - 4$) the largest shift $\Delta\nu_e$ is observed for the cyclic structure $(H_2O...HF)_2$ with $D_e^0 = -14.68$ kcal/mol, namely, $\Delta\nu_e = 1.06$ eV. For the olygomer structures $(H_2O...HF)_3$ and $(H_2O...HF)_4$ with $D_e^0 = -7.59$ kcal/mol and $D_e^0 = -8.39$ kcal/mol the corresponding values $\Delta\nu_e$ are 0.84 eV and 0.94 eV. The optimum geometry of the $(H_2O)_n$ complexes, $n = 2 - 6$, can be found in Refs. 16 and 17, while the optimum geometry of the $(H_2O...HF)_n$ complexes, $n = 1 - 4$, is presented in Figs. 2–4 and Tables 3–6.

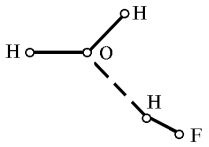

Fig. 2.

812 Atmos. Oceanic Opt. /September 1999/ Vol. 12, No. 9 N.A. Zvereva et al.

Table 3. Geometry of the $H_2O...HF$ complex

Bond length, Å		Bond angles, deg		Torsion angles, deg	
$R(OH)$	0.949	HOH	106.4	FH...OH	88.2
$R(H...O)$	1.805	FH...O	172.9	–	
$R(FH)$	0.921	H...OH	125.0	–	
$R(FO)$	2.720				

Table 4. Geometry of the $(H_2O...HF)_2$ complex

Bond length, Å		Bond angles, deg		Torsion angles, deg	
$R(O_1O_2)$	2.769	$F_3O_2O_1$	84.0	$F_4F_3O_2O1$	0
$R(FO)$	2.827	$H_5O_1O_2$	126.0	$H_5O_1O_2F_3$	180
$R(F_3F_4)$	2.588	$H_6O_2F_3$	92.6	$H_6O_2F_3F_4$	0
$R(H_8O_2)_b$	0.953	$H_7O_2F_3$	119.6	$H_7O_2F_3F_4$	180
$R(H_6O_1)_b$	0.958	$H_8F_3F_4$	96.6	$H_8F_3F_4O_1$	0
$R(H_5O_1)_f$	0.946	$H_9F_3O_2$	98.7	H_9F3O2O_1	0
$R(H_7O_2)_f$	0.947	$H_{10}F_4F_3$	102.5	$H_{10}F_4F_3O_2$	0
$R(H_6...O_2)$	1.874	–		–	
$R(H_8...F_3)$	1.908	–		–	
$R(H_9F_3)$	0.929	–		–	
$R(H_{10}F_4)$	0.940	–		–	

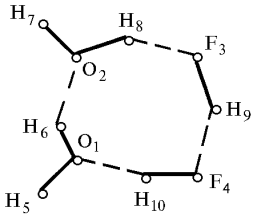

Fig. 3. Geometrical structure of the $(H_2O ... HF)_2$ complex.

Table 5. Geometry of the $(H_2O...HF)_3$ complex

Bond length, Å		Bond angles, deg		Torsion angles, deg	
$R(O_2H_1)_f$	0.949	$H_3O_2H_1$	105.0	$F_4H_3O_2H_1$	180
$R(O_2H_3)_b$	0.953	$H_7O_6O_8$	107.3	$H_5F_4H_3O_2$	0
$R(F_4H_3)$	1.994	$H_{12}O_{11}H_{13}$	107.5	$O_6H_5F_4H_3$	0
$R(F_4H_5)$	0.929	$F_4H_3O_2$	190.8	$H_7O_6F_4H_3$	0
$R(H_6...O_5)$	1.724	$H_5F_4H_3$	120.8	$H_8O_6F_4H_3$	180
$R(O_6H_7)_f$	0.947	$H_7O_6H_5$	127.7	$F_9O_6F_4H_3$	180
$R(O_6H_8)_b$	0.955	$H_{10}F_9H_8$	131.3	$H_{10}F_9O_6F_4$	180
$R(F_9...H_8)$	1.876	$H_{12}O_{11}H_{10}$	129.1	$O_{11}F_9O_6F_4$	180
$R(H_{10}F_9)$	0.929	$H_{15}F_{14}H_{13}$	139.3	$H_{12}O_{11}F_9O_6$	0
$R(O_{11}H_{10})$	1.721	$F_9H_8O_6$	180.0	$H_{13}O_{11}F_9O_6$	180
$R(O_{11}H_{12})_f$	0.948	$O_6H_5F_4$	180.0	$F_{14}O_{11}F_9O_6$	180
$R(O_{11}H_{13})_b$	0.952	–		$H_{15}O_{11}F_9O_6$	180
$R(F_{14}H_{13})$	1.989	–		–	
$R(F_{14}H_{15})$	0.914	–		–	

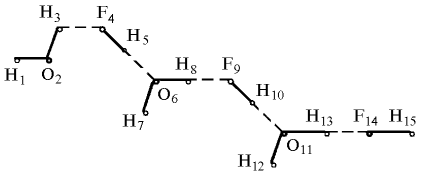

Fig. 4. Geometrical structure of the $(H_2O ... HF)_3$ complex.

Table 6. Geometry of the $(H_2O...HF)_4$ complex

N	Coordinates, Å			
	Atom	X	Y	Z
1	H	0.000	0	0.000
2	O	0.000	0	0.946
3	H	0.919	0	1.192
4	F	2.907	0	1.303
5	H	3.432	0	0.534
6	O	4.421	0	−0.863
7	H	4.140	0	−1.766
8	H	5.376	0	−0.863
9	F	7.234	0	−0.896
10	H	7.790	0	−1.644
11	O	8.821	0	−2.980
12	H	8.600	0	−3.900
13	H	9.773	0	−2.916
14	F	11.650	0	−2.822
15	H	12.274	0	−3.508
16	O	13.446	0	−4.755
17	H	14.381	0	−4.588
18	H	13.324	0	−5.700
19	F	13.030	0	−7.671
20	H	13.670	0	−8.389

Conclusions

In the complexes considered the excitation energy is localized in the O–H bond of one of the component H_2O molecules. This results in preservation of the Rydberg nature of the $S_0 \rightarrow S_1$ transition and the photodissociative type of the absorption bands corresponding to this transition, as in the water monomer.

As a result of the interaction of molecules in the complex, the absorption bands of $(H_2O...HF)_n$, $n = 1 - 4$, and $(H_2O)_n$, $n = 2 - 6$, complexes broaden, and their maximum shifts toward shorter waves with respect to the corresponding absorption bands of the water monomer.

The estimates show that this shift for the $(H_2O)_n$, $n = 2 - 6$, complexes is from 5566 cm^{-1} (dimer) to 7259 cm^{-1} (cluster), and for the $(H_2O...HF)_n$ complexes (olygomer structure, $n = 1, 3, 4$) it is from 6211 cm^{-1} ($n = 1$) to 7582 cm^{-1} ($n = 4$) and 8550 cm^{-1} (cyclic structure, $n = 2$).

Acknowledgments

This work was partially supported by the Russian Foundation for Basic Research (Project No. 99–05–64564).

References

1. S. Zdenek, Chem. Phys. Lett. **172**, 367–371 (1990).
2. P.R. Bunker, J. Chem. Phys. **92**, 7432–7440 (1990).
3. V.I. Starikov and Vl.G. Tyuterev, *Intramolecular Interaction and Theoretical Methods in Spectroscopy of Non-Rigid Molecules* (Publishing House of the Siberian Branch of the Russian Academy of Sciences, Tomsk, 1997), 230 pp.
4. Sh.Sh. Nabiev and L.P. Sukhanov, Izv. Akad. Nauk, Ser. Khim., No. 8 (1999).

5. C.C.J. Roothan, Rev. Mod. Phys. **32**, 179–185 (1960).
6. K. Hirao and N. Nakatsuji, J. Chem. Phys. **59**, 1457–1462 (1973).
7. K. Hirao, J. Chem. Phys. **60**, 3215–3222 (1974).
8. R. Carbo and J.M. Riera, *Lecture Notes in Chemistry*. Vol. 5. *A General SCF Theory* (Springer Verlag, Berlin, 1978).
9. R. Fletcher, Computer J. **13**, 317 (1970).
10. M. Peterson and R. Poirer, *MONSTERGAUSS-90*, Department of Chemistry, University of Toronto and Memorial University of Newfoundland, St. John's, Newfoundland.
11. V.P. Bulychev, in: *Molecular Spectroscopy*, ed. by G.S. Denisov (Leningrad State University Publishing House, Leningrad, 1973), pp. 3–10.
12. J.E. Del Bene, J. Phys. Chem. **92**, 2874–2881 (1988).
13. Sh.Sh. Nabiev and Yu.N. Ponomarev, Atmos. Oceanic Opt. **11**, 1093–1098 (1998).
14. A.M. Pravilov, *Photoprocesses in Molecular Gases* (Energoatomizdat, Moscow, 1992), 350 pp.
15. T.G. Meister, *Electronic Spectra of Polyatomic Molecules*, ed. by G.A. Grigench (Leningrad State University Publishing House, Leningrad, 1969), 206 pp.
16. N.A. Zvereva, M.A. Buldakov, I.I. Ippolitov, and A.F. Terpugova, Izv. Vyssh. Uchebn. Zaved., Ser. Fizika **36**, No. 3, 11–15 (1993).
17. S.S. Xantheas and T.N. Dunning, J. Chem. Phys. **99**, No. 11, 8774–8792 (1993).

Optics and Spectroscopy, Vol. 91, No. 4, 2001, pp. 604–608. Translated from Optika i Spektroskopiya, Vol. 91, No. 4, 2001, pp. 640–644.

MOLECULAR SPECTROSCOPY

Theoretical Description of the Photodissociation Spectrum of Monomer and Dimer Forms of Water

N. A. Zvereva

Institute of Atmospheric Optics, Siberian Division, Russian Academy of Sciences, Tomsk, 643055 Russia

Received June 9, 2000; in final form, February 7, 2001

Abstract—Electronic absorption spectra caused by the transition to the repulsive electronic term $\tilde{A}^1B_1$ for monomers and dimers of water are theoretically studied. It is proposed to describe the absorption cross section in the continuum by using the model of the linear potential $U(x) = E(R_0) - Fx$ ($x = R - R_0$ is the coordinate calculated from the equilibrium internuclear separation R_0) for which the repulsive term of an excited electronic state is described by Airy functions (such as the solution of the Schrödinger equation in a uniform field). The form of the potential $U(x)$ is determined using the calculated *ab initio* values of potential energy $U(x)$ for the corresponding values of x. The sections of potential surfaces of the lower electronic states are determined from *ab initio* calculations using the Hartree–Fock method [the self-consistent field approximation (SCF)], the configuration interaction (CI), and the multiconfiguration interaction (MC SCF). It is shown on the basis of the analysis of changes in electron density for the $S_0 \longrightarrow S_1$ transition on moving along the coordinate of reaction and mixing of different vibrational modes in the formation process of water dimers that the model is suitable for the description of photodissociation spectra (for the first absorption band) of monomer and dimer forms of water. The dependence of the absorption spectrum on the radiation frequency ω for monomer and dimer forms of water is constructed. The absorption cross section calculated for water molecules using the model proposed in the paper is compared with the experimental cross section and the absorption cross section calculated using the replacement of Airy functions with the δ function. The results obtained within the framework of the model using Airy functions agree well with the experiment. The replacement of Airy functions with δ functions leads to a larger deviation of the form of the absorption band from the experimental one. The absorption band of water dimers $(H_2O)_2$, like the band of water monomers, has no structure. The absorption band of dimers (with a peak at $\lambda \sim 162$ nm) is shifted to the short-wavelength region with respect to the band of water monomers H_2O ($\lambda \sim 167$ nm). © *2001 MAIK "Nauka/Interperiodica".*

INTRODUCTION

Photodissociation continuous absorption spectra of diatomic molecules were calculated by different approximate methods in [1–13]. For the description of photodissociation processes of triatomic molecules and the corresponding photodissociation spectra, the method of classical trajectories [14–23], the statistical model, and the Franck–Condon model [24–27] were used. However, these models possess no predictability; i.e., they cannot be applied to an arbitrary triatomic molecule. The water molecule is one of a few molecules for which the first absorption band corresponding to the $\tilde{X} \longrightarrow \tilde{A}$ transition was theoretically studied in detail [28]. The photodissociation of water in the first absorption band ($\lambda \sim 167$ nm)

$$\begin{aligned} &H_2O(\tilde{X}\,^1A_1) + \hbar\omega \\ &\longrightarrow H_2O(\tilde{A}\,^1B_1) \longrightarrow H(^2S) + OH(\tilde{X}^2\Pi) \end{aligned} \quad (1)$$

is a prototype of a system for the direct dissociation reaction. It is well known that the first excited state of the water molecule $\tilde{A}\,^1B_1$, via which process (1) proceeds, is characterized by the absence of crossing with other high-lying terms or a strong approach to them, and one may neglect nonadiabatic effects throughout the course of reaction. Because of this, the given process is ideally suited for the study of direct photodissociation. The number of electrons in a water molecule is not too large, which enables one to carry out *ab initio* calculations of potential energy and total absorption cross section [28]. The hydrogen bond between water molecules leads to the formation of systems whose exact quantum-mechanical description is a more complicated problem. Because of this, here we propose to calculate the Franck–Condon factor, which determines the absorption cross section in the continuous spectrum, by using the pseudopotential whose parameters are determined using data of an exact quantum-mechanical calculation.

THEORY

The dependence of the cross section for absorption in the continuous spectrum on the radiation frequency ω is determined by the approximate formula, which includes the square of the overlap integral for the radial

0030-400X/01/9104-0604$21.00 © 2001 MAIK "Nauka/Interperiodica"

wave function and the wave function of a state in the continuum, which is called the Franck–Condon factor $\Phi_v(E)$ (the golden rule [29]),

$$\sigma_v(\omega) \sim \omega|\Phi_v(E)|^2 = \omega\left|\int_0^\infty \Psi_v(R)\Psi_E(R)dR\right|^2, \quad (2)$$

where R is the internuclear spacing, $\Psi_v(R)$ is the radial wave function of the vibrational state v, $\Psi_E(R)$ is the wave function of the continuum with the energy $E = E_v + \hbar\omega$, and E_v is the energy of the initial vibrational state.

For a moderate electronic excitation, when the vibration energy of the mode being excited does not exceed 15% of the photodissociation energy D_0, one may conclude that the section of the potential energy along the coordinate of reaction is a parabola. This conclusion was made on the basis of estimating the deviation of the real potential energy curve $U(x)$ for the ground electronic state from the parabola $U(x) = (1/2)Kx^2$ (taking into account the typical value $\rho_0 \sim 1.4 \times 10^{-9}$ cm for the amplitude of molecular vibrations of water with the frequency of harmonic vibrations $\nu_{as} = 3966$ cm^{-1}, one can find that $U(x) = (1/2)Kx^2$ is about 18% of the photodissociation energy $D_0 = 37108$ cm^{-1}; the frequency correction for anharmonicity of water molecules is about 210 cm^{-1}, and the fundamental frequency becomes equal to 3756 cm^{-1}, which decreases the energy of zero vibrations by ~3% of the dissociation energy D_0). The wave functions of a harmonic oscillator [30]

$$\Psi_v(x) = N_v \frac{1}{(2^v v!)^{1/2}} \exp(-x^2/\rho^2) H_v(\sqrt{2}x/\rho) \quad (3)$$

should be taken as wave functions of the ground electronic state. Here, N_v is the normalization constant, $\rho = (2\hbar/\mu\Omega)^{1/2}$, Ω is the vibration frequency, $x = R - R_0$ is the coordinate measured from the equilibrium internuclear separation R_0, and H_v are Hermitian polynomials.

The wave functions of an electronic state depend on the form of the potential energy curve. The dominant contribution to integral (2) is made by the region with the width of the order of the amplitude of molecular vibrations $\rho_0 \sim 10^{-9}$ cm near the equilibrium position R_0. Typical changes in the atom–atom repulsion strength correspond to changes in interatomic separation by $R_0 \sim 10^{-8}$ cm. In the region making the dominant contribution to integral (2), the potential may be assumed to be uniform, $U(x) = E(R_0) - Fx$. A repulsive potential curve may be approximated by a straight line (with the accuracy $\Delta U(x) \sim 0.002$ au) for $\Delta R = R - R_0$ in the range from 0 to ~0.3 Å (Fig. 1), which agrees with the quantum-mechanical calculations.

The motion in the uniform field $U = -Fx + \text{const}$ (the field is directed along the x-axis) is described by the Schrödinger equations [30], whose solution is given by Airy functions

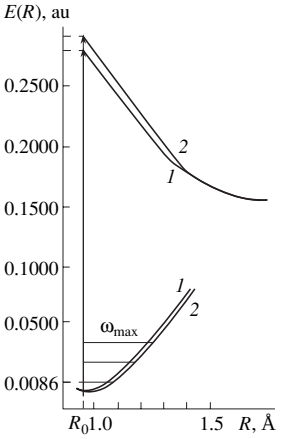

Fig. 1. Sections of potentials surfaces along the coordinate of reaction R(OH) for (*1*) the monomer and (*2*) the dimer of water for S_0 (the sections of the potential surfaces for S_0 states of monomers and dimers of water are made coincident) and S_1 electronic states.

$$\Psi_{v,E}(x) = N_{v,E}\int_0^\infty \cos\left(\frac{z^3}{3} + \tilde{\nu}\beta^{-2/3}z - 2\beta^{1/3}\frac{x}{\rho}z\right)dz, \quad (4)$$

where $\beta = \rho^3 mF/4\hbar^2$, $\tilde{\nu} = (E(R_0) - E)/\hbar\Omega$, and $N_{v,E}$ is the normalization constant. Wave function (4) describes the reflected wave. Because of this, the approximation using the uniform potential $U(x) = E(R_0) - Fx$ and wave functions (4) is sometimes called the reflective approximation [25].

By using wave functions (3) and (4), one can represent the Franck–Condon factors in the form

$$\Phi_v(\tilde{\nu}) = c\frac{(-i)^v}{(2^v v!)^{1/2}}\int_{-\infty}^{+\infty}\exp\left[-\beta^{2/3}z^2 + i\left(\frac{z^3}{3} + \tilde{\nu}\beta^{-2/3}z\right)\right]H_v(\sqrt{2}\beta^{1/3}z)dz, \quad (5)$$

where c is the normalization constant.

The first absorption band in the UV spectrum of water is determined by the asymmetric valence vibration of the OH bond. Small oscillations observed in the $\tilde{A}$ band are attributed to the summation of several partial absorption cross sections (Fig. 2) [28]. When calculating the dissociation spectrum of UV absorption, one may treat in the first approximation an H_2O molecule as a quasi-diatomic molecule under the assumption that

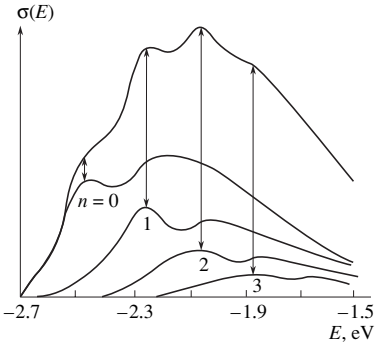

Fig. 2. The total absorption cross section $\sigma(E)$ and the partial absorption cross sections $\sigma_n(E)$ for dissociation of the (0, 0, 0) vibrational state of an H_2O molecule for the fixed deformation angle $\alpha = 104°$. The arrows show identities in the shape of curves for the total and partial absorption cross sections.

the dominant contribution to changes in electronic absorption is made by the valence vibration ν_{as} = 3756 cm^{-1}.

With functions (4) replaced by δ functions at the classical turning points, the cross section for the electronic transition from the vibrational level v of mode ν is determined by the expression [25]

$$\sigma_v(\nu) = B\nu N_v^2 \exp(-\xi^2) H_v^2(\xi), \quad (6)$$

where $\xi = \sqrt{2}/\rho(R - R_0) = \sqrt{2}/\rho F(\omega_{max} - v\nu - \omega)$ is a dimensionless parameter, ω_{max} corresponds to the maximum of the spectrum of absorption from the lowest vibrational level ($v = 0$), $\rho = (2\hbar/\mu\Omega)^{1/2}$. In this paper, we numerically studied the effect of replacement of function (4) with the δ function on the frequency dependence of the absorption cross section for water molecules.

The absorption at a fixed frequency ω represents the sum of absorptions from all vibrational levels

$$\sigma(\omega) = \sum_v N_v \sigma_v(\omega), \quad (7)$$

where N_v is the relative population of the vth level of mode ν. In the equilibrium gas, the distribution of molecules over vibrational levels is described by the Boltzmann distribution. At room temperature, molecules of water in the ground electronic state are found predominantly on the zero vibrational level of the vibrational mode under consideration. However, as shown in [28], the total cross section for absorption from the zero vibrational level of a water molecule is determined by the sum of partial cross sections $\sigma(n|\lambda)$ for dissociation accompanied by the formation of an OH radical in a certain vibrational state n, and this distribution over the vibrational states depends on the wavelength.

The experimental studies [31, 32] show that the cross sections for the first three vibrational levels are in the ratio $\sigma_0 : \sigma_1 : \sigma_2 = 1 : 0.96 : 0.58$ (the quantum-mechanical calculation gives a close result 1 : 0.81 : 0.53 [32]). In the paper, calculations were made for the total cross section $\sigma(\lambda)$ for absorption from the zero vibrational level of the antisymmetric vibrational mode ν_{as} of water molecules in the case of dissociation taking into account the experimental vibrational distribution for OH radicals (1 : 0.96 : 0.58).

The *ab initio* quantum-mechanical calculation (by the MC SCF, SCF, and CI methods) of the electronic states S_0 and S_1 of water dimers [33–36] shows that the electronic concentration is localized only on one of the water molecules, and the stretching of the OH bond causes considerable changes in electron density only on one OH bond of the water molecule. It follows from the vibrational analysis of water dimers $(H_2O)_2$ that the antisymmetric valence vibration is determined by a change of valence OH bonds only for the water molecule that does not lie in the symmetry plane of a water dimer, and with those hydrogen atoms H which are not involved in the O–H···O bond (here, the linear open form of the water dimer, which corresponds to the global energy minimum with $\Delta E = -4.6$ kcal/mol, is considered). The force constants corresponding to the interaction of free OH_f bonds with the intermolecular O…H bond are very small (k = 0.0084 and 0.0081 mdyn/Å), whereas the force constant for the interaction of O…H and OH_b, which is involved in hydrogen bonding, is 0.21 mdyn/Å. The corresponding frequency shifts $\Delta\nu$ with respect to water monomers are about 33 and 125 cm^{-1}. In the case of dimer formation, the hydrogen bond for water molecules may be treated as a weak perturbation $\Delta W \sim \Delta E_{bond}$. The *ab initio* calculation made for the water dimer (Fig. 1, curve *2*) shows that the potential curve of the excited electronic state may be approximated, as before, by one straight line with the slope F near the equilibrium position R_0 ($\Delta R \sim 0.3$ Å) and $U(x) = E(R_0) - Fx$. The energy $E(R_0)$ determined from the MC SCF calculations is 7.65 eV, and virtually coincides with the value $E(R_0)$ = 7.6 eV determined from perturbation theory in the first approximation as $(E(S_1)_{monomer} - E(S_0)_{monomer}) + (\Delta E(S_1) - \Delta E(S_0)) = E(R_0) + \Delta E(R_0)$. For the water dimer, where perturbation ΔE is rather small (~0.01% of the total energy), one may describe the wave functions of the reflective electronic term by using the reflective approximation.

CALCULATION RESULTS AND DISCUSSION

By using the SCF + CI and MC SCF methods and the Monstergauss code [37], we constructed the depen-

dence $E(R)$ and determined the slope F of the repulsive term for monomer and dimer forms of water: F = 53821 cm^{-1} Å^{-1}, ω_{max} = 59696 cm^{-1}, and ν = 3756 cm^{-1} for monomers and F = 54235 cm^{-1} Å^{-1}, ω_{max} = 61713 cm^{-1}, and ν = 3722 cm^{-1} for dimers. The absorption cross section was calculated taking into account formulas (2)–(5) and the distribution of OH radicals over the lower vibrational levels (1 : 0.96 : 0.58). For water monomers, we also calculated the absorption cross section using δ functions [formula (6)] and compared the results. Figure 3 presents (*3*) the experimental absorption cross section [38], (*4*) the absorption cross section calculated by using δ functions, and the absorption cross section calculated for (*1*) monomers and (*2*) dimers of water by formulas (2)–(5). One can see from the figure that $\sigma(\omega)$ obtained by replacing integral (4) with the δ function deviates from σ_{exp} more strongly than $\sigma(\omega)$ obtained by using function (4). The maximum of the absorption spectrum for water dimers is shifted to the short-wavelength region ($\lambda \sim 162$ nm) with respect to the monomer maximum ($\lambda \sim 167$ nm). The band has a similar structureless form and is broadened because of the interaction with the other water molecule. For dimers, the half-width of the band is wider by a factor of 1.2 than for monomers, and $\sigma_{dim}^{max}/\sigma_{mon}^{max}$ = 1.05. The effect of the hydrogen bond manifested itself in the value of the vibration frequency ν and the form of the curve and, therefore, in the slope F of the repulsive term, which entered into the formulas for calculating the absorption cross section $\sigma(\omega)$ and determined the form of $\sigma(\omega)$ for the water dimer. In these calculations, the function of the dipole moment $\mu(R)$ was assumed to be a constant, which is quite reasonable for such a narrow transition region ($\Delta R \sim 0.2$ Å).

Figure 4 illustrates the influence of hydrogen bonding on the absorption cross section $\sigma_{exp}(\omega)$ for a change from the gas phase (water vapor) [39] to liquid water [40] and ice [41]. One can see wide structureless bands for different forms of water, which are shifted to the short-wavelength region in comparison with the absorption of water vapor. In accordance with my previous papers [33, 34], in the case of formation of larger complexes of water $(H_2O)_n$, the electronic excitation, as in the case of a water dimer, is localized only on one molecule of the complex and leads to the rupture of one of the OH bonds and the shift of the absorption band peak for the $S_0 \longrightarrow S_1$ transition to the short-wavelength region. The shift increases with increasing n in $(H_2O)_n$, but it saturates at $n \sim 4$ and remains almost unchanged for larger n. The shift of the absorption band is determined by the interaction of the molecule on which absorption is localized with the nearest neighborhood. It is shown in [42] that the dominant contribution to the interaction energy of a complex is made by two- and three-particle potentials, whereas the contributions of E_i with $i \geq 4$ are negligibly small.

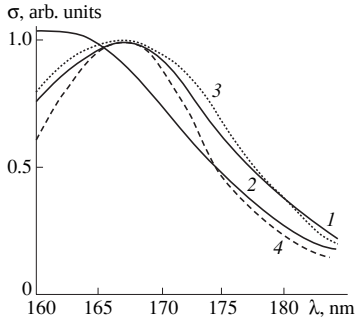

Fig. 3. Absorption cross sections $\sigma(\omega)$ for (*1*, *3*, *4*) the monomer and (*2*) the dimer of water. (*1*, *2*) The calculations using Airy functions, (*4*) calculation using δ functions, and (*3*) experiment [38].

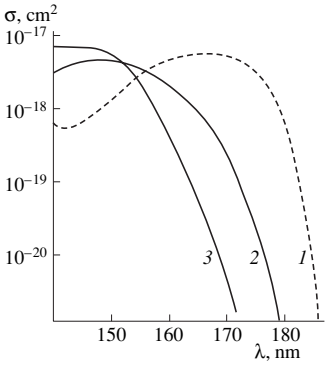

Fig. 4. Absorption cross sections of water. (*1*) Water vapor [39], (*2*) liquid water [40], and (*3*) ice [41].

Thus, both for the water dimer and for larger $(H_2O)_n$ complexes, the form of absorption bands for the transition to the first singlet state is determined by the photodissociation electronic term of one of the water molecules on which the electronic excitation is localized. The absorption spectrum broadens because of the interaction with other water molecules and shifts to the short-wavelength region to ~162 nm for $(H_2O)_2$, ~157 nm for n = 3, and ~150 nm for n = 4, which correlates with $\lambda_{max} \sim 150$ nm for liquid water ($\lambda \sim 145$ nm for the crystalline lattice of ice). The form of the cross section for the photodissociation spectrum of the dimer form of water can be successfully described within the framework of the model proposed here.

REFERENCES

1. E. C. G. Stueckelberg, Phys. Rev. **42**, 522 (1932).
2. A. S. Goolidge, H. M. James, and R. D. Present, J. Chem. Phys. **4**, 193 (1936).
3. N. S. Bayliss, Proc. R. Soc. London **158**, 551 (1937).
4. P. Fink and C. F. Goodeve, Proc. R. Soc. London, Ser. A **163**, 592 (1937).
5. A. A. Makarov, Author's Abstract of Candidate's Dissertation (Inst. Spektroskopii Akad. Nauk SSSR, Troitsk, 1977).
6. A. D. Pradhan, K. P. Kirby, and A. Dalgarno, J. Chem. Phys. **95**, 9009 (1991).
7. V. S. Ivanov and V. V. Sovkov, Opt. Spektrosk. **70**, 306 (1991) [Opt. Spectrosc. **70**, 178 (1991)].
8. L. D. A. Siebbeles, J. M. Schins, W. J. van der Zande, *et al.*, Phys. Rev. A **44**, 343 (1991).
9. D. P. Murtagh, in *Proceedings of the 9th ESA/PAC Symposium on European Rocket and Balloon Programmes and Related Research, Lahnstein, 1989, Noorofwiy'k, 1988*, p. 49.
10. P. Kowalczyk, Acta Phys. Pol. A **72**, 463 (1987).
11. C. W. Zucker and E. E. Eyler, J. Chem. Phys. **85**, 7180 (1986).
12. S. J. Singer, K. F. Freed, and Y. B. Band, J. Chem. Phys. **81**, 3064 (1984).
13. S. J. Singer, K. F. Freed, and Y. B. Band, J. Chem. Phys. **81**, 3091 (1984).
14. E. M. Goldfield, P. L. Houston, and G. S. Ezra, J. Chem. Phys. **84**, 3120 (1986).
15. R. Shinke, J. Chem. Phys. **92**, 3195 (1988).
16. V. Engel and R. Schinke, J. Chem. Phys. **88**, 6831 (1988).
17. K. Weide and R. Schinke, J. Chem. Phys. **87**, 4627 (1987).
18. H. Guo and J. N. Murrell, Mol. Phys. **65**, 821 (1988).
19. H. Guo and J. N. Murrell, J. Chem. Soc., Faraday Trans. 2 **84**, 949 (1988).
20. S. Goursard, M. Sizun, and F. Fiquet-Fayard, J. Chem. Phys. **65**, 5453 (1976).
21. A. Untch, S. Henning, and R. Schinke, Chem. Phys. **126**, 181 (1988).
22. R. C. Brown and E. J. Heller, J. Chem. Phys. **75**, 186 (1981).
23. K. Kuhl and R. Schinke, Chem. Phys. Lett. **158**, 81 (1989).
24. M. Shapiro and R. Bersohn, Annu. Rev. Phys. Chem. **33**, 409 (1982).
25. V. S. Letokhov, *Nonlinear Selective Photoprocesses in Atoms and Molecules* (Nauka, Moscow, 1983).
26. K. F. Freed and Y. B. Band, in *Excited States*, Ed. by F. C. Lim (Academic, New York, 1977), Vol. 3.
27. R. Schinke, V. Engel, and V. Staemmler, Chem. Phys. Lett. **116**, 165 (1985).
28. V. Engel, R. Schinke, and V. Staemmler, J. Chem. Phys. **88**, 129 (1988).
29. G. Balint-Kurti and M. Shapiro, in *Photodissociation and Photoionization*, Ed. by K. P. Lawley (Wiley, New York, 1985), p. 403.
30. L. D. Landau and E. M. Lifshitz, *Quantum Mechanics: Non-Relativistic Theory* (Fizmatgiz, Moscow, 1963; Pergamon, New York, 1977).
31. P. Andresen, G. S. Ondrey, B. Titze, and E. W. Rothe, J. Chem. Phys. **80**, 2548 (1984).
32. S. Henning, V. Engel, and R. Shinke, J. Chem. Phys. **84**, 5444 (1986).
33. N. A. Zvereva and I. I. Ippolitov, Izv. Vyssh. Uchebn. Zaved., Fiz. **42** (4), 8 (1999).
34. N. A. Zvereva, Izv. Vyssh. Uchebn. Zaved., Fiz. **42** (9), 87 (1999).
35. N. A. Zvereva and I. I. Ippolitov, Proc. SPIE **3090**, 88 (1997).
36. N. A. Zvereva, Proc. SPIE **3583**, 113 (1998).
37. M. Peterson and R. Poirer, *MONSTERGAUSS-90* (Department of Chemistry, University of Toronto and Memorial University of Newfoundland, 1990).
38. H. T. Wang, W. S. Felps, and S. P. McGlynn, J. Chem. Phys. **67**, 2614 (1977).
39. G. Herzberg, *Molecular Spectra and Molecular Structure* (Van Nostrand, New York, 1966; Mir, Moscow, 1969).
40. L. R. Painter, R. D. Birkhoff, and E. T. Arakawa, J. Chem. Phys. **51**, 243 (1969).
41. K. Dressler and O. Schnepp, J. Chem. Phys. **33**, 270 (1960).
42. S. S. Xantheas, J. Chem. Phys. **100**, 7523 (1994).

Translated by A. Kirkin

Russian Physics Journal, Vol. 44, No. 4, 2001

A THEORETICAL DESCRIPTION OF THE PHOTODISSOCIATION SPECTRUM OF THE H_2O...HCl COMPLEX

N. A. Zvereva and A. F. Terpugova 551. 508. 769

The effect of association of the water molecule and hydrogen chloride on the UV absorption bands is studied. Complete ab initio calculations for the H_2O...HCl *complex in the* S_1 *and* S_2 *states are performed. A mathematical model using Airy functions is developed to describe the absorption cross-sections in a continuous spectrum. The form of the potential is determined by accurate ab initio calculations. The cross-sections of potential surfaces of lower electron states are found from ab initio calculations using the Hartree–Fock, configurational interaction, and multi-configurational interaction techniques. A complete vibrational analysis and an analysis of the change in the electron density for the* $S_0 \rightarrow S_1$ *transition on moving along the reaction coordinate allow a conclusion to be made on the feasibility of applying the model proposed to the* H_2O...HCl *complex. The results obtained in the framework of the model using Airy functions show reasonably good agreement with the experiment. For the* H_2O...HCl *heterodimer, the absorption band has the same structureless form as for the water monomer. The absorption band (peaking at* $\lambda \sim 161$ *nm) is seen to shift towards short wavelengths as compared with the water monomer* H_2O *(*$\lambda \sim 167$ *nm).*

INTRODUCTION

In recent years, studies of intermolecular interactions and their spectral manifestations have received much attention. Considerable progress has been made in the experimental investigation of systems with hydrogen bonding in the gas phase [1–8]. Most of the works on the subject consider the contribution of these systems to the absorption of gas-phase particles in the IR region of the spectrum. The problem of the effect of hydrogen bonding on absorption of UV radiation by molecular systems is poorly understood. The major emphasis was placed on systems with fairly high and moderate energies. For example, a practically complete IR spectrum was obtained for H_2O...HF in the gas phase [9]. Weak hydrogen bonds, such as H_2O...HCl, are less studied, despite their chemical significance. The geometry of the complex was determined by methods of rotational spectroscopy [10]. The data on vibrational spectra were available only for intramolecular modes in solid matrices [11–13].

The problem of the dissociation dynamics of excited states of polyatomic molecules on photodissociation is very important but difficult to solve. There are scarcely any data on the form of the potential energy surface of excited states even for triatomic molecules. As an exact numerical solution to the problem of dissociation dynamics is difficult, use is made of different approximations, in particular, of a statistical model, the Franck–Condon model, the classical trajectory method, etc. These models cannot currently be applied to a description of any specified molecule. The water molecule belongs to the few molecules for which a detailed theoretical investigation of the first absorption band at the $\tilde{X} \rightarrow \tilde{A}$ transition was performed in [14]. Photochemical water dissociation in the first absorption band ($\lambda \sim 167$ nm)

$$H_2O(\tilde{X}\,^1A_1) + \hbar\omega > H_2O(\tilde{A}\,^1B_1) \rightarrow H(^2S) + OH(\tilde{X}\,^2P) \quad (1)$$

is a prototype system for the direct dissociation reaction. It is well known, that the first excited state $\tilde{A}^1B_1$ of the water molecule, where process (1) occurs, is well separated from other high-lying states, and nonadiabatic effects can be neglected in the course of the reaction. Therefore, this process is perfectly suited for examination of direct photodissociation. The

Tomsk State University. Translated from Izvestiya Vysshikh Uchebnykh Zavedenii, Fizika, No. 4, pp. 24–29, April, 2001. Original article submitted June 27, 2000.

 1064-8887/01/4404-0358$25.00

number of electrons in a water molecule is not large. This allows accurate calculations of the potential energy and total absorption cross-section [14]. Hydrogen bonding between water and HCl molecules gives rise to the formation of systems that are more difficult to treat within quantum mechanics. It is the object of this paper to use a preudopotential, whose parameters are determined from accurate quantum-mechanical calculations, to estimate the Franck–Condon factor defining the absorption cross-section in a continuous spectrum. The ab initio methods of the restricted Hartree–Fock (RHF), self-consistent field (SCF), configurational interaction (CI), and multi-configurational interaction (MC SCF) are used to study molecular systems. The calculations are performed in the 4-31*G* and 6-31*G*** basis sets using the MONSTERGAUSS package [15].

1. THEORY

The dependence of the absorption cross-section in the continuous spectrum on the radiation frequency ω is given by the Frank–Condon factor $\Phi_v(E)$ ("golden rule" [16])

$$\sigma_v(\omega) \sim \omega|\Phi_v(E)|^2 = \omega\left|\int_0^\infty \Psi_v(R)\Psi_E(R)\,dR\right|^2, \tag{2}$$

Here R is the internuclear distance, $\Psi_v(R)$ is the radial wave function of the vibrational state v, and $\Psi_E(R)$ is the wave function for a continuous spectrum of energy $E = E_v + \hbar\omega$, where E_v is the energy of the initial vibrational state.

The cross-section of the potential surface for the reaction coordinate can be assumed to be a parabola for moderate excitation of an electron. The following harmonic oscillator wave functions can be taken as wave functions for the ground electron state [17]:

$$\Psi_v(x) = N_v \frac{1}{(2^v v!)^{1/2}} \exp(-x^2/\rho^2) H_v(\sqrt{2}\,x/\rho), \tag{3}$$

where N_v is the normalized constant, $\rho = (2\hbar/\mu\Omega)^{1/2}$, Ω is the vibration frequency, $x = R - R_0$ is the coordinate reckoned from the equilibrium internuclear distance R_0, and H_v are Hermite polynomials.

The wave functions of the repulsive electron state depend on the shape of the potential energy curve. The major contribution to integral (2) is made by the region whose size nearly equals the amplitude $\rho_0 \sim 10^{-9}$ cm of molecular vibrations in the vicinity of the equilibrium position R_0. Characteristic changes in the repulsive forces of atoms occur as the atomic spacing R_0 is increased or decreased by $\sim 10^{-8}$ cm. In the region that makes the greatest contribution to integral (2), the potential can be assumed homogeneous, i.e., $U(x) = E(R_0) - Fx$. The repulsive potential curve can be approximated by a straight line as $\Delta R = R - R_0$ changes in the range from 0 to ~ 0.3 Å. This is consistent with our quantum-mechanical calculations.

The motion in the homogeneous field $U = -Fx + \text{const}$ (the field is directed along x) is described by the Schrödinger equation [17]:

$$\frac{d^2\Psi}{dx^2} + \frac{2m}{\hbar^2}(E - E_0 + Fx)\Psi = 0\,, \tag{4}$$

since $U \to +\infty$ at $x \to -\infty$ and $U \to -\infty$ at $x \to +\infty$. Hence, the energy levels form a continuous spectrum in the entire range from $-\infty$ to $+\infty$. All these eigenvalues are nondegenerate and correspond to motion that is finite for $x = -\infty$ and infinite for $x \to +\infty$. If the following dimensionless variable is substituted for x

$$\xi = (x + (E - E_0)/F)(2mF/\hbar^2)^{1/3}, \tag{5}$$

Eq. (4) becomes

$$\Psi'' + \xi\Psi = 0. \tag{6}$$

The energy parameter does not appear in Eq. (6). Therefore, once a solution to Eq. (6) satisfying the necessary finiteness condition is obtained, we derive an eigenfunction for an arbitrary energy value. The solution to Eq. (6) is finite for all x and we have

$$\Psi(\xi) = A\,\Phi(-\xi), \tag{7}$$

where $\Phi(\xi) = \frac{1}{\sqrt{\pi}}\int_0^{\infty}\cos\left(\frac{u^3}{3}+u\xi\right)du$ is the Airy function and A is the normalized factor ($A = (2m)^{1/3}/(\pi^{1/2}F^{1/6}\hbar^{2/3})$). A more convenient form of the Airy functions is written using the dimensionless values $\beta = \rho^3 mF/4\hbar^2$ and $\tilde{\nu} = (E(R_0) - E)\hbar\Omega$ to give

$$\Psi_{v,E}(x) = N_{v,E}\int_0^{\infty}\cos\left(\frac{z^3}{3}+\tilde{\nu}\beta^{-2/3}z - 2\beta^{1/3}\frac{x}{\rho}z\,dz\right), \tag{8}$$

where $N_{v,E}$ is the normalized constant. Wave function (7) and (8) describe a reflected wave. This approximation is referred to as reflective [18].

Using wave functions (3) and (8) we can represent the Frank–Condon factors as

$$\Phi_v(\tilde{\nu}) = c\frac{(-i)^v}{(2^v v!)^{1/2}}\int_{-\infty}^{+\infty}\exp[-\beta^{2/3}z^2 + i\left(\frac{z^3}{3}+\tilde{\nu}\beta^{-2/3}z\right)]H_v(\sqrt{2}\,\beta^{1/3}z)dz\,, \tag{9}$$

where c is the normalized constant. Changing variables, substituting explicit forms of the Hermite polynomials, and integrating Eq. (9) by parts, we can write the Franck–Condon factors for the long-wavelength edge of the absorption band ($\nu > 0$ and $\nu + \beta^2 > 0$) in the following form:

$$\Phi_0(\tilde{\nu}) = cM(\beta,\tilde{\nu})R_1(A)\,, \tag{10}$$

$$\Phi_1(\tilde{\nu}) = cM(\beta,\tilde{\nu})[2(B-\beta)R_1(A) + \beta^{2/3}R_2(A)/B)]\,, \tag{11}$$

$$\Phi_2(\tilde{\nu}) = c\sqrt{2}M(\beta,\tilde{\nu})\{[2(B-\beta)^2 + 1/2]R_1(A) - 2\beta^{5/3}R_2(A)/B\}\,, \tag{12}$$

where $M(\beta,\tilde{\nu}) = \exp\left[-\frac{1}{3\beta}(B-\beta)^2(2B+\beta)\right]$, $A = \beta^{-1/3}B$, $B = (\beta^2+\tilde{\nu})^{1/2}$,

$$R_1(A) = \int_{-\infty}^{\infty}\exp(-Ax^2)\cos\frac{x^3}{3}dx\,, \tag{13}$$

$$R_2(A)\int_{-\infty}^{\infty}x^2\exp(-Ax^2)\cos\frac{x^3}{3}dx\,. \tag{14}$$

The first absorption band in the UV spectrum of the water molecule is determined by the asymmetric stretching vibration of the OH bond. Small oscillations observed in the $\tilde{A}$-band are accounted for by the summation of several individual absorption cross-sections. The fairly rough agreement between the progression of symmetrical stretching vibrations in the $\tilde{A}$-band and deformation frequencies in the $\tilde{X}$-state is purely coincidental. This is shown in [14], where a complete ab initio study of the photodissociation dynamics of water molecule was performed and absorption cross-sections

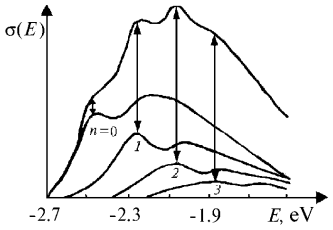

Fig. 1

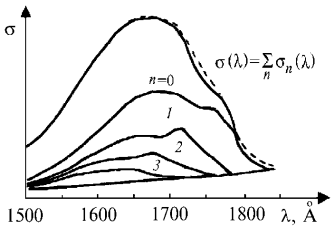

Fig. 2

Fig. 1. Absorption cross-sections $\sigma(E)$ for a fixed angle $\gamma = 104°$.

Fig. 2. Total theoretical and experimental absorption cross-sections $\sigma(\lambda)$ and individual cross-sections $\sigma_n(\lambda)$ for H_2O.

for each orientation angle γ were constructed. The results for $\gamma = 104°$ are shown in Fig. 1. It is clearly seen that vibrational structures already exist for a fixed γ. Their structures are even more distinct for absorption cross-sections averaged over γ (Fig. 2). These results argue against the hypothesis of selective excitation of the deformation mode ν_2. According to the model from [19], the shifts of individual absorption cross-sections $\sigma_n(\omega)$ are correlated with the energy of the levels of the symmetric mode of stretching vibrations at the top of the barrier of the ground H_2O state. The Pack model in [19] accounts for structural features of the total absorption cross-sections $\sigma(\omega)$ on summation of narrow yet structureless individual absorption cross-sections $\sigma_n(\omega)$. In [14], the total absorption cross-section is attributed to the summation of broad yet structural individual absorption cross-sections. Thus, the sum of several fairly broad individual absorption cross-sections $\sigma_n(\omega)$ is responsible for the presence of structure in the total absorption cross-section. The individual absorption cross-sections shift according to energy levels of the symmetrical mode ν_1 at the top of the barrier of the excited electron state. This provides the "vibrational progression," even though no selective excitation of this mode or a deformation mode occurs. In calculating the dissociation of the UV absorption spectrum, the water molecule can be regarded, in the first approximation, as being a quasi-diatomic one. In doing so, we believe that the major contribution to the change in the electron absorption is made by the asymmetric stretching vibration $\nu_{as} = 3755$ cm^{-1}. In [2], functions (8) are replaced by the δ-functions at classical points of rotation. Reasonably good results were obtained for diatomic molecules. In this approximation, the cross-section of the electron transition from the vibrational level ν of the ν mode is determined by the following relation:

$$\sigma_\nu(\nu) = B\nu N_\nu^2 \exp(-\xi^2) H_\nu^2(\xi), \tag{18}$$

where the dimensionless parameter $\xi = \sqrt{2}/\rho(R - R_0) = \sqrt{2}/\rho F(\omega_{max} - \nu\nu - \omega)$, ω_{max} corresponds to the peak of absorption spectrum from the lowest vibrational level ($\nu = 0$), and $\rho = (2\hbar/\mu\Omega)^{1/2}$. In the present paper, we demonstrate the effect of substitution of the δ-function of the frequency dependence of the absorption cross-section for the water molecule for function (8).

The absorption at a fixed frequency ω is the sum of the absorptions from all vibrational levels,

$$\sigma(\omega) = \sum_\nu N_\nu \sigma_\nu(\omega), \tag{19}$$

where N_ν is the relative occupancy of the level ν of the ν mode.

The simple Franck–Condon theory [20, 21] would give a fairly large absorption cross-section for the ground state $n = 0$ alone (in view of the similarity between free radical OH with $R_0 = 0.9706$ Å and $\nu = 3735$ cm^{-1} and OH in the water

TABLE 1. Calculated Geometric Parameters H_2O...HCl

r(OH)	*R*(O...H)	*r*(HCl)	*R*(ClO)
0.943	1.975	1.277	3.25
α(HOH)	θ(O...HCl)	β(HO...H)	χ(HO...HH)
107.0	178.8	119.9	115.0

molecule with R_0 = 0.956 Å, ν_s = 3657 cm^{-1}, and ν_{as} = 3755 cm^{-1}). An experimental study, however, shows that this ratio is $\sigma_0 : \sigma_1 : \sigma_2$ = 1 : 0.96 : 0.58 (at λ = 157 nm) for the first three vibrational levels (for OH radical) [22]. Quantum-mechanical calculations give a similar ratio: 1 : 0.81 : 0.53 [14, 23]. Our ab initio calculations show that the Franck–Condon excitation switches the molecule to a repulsive term and that electronic excitation primarily affects both OH bonds to the same extent. The excitation is localized on one of the bonds only after the reaction route is determined, hence only the antisymmetric mode takes part in the dissociation. This is in good agreement with the ab initio calculations performed elsewhere [14, 21, 22]. This vibrational pre-dissociation model is typical for symmetrical triatomic molecules *ABA* experiencing vibrational excitation at photofragmentation *AB* (H_2S, NO_2, O_3, CO_2, and SO_2). The degree of vibrational excitation depends on the saddle point position relative to the ground electron state of the slope of the repulsive curve for the $^1B_1$-state. We calculated the individual absorption cross-sections σ_0, σ_1, and σ_2 and the total absorption cross-section σ(ω) for OH dissociation in a certain vibrational state (for the population ratio 1 : 0.96 : 0.58).

Our accurate quantum-mechanical calculations of the S_0 and S_1 electron states of the H_2O....HCl heterodimer (using MC SCF, SCF and CI methods) show that the electronic excitation is concentrated on just one of the water molecules and significant changes in electron density occur on just one OH-bond of the molecule on OH-bond stretching. It follows from the vibrational analysis for the water heterodimer H_2O...HCl that the antisymmetric stretching vibration depends on the change in the OH valence bonds alone. Geometric parameters of the heterodimer calculated using the valence-split basis with polarization functions for all atoms 6-31*G*** are summarized in Table 1 (*R* (Å) and α (degrees))).

The calculated (6-31*G***) force constants corresponding to the interaction between free O–H bonds and intermolecular hydrogen O...H bond of water and hydrogen chloride molecules are very small: *k* = 0.011 and 0.027 mdynes/Å (*k*, dyne/cm = $6.365 \cdot 10^{-2}$ *k*, cm^{-2}), whereas the force constant of the O...H and HCl interaction involved in hydrogen bonding is 0.131 mdynes/Å. The corresponding frequency shifts Δν as compared to those of the water monomer are ~ 0–4 cm^{-1} and 100 cm^{-1}, respectively. On formation of the heterodimer, the hydrogen bond for H_2O can be regarded as a small perturbation $\Delta W \sim \Delta E_{bond}$. Our ab initio calculations show that the potential excitation function for the heterodimer can be approximated, as before, by a straight line with a slope *F* near the equilibrium position R_0 (ΔR ~ 0.3 Å). The function $U(x) = E(R_0) - Fx$, $E(R_0)$ determined from the calculations using the MC SCF method is 7.69 eV and, in fact, coincides with $E(R_0)$ = 7.64 eV found by the perturbation theory in the first approximation. For the H_2O...HCl heterodimer, where the perturbation Δ*E* is rather small (~0.0015% of the total energy), the "reflective" approximation can be used to describe the wave functions of the repulsive electron term.

RESULTS AND DISCUSSION

Using the SCF + CI and MC SCF theoretical methods we have constructed *E*(*R*) and determined the slope of the repulsive term *F* for the water molecule and the H_2O...HCl heterodimer: *F* = 53821· $cm^{-1}\cdot$ $Å^{-1}$, ω_{max} = 59696 cm^{-1}, and ν = 3755 cm^{-1} for the water dimer and *F* = 54765 cm^{-1}, ω_{max} = 62035 cm^{-1}, and ν = 3753 cm^{-1} for the H_2O...HCl heterodimer. The absorption cross-sections for ν = 0, 1, and 2 were calculated from Eqs. (13)–(18). The absorption cross-section was also calculated for the water monomer using δ-functions (Eq.(16)), and the results were compared. Figure 3 shows experimental absorption cross-sections [24], and the absorption cross-sections calculated by using the δ-function and Eqs. (13)–(15) for monomer (1) and heterodimer (2). As is seen from Fig. 3, substituting the δ-function for integral (8) causes a more pronounced deviation of δ(ω) from δ_{exp} than δ(ω) derived by Eq. (8). The peak of the absorption cross-section for H_2O...HCl shifts to the short wavelength region (λ ~ 161 nm) as compared to that of the water monomer (λ ~ 167 nm). The band is also structureless in character and is broadened due to interaction with another water molecule. The band halfwidth (when the absorption cross-section is half as large) is 1.2 as large as that for the water monomer

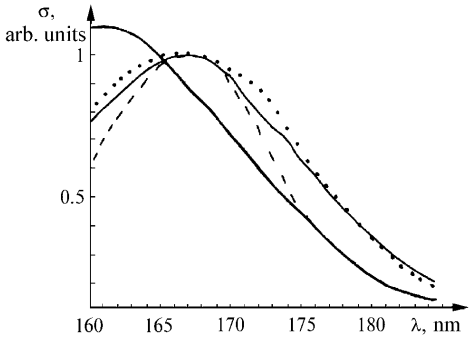

Fig. 3

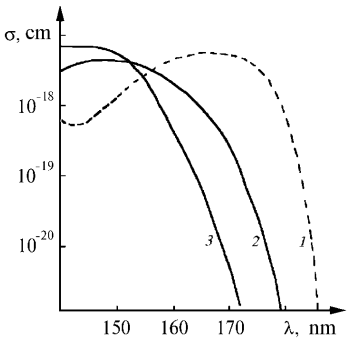

Fig. 4

Fig. 3. Absorption cross-sections σ(λ) for the water monomer and H_2O...HCl heterodimer using the Airy functions (solid curve), δ-functions (dashed curve), and experiment (dotted curve) [19].

Fig. 4. Experimental absorption cross-sections σ(λ) for gas (*1*) and liquid (*2*) water phases and ice (*3*).

$\sigma^{max}_{H_2O...HCl}/\sigma^{max}_{H_2O}$ = 1.1. The vibration frequency ν and the shape of the potential curve and, hence, the slope *F* of the repulsive term (appearing in the formulas for calculating the absorption cross-section σ(ω) and determining the associated form of σ(ω) for the water dimer) are affected by the hydrogen bonding. The dipole moment function μ(*R*) in our calculations was assumed to be constant, which is acceptable for this narrow transition region (Δ*R* ~ 0.2 Å). The effect of hydrogen bonding on the absorption cross-section $\sigma_{exp}(\omega)$ in transition from the gaseous phase (water vapor) [25] to water [26] and ice [27] is shown in Fig. 4. For different states of water we see broad structureless bands shifted to the short wavelength region as compared with the water vapor absorption bands. For H_2O...HCl and for the $(H_2O)_n$ complexes, the shape of the absorption band spectra in transition to the first singlet state is determined by the photodissociative electron term of one of the water molecules where the electron excitation is localized. The absorption spectrum is broadened due to interaction with other molecules and is shifted to short wavelengths from ~161 nm for H_2O...HCl and ~162 nm for $(H_2O)_2$ to ~ 157 nm (*n* = 3) and ~ 150 nm (*n* = 4), which correlates with λ_{max} ~ 150 nm for liquid water.

The shape of the absorption cross-section of the photodissociative H_2O...HCl spectrum can be adequately described within the model under discussion.

REFERENCES

1. T. R. Dyke, Top. Curr. Chem., **120**, 85 (1984).
2. F. G. Celli and K. S. Janda, Chem. Rev., **86**, 507 (1986).
3. R. E. Miller, J. Phys. Chem, **90**, 3301 (1986).
4. E. Knözinger and O. Schrems, Vibrational Spectra and Structure, J. R. During (ed.), Elsevier, Amsterdam (1987).
5. A. J. Barnes, Molecular interactions, H. Ratajczak and W. J. Orville - Thomas (eds.), Wiley, Chichester (1980).
6. A. J. Barnes, J. Mol. Struct., **100**, 259 (1983).
7. J. Howard and T. C. Waddington, Advances in Infrared and Raman Spectroscopy, R. H. Clark and R. E. Hester (eds.), Heyden, London (1980).
8. Chemical Applications of Thermal Neutron Scattering, B. T. M. Willes (ed.), Oxford University, London (1973).
9. R. K. Thomas, R. Soc. Lond. A, **344**, 579 (1975).
10. A. C. Legon and L. C. Willoughby, Chem. Phys. Lett., **95**, 37 (1983).

11. B. C. Ault and G. C. Pimentel, J. Phys. Chem., **77**, 37 (1973).
12. G. P. Ayers and A. D. E. Pullin, Spectr. Acta. Part A, **32**, 1641 (1976).
13. A. Schriver, B. Silvi, D. Maillard, and J. P. Perchard, J. Chem. Phys., **81**, 2095 (1977).
14. V. Engel, R. Schinke, and V. Staemmler, J. Chem. Phys., **88**, 129 (1988).
15. M. R. Peterson and R. Poirer, Monstergauss, Dept. of Chem., Univ. of Toronto (1990).
16. G. Balint-Kurti and M. Shapiro, Photodissociation and Photoionization, K. P. Lawley (ed.), Wiley, New York (1985).
17. L. D. Landau and E. M. Lifshits, Quantum Mechanics [in Russian], Gos. Izd. Fiz. Mat. Literatury, Moscow (1963).
18. V. S. Letokhov, Nonlinear Selective Photoprocesses in Atoms and Molecules [in Russian], Nauka, Moscow (1983).
19. R. T. Pack, J. Chem. Phys., **65**, 4765 (1976).
20. K. F. Freed and Y. B. Band, Excited States, F. C. Lim (ed.), Academic Press, New York (1977).
21. R. Schinke, V. Engel, and V. Staemmler, Chem. Phys. Lett., **116**, 165 (1985).
22. P. Andresen, G. S. Ondrey, B. Titze, and E. W. Rothe, J. Chem. Phys., **80**, 2548 (1984).
23. S. Henning, V. Engel, and R. Schinke, J. Chem. Phys., **84**, 5444 (1986).
24. H. T. Wang, W. S. Felps, and S. P. McGlynn, J. Chem. Phys., **67**, 2614 (1977).
25. G. Herzberg, Electronic Spectra and the Structure of Polyatomic Molecules, Van Nostrand, New York (1966).
26. L. R. Painter, R. D. Birkhoff, and E. T. Arakawa, J. Chem. Phys., **51**, 243 (1969).
27. K. Dressler and O. Schnepp, J. Chem. Phys., **33**, 270 (1960).

Journal of Structural Chemistry, Vol. 42, No. 5, pp. 730-738, 2001

AB INITIO STUDY OF H_2O–HCl (1:1, 1:2, 2:1) COMPLEXES

N. A. Zvereva

UDC 551.508.769

*This paper reports on an ab initio (6-31G**) study of 1:1, 1:2, and 2:1 $(H_2O)_n(HCl)_m$ complexes. Stable configurations of the 1:2 and 2:1 $(H_2O)_n(HCl)_m$ complexes and their geometrical and energy characteristics were determined. The vibrational analysis of the complexes was carried out. The effect of hydrogen bonding due to $S_0 \rightarrow S_1$ and $T_0 \rightarrow T_1$ electronic excitations is considered.*

INTRODUCTION

In recent years, there has been growth of interest in investigation of intermolecular interactions and their spectral characterization. Formation of structurally nonrigid molecular complexes of H_2O with chemically active and toxic molecules of anthropogenic origin and their stability and optical activity are among major challenges in modern physics and chemistry of atmosphere. Loosely bonded molecular complexes may be the reason for additional radiation losses in atmosphere over some industrial regions and variations in solar energy flux. Among other methods, *ab initio* studies of the structure and vibrational spectra of the above complexes are expected to provide a clue to this problem. The complexes are characterized by several types of large-amplitude motions, leading to transformation of the vibrational spectra of the monomer molecules constituting the complex and giving rise to new bands corresponding to intermolecular vibrations.

Considerable progress has been achieved in gas-phase experimental studies of hydrogen-bonded systems [1-14]. However, the low concentration of the complexes and interference in the far infrared (IR) region caused by the very intense rotational spectra make spectrum interpretation a very complex problem. A full set of intermolecular vibrations has been obtained for a very limited number of hydrogen complexes. The attention of researchers mainly concentrated on systems with large and medium binding energies, as H_2O...HF [15], for which a complete IR spectrum was obtained in the gas phase. Weak hydrogen bonds such as H_2O...HCl were studied to a lesser extent, although they are of great chemical importance. The geometry of the complex was studied by rotational spectroscopy [16], whereas vibrational spectral data were restricted to intramolecular modes in solid matrices [17-19]. *Ab initio* quantum mechanical calculations of H_2O...HCl were reported in [20], where its vibrational frequencies and geometry were determined.

The purpose of this work is a quantum mechanical study of the structure, stability, and vibrational spectra of the 1:2 and 2:1 $(H_2O)_n(HCl)_m$ complexes. A correct quantum chemical investigation demands an optimal choice of the calculation procedure. The most consistent and reliable method today is the *ab initio* Hartree–Fock–Roothaan technique [21]. For structurally nonrigid molecules with large-amplitude nuclear displacements which are just the case of intermolecular complexes, it was shown [22, 23] that for widely separated electronic states the displacements with anomalously large amplitudes do not violate the Born–Oppenheimer approximation. This follows from the estimates of nonadiabatic matrix elements. The estimates for ordinary and nonrigid molecules were compared, and it was concluded that for nonrigid systems the adiabatic approximation is valid with greater accuracy than for ordinary molecules.

CALCULATION PROCEDURE

The *ab initio* calculations were carried out using the MONSTERGAUSS program complex [24]. To investigate

Siberian Physicotechnical Institute, Tomsk State University. Translated from *Zhurnal Strukturnoi Khimii*, Vol. 42, No. 5, pp. 874-883, September-October, 2001. Original article submitted January 11, 2001.

 0022-4766/01/4205-0730$25.00

TABLE 1. Calculated Properties of H_2O and HCl and Their Complex [20]

	Method	6-31G**	+VP^s	+VP^s(2*d*)^s	Experiment
			H_2O		
r(OH), Å	SSP	0.943	0.943	0.943	0.9575 [41]
α(HOH), deg	SSP	106.0	106.4	106.0	104.5 [41]
E, au	SSP	–76.02361	–76.03576	–76.03885	
	MP2	–0.19544	–0.20956	–0.22362	
∝, D	SSP	2.147	2.226	1.991	1.847 [42]
	MP2	–0.085	–0.048	–0.036	
			HCl		
r(HCl), Å	SSP	1.266	1.269	1.267	1.274 [41]
	MP2			1.274	
E, au	SSP	–460.06603	–460.06816	–460.07012	
	MP2	–0.14932	–0.15146	–0.17212	
∝, D	SSP	1.469	1.511	1.231	1.093 [43]
	MP2	–0.049	–0.046	–0.040	
			H_2O...HCl		
R(O...Cl), Å	SSP	3.250	3.303	3.369	
	MP2			3.235	
θ(OClH), deg	SSP	2.2	2.9	3.2	
	MP2			3.5	
r(OH), Å	SSP	0.943	0.944	0.943	
	MP2			0.943	
α(HOH), deg	SSP	107.1	107.1	106.7	
	MP2			106.7	
r(HCl), Å	SSP	1.277	1.278	1.275	
	MP2			1.286	

TABLE 2. Calculated Geometrical Parameters of H_2O...HCl [this work, 6-31G**, *R*(Å), α(deg)]

r(OH)	*R*(O...H)	*r*(HCl)	*R*(ClO)
0.943	1.975	1.277	3.25
α(HOH)	θ(OClH)	β(HO...H)	χ(HO...HH)
107.0	2.2	119.9	115.0

TABLE 3. Vibration Frequencies (cm^{-1}) of Water Molecules

	ν_1	ν_2	ν_3
6-31G** [20]	4149	1770	4267
6-31G** [This work]	4065	1754	4164
+VP^s [20]	4129	1727	4242
+VP^s(2*d*)^s [20]	4139	1759	4244
Experiment [44]	3657	1595	3756
Experiment [35]$^{harm.\ freq.}$	3832	1648	3942

TABLE 4. Vibration Frequencies of the HCl Molecule (cm^{-1})

	6-31G**	+VP^s [20]	+VP^s(2*d*)^s [20]	[7*s*6*p*2*d*/4*s*1*p*] [20]	Experiment [36]	Experiment [45]
ν	3178 [20] 3073*	3174	3174	3141	2990	3042

*This work.

TABLE 5. Intramolecular Vibration Frequencies of H_2O...HCl (cm^{-1})

Assignment	ν(6-31G**)	Δν	Δν*	ν_{cor}	$\Delta\nu_{cor}$
HCl	2991	–82	–105	2870	–78
$(OH)_1$	4065	0	–4	3883	0
$(OH)_2$	4164	0	–3	3977	0
HOH	1760	+6	+1	1707	+5

*+VP^s(2*d*)^s [20].

the 1:2 and 2:1 $(H_2O)_n(HCl)_m$ complexes we chose the split valence-shell basis 6-31G**, containing polarization functions on all atoms. The complementary diffuse *sp*-shells on heavy atoms and the additional set of *d*-functions on the O and Cl atoms do not significantly affect the geometrical structure and vibrational frequencies (Tables 1-5). The accuracy of the *ab initio* calculations of the molecular properties depends not only on the quality of wave function description but also on the numerical methods of determination. Spectroscopic constants are especially sensitive to this factor because the inadequate numerical method in this case may lead to effects that may be attributed to the basis or electron correlation. For geometry optimization and construction of the force constant matrix we chose the method minimizing the sum of the squares of the *m* functions (states) of each of *n* variables and using the Newton–Raphson combination, the gradual descent method, and the Marquardt algorithm (similar to the one described in [25]). For application of this method, the choice of the step Δ*S* (Euclidean distance between the starting point and the point being optimized) is important. Calculations for various nonrigid systems [26] showed that the optimal Δ*S* = 0.1 au. On the one hand, the step must be small enough to ensure the validity of the harmonic approximation; on the other hand, with too small Δ*S* the energy changes Δ*E* may become comparable in magnitude to the uncertainties in the energy itself. The step Δ*S* = 0.1 au leads to numerical errors in determining the harmonic force constants ~0.001 mdyn/Å. The required accuracy of length gradients ACC (from ''accuracy'' — the threshold of convergence in energy gradients) was chosen to be $5\cdot10^{-4}$; when it changes to $5\cdot10^{-5}$, the changes in the minimized energy take place in the 6th decimal place. Thus for the given parameters, the *E* value may be taken to the 5th decimal place. The frequencies of normal vibrations and the matrix elements of the eigenvectors of the vibrational problem were calculated from the known force constant matrix *F* and the kinematic coefficient matrix *T*. Diagonalization of the matrix $D = F\cdot T$ gives the frequencies of normal vibrations, whose values and, most importantly, signs are related to the type of the fixed point.

The accuracy of the geometrical parameters compared to the experimental data and MP2 calculations is ~0.01-0.02 Å for the intramolecular distances *r* and ~0.12 Å for the intermolecular distances *R*, ~1.5° for the deformation intramolecular angles α, and ~1.5-10° for the deformation intermolecular angles θ.

For the estimated harmonic force constants (and hence for normal vibration frequencies), one would expect systematically exaggerated values compared to the experimental data (one-configuration approximation of the Hartree–Fock–Roothaan method, SCF). The total energy of the molecule whose nuclei mildly oscillate around the equilibrium position may be represented as [27]

$$E = E_0 + \frac{1}{2}\sum_{n=1}^{k} Q_n^2 \langle\Psi_0|(\partial^2 U/\partial Q_n^2)_0|\Psi_0\rangle + \sum_{n}^{k} Q_n^2 \sum_{i} \frac{|\langle\Psi_0|(\partial U/\partial Q_n)_0|\Psi_i\rangle|^2}{E_0 - E_i} + \upsilon(Q_n^3) =$$

$$E_0 + \frac{1}{2}\sum_{n=1}^{k} (f_{00_n} + f_{0i_n})Q_n^2 + \upsilon(Q_n^3). \quad (1)$$

TABLE 6. Expansion of the Binding Energy of SCF (6-31G**) in Terms of the CI Method (kcal/mole)

	ex	ct	es	pl	MIX
$(H_2O)_2$	4.223	–1.44	–7.4	–0.5	–0.08
$H_2O...HCl$	6.91	–3.03	–9.5	–0.78	0.226

Here Ψ_0 is the wave function of the ground electronic state with an energy E_0 for the equilibrium configuration; Ψ_i, the wave function of the excited state with an energy E_i; U, the potential energy of the molecule corresponding to the nucleus–nucleus and nucleus–electron interactions; Q_n, the displacement along the normal coordinate corresponding to the nth vibration mode, where $n = 1, ..., k$; $k = 3N_A - 6$ and $3N_A - 5$ for the nonlinear and linear N_A-atomic molecules, respectively. The sums of f_{00_n} and f_{0i_n} are the harmonic force constants of the nth vibration mode determined from spectroscopic measurements. If, for any Q_n, $f_{00_n} > 0$, then $f_{0i_n} < 0$, since $E_0 - E_i < 0$. The one-configuration approximation of the Hartree–Fock–Roothaan method ignores the interaction with the excited electronic states, thus neglecting the relaxation terms with f_{0i_n} in expansion (1). The harmonic force constants calculated at the level of the Hartree–Fock limit for molecular systems are overestimated by ~10-20%, and the harmonic vibration frequencies are exaggerated by 5-10%. Inclusion of electron correlation by using the configuration interaction (CI) method [30] or Möller–Plesset second-order perturbation theory [21, 29, 30] leads to the normal vibration frequencies decreased by ~4%. The stretching frequencies, however, remain exaggerated compared to the experimental values (for example, for H_2O and HF molecules, the difference between the frequencies is ~200 cm^{-1} [30]).

It is suggested here that the vibration frequencies be corrected by using a linear calibrating function

$$\nu_{cor} = a \cdot \nu_{calc} + b, \tag{2}$$

where ν_{calc} are the *ab initio* calculated frequencies; ν_{cor}, the corrected frequencies; a and b, the calibrating coefficients, found by the least-squares procedure by comparing the experimental ν_{exp} and calculated ν_{calc} frequencies in the IR spectra of H_2O and HCl.

The interaction energies ΔE of the complexes were calculated by using the scheme of expansion of the SCF energy suggested by Kitaura and Morokuma [31-33] in terms of CI calculations:

$$\Delta E_{SCF} = \Delta E_{ex} + \Delta E_{ct} + \Delta E_{mix} + \Delta E_{es} + \Delta E_{pl}, \tag{3}$$

where $\Delta E_{ex} + \Delta E_{es}$ are the exchange and electrostatic interaction energies corresponding to the first-order contribution, or to the inner part of the matrix including only occupied orbitals in terms of CI matrix; ΔE_{pl} is the polarization energy, resulting from the interaction between the occupied and virtual orbitals of one subsystem; ΔE_{ct}, the charge transfer energy, resulting from the interaction between the occupied orbitals of one subsystem and the virtual orbitals of the other; ΔE_{mix}, additional term determined by different types of matrix element.

The expansion of energy for $H_2O...HCl$ compared to the water dimer $(H_2O)_2$ is given in Table 6. The basis set superposition error (BSSE) was included in the calculation by using the method suggested in [34]; for $H_2O...HCl$, ΔE(BSSE) = 1 kcal/mole (~20% of the total energy of interaction). The interaction energy ΔE(SCF, 6-31G**) – ΔE(BSSE) = 5.2 kcal/mole, $\Delta E(+VP^s(2d)^s$, SCF + MP2 – ΔE(BSSE)) = 4.74 kcal/mole [20] ($\Delta E_{el.cor.}$ ~ 12% of the total energy of interaction for 6-31G** including ΔE(BSSE)).

RESULTS OF CALCULATIONS

Table 7 lists the calculated harmonic ν_{calc} (cm^{-1}), experimental [35, 36] ν_{exp} (cm^{-1}), and corrected ν_{cor} (cm^{-1}) frequencies (least-squares procedure) for H_2O and HCl monomers. The coefficients a and b of the linear correction function $\nu_{cor} = a \cdot \nu_{calc} + b$ determined by using the experimental values are 0.944 and 46 cm^{-1}, respectively. The coefficient of correlation between the experimental and calculated harmonic frequencies for the given a and b equals 0.9991. The mean absolute deviation of the predicted values from the experimental harmonic frequencies of H_2O and HCl is 46 cm^{-1}. Therefore

TABLE 7. Experimental and Calculated Harmonic Frequencies (cm^{-1}) for H_2O and HCl Molecules

Assignment	ν_{calc}	ν_{exp}	ν_{cor}
HCl	3073	2990	2947
OH^s	4065	3832	3883
OH^{as}	4164	3942	3977
HOH	1754	1648	1702

TABLE 8. Intermolecular Frequencies, Binding Energies, and Dipole Moments of H_2O...HCl Compared with Other Complexes

Complex	ΔE, 6-31G**, kcal/mole	ν_a, cm^{-1}	ν_b, cm^{-1}	ν_c, cm^{-1}	ν_{β_1}, cm^{-1}	ν_{β_2}, cm^{-1}	∞, D	∞, D (monomer)
H_2O...HCl	–5.2	139 100[20]	436 460[20]	289	131	73	4.26	1.09
H_2O...H_2O	–4.63	186	645	345	157	98	2.74	1.85
H_2O...HF	–9.2	190 180[15]	740 696[15]	672 666[15]	220 170[15]	169 145[15]	4.3	1.91

it is believed that *ab initio* quantum mechanical calculations (6-31G**) using the estimated correction coefficients permit the evaluation of the vibration frequencies of the compounds to an accuracy of ±50 cm^{-1}.

The calculated structural parameters of the H_2O...HCl heterodimer (Fig. 1) are presented in Table 2. The calculated ν_{calc} (6-31G**) corresponding to the given geometrical parameters and the corrected ν_{cor} harmonic intramolecular frequencies and displacements $\Delta\nu$ relative to the H_2O monomers and the HCl molecule are given in Table 5. In contrast to the OH stretching modes of the water molecule, the stretching mode of HCl experiences a considerable low-frequency shift ~100 cm^{-1}. Ault and Pimentel [11] observed a red shift of ~216 cm^{-1} for H_2O...HCl in the N_2-matrix, which was ~1.8 times greater than the shift in the gas phase for compounds of the same type.

The next group of frequencies corresponds to the intermolecular vibrations and is represented in Table 8. The intermolecular O...H stretching mode has frequencies ν = 139 cm^{-1}; 118 cm^{-1} (+$VP^s(2d)^s$) [20], which agree fairly well with the data of Pimentel and Ault [19] ($\nu \sim 100$ cm^{-1}) and with $\nu \sim 119$ cm^{-1} for the analogous compound $(CH_3)_2O$...HCl in the gas phase [39]. The intermolecular deformation vibrations O...H–Cl are assigned the frequencies 436 cm^{-1} (6-31G**); 459 cm^{-1} (+$VP^s(2d)^s$) [20] and 289 cm^{-1} (6-31G**); 351 cm^{-1} (+$VP^s(2d)^s$) [20], corresponding to the bending vibrations in the symmetry plane of the complex and to the vibrations with H-bond deviation from the symmetry plane of the complex. These calculated data agree well with the experimental data of Ault and Pimentel [19], who observed a wide band in the region 460 cm^{-1} and assigned it to the deformation vibrations of the H-bond.

The deformation vibrations of the acceptor proton of H_2O were assigned lower frequencies: 131 and 73 cm^{-1} (6-31G**); 143 and 94 cm^{-1} (+$VP^s(2d)^s$) [20], which agree with the experimental frequencies of 157 and 64 cm^{-1} for the H_2O...HF complex in the gas phase [38].

Summing up the results for H_2O...HCl, one can say that for the intermolecular frequencies of complexes with weak hydrogen bonding good agreement is observed even at the SCF (6-31G**) level of *ab initio* calculations.

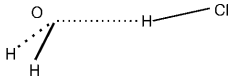

Fig. 1. Geometrical structure of the H_2O...HCl heterodimer.

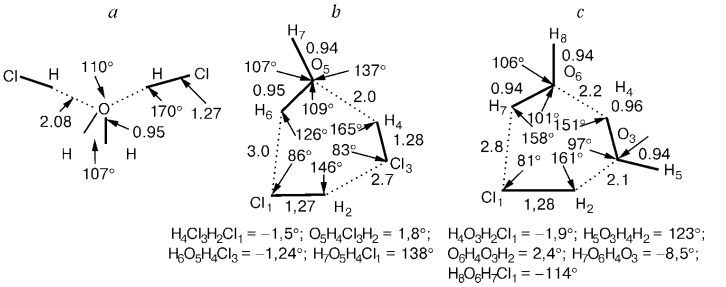

Fig. 2. Geometrical structure of the $(HCl)_2...H_2O$ complex (bond lengths in Å): configuration 1 (*a*), configuration 2 (*b*), configuration 3 (*c*).

Based on the results obtained for $H_2O...HCl$ we have carried out a theoretical investigation of the structure, stability, and vibrational IR spectra of the 1:2 and 2:1 complexes of water with hydrogen chloride $H_2O...(HCl)_2$ and $(H_2O)_2...HCl$.

The energy optimization data show that there are three most stable configurations. The interaction between H_2O and HCl in a 1:2 ratio leads to one of two configurations. The first configuration corresponds to a complex with C_{2v} symmetry (Fig. 2*a*, configuration 1) with a symmetry plane through the H_2O molecule and a plane of HCl molecules perpendicular to the first one [$E = -996.17165$ au; $\Delta E = -9.8$ kcal/mole (SCF, 6-31G**) and −8.5 kcal/mole (SCF–BSSE)]. The second configuration corresponds to a C_1 complex (Fig. 2*b*, configuration 2) with $E = -996.17011$ au and $\Delta E = -8.84$ kcal/mole (SCF, 6-31G**) and −7.64 kcal/mole (SCF–BSSE). The interaction between H_2O and HCl in a 2:1 ratio leads to a closed structure (Fig. 2*c*, configuration 3) with $E = -612.13414$ au and $\Delta E = -13$ kcal/mole (SCF, 6-31G**) and −11.1 kcal/mole (SCF–BSSE).

The complex corresponding to configuration 3 is the most stable complex in agreement with the calculated interaction energies with $\Delta E = 11.1$ kcal/mole. The complex corresponding to configuration 1 has two Cl–O...H bonds with $D_e = -3.71$ kcal/mole (SCF, 6-31G**); −3.053 kcal/mole (SCF–BSSE); structure 2 has one Cl–H...O bond and two weaker bonds H–Cl...H ~ −1.4 kcal/mole (SCF, 6-31G**), −1.3 kcal/mole (SCF–BSSE). This accounts for the fact that according to the calculated ΔE values complex 1 with an open structure is more stable than complex 2 with a closed structure. Complex 3 has hydrogen bonds with D_e(H–O...H) ~ D_e(Cl–H...O) > D_e(Cl...H–O) ~ D_e(Cl–H...Cl).

Hydrogen bonding between H_2O and HCl molecules and formation of 1:2 and 2:1 complexes leads to the following structural changes in the monomers: bond lengthening for HCl ~ 0.01 Å and OH_b (involved in hydrogen bonding) ~0.01-0.02 Å; variation of the HOH bond angle within 1°. The deviation of the Cl–H...O hydrogen bond from the quasilinear bond compared to the heterodimer $H_2O...HCl$ ($\theta \sim 179°$) is 9° (configuration 1), 14° (configuration 2), and 18° (configuration 3), and there is an insignificant lengthening of Cl–O...H ~ 0.1-0.2 Å.

The calculated and corrected harmonic intramolecular vibration frequencies of the complexes are presented in Tables 9-11. The intermolecular stretching vibrations O...H–Cl of the optimal structure are assigned the frequencies 124 and 138 cm^{-1} (6-31G**), differing slightly from the stretching vibrations of the O...H–Cl bond in the $H_2O...HCl$ heterodimer. The deformation intermolecular vibrations of the complex are assigned the following frequencies: 306, 269 cm^{-1} (Cl–H...O);

TABLE 9. Intramolecular Frequencies of $H_2O...(HCl)_2$ (open form, cm^{-1})

Assignment	ν(6-31G**)	ν_{cor}	Δν	$\Delta\nu_{cor}$
$(OH)_1$	4046	3865	–19	–18
$(OH)_2$	4135	3949	–29	–28
HOH	1771	1718	+11	+11
$(HCl)_1$	2990	2869	–83	–78
$(HCl)_2$	2995	2873	–78	–74

TABLE 10. Intramolecular Frequencies of $H_2O...(HCl)_2$ (closed form, cm^{-1})

Assignment	ν(6-31G**)	ν_{cor}	Δν	$\Delta\nu_{cor}$
$(OH)_1$	4024	3845	–41	–38
$(OH)_2$	4123	3938	–41	–39
HOH	1750	1698	–4	–4
$(HCl)_1$	2917	2800	–156	–147
$(HCl)_2$	2927	2809	–146	–138

TABLE 11. Intramolecular Frequencies of $HCl...(H_2O)_2$ (cm^{-1})

Assignment	ν (6-31G**)	ν_{cor}	Δν	$\Delta\nu_{cor}$
O_3H_4	3842	3673	–223	–210
O_3H_5	3947	3772	–217	–295
O_6H_7	4014	3835	–51	–48
O_6H_8	4113	3929	–51	–48
$H_8O_6H_7$	1727	1676	–42	–26
$H_5O_3H_4$	1729	1678	–25	–24
Cl_1H_2	2982	2861	–91	–86

220, 159 cm^{-1} (H...O...H); ν = 182 and 174 cm^{-1} associated with the proton-accepting molecule. The frequencies 175 and 169 cm^{-1} may be assigned to the torsion vibrations.

Complex 2 possessing an optimal configuration has the following frequencies of intermolecular vibrations (6-31G**): 61, 84, and 154 cm^{-1} for the stretching vibrations of $O_5–H_6...Cl$, $Cl_1–H_2...Cl_3$, and $O_5...H_4–Cl_3$; 285, 292, 314, 473, 523, 778, and 1264 cm^{-1} for the deformation vibrations of $Cl_1–H_2...Cl_3$, $Cl_1...H_6–O_5$, $Cl_3–H_4...O_5$, $H_7–O_5...H_4$, $H_4–O_5...H_6$, $H_2...Cl_3–H_4$, and $H_2–Cl_1...O_6$, respectively. The assignment of the deformation vibrations is slightly idealized because of the strong mixing of these modes (the assignment was done based on the maximal contribution to the corresponding normal vibration).

Complex 3 having an optimal structure corresponds to the following intermolecular frequencies (6-31G**): 87, 153, and 154 cm^{-1} for the stretching vibrations of $Cl_1...H_7–O_6$, $O_6...H_4–O_3$, and $O_3...H_2–Cl_1$; 304, 384, 421, 507, 617, 649, 917, and 1322 cm^{-1} for the deformation vibrations of $H_8–O_6...H_4$, $H_7–O_6...H_4$, $O_6...H_4–O_3$, $O_3...H_2–Cl_1$, $H_4–O_3...H_2$, $O_6–H_7...Cl_1$, $H_5–O_3...H_2$, and $H_2–Cl_1...H_7$, respectively.

In the systems under study, electronic excitation affects only one water molecule and is of mixed valence-Rydberg character. The $S_0 \rightarrow S_1$ and $T_0 \rightarrow T_1$ transitions for the complexes are characterized by increased excitation energies ε compared to the water monomer. For the $S_0 \rightarrow S_1$ transition: 8.68 eV [restricted Hartree–Fock (RHF) method], 8.2 eV [multiconfiguration interaction self-consistent field (MC SCF) method] for configuration 1 (σ→σ* type transition); 8.53 (RHF), 8.03 eV (MC CSF) for configuration 2 (σ→σ* type transition); 8.52 (RHF), 8.02 eV (MC CSF) for configuration 3 (σ→σ* type transition); for the $T_0 \rightarrow T_1$ transition: 7.89 (RHF), 7.4 eV (MC SCF) for configuration 1 (σ→σ* type transition), 7.79 (RHF), 7.3 eV (MC SCF) for configuration 2 (σ→σ* type transition); 7.83 (RHF), 7.33 eV (MC SCF) for configuration 3 (σ→σ* type transition). For the $H_2O...HCl$ heterodimer, the excitation energies ε of the $S_0 \rightarrow S_1$ and $T_0 \rightarrow T_1$ transitions are 8.39 (RHF), 7.7 (MC SCF), and 7.67 (RHF), 7.27 eV (MC SCF), respectively (π→σ* type transition).

CONCLUSIONS

The 1:2 intermolecular complexes $(H_2O)_n(HCl)_m$ have two configurations corresponding to the energy minimum: one is open and the other closed with interaction energies $\Delta E = -8.5$ and −7.64 kcal/mole, respectively. The 2:1 complex with two water molecules is a closed structure with $\Delta E = -11.1$ kcal/mole. For the corresponding complexes with a stronger hydrogen bond, $(H_2O)_n(HF)_m$, the interaction energies are (6-31G**): −14.79, −21.16, and −20.24 kcal/mole. For these

complexes, the closed (cyclic) structures are more stable. For the 1:2 water complexes with hydrogen chloride it was shown that cyclic structures are not always more stable.

The formation of the 1:2 and 2:1 complexes of H_2O and HCl leads to the following structural changes in the monomers: bond lengthening ~0.01 Å for HCl and ~0.01-0.02 Å for OH_b (involved in hydrogen bonding). For the Cl–H...O hydrogen bond, its deviation from the quasilinear bond compared to the H_2O...HCl heterodimer ($\theta \sim 179°$) is 9° (configuration 1), 14° (configuration 2), and 18° (configuration 3); the Cl–O...H bond is lengthened by ~0.1-0.2 Å.

Analysis of the harmonic vibration frequencies v for the complexes under study showed that the H–Cl stretching vibrations undergo a low-frequency shift ($\Delta\nu$): ~80 [H_2O...$(HCl)_2$, open form], ~150 [H_2O...$(HCl)_2$, closed form], and ~90 cm^{-1} [HCl...$(H_2O)_2$]. For H_2O...$(HCl)_2$ complexes, the O–H stretching vibration frequencies experience a minor low-frequency shift, ~20-40 cm^{-1}. A significant ''red'' shift, ~200 cm^{-1}, was observed for the O–H stretching frequencies for the HCl...$(H_2O)_2$ complex. (The corresponding shift for the water dimer $(H_2O)_2$ is ~112-175 cm^{-1} [39, 40]). Hydrogen bonding also leads to a new group of low-frequency intermolecular modes.

For the 1:2 and 2:1 $(H_2O)_n(HCl)_m$ complexes, hydrogen bonding results in longer HCl bonds and a significant long-wave shift of the band of HCl stretching vibrations.

For the 1:2 and 2:1 $(H_2O)_n(HCl)_m$ complexes, electron excitation during the $S_0 \rightarrow S_1$ and $T_0 \rightarrow T_1$ transitions leads to a displacement of the absorption band to the short-wave region.

This work was supported by RFFR grant No. 00-05-64919.

REFERENCES

1. T. R. Dyke, *Top. Curr. Chem.*, **120**, 85 (1984).
2. F. G. Celli and K. S. Janda, *Chem. Rev.*, **86**, 507 (1986).
3. R. E. Miller, *J. Phys. Chem.*, **90**, 3301 (1986).
4. E. Knözinger and O. Schrems, *Vibrational Spectra and Structure*, Vol. 16, J. R. During (ed.), Elsevier, Amsterdam (1987).
5. A. J. Barnes, *Molecular Interactions*, Vol. 1, H. Ratajczak and W. J. Orville-Thomas (eds.), Wiley, Chichester (1980), pp. 273-299.
6. A. J. Barnes, *J. Mol. Struct.*, **100**, 259 (1983).
7. J. Howard and T. C. Waddington, *Advances in Infrared and Raman Spectroscopy*, Vol. 7, R. H. Clark and R. E. Hester (eds.), Heyden, London (1980), p. 86.
8. B. T. M. Willes (ed.), *Chemical Applications of Thermal Neutron Scattering*, Oxford University, London (1973).
9. E. G. Tarakanova, F. Huisken, and M. Kaloudis, *12th Symposium and School on High-Resolution Molecular Spectroscopy*, L. N. Sinitsa (ed.), Proceedings of SPIE, Washington (1996), pp. 180-182.
10. A. C. Legon, J. Millen, S. L. A. Adebayo, et al., *J. Chem. Soc., Faraday Trans.*, **87**, 443 (1991).
11. A. C. Legon and J. Millen, *Chem. Soc. Rev.*, 71 (1992).
12. Y. Hannachi, B. Silvi, and Y. Bouteiller, *J. Chem. Phys.*, **94**, 2915 (1991).
13. I. Pak, L. A. Surin, D. A. Roth, et al., *Abstracts from the NATO Advanced Research Workshop Spectroscopy from Space*, Bratislava (2000), p. 47.
14. J. N. Harvey, J. O. Jung, and R. B. Gerber, *J. Chem. Phys.*, **109**, 8747-8750 (1998).
15. R. K. Thomas, *R. Soc. Lond. A*, **344**, 579-593 (1975).
16. A. C. Legon and L. C. Willoughby, *Chem. Phys. Lett.*, **95**, 37 (1983).
17. B. S. Ault and G. C. Pimentel, *J. Phys. Chem.*, **77**, 37 (1973).
18. G. P. Ayers and A. D. E. Pullin, *Spectrochim. Acta A*, **32**, 1641 (1976).
19. A. Shriver, B. Silvi, D. Maillard, and J. P. Perchard, *J. Chem. Phys.*, **81**, 2095 (1977).
20. Z. Latajka and S. Scheiner, *ibid.*, **87**, 5928-5936 (1987).
21. L. Zülicke, *Quantum Chemie* [Russian translation], Mir, Moscow (1972).
22. V. N. Lunichev, ''Structural specifics of nonrigid molecules with large nuclear displacements,'' Physical and Mathematical Sciences Candidate's Dissertation, Moscow (1979).
23. V. N. Lunichev, *Zh. Strukt. Khim.*, **20**, No. 1, 20-25 (1979).

24. M. R. Peterson and R. Poirer, *MONSTERGAUSS*, University of Totonto, Toronto. Memorial University of Newfoundland, Newfoundland (1990).
25. M. J. D. Powell, *Numerical Methods for Nonlinear Algebraic Equations*, P. Rabinowitz (ed.), Gordon and Breach (1970), p. 87.
26. L. P. Sukhanov, ''Theoretical study of physicochemical properties of light metal hydrides oligomers,'' Physical and Mathematical Sciences Candidate's Dissertation, Moscow (1983).
27. R. G. Pearson, *Symmetry Rules for Chemical Reactions*, Wiley, New York (1976).
28. Y. Yamaguchi and H. F. A. Schaefer III, *J. Chem. Phys.*, **73**, No. 5, 2310-2318 (1980).
29. R. F. Hout, B. A. Levi, and W. J. Hehre, *J. Comput. Chem.*, **3**, No. 2, 234-250 (1982).
30. M. J. Frisch, J. E. Del Bene, J. S. Binkley, and H. F. Schaefer III, *J. Chem. Phys.*, **84**, 2279 (1986).
31. K. Kitaura and K. Morokuma, *Int. J. Quant. Chem.*, **10**, 325-340 (1976).
32. K. Morokuma, *Acc. Chem. Res.*, **10**, 294-300 (1977).
33. K. Morokuma and K. Kitaura, in: *Chemical Applications of Atomic and Molecular Electrostatic Potentials*, P. Politzer and D. G. Truhlar (eds.), Plenum, New York (1981), pp. 215-242.
34. R. Cammi, R. Bonaccorsi, and J. Tomasi, *Theor. Chim. Acta*, **68**, 271-283 (1985).
35. A. J. Barnes and W. J. Orville-Thomas, *J. Mol. Spectrosc.*, **84**, 391 (1980).
36. T. Shimanouchi, *Tables of Molecular Vibration Frequencies*, Natl. Stand. Ref. Data Scr. Natl. Bur. Stand. No. 39, Vol. 1, National Bureau of Standards, Washington (1972).
37. J. E. Berti and M. V. Falk, *Can. J. Chem.*, **51**, 1713 (1973).
38. Z. Kisiel, A. C. Legon, and D. J. Millen, *Proc. R. Soc. Lond. A*, **381**, 419 (1982).
39. D. F. Coker, R. E. Miller, and R. O. Watts, *J. Chem. Phys.*, **82**, 3554-3562 (1985).
40. S. Wuelfert, D. Herren, and S. Leutwylen, *ibid.*, **86**, 3751-3753 (1987).
41. K. P. Huber and G. Herzberg, *Molecular Spectra and Molecular Structure*, Vol. 14, Van Nostrand Reinhold, New York (1979).
42. S. A. Clough, Y. Bears, G. P. Klein, and L. S. Rothman, *J. Chem. Phys.*, **59**, 2254 (1973).
43. F. H. Deleeuw and A. Dymanus, *J. Mol. Spectrosc.*, **48**, 427 (1973).
44. W. S. Benedict, W. Gailer, and E. K. Plyier, *J. Chem. Phys.*, **24**, 1139 (1956).
45. D. R. Stull and J. Prophet, *JANAF Thermochemical Tables*, Natl. Stand. Ref. Data Scr. Natl. Bur. Stand., Vol. 37, National Bureau of Standards, Washington (1971).

Russian Chemical Bulletin, International Edition, Vol. 52, No. 1, pp. 45—54, January, 2003 45

Structurally nonrigid molecular complexes $(HF)_n(H_2O)_m$ ($n + m \geq 2$) and their spectroscopic features

*N. A. Zvereva,[a] Sh. Sh. Nabiev,[b] Yu. N. Ponomarev,[c] and L. P. Sukhanov[b]**

[a] *Tomsk State University,*
36 prosp. Lenina, 634050 Tomsk, Russian Federation.
Fax: +7 (382 2) 23 3034. E-mail: zvereva@phys.tsu.ru
[b] *Russian Scientific Center "Kurchatov Institute",*
1 pl. I. V. Kurchatova, 123182 Moscow, Russian Federation.
Fax: +7 (095) 194 1994. E-mail: nabiev@imp.kiae.ru, sukhanov@imp.kiae.ru
[c] *Institute of Atmospheric Optics, Siberian Branch of the Russian Academy of Sciences,*
1 Akademicheskii prosp., 634055 Tomsk, Russian Federation.
Fax: +7 (382 2) 25 9086. E-mail: yupon@asd.iao.ru

The problem of the formation and stability of structurally nonrigid, donor—acceptor molecular complexes is considered. These complexes are formed between the molecules of water and hydrogen fluoride, the latter being the hydrolysis product of the chemical, radiochemical, and metallurgical industrial wastes. Based on the results of *ab initio* quantum-chemical calculations of the potential energy surfaces by the Hartree—Fock—Roothaan method, the equilibrium configurations of the $(H_2O)_n(HF)_m$ complexes ($n : m$ = 1 : 1; 1 : 2; 2 : 1; 2 : 2; and 3 : 3) were determined. These configurations are necessary for correct interpretation of the IR absorption spectra and for routine remote monitoring of such environmentally hazardous complexes in the Earth atmosphere. The harmonic vibrational frequencies of the $(H_2O)_n(HF)_m$ complexes ($n + m \geq 2$) were calculated and the interaction energies between the monomers were found. The influence of UV radiation on the $(H_2O)_n(HF)_n$ complexes (n = 1—3) upon the transition from the ground to the lowest excited singlet electronic state was studied. Characteristic spectroscopic features of the $(H_2O)_n(HF)_m$ complexes were established.

Key words: remote probing, lasers, atmosphere, structural nonrigidity, donor—acceptor molecular complexes, quantum-chemical calculations.

Solving problems of on-line monitoring of the gas and aerosol industrial discharges requires obtaining reliable information on the concentrations and molecular compositions of the discharges in the real-time mode. At present, remote probing methods based on the use of the near and mid-IR lasers are thought to be the most promising for this purpose.[1] Efficient use of these instruments as well as the development of physical foundations of novel probing techniques requires detailed information on the vibrational spectra of the radioactive and toxic discharge components. Chemically active antropogenic toxicants (fluorides, hydrides, *etc.*) can readily interact with the main molecular atmospheric gases and first of all with water vapor present in the Earth atmosphere in rather large amounts (0.02 to 4 mass.% at low altitude).[2]

In addition to the products of chemical transformations that can mainly occur involving the species present in relatively high concentrations, the donor—acceptor molecular complexes with the bonding energies varying from several tens of calories to several kilocalories can form under the atmospheric conditions.[3,4] The optical activity of such complexes can be rather high. Therefore, they can be responsible for additional radiation loss in the atmosphere in some industrial areas (*e.g.*, in the areas with a large number of chemical, radiochemical, electronic, and metallurgical productions, *etc.*) as well as for variations of the solar flux.[4] Usually, the gas-phase donor—acceptor complexes are characterized by a number of large-amplitude nuclear motions,[4—6] which alter their vibrational spectra (and parameters of the spectral components) and cause the appearance of new bands corresponding to intermolecular vibrations. In turn, these factors are responsible for severe difficulties when detecting and estimating the concentrations of the molecular complexes in the Earth atmosphere using modern remote probing techniques.

Earlier,[3—5] we have studied the spectrochemical aspects of the remote monitoring of accidental discharges on nuclear fuel cycle installations and on some productions that employ volatile fluorine-containing compounds

Published in Russian in *Izvestiya Akademii Nauk. Seriya Khimicheskaya,* No. 1, pp. 43—51, January, 2003.

1066-5285/03/5201-45 $25.00

including strong inorganic fluoro oxidants.[7,8] Analysis showed that the most toxic and chemically reactive components of the discharge plumes of the above-mentioned productions include UF_6, SiF_4, and interhalides like XF_3 and XF_5 (X = Cl, Br). At the same time, virtually all stages of hydrolysis of these compounds in the Earth atmosphere involve the formation of HF, which is one of the most environmentally hazardous antropogenic, minor gas component of the Earth atmosphere.[9]

Though the parameters of the HF molecule are well known[10] and are available from virtually all spectroscopic database systems (see, *e.g.*, Ref. 11), their use when solving problems of on-line laser monitoring of atmosphere is not always appropriate. This is due to the possibility for stable, structurally nonrigid complexes of general formula $(HF)_n(H_2O)_m$ $(n + m \geq 2)$ to be formed in the interaction between HF and H_2O.[3–5,8,12] The rovibrational spectra of such complexes can be appreciably different from those of pure HF and H_2O. The formation conditions of stable and long-lived (in the Earth atmosphere) complexes and the parameters of their absorption spectra, which can be employed in developing novel efficient methods for detecting these environmentally hazardous compounds, have virtually not been studied so far.

The aim of this work was to carry out a quantum-chemical study of the structure, stability, and vibrational spectra of the $(HF)_n(H_2O)_m$ complexes $(n + m \geq 2)$ and of the influence of UV radiation on such complexes on going from the ground to the lowest excited singlet electronic state.

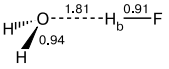

Fig. 1. Geometric parameters of $H_2O...HF$ complex (C_s symmetry) obtained from HFR/6-31G**calculations; E_{tot} = −176.0497 au, the H—O—H angle is 107° and the O—H_b—F angle is 176°. The internuclear distances are given in Å; H_b is the bridging hydrogen atom.

Calculation Procedure

The potential energy surfaces (PES) of the $(HF)_n(H_2O)_m$ complexes were calculated by the Hartree—Fock—Roothaan (HFR) method using the MONSTERGAUSS [13] and GAUSSIAN-98 [14] program packages which were adapted for personal computers with Pentium® CPUs. The 6-31G** split valence basis set (see, *e.g.*, Ref. 15) employed in this work includes the outer polarization d-functions on the F and O atoms and p-functions on H atoms.

The calculated geometric parameters and energy characteristics of the HF and H_2O molecules and of the $H_2O...HF$ complex with C_s symmetry in the configuration corresponding to the absolute minimum on the PES (Fig. 1) are listed in Table 1. The harmonic vibrational frequencies of the monomers and the complex calculated with an increment of ±0.1 au along the vibrational coordinates are listed in Table 2. For comparison, Tables 1 and 2 also list the experimental values and the results of more precise calculations performed using the Møller—Plesset (MP) perturbation theory with inclusion of electron correlation effects.

As can be seen from the data in Table 1, the calculated equilibrium internuclear distances and the H—O—H bond angle in the monomer molecules differ from the experimental values

Table 1. Geometric parameters and energy characteristics of the HF and H_2O monomers and $H_2O...HF$ complex calculated by different methods and corresponding experimental values[a]

Molecule	Symmetry	Computational method	ΔE /kcal mol^{-1}	R_e/Å			Angle/deg		
				H_b—F	O—H	O—F	H—O—H	α	H_b—F—O
HF	$C_{\infty v}$	HFR/6-31G**[b]	—	0.90	—	—	—	—	—
		Experiment[16]	—	0.92	—	—	—	—	—
H_2O	C_{2v}	HFR/6-31G**[b]	—	—	0.94	—	106	—	—
		Experiment[17]	—	—	0.96	—	105	—	—
$H_2O...HF$	C_s	HFR/6-31G**[b]	9	0.91	0.94	2.72	107	134	4
		MP2/6-31G**[b]	11	0.93	0.96	2.67	105	131	6
		MP2/6-311G**[18]	11	0.92	0.96[c]	2.64	105[c]	129	5
		MP3/6-311G**[18]	11	0.92	0.96[c]	2.65	105[c]	133	3
		Experiment[18,19]	—	—	—	2.66	—	134	—
		MP4/6-311+G(2d,2p)[20]	9[d]	0.92[d]	—	2.72[d]	—	—	5[d]
		Experiment[21]	10	—	—	—	—	—	—

[a] For the atomic numbering scheme, see Fig. 1; ΔE is the bonding energy of monomers in the complex; and α is the angle between the O—F axis and the bisectrix of the H—O—H angle.
[b] This work.
[c] Calculations[18] at the second- and third-order Møller—Plesset level of perturbation theory (MP2 and MP3, respectively) were carried out with the experimental[17] geometric parameters of the H_2O molecule.
[d] Obtained from calculations at the fourth-order Møller—Plesset level of perturbation theory (MP4) performed with the geometric parameters optimized by the HFR/6-31G* method.

Table 2. Harmonic vibrational frequencies (ω_i/cm^{-1}) of the HF and H_2O monomers and H_2O...HF complex

H_2O...HF			H_2O			HF		
Calculation[a]	Experiment[22]	Assignment[b]	Calculation[a]	Experiment[17]	Assignment[b]	Calculation	Experiment[16]	Assignment[b]
4270	3608±2	ν(H_bF)	4265 [a]	3939	ν^{as}(OH)	4493 [a]	4138	ν(HF)
4258	3756	ν^{as}(OH)	4052 [c]	—	—	4212 [c]	—	—
4142	3657	ν^{s}(OH)	4010 [d]	—	—	4119 [d]	—	—
1765	1595	δ(HOH)	4148 [a]	3835	ν^{s}(OH)	—	—	—
760	696±30	$\delta_i(OH_bF)$	3909 [c]	—	—	—	—	—
626	666±30	$\delta_o(OH_bF)$	3863 [d]	—	—	—	—	—
236	180±30	ν($H_2O...H_bF$)	1770 [a]	1648	δ(HOH)	—	—	—
206	145±50	$\delta_o(HOH_b)$	1674 [c]	—	—	—	—	—
194	170±50	$\delta_i(HOH_b)$	1620 [d]	—	—	—	—	—

[a] This work.
[b] The frequencies (ν)[22] of fundamental transitions are reported for the complex (see Fig. 1). Notations: ν^s and ν^{as} are the symmetrical and asymmetrical stretching vibrations, respectively, and δ denotes the deformation vibrations in plane (δ_i) and out of plane (δ_o) of the H_2O molecule.
[c] Obtained from our MP2/6-31G** calculations.
[d] Obtained from MP2/6-31++G** calculations.[23]

by at most 0.02 Å and 1°, respectively. The harmonic vibrational frequencies of the monomers (see Table 2) are overestimated (up to 9%) compared to the experimental values. Partial inclusion of electron correlation at the second-order Møller—Plesset (MP2) level of perturbation theory reduces the frequencies and the differences between the calculated and experimental data down to 2%. This agreement between the calculated molecular constants of the monomers and the corresponding experimental values allows the 6-31G** basis set to be used in theoretical studies of the molecular characteristics of the H_2O...HF complex.

Analysis of the data listed in Table 1 and comparison of the results of our calculations of the $H_2O...(HF)_2$ and $HF...(H_2O)_2$ complexes with the corresponding data obtained from more precise MP2 calculations[23] showed that the computational method employed in this work (HFR/6-31G**) for theoretical studies of the $(HF)_n(H_2O)_m$ complexes provides the errors of at most 0.01—0.04 Å for the equilibrium bond lengths in the monomers, 0.05—0.10 Å for the hydrogen bond lengths, 2—10 degrees for the bond angles and dihedral angles, and 1—2 kcal mol^{-1} for the complexation energies. The harmonic vibrational frequencies (ω_i) of the H_2O...HF complex calculated in this work (see Table 2) are, as a rule, overestimated up to 18 and 42% compared to the experimental frequencies of fundamental transitions (ν_i) corresponding to intramolecular and intermolecular modes, respectively.[22] Anharmonicity of the molecular vibrations, which contributes to the frequencies of the fundamental transitions, introduces an additional contribution to an increase in discrepancies with the calculated harmonic frequencies and is significant when describing the vibrational spectra of loosely bound hydrogen-bonded complexes.

The stationary points on the PES of the complexes under study were located using full geometry optimization by the Broiden—Fletcher—Goldfarb—Shanno[24] and using a combination of the Newton—Raphson methods.[25] Calculations were carried out until a total energy gradient of $5 \cdot 10^{-4}$ hartree Bohr^{-1}. This allowed calculations with an accuracy of 0.001 Å for the equilibrium internuclear distances, 3 degrees for the bond angles and dihedral angles, 0.001 kcal mol^{-1} for the complexation energies, and ~1 cm^{-1} for harmonic vibrational frequencies. This accuracy of the geometry optimization can be considered reasonable taking into account rather large errors of determination of the parameters of the complexes under study due to incompleteness of the basis set employed and to neglect of electron correlation effects in the HFR computational procedure.

The energies (ε) of the $S_0 \rightarrow S_1$ vertical electronic transitions were calculated by the restricted Hartree—Fock method for open-shell systems[26—29] from the total energy differences between the complex in the first excited singlet state, $E_{tot}(S_1)$, and in the ground singlet state, $E_{tot}(S_0)$. The excited electronic state S_1 corresponds to transition of an electron from the highest occupied MO, φ_{occ}, of the ground state S_0 to the lowest unoccupied MO, φ_{vac}, with retention of symmetry of the spin function. The ε values calculated for the HF and H_2O monomers (9.7 and 7.8 eV, respectively) are in good agreement with the experimental data[30] (10±0.2 and 7.4 eV, respectively). This allowed the use of the computational procedure described above for studying the influence of UV radiation on such complexes in the spectral region corresponding to electronic transitions between the lowest singlet states.

Results and Discussion

The first experimental IR study[22] revealed the existence of the $(H_2O)_n(HF)_m$ complexes (n, $m \geq 2$) at high pressures; however, measurements were carried out only for the H_2O...HF (1 : 1) complex. The enthalpy of complex formation, $\Delta H°_{298}$, was estimated at −6.2 kcal mol^{-1},[22] which corresponds to the dissociation energy D_0 = −5.5 kcal mol^{-1} and to the total dissociation energy D_e = −7.1 kcal mol^{-1}. Here $|D_e| = |D_0| + \Delta\varepsilon_0$, where $\Delta\varepsilon_0 = (\varepsilon_0(H_2O...HF) - \varepsilon_0(H_2O) - \varepsilon_0(HF))$ is the zero-point vibrational energy correction for the complex and the

monomers. Further microwave spectroscopy studies[31—33] of thermodynamically equilibrated $H_2O...HF$ gas hydrate ($n(H_2O) = 1.85 \cdot 10^{19}$, $n(HF) = 6.66 \cdot 10^{20}$, $n(H_2O...HF) = 10.03 \cdot 10^{15}$ m^{-3}) showed that the dissociation energy, D_0, equals −8.1 kcal mol^{-1}. The estimate of the total dissociation energy ($D_e = -10.2$ kcal mol^{-1}) is in good agreement with the results of *ab initio* quantum-chemical calculations[20] (−8.8 kcal mol^{-1}). It should be noted that the latter value is much higher than that obtained from the IR spectra (−7.1 kcal mol^{-1}),[22] whereas the formation enthalpy of the complex obtained from the IR spectroscopic study insignificantly differs from the calculated value[20] ($\Delta H°_{298} = -6.2$ and −7.4 kcal mol^{-1}, respectively).

The IR spectrum of a HF—H_2O mixture in an Ar matrix at 12 K revealed[34] the presence of three different types of hydrogen-bonded complexes, namely, $H_2O...(HF)_2$, $H_2O...HF$, and HF...HOH (listed in the order of increasing stability). Despite the lack of experimental data, the existence of the $(H_2O)_2...HF$ complex was suggested based on the observation of a strong absorption band in the IR spectrum in the region corresponding to vibrations of the $(H_2O)_2$ dimer.[34]

A systematic theoretical study[23] of the structure, stability, and IR spectra of the $H_2O...(HF)_2$ and $(H_2O)_2...HF$ complexes allowed the determination of a total of three stable equilibrium structures among all possible configurations of these complexes. However, the existence of the HF...HOH complex was not established.

In this work we carried out *ab initio* HFR quantum-chemical calculations of the following molecular systems: $H_2O...HF$, $H_2O...(HF)_2$, $(H_2O)_2...HF$, $(H_2O...HF)_2$, and $(H_2O...HF)_3$.

Stability of $(H_2O)_n(HF)_m$ complexes. The geometry of the $H_2O...HF$ complex (C_s symmetry) characterized by a bonding energy, ΔE, of 9 kcal mol^{-1} (see Table 3) and corresponding to the absolute minimum on the PES is shown in Fig. 1. According to our calculations, the energy of the planar structure of this complex with a linear hydrogen bond (C_{2v} symmetry) is 0.05 kcal mol^{-1} higher (*cf.* 0.13 kcal mol^{-1} obtained from the HFR calculations[18] with the extended 6-311G** basis set and 0.49 and 0.41 kcal mol^{-1} according to calculations[18] performed with the same basis set and inclusion of electron correlation by the MP2 method and at the third-order Møller—Plesset (MP3) level of perturbation theory, respectively).

For the $H_2O...(HF)_2$ complex our calculations predict two stable configurations ($\Delta E = 15$ and 21 kcal mol^{-1}, see Table 3) corresponding to the open and cyclic structures (Fig. 2, *a*, *b*). This is in excellent agreement with the published results.[23] The cyclic configuration of the $H_2O...(HF)_2$ complex is more stable.

Similarly to the earlier study,[23] the $(H_2O)_2...HF$ complex corresponds to the cyclic structure (Fig. 2, *c*) with $\Delta E = 20$ kcal mol^{-1} (see Table 3). The cyclic structure of the $(H_2O)_2(HF)_2$ complex (Fig. 3) is characterized by $\Delta E = 33$ kcal mol^{-1} (see Table 3), while the $(H_2O)_3(HF)_3$ complex can be formed as both the chain structure with $\Delta E = 36$ kcal mol^{-1} (Fig. 4) and as the cyclic structure with $\Delta E = 55$ kcal mol^{-1} (Fig. 5, see Table 3). Attempts at locating other local minima corresponding to the positive-definite matrix of the second derivatives of the total energy on the PES of the 2 : 1, 2 : 2, and 3 : 3 complexes failed. As follows from Table 3 and Fig. 1—5, the cyclic structure of the $(H_2O)_3...(HF)_3$ complex is the most stable among all configurations of the $(H_2O)_n(HF)_m$ complexes ($n + m \geq 2$) studied in this work from the standpoint of the bonding energy per H-bond.

More detailed analysis of the data listed in Table 3 showed that all the $(H_2O)_n(HF)_m$ complexes, except for the chain configuration of the $(H_2O)_3(HF)_3$ complex (see Fig. 4), are energetically stable toward all types of gas-phase monomolecular decomposition. The chain structure of the $(H_2O)_3(HF)_3$ complex is unstable toward the decomposition into the 2 : 2, 1 : 1, 2 : 1, and 1 : 2 complexes. Nevertheless, as will be shown below, this

Table 3. Monomolecular decomposition energies (ΔE) of the $(H_2O)_n(HF)_m$ complexes, obtained from HFR/6-31G** calculations

Complex	Decomposition products	ΔE /kcal mol^{-1}
$(H_2O)(HF)$	$H_2O + HF$	9
$(H_2O)(HF)_2$	$(H_2O)(HF) + HF$	12
	$H_2O + 2\ HF$	21
$(H_2O)_2(HF)$	$(H_2O)(HF) + H_2O$	11
	$2\ H_2O + HF$	20
$(H_2O)_2(HF)_2$	$(H_2O)(HF)_2 + H_2O$	12
	$(H_2O)_2(HF) + HF$	12
	$2\ (H_2O)(HF)$	15
	$(H_2O)(HF) + H_2O + HF$	24
	$2\ H_2O + 2\ HF$	33
$(H_2O)_3(HF)_3$	$(H_2O)_2(HF)_2 + (H_2O)(HF)$	14
	$(H_2O)_2(HF)_2 + H_2O + HF$	23
	$(H_2O)_2(HF) + (H_2O)(HF)_2$	14
	$(H_2O)_2(HF) + (H_2O)(HF) + HF$	26
	$(H_2O)_2(HF) + H_2O + 2\ HF$	35
	$(H_2O)(HF)_2 + (H_2O)(HF) + H_2O$	25
	$(H_2O)(HF)_2 + 2\ H_2O + HF$	34
	$3\ (H_2O)(HF)$	28
	$2\ (H_2O)(HF) + H_2O + HF$	37
	$(H_2O)(HF) + 2\ H_2O + 2\ HF$	46
	$3\ H_2O + 3\ HF$	55

Note. The energy, ΔE, of the decomposition reaction $A \rightarrow \sum_i A_i$ is given by the formula $\Delta E = \sum_i E_{tot}(A_i) - E_{tot}(A)$, where $E_{tot}(A)$ and $E_{tot}(A_i)$ are the total energies of the complex, A, and the decomposition products, A_i, in the lowest energy configurations; $E_{tot}(H_2O) = -76.0236$ au and $E_{tot}(HF) = -100.0117$ au. For the total energies of other molecular systems, see Notes to Figs. 1—5.

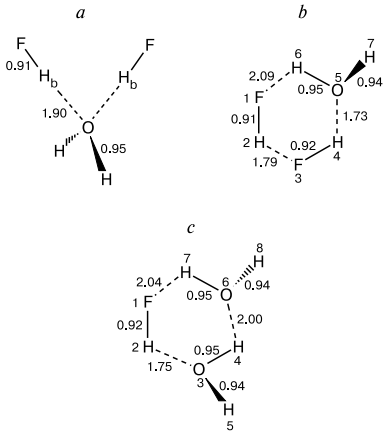

Fig. 2. Geometric parameters of the complexes $H_2O...(HF)_2$ with C_{2v} symmetry (*a*), $H_2O.....(HF)_2$ with C_1 symmetry (*b*), and $(H_2O)_2.....HF$ with C_1 symmetry (*c*), obtained from HFR/6-31G** calculations. The internuclear distances are given in Å. The values of the angles (ω) are listed below.

Complex (symmetry) [$-E_{tot}$/au]	Angle	ω/deg
$H_2O...(HF)_2$	F—H_b—O	166
(C_{2v})	H_b—O—H_b	115
[276.0706]	H—O—H	107
$H_2O.....(HF)_2$	H(6)—O(5)—H(4)	98
(C_1)	H(2)—F(3)—H(4)	93
[276.0807]	F(3)—H(4)—O(5)	154
	F(1)—H(2)—F(3)	150
	H(6)—O(5)—H(7)	107
	H(4)—O(5)—H(7)	123
	H(4)—F(3)—H(2)—F(1)	−2
	O(5)—H(4)—F(3)—H(2)	0
	H(6)—O(5)—H(4)—F(3)	−3
	H(7)—O(5)—H(4)—F(3)	114
$(H_2O)_2.....HF$	F(1)—H(2)—O(3)	158
(C_1)	H(2)—O(3)—H(4)	95
[252.0912]	O(3)—H(4)—O(6)	144
	H(7)—O(6)—H(4)	91
	H(2)—O(3)—H(5)	120
	H(8)—O(6)—H(4)	124
	H(5)—O(3)—H(4)	107
	H(7)—O(6)—H(8)	107
	H(4)—O(3)—H(2)—F(1)	−4
	O(6)—H(4)—O(3)—H(2)	5
	H(8)—O(6)—H(4)—O(3)	−113
	H(5)—O(3)—H(2)—F(1)	109
	H(7)—O(6)—H(4)—O(3)	−2

configuration also corresponds to a minimum on the PES and the harmonic force constant matrix is positive-definite in the vicinity of this point. It should also be noted

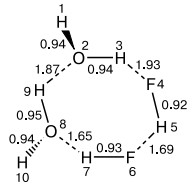

Fig. 3. Geometry of $(H_2O...HF)_2$ complex with C_1 symmetry calculated by the HFR/6-31G** method; $E_{tot} = -352.1227$ au. The internuclear distances are given in Å. The values of the angles (ω) are listed below.

Angle	ω/deg	Angle	ω/deg
H(1)—O(2)—H(3)	108	H(1)—O(2)—H(3)—F(4)	115
H(9)—O(8)—H(10)	110	H(5)—F(4)—H(3)—O(2)	15
O(2)—H(3)—F(4)	161	F(6)—H(5)—F(4)—H(3)	1
F(4)—H(5)—F(6)	167	H(7)—F(6)—H(5)—F(4)	0
F(6)—H(7)—O(8)	166	O(8)—H(7)—F(6)—H(5)	1
H(3)—F(4)—H(5)	106	H(9)—O(8)—H(7)—F(6)	−6
H(5)—F(6)—H(7)	106	H(10)—O(8)—H(9)—O(2)	−47
H(7)—O(8)—H(9)	116		

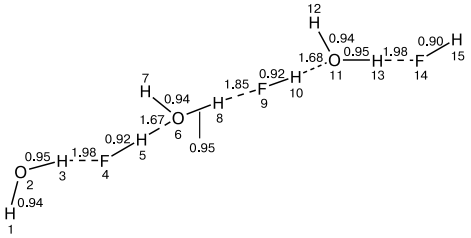

Fig. 4. Geometric parameters of the chain configuration of the $(H_2O...HF)_3$ complex with C_1 symmetry, obtained from HFR/6-31G** calculations; $E_{tot} = -528.1632$ au. The internuclear distances are given in Å. All torsion angles are equal to 0 and 180°. The values of other angles (ω) are listed below.

Angle	ω/deg	Angle	ω/deg
H(1)—O(2)—H(3)	106	H(8)—F(9)—H(10)	133
O(2)—H(3)—F(4)	169	F(9)—H(10)—O(11)	180
H(3)—F(4)—H(5)	122	H(10)—O(11)—H(12)	129
F(4)—H(5)—O(6)	180	H(12)—O(11)—H(13)	108
H(5)—O(6)—H(7)	127	O(11)—H(13)—F(14)	180
H(7)—O(6)—H(8)	108	H(13)—F(14)—H(15)	140
O(6)—H(8)—F(9)	180		

that the elimination energies of the H_2O and HF monomers from the 1 : 2, 2 : 1, and 2 : 2 complexes virtually coincide, being somewhat higher than the bonding energy in the $H_2O...HF$ heterodimer.

Structural features of some $(H_2O)_n(HF)_n$ complexes. The following trends of changes in the structural param-

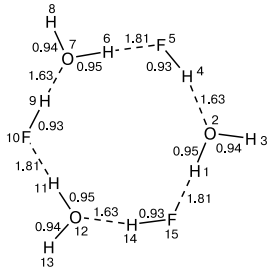

Fig. 5. Geometric parameters of the cyclic configuration of the $(H_2O...HF)_3$ complex with C_1 symmetry according to HFR/6-31G** calculations; E_{tot} = −528.1943 au. The internuclear distances are given in Å. All torsion angles are equal to 0 and 180°. The values of other angles (ω) are listed below.

Angle	ω/deg	Angle	ω/deg
H(1)—O(2)—H(3)	108	F(10)—H(9)—O(7)	178
H(4)—O(2)—H(3)	126	H(11)—F(10)—H(9)	116
F(5)—H(4)—O(2)	177	O(12)—H(11)—F(10)	179
H(6)—F(5)—H(4)	116	H(13)—O(12)—H(11)	108
O(7)—H(6)—F(5)	178	H(14)—O(12)—H(13)	126
H(8)—O(7)—H(6)	108	F(15)—H(14)—O(12)	177
H(9)—O(7)—H(8)	126		

eters of the $(H_2O)_n(HF)_n$ complexes (n = 1—3) can be pointed out. The H_b—F bond is lengthened by 0.01 Å (n = 1) and by 0.02—0.03 Å (n = 2, 3) compared to the equilibrium bond length in free HF molecule (see Table 1, Figs. 1, 3—5). The like H-bonds (O...H_b) are 0.16 Å (n = 2) and 0.13—0.18 Å (n = 3) shorter than in the $H_2O...HF$ complex. A feature of the cyclic structure (n = 2) is appreciable deviation of the F—H_b...O angle from 180° (by 14°) whereas this parameter for the $H_2O...HF$ complex is ~4°. The F—H_b...O angle is 180° in the chain structure of the complex with n = 3 while differs from this value only by 2—3° in the cyclic structure. In all complexes the O—H bond involving the terminal H atom of the H_2O molecule has the same length (0.94 Å). The maximum elongation of the bridging O—H_b bond compared to its analog in free H_2O molecule is 0.01 Å (n = 2, 3).

Vibrational spectra of $(H_2O)_n(HF)_m$ complexes. As mentioned above, the harmonic vibrational frequencies (ω_i) calculated in this work differ (sometimes appreciably) from the corresponding experimental frequencies (ν_i) of fundamental vibrational transitions. These discrepancies are due to both the errors of the HFR method when calculating the ω_i values and to the large anharmonicity contribution to the vibrational frequencies of H-bonded complexes. An efficient model has been proposed and theoretically substantiated,[35] which provides a rather accurate and simple procedure for the inclusion of the contribution of the anharmonicity corrections to the stretching vibration frequencies (ν_i) of the Y monomer which forms a $H_2O...Y$ complex with a quasi-linear hydrogen bond in the Earth atmosphere. In this work, the vibrational frequencies were corrected using the linear calibration function

$$\nu_{corr} = b\omega_{calc} + a, \quad (1)$$

where ω_{calc} and ν_{corr} are the calculated harmonic and corrected vibrational frequencies, respectively, and a and b are the calibration coefficients that can be found by the least-squares method using the experimental[22] and calculated data for the $H_2O...HF$ complex. The coefficients b and a were found to be 0.84 and 108 cm^{-1}, respectively, while the correlation coefficient between the experimental and calculated frequencies was 0.998.

Table 4 lists the experimental and calculated vibrational frequencies used in the fitting of the a and b coefficients and corresponding to intramolecular modes of the $H_2O...HF$ complex (see Fig. 1). The mean absolute deviation of ν_{corr} from ν_{exp} was 58 cm^{-1}. The harmonic vibrational frequencies of the HF molecule and the HF fragment of the $H_2O...HF$ complex obtained from HFR calculations differ by 223 cm^{-1} (see Table 2, *cf.* a value of 351 cm^{-1} obtained from the experimental[16,22] frequencies). Thus, calculations in the HFR/6-31G** approximation underestimate the shift of the vibrational frequency of the HF monomer upon the formation of the F—H...O hydrogen bond by 130 cm^{-1}. A complete set of the vibrational frequencies of the $H_2O...HF$ complex is listed in Table 2.

In Table 5 we present the calculated intramolecular frequencies ω_i and $\nu_{i,corr}$ and the results of MP2 calculations[23] of the $H_2O...(HF)_2$ and $(H_2O)_2...HF$ complexes. Given for the cyclic structure of the $H_2O...(HF)_2$ complex are also the results of study,[36] the authors of which used a semiempirical model in the method of the F—G matrix using the experimental data. The vibrational frequencies $\nu_{i,corr}$ obtained in this work are in reasonable agreement with the results of the earlier study[36] and of the IR spectroscopic study[34] of a HF—H_2O mixture in the low-temperature Ar matrix. The vibrational frequencies corresponding to the intermolecular modes of the $(H_2O)_n(HF)_m$ complexes ($n : m$ = 2 : 1; 1 : 2) are listed in

Table 4. Experimental[22] (ν_{exp}) and calculated intramolecular vibrational frequencies (cm^{-1}) of $H_2O...HF$ complex (see Fig. 1)

ω_{calc}	ν_{exp}[22]	ν_{corr}	Assignment*
4270	3608	3695	$\nu(H_bF)$
4258	3756	3685	$\nu^{as}(OH)$
4142	3657	3587	$\nu^{s}(OH)$
1765	1595	1591	δ(HOH)

Note. For notations of vibrations, see note[b] to Table 2.

Table 5. Intramolecular vibrational frequencies (cm^{-1}) of the $H_2O...(HF)_2$ complex with the chain (see Fig. 2, *a*) and cyclic (see Fig. 2, *b*) structures and those of the $(H_2O)_2...HF$ complex (see Fig. 2, *c*)

Complex (symmetry)	ω_i		$\nu_{i,\mathrm{corr}}$ [a]	Assignment
	I [b]	II [c]		
$(H_2O)\cdot(HF)_2$	1765 (121)	1636 (98)	1591	δ(HOH) (A_1)
(C_{2v})	4120 (81)	3820 (160)	3567	ν(OH) (A_1)
	4230 (152)	3851 (1066)	3661	ν(OH) (B_1)
	4331 (839)	3897 (229)	3746	$\nu(H_bF)$ (B_2)
	4357 (142)	3957 (144)	3768	$\nu(H_bF)$ (A_1)
$(H_2O)\cdot(HF)_2$	1777 (112)	1646 (89)	1601	$\delta(H_6O_5H_7)$
(C_1)	4024 (555)	3374 (1111)	3488 [3329, 3272] [d]	$\nu(H_4F_3)$
	4103 (190)	3807 (168)	3555 [3590] [d]	$\nu(O_5H_6)$
	4228 (154)	3823 (465)	3660 [3715] [d]	$\nu(O_5H_7)$
	4268 (544)	3969 (154)	3693 [3703, 3690] [d]	$\nu(H_2F_1)$
$(H_2O)_2\cdot HF$	1785 (142)	1640 (154)	1607	δ(HOH)
(C_1)	1788 (77)	1653 (21)	1610	δ(HOH)
	4018 (166)	3440 (1001)	3483	ν(HF)
	4084 (494)	3703 (345)	3539	ν(HO)
	4115 (385)	3805 (117)	3565	ν(HO)
	4229 (122)	3954 (129)	3660	ν(HO)
	4239 (143)	3974 (126)	3669	ν(HO)

[a] Listed are the frequencies of fundamental vibrational transitions corrected using formula (1).
[b] This work; listed are the harmonic frequencies, ω_i, and the transition intensities in the IR spectra (in km mol^{-1}) calculated by the HFR/6-31G** method (figures in parentheses).
[c] Harmonic frequencies, ω_i, and transition intensities in the IR spectra (in km mol^{-1}) obtained from MP2/6-31++G** calculations[23] (figures in parentheses).
[d] Given in square brackets are the vibrational frequency obtained in the framework of the semiempirical model[36] using the F—G matrix method followed by the frequency found in the IR spectroscopic study[34] of a HF—H_2O mixture in Ar matrix at 12 K.

Table 6. Intermolecular harmonic vibrational frequencies (ω_i) of $H_2O\cdot(HF)_2$ and $(H_2O)_2\cdot HF$ complexes

Complex (symmetry)	ω_i/cm^{-1}		Complex (symmetry)	ω_i/cm^{-1}	
	I [a]	II [b]		I [a]	II [b]
$H_2O\cdot(HF)_2$	691 (65)	782 (390)	$H_2O\cdot(HF)_2$	266 (6)	275 (15)
(C_{2v})	690 (349)	753 (0)	(C_1)	236 (103)	218 (94)
	647 (238)	712 (253)		223 (7)	209 (4)
	592 (362)	653 (296)		162 (11)	111 (17)
	250 (114)	314 (85)	$(H_2O)_2\cdot HF$	1017 (115)	1077 (162)
	199 (23)	231 (0)	(C_1)	805 (359)	903 (274)
	175 (0)	212 (1)		644 (264)	658 (249)
	167 (3)	184 (0)		544 (322)	500 (189)
	100 (0)	144 (1)		374 (72)	388 (72)
	32 (12)	33 (10)		299 (13)	326 (69)
$H_2O\cdot(HF)_2$	1055 (121)	1117 (144)		260 (90)	293 (111)
(C_1)	805 (409)	902 (300)		258 (5)	266 (5)
	669 (378)	654 (344)		202 (2)	215 (11)
	548 (91)	583 (99)		175 (188)	196 (164)
	522 (240)	477 (204)		159 (8)	127 (11)
	334 (60)	355 (82)			

[a] See note[b] to Table 5.
[b] See note[c] to Table 5.

Table 6. The vibrational frequencies corresponding to the intra- and intermolecular modes of the $(H_2O...HF)_2$ complex calculated in this work are listed in Tables 7 and 8, respectively.

Table 7. Intramolecular vibrational frequencies (in cm^{-1}) of $(H_2O)_2...(HF)_2$ complex (see Fig. 3)

ω_i[a]	$\nu_{i,corr}$[b]	Assignment
1764 (147)	1590	δ(HOH)
1776 (62)	1600	δ(HOH)
3844 (1038)	3337	ν(HF)
4009 (422)	3476	ν(HO)
4139 (526)	3585	ν(HF)
4171 (385)	3612	ν(HO)
4256 (50)	3683	ν(HO)
4263 (38)	3689	ν(HO)

[a] See note[b] to Table 5.
[b] See note[a] to Table 5.

Table 8. Intermolecular harmonic vibrational frequencies (ω_i/cm^{-1}) of the $(H_2O)_2...(HF)_2$ and $(H_2O)_3...(HF)_3$ complexes in the chain and cyclic configurations and the band intensities in the IR spectra (A/km mol^{-1}), obtained from HFR/6-31G** calculations

Complex (symmetry, configuration)	ω_i	A	Complex (symmetry, configuration)	ω_i	A
$(H_2O)_2 \cdot (HF)_2$	39	56	$(H_2O)_3 \cdot (HF)_3$	411	0
(C_1)	52	51	(C_1, chain	471	27
	99	70	configuration,	479	174
	162	106	see Fig. 4)	653	90
	185	1		687	127
	214	9		717	455
	240	18		916	259
	249	76		956	184
	293	27	$(H_2O)_3 \cdot (HF)_3$	30	0
	408	83	(C_1, cyclic	30	0
	491	137	configuration,	39	3
	636	77	see Fig. 5)	51	4
	728	97		51	4
	762	400		104	0
	853	341		147	0
	1099	215		199	44
$(H_2O)_3 \cdot (HF)_3$	12	10		200	44
(C_1, chain	19	6		229	450
configuration,	20	1		240	0
see Fig. 4)	23	2		240	0
	43	0		308	4
	74	3		308	4
	86	13		339	0
	115	308		386	0
	128	1		447	46
	154	21		448	47
	168	147		518	0
	193	109		518	0
	222	170		548	356
	247	105		751	0
	277	11		751	0
	306	3		777	778
	347	39		1003	199
	370	145		1003	299
	402	52		1003	0

Table 9. Intramolecular vibrational frequencies (in cm^{-1}) of the chain configuration of $(H_2O)_3...(HF)_3$ complex (see Fig. 4)

ω_i[a]	$\nu_{i,corr}$[b]	Assignment
1779 (87)	1602	δ(HOH)
1804 (204)	1623	δ(HOH)
1811 (6)	1629	δ(HOH)
3919 (1012)	3400	ν(HO)
4006 (1180)	3473	ν(HF)
4012 (586)	3478	ν(HF)
4123 (137)	3571	ν(HO)
4144 (129)	3589	ν(HO)
4256 (98)	3683	ν(HO)
4266 (102)	3691	ν(HO)
4274 (213)	3698	ν(HO)
4453 (209)	3849	ν(HF)

[a] See note[b] to Table 5.
[b] See note[a] to Table 5.

Table 10. Intramolecular vibrational frequencies (in cm^{-1}) of the cyclic configuration of $(H_2O)_3...(HF)_3$ complex (see Fig. 5)

ω_i[a]	$\nu_{i,corr}$[b]	Assignment
1802 (146)	1622	δ(HOH)
1802 (145)	1622	δ(HOH)
1810 (0)	1628	δ(HOH)
3829 (0)	3324	ν(HF)
3889 (2291)	3375	ν(HF)
3889 (2291)	3375	ν(HF)
4074 (345)	3530	ν(HO)
4074 (346)	3530	ν(HO)
4077 (0)	3533	ν(OH)
4262 (211)	3688	ν(OH)
4261 (212)	3687	ν(OH)
4262 (1)	3688	ν(OH)

[a] See note[b] to Table 5.
[b] See note[a] to Table 5.

Analysis of the data presented in Tables 2, 4, 5, 7, 9, and 10 revealed an appreciable low-frequency shift of the stretching vibration frequencies of the HF monomer upon the formation of hydrogen-bonded complexes $(H_2O)_n(HF)_m$. This shift varies from 223 cm^{-1} for the heterodimer up to 664 cm^{-1} for the cyclic configuration of the $(H_2O...HF)_3$ complex (see Table 10).

Electronic transitions between the lowest singlet states of $(H_2O)_n(HF)_n$ complexes. Analysis of the electron density redistribution on the atoms of the complexes under study upon the $S_0 \rightarrow S_1$ electronic excitation showed that the excitation is, as a rule, localized on one of the water molecules constituting a particular complex. The shape of the cross-section of the PES along the R(O—H) coordinate in the H_2O molecule on which the excitation is localized clearly indicates the dissociation character of the

$E(S_1)$ electronic term.[5] The photodissociation character of the $\tilde{A}^1B_1$ state corresponding to the first absorption band of the water monomer ($\lambda \approx 165$ nm) is well known.[30,37]

$$H_2O\,(\tilde{X}^1A_1) + h\nu \longrightarrow H_2O\,(\tilde{A}^1B_1) \longrightarrow$$
$$\longrightarrow H\,(^2S) + OH\,(\tilde{X}^2\Pi) \qquad (2)$$

The complexes under study exhibit a Rydberg character of the S_1 electronic state (as in the case of water monomer). The $S_0 \rightarrow S_1$ electronic transition can be described as a $\pi \rightarrow \sigma^*$ ($[2p_z](O) \rightarrow [3s,3p_y](O)$) transition.

According to our calculations, one can expect a high-frequency shift of maxima of the absorption bands of the complexes under study relative to the absorption band of the water monomer upon the $S_0 \rightarrow S_1$ electronic transition (Fig. 6). For the $H_2O...HF$ complex, this shift is $\Delta\nu_e^{el} = \varepsilon(H_2O...HF) - \varepsilon(H_2O) = 8.57$ eV $- 7.80$ eV $= 0.77$ eV (ε is the energy of the corresponding vertical electronic transition). Among the $(H_2O)_n...(HF)_m$ complexes with $n = m = 1—3$, the largest frequency shift $\Delta\nu_e^{el}$ (1.20 eV) is expected for the cyclic structure of the $(H_2O)_3...(HF)_3$ complex. The $\Delta\nu_e^{el}$ parameters for the chain configuration of the $(H_2O)_3...(HF)_3$ complex and the cyclic structure of the $(H_2O)_2...(HF)_2$ complex are 0.84 and 1.06 eV, respectively.

The vertical ionization potentials (IPs) for all complexes calculated in this work from the differences between the total energies of the molecular systems lie in the range 12.8—13.6 eV and are close to that calculated for the H_2O monomer (12.6 eV), which virtually coincides with the experimental value (see, *e.g.*, Ref. 38). Close values of the IPs of the complexes and monomer indicate that ionization of the complexes usually leads to detachment of an electron from one of the water molecules in the complexes. The energies of the electronic transitions to the continuous spectrum are 4—5 eV higher than those of the $S_0 \rightarrow S_1$ electronic excitations.

Thus, in addition to the previously studied $(H_2O)_n...(HF)_m$ complexes ($n : m = 1 : 1$, $1 : 2$, and $2 : 1$), in this work we studied the complexes with $n : m = 2 : 2$ and $3 : 3$, which allowed us to obtain valuable information required for correct interpretation of the IR and UV spectra of a mixture of water vapor with HF under the atmospheric conditions. Using the same computational approach, we revealed some trends of formation of the energy, structural, and spectroscopic characteristics of the above-mentioned complexes with an increase in the number of the monomer molecules.

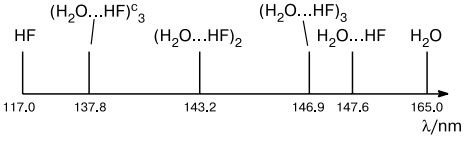

Fig. 6. Positions of the UV absorption band maxima of $(H_2O...HF)_n$ complexes in the spectral region corresponding to electronic transitions between the lowest singlet states.

With respect to the intermolecular interaction energy per H-bond the cyclic structure of the $(H_2O)_3...(HF)_3$ complex is the most stable among all stable configurations of the $(H_2O)_n(HF)_m$ complexes ($n + m \geq 2$) studied in this work. According to our calculations, the cyclic configurations of the $(H_2O)_n(HF)_m$ complexes (at least, at $n + m \leq 6$) are more energetically favorable than other structures including the open-chain structures. Analogous results were obtained for both the $(H_2O)_n$ complexes (see, *e.g.*, Refs. 39 and 40), and the $(HF)_n$ clusters (see, *e.g.*, Ref. 41) at $n \leq 6$.

Among the vibrational frequencies corresponding to intramolecular modes of the complexes studied, the stretching vibration frequency of HF is changed to the greatest extent upon complexation. For all the complexes, the ν(HF) frequency experiences a low frequency shift. The second group of low-frequency vibrations corresponds to intermolecular modes of the $(H_2O...HF)_n$ complexes and falls in the frequency range from nearly 10 to 1100 cm^{-1}.

The $S_0 \rightarrow S_1$ electronic excitation in the $(H_2O...HF)_n$ complexes is localized on the O—H bond of one of the H_2O molecules. Similarly to the H_2O molecule, the complexes also exhibit a Rydberg character of the $S_0 \rightarrow S_1$ transition and the photodissociation type of the corresponding absorption band. Intermolecular interactions in the $(H_2O...HF)_n$ complexes ($n = 1—3$) cause a shift of the absorption band maxima toward the short-wavelength region (similarly to the $(H_2O)_n$ clusters with $n = 2—6$)[42,43] compared to the corresponding bands in the water monomer spectrum. These shifts are 0.77 eV ($n = 1$), 1.06 eV ($n = 2$, cyclic structure), 0.84 eV ($n = 3$, chain structure), and 1.20 eV ($n = 3$, cyclic structure).

This work was carried out with the financial support of the Russian Foundation for Basic Research (Project No. 00-05-64919).

References

1. V. E. Zuev, Yu. S. Makushkin, and Yu. N. Ponomarev, *Sovremennye problemy atmosfernoi optiki. 3. Spektroskopiya atmosfery* [*Modern Problems of Atmospheric Optics. Atmospheric Spectroscopy*], Gidrometeoizdat, Leningrad, 1987, 247 pp. (in Russian).
2. J. Heichlen, *Atmospheric Chemistry*, Academic Press, New York, 1976, 412 pp.
3. Sh. Sh. Nabiev and Yu. N. Ponomarev, *Optika Atmosfery i Okeana* [*Atmospheric and Ocean Optics*], 1998, **11**, 1274 (in Russian).
4. Sh. Sh. Nabiev, P. G. Sennikov, and Yu. N. Ponomarev, *Abstrs. Vth Colloq. "Atmospheric Spectroscopy Applications"*, Reims, France, 1999, CP2.

5. N. A. Zvereva, Sh. Sh. Nabiev, and Yu. N. Ponomarev, *Optika Atmosfery i Okeana* [*Atmospheric and Ocean Optics*], 1999, **12**, 843 (in Russian).
6. Sh. Sh. Nabiev and L. P. Sukhanov, *Izv. Akad. Nauk*, *Ser. Khim.*, 1999, 1415 [*Russ. Chem. Bull.*, 1999, **48**, 1397 (Engl. Transl.)].
7. Sh. Sh. Nabiev, *Optika Atmosfery i Okeana* [*Atmospheric and Ocean Optics*], 2000, **13**, 123 (in Russian).
8. Sh. Sh. Nabiev, A. N. Trotsenko, S. K. Ignatov, P. G. Sennikov, N. A. Zvereva, and Yu. N. Ponomarev, *Tez. Dokl. Mezhdunar. Simp. "Atmosfernaya Radiatsiya"* [*Abstrs. Int. Symp. on Atmospheric Radiation*], Izd-vo SPbGU, Sankt-Peterburg, 1999, 127 (in Russian).
9. K. Wark and C. F. Warner, *Air Pollution. Its Origin and Control*, Harper and Row, New York, 1976.
10. K. Nakamoto, *Infrared and Raman Spectra of Inorganic and Coordination Compounds*, Wiley, New York—Chichester—Toronto, 1986.
11. N. Husson, B. Bonnett, N. Scott, and A. Chedin, *J. Quant. Spectrosc. Radiat. Transfer*, 1992, **48**, 509.
12. N. A. Zvereva, Sh. Sh. Nabiev, and Yu. N. Ponomarev, *Proc. SPIE*, 1999, **3983**, 9.
13. M. Peterson and R. Poirer, *MONSTERGAUSS-90*, University of Toronto and Memorial University of Newfoundland, St. John´s Newfoundland, 1990.
14. M. J. Frisch, G. W. Trucks, H. B. Schlegel, G. E. Scuseria, M. A. Robb, J. R. Cheeseman, V. G. Zakrzewski, J. A. Montgomery, Jr., R. E. Stratmann, J. C. Burant, S. Dapprich, J. M. Millam, A. D. Daniels, K. N. Kudin, M. C. Strain, O. Farkas, J. Tomasi, V. Barone, M. Cossi, R. Cammi, B. Mennucci, C. Pomelli, C. Adamo, S. Clifford, J. Ochterski, G. A. Petersson, P. Y. Ayala, Q. Cui, K. Morokuma, D. K. Malick, A. D. Rabuck, K. Raghavachari, J. B. Foresman, J. Cioslowski, J. V. Ortiz, B. B. Stefanov, G. Liu, A. Liashenko, P. Piskorz, I. Komaromi, R. Gomperts, R. L. Martin, D. J. Fox, T. Keith, M. A. Al-Laham, C. Y. Peng, A. Nanayakkara, C. Gonzalez, M. Challacombe, P. M. W. Gill, B. G. Johnson, W. Chen, M. W. Wong, J. L. Andres, M. Head-Gordon, E. S. Replogle, and J. A. Pople, *GAUSSIAN-98*, *Revision A.3*, Gaussian, Inc., Pittsburgh (PA), 1998.
15. T. Clark, *A Handbook of Computational Chemistry*, Wiley, New York, 1985.
16. K. P. Huber and G. Herzberg, *Constants of Diatomic Molecules*, Van Nostrand Reinhold, Toronto, 1979.
17. *Molekulyarnye postoyannye neorganicheskikh soedinenii* [*Molecular Constants of Inorganic Compounds*]: *A Handbook*, Ed. K. S. Krasnov, Khimiya, Leningrad, 1979, 448 pp. (in Russian).
18. M. M. Szczesniak, S. Scheiner, and Y. Bouteiller, *J. Chem. Phys.*, 1984, **81**, 5024.
19. J. W. Bevan, Z. Kisiel, A. C. Legon, D. J. Millen, and S. C. Rogers, *Proc. R. Soc. London, Ser. A*, 1980, **372**, 441.
20. J. E. Del Bene, *J. Phys. Chem*., 1988, **92**, 2874.
21. S. L. A. Adebayo, A. C. Legon, and D. J. Millen, *J. Chem. Soc.*, *Faraday Trans*., 1991, **87**, 443.
22. R. K. Thomas, *Proc. R. Soc. London, Ser. A*, 1975, **344**, 579.
23. C. Rovira, P. Constants, M. H. Whangbo, and J. J. Novoa, *Int. J. Quant. Chem*., 1994, **52**, 177.
24. R. Fletcher, *Comput. J*., 1970, **13**, 317.
25. M. J. D. Powell, *Numerical Methods for Nonlinear Algebraic Equations*, Gordon and Breach, London, 1970, 87.
26. C. C. J. Roothaan, *Rev. Mod. Phys.*, 1960, **32**, 179.
27. K. Hirao and H. Nakatsuji, *J. Chem. Phys*., 1973, **59**, 1457.
28. K. Hirao, *J. Chem. Phys.*, 1974, **60**, 3215.
29. R. Carbo and J. M. Riera, *Lecture Notes in Chemistry*. **5**. *A General SCF Theory*, Springer, Berlin, 1978.
30. A. M. Pravilov, *Fotoprotsessy v molekulyarnykh gazakh* [*Photoprocesses in Molecular Gases*], Energoatomizdat, Moscow, 1992, 350 pp. (in Russian).
31. A. C. Legon, D. J. Millen, and H. M. North, *Chem. Phys. Lett*., 1987, **135**, 303.
32. G. Gazzoli, P. G. Favero, D. G. Lister, A. C. Legon, D. J. Millen, and Z. Kisiel, *Chem. Phys. Lett*., 1985, **117**, 543.
33. S. P. Belov, V. M. Demkin, N. F. Zobov, E. N. Karyakin, A. F. Krupnov, I. N. Kozin, O. L. Polyanskii, and M. Yu. Tret´yakov, *Prepr. IPF Akad. Nauk SSSR* [*Prepr. Int. Appl. Phys., USSR Acad. Sci.*] *No. 192*, Gor´kii, 1988, 17 pp. (in Russian).
34. L. Andrews and G. L. Johnson, *J. Chem. Phys*., 1983, **79**, 3670.
35. L. P. Sukhanov, V. V. Zheleznyakov, and N. L. Zakamskaya, *Zh. Fiz. Khim*., 2001, **75**, 1972 [*Russ. J. Phys. Chem*., 2001, **75**, 1808 (Engl. Transl.)].
36. E. G. Tarakanova, F. Huisken, and M. Kaloudis, *Proc. SPIE*, 1997, **3090**, 180.
37. T. G. Meister, *Elektronnye spektry mnogoatomnykh molekul* [*Electronic Spectra of Polyatomic Molecules*], Izd-vo LGU, Leningrad, 1969, 206 pp. (in Russian).
38. W. R. Wadt and W. A. Goddard, *Chem. Phys*., 1976, **18**, 1.
39. S. S. Xantheas and T. H. Dunning, Jr., *J. Chem. Phys*., 1993, **99**, 8774.
40. S. S. Xantheas, *J. Chem. Phys*., 1995, **102**, 4505.
41. F. Huisken, E. G. Tarakanova, A. A. Vigasin, and G. V. Yukhnevich, *Chem. Phys. Lett*., 1995, **245**, 319.
42. N. A. Zvereva, M. A. Buldakov, I. I. Ippolitov, and A. F. Terpugova, *Izv. Vuz. Fiz.,* 1993, **36**, 11 [*Bull. Vuz. Physics*, 1980 (Engl. Transl.)].
43. N. A. Zvereva and I. I. Ippolitov, *Proc. SPIE*, 1997, **3090**, 88.

Received August 31, 2001;
in revised form May 22, 2002

N.A. Zvereva et al. Vol. 14, No. 12 /December 2001/ Atmos. Oceanic Opt. 1009

IR spectra of HF and its complexes with water under atmospheric conditions

N.A. Zvereva,[1] Sh.Sh. Nabiev,[2] A.I. Nadezhdinskii,[3] Yu.N. Ponomarev,[4] D.B. Stavrovskii,[3] S.M. Chernin,[3] and T.A. Shubenkina[3]

[1] *Tomsk State University*
[2] *Russian Scientific Center "Kurchatov Institute," Moscow*
[3] *Natural Sciences Center at General Physics Institute, Russian Academy of Sciences, Moscow*
[4] *Institute of Atmospheric Optics, Siberian Branch of the Russian Academy of Sciences, Tomsk*

Received December 4, 2001

IR spectra of H_2O–HF mixture have been recorded in the spectral region from 700 to 4000 cm^{-1} using a VECTOR-22 Fourier transform spectrometer. Analysis of the spectroscopic data enabled us to reveal some peculiarities in the spectra, in particular, a larger number of bands are observed as compared to that known from literature data. Based on *ab initio* quantum chemical calculations, experimental vibrational frequencies have been tentatively assigned. Our experiments show that in the atmosphere H_2O and HF form various complexes.

Solution of the problems in real-time monitoring of gas and aerosol emissions from chemical, radiochemical, and metallurgical plants requires reliable data on the concentration and molecular composition of the emissions. Today methods of remote laser sensing are most promising for this purpose. To implement these methods successfully, one needs detailed information on the absorption and emission spectra of molecular components and their interaction with water vapor and other atmospheric gases.[1–3] Such an interaction may produce molecular complexes with the bond energy from several tens of calories to several kilocalories.[4] The optical activity of such donor-acceptor or H-bonded complexes may be rather high, what can cause additional radiation losses in the atmosphere of industrial regions and variations of the solar radiation flux. Gas-phase complexes of water molecules are characterized, as a rule, by several types of large-amplitude motions.[5] In the atmosphere, this, in its turn, leads to transformation of vibrational spectra of their components (shifts of spectral features relative to those of free molecules may range from several wave numbers to even hundreds of wavenumbers) and to appearance of new bands corresponding to intermolecular vibrations.[4] These changes can be traced using the method of remote laser sensing. The aim of this paper is to study FTIR spectra of HF and $(H_2O)_n(HF)_m$ complexes under nearly atmospheric conditions.

Experiment

The IR spectra were recorded with a VECTOR-22 Fourier transform spectrometer (manufactured by Bruker) in the spectral region from 700 to 4000 cm^{-1} (resolution of 0.5 cm^{-1}). A multipass cell with the optical length of 4 m was filled with the mixture of gaseous HF with atmospheric air at room temperature. The HF concentration was $1 \cdot 10^{17}$ cm^{-3}, and the water vapor concentration was $1.3 \cdot 10^{17}$ cm^{-3}. In processing the recorded spectra, water vapor absorption spectrum obtained by the same method on the same spectrometer was subtracted from the initial spectrum.

Calculations of IR bands of $(H_2O)_n(HF)_m$ complexes

Potential energy surfaces and harmonic frequencies of $(HF)_n(H_2O)_m$ complexes were calculated by Hartree–Fock–Roothaan (HFR) method with the use of the MONSTERGAUSS (Ref. 11) and GAUSSIAN 98 (Ref. 12) software packages adapted for use on Pentium IBM PCs. We used the 6-31G** Pople basis set including external polarization *d*- and *p*-functions at the atoms of F, O, and H, respectively. Table 1 gives vibrational frequencies of the hetero-dimer H_2O...HF. For a comparison Table 1 also presents, along with the experimental results, the corresponding data of more accurate calculations taking into account the effects of electron correlation by the Moller–Plesset (MP) perturbation theory.

As is seen from Table 1, the partial allowance for the effects of electron correlation within the Moller–Plesset perturbation theory up to the second order inclusive (MP2) leads to a decrease in the frequencies of the intramolecular normal vibrations thus improving the agreement with the experimental data. However, for intermolecular vibrational modes, the smallest deviation from the experimental frequencies results from calculation with the use of the 6-31G** basis set and the Hartree–Fock–Roothaan method. The calculated harmonic frequencies ω_i may differ markedly from the experimentally observed frequencies ν_i of the fundamental vibrational transitions. This discrepancy may be caused by significant contributions of the anharmonic terms to ν_i in description of vibrational spectra of complexes with H-bonds.

0235-6880/01/12 1009-03 $02.00

1010 Atmos. Oceanic Opt. /December 2001/ Vol. 14, No. 12 N.A. Zvereva et al.

Table 1. Vibrational frequencies, cm^{-1}, of the $H_2O...HF$ hetero-dimer

HFR/6-31G**	MP2/6-31G**	HFR/6-31++ G**	MP2/6-31++ G**	HFR/aug-cc-pVDZ	MP2/aug-cc-pVDZ	Exp., Ref. 6	Assignment
4258	4012	4261	3991	4231	3919	3756	ν_{as}(OH)
4270	3908	4209	3728	4172	3664	3608±2	$\nu(H_bF)$
4142	3869	4142	3854	4124	3792	3657	ν_s(OH)
1765	1675	1745	1641	1746	1626	1595	δ(HOH)
760	821	795	886	775	852	666±30	$\delta_o(OH_bF)$
626	702	648	731	661	733	696±30	$\delta_i(OH_bF)$
236	269	217	222	216	236	180±30	$\nu(O..H_bF)$
206	208	224	276	230	268	145±50	$\delta_o(HOH_b)$
194	212	162	281	186	280	170±50	$\delta_i(HOH_b)$

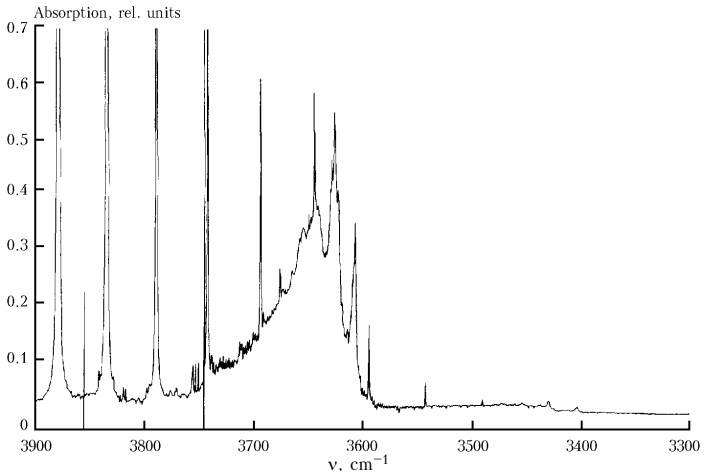

Fig. 1. IR absorption spectrum of the HF mixture with air in the region of 3300–3900 cm^{-1}.

An efficient model rather accurately and simply allowing for the anharmonic contributions to the frequencies ν_i of the stretching vibrations of a monomer Y, when it produces a complex $H_2O...Y$ with the quasi-linear hydrogen bond under atmospheric conditions, was developed and justified in Ref. 13. In this paper, the vibrational frequencies of complexes with the nonlinear bond were corrected with the use of linear calibration function

$$\nu_{cor} = b\omega_{calc} + a, \quad (1)$$

where ω_{calc} are the harmonic vibrational frequencies calculated *ab initio*; ν_{cor} are the corrected values of the vibrational frequencies; *a* and *b* are the calibration coefficients, which are determined from the least-squares fitting to the experimental data[6] for the $H_2O...HF$ complex. These coefficients *b* and *a* proved to be equal to 0.84 and 108 cm^{-1}, respectively, and the correlation coefficient between the experimental and calculated frequencies was 0.998. In this case, the mean absolute deviation of ν_{calc} from ν_{exp} was 58 cm^{-1}.

Discussion

For the first time, the existence of $m_2n...mF$ complex in the gas phase under equilibrium conditions at 315K temperature was found experimentally by Thomas[6] with the use of the method of traditional IR spectroscopy. In Thomas' opinion, three bands pointed to the existence of the complex: one corresponding to the stretching vibrations of the mF molecule, the second corresponding to the bending vibrations of the water molecule, and the third corresponding to two bending vibrations of the hydrogen bond itself. The energy for the formation of the complex with the allowance for zero vibrations was determined from the spectroscopic data as 7 kcal·mol^{-1}. The rotational spectrum of this complex was studied in Refs. 7 and 8. Under equilibrium conditions in the gas phase, intensities of rotational transitions were measured in the ground state of the molecules m_2n and mF and the complex $m_2n...mF$ and the equilibrium constant of complex formation was calculated, as well as the energy of the formation with the allowance for zero vibrations, which proved to be equal to 10.2 kcal·mol^{-1} (Ref. 8).

A fragment of the IR spectrum of the HF mixture with air in the region of 3300–3900 cm^{-1} is shown on Fig. 1. The values of the experimental and calculated (with allowance for the systematic error) vibrational frequencies for the complexes of HF with H_2O and their tentative assignments are tabulated below in

Table 2. For a comparison, Table 2 also gives the experimental vibrational frequencies for the complex HF…H_2O taken from Ref. 6.

Table 2. Experimental (ν_{exp}) and calculated (ν_{theor}) vibrational frequencies for the complexes $(HF)_m…(H_2O)_n$ and their tentative assignments

ν_{exp}, cm^{-1}	ν_{exp} (Ref. 1), cm^{-1}	ν_{theor}, cm^{-1}	Tentative assignment
3726 w	3756	3740	HF…H_2O,
		3720	$(HF)_2…H_2O$
		3740, 3750	$(HF)_2…(H_2O)_2$, $(HF)_3…(H_2O)_3$
3676 ar		3670	$(HF)_2…(H_2O)_2$
		3690	$(HF)_2…H_2O$
3665 ar		3670	$(HF)_2…(H_2O)_2$
3655 ar	3657	3650	HF…H_2O
3643 m		3645, 3635	$(HF)_2…H_2O$
3625 s		3623	HF…$(H_2O)_2$
3607 s	3608	3610	HF…H_2O, $(HF)_2…H_2O$
3471 ar		3534	$(HF)_2…(H_2O)_2$
3453 w		3527	$(HF)_2…(H_2O)_2$
3429 w		3430	$(HF)_2…H_2O$
3403 w		3425	HF…$(H_2O)_2$
1620 ar		1622, 1628	$(HF)_3…(H_2O)_3$,
1612 m	≈ 1600	1607, 1610	HF…$(H_2O)_2$
1594 ar		1601, 1600	$(HF)_2…H_2O$, $(HF)_2…(H_2O)_2$
		1595	$(HF)_2…(H_2O)_2$
		1590	$(HF)_2…(H_2O)_2$
		1591	HF…H_2O, $(HF)_2…H_2O$

Note. s means strong band, m means medium band, and w means weak band; ar denotes an arm.

The analysis of obtained spectroscopic data (see Table 2) revealed some peculiarities in the spectra. Thus, the number of the observed bands is larger than that known from the literature data.[6] In the region of 3600–3750 cm^{-1}, four new bands were found, while only two bands were observed in Ref. 6. In the region of bending vibration of the water molecule (1550–1650 cm^{-1}), three allowed spectral bands were observed, but only one band was found in Ref. 6. In addition, new, not reported earlier, bands were found in the region of 3400–3450 cm^{-1}. Structures possibly connected with the rotation of one of the complex fragments were observed nearby 3700 and 3600 cm^{-1}.

It follows from Table 2 that the bands in the region of 3750–3600 cm^{-1} can be tentatively assigned to the stretching vibrations of HF and H_2O in such complexes as HF…H_2O (1:1), $(HF)_2…H_2O$ (2:1), HF…$(H_2O)_2$ (1:2), $(HF)_2…(H_2O)_2$ (2:2), $(HF)_3…(H_2O)_3$ (3:3). The gas phase complex of the composition 1:1 was observed experimentally in the gas medium only in Ref. 6, and the complexes of the composition 1:2 and 2:1 were observed only under conditions of low-temperature matrix isolation.[9] The energy, structure, and vibrational spectra of complexes of HF with H_2O up to the composition 3:3 were calculated in Ref. 10. The bands in the region of 1650–1550 cm^{-1} can be tentatively assigned to the bending vibrations of H_2O in the complexes mentioned above. As to the bands in the region of 3400–3450 cm^{-1}, according to quantum chemical calculations, they can be assigned to the vibration of HF in the complexes with the composition 1:2, 2:1, and 2:2.

Thus, the experiments conducted evidence that HF produces in the atmosphere various complexes with water. More strict assignment of bands in the IR spectra will likely become possible after recording of spectra with a higher resolution.

Acknowledgments

This work was partly supported by the Russian Foundation for Basic Research (Project No. 00–05–64919).

References

1. Sh.Sh. Nabiev and Yu.N. Ponomarev, Atmos. Oceanic Opt. **11**, No. 12, 1093–1098 (1998).
2. N.A. Zvereva, Sh.Sh. Nabiev, and Yu.N. Ponomarev, in: *Abstracts of the NATO Adv. Research Workshop Spectroscopy from Space* (Bratislava, 2000), p. 55.
3. Sh.Sh. Nabiev, P.G. Sennikov, and Yu.N. Ponomarev, in: *Abstracts Vth Colloq. on Atmospheric Spectroscopy Applications* (Reims, France, 1999), p. CP2.
4. Sh.Sh. Nabiev and P.G. Sennikov, Atmos. Oceanic Opt. **14**, No. 3, 170–191 (2001).
5. Sh.Sh. Nabiev and L.P. Sukhanov, Izv. Ros. Akad. Nauk, Ser. Khim., No. 8, 1415–1441 (1999).
6. R.K. Thomas, Proc. Roy. Soc. London A **344**, 579–592 (1975).
7. A.C. Legon and L.C. Willoughby, Chem. Phys. Lett. **92**, 333 (1982).
8. A.C. Legon, J. Millen, and S.L. Adebayo, J. Chem. Soc. Faraday Trans. **87**, 443 (1991).
9. L. Andrews and G.L. Johnson, J. Chem. Phys. **79**, 3670–3676 (1983).
10. N.A. Zvereva, Sh.Sh. Nabiev, and Yu.N. Ponomarev, in: *Abstracts of VIII Joint Intern. Symp. Atmospheric and Ocean Optics. Atmospheric Physics* (Irkutsk, 2001), p. 94.
11. M. Peterson and R. Poirer, MONSTERGAUSS-90 (University of Toronto and Memorial University of Newfoundland, St. John's Newfoundland, 1990).
12. M.J. Frisch, G.W. Trucks, H.B. Schlegel, G.E. Scuseria, M.A. Robb, J.R. Cheeseman, V.G. Zakrzewski, J.A. Montgomery, Jr., R.E. Stratmann, J.C. Burant, S. Dapprich, J.M. Millam, A.D. Daniels, K.N. Kudin, M.C. Strain, O. Farkas, J. Tomasi, V. Barone, M. Cossi, R. Cammi, B. Mennucci, C. Pomelli, C. Adamo, S. Clifford, J. Ochter-ski, G.A. Petersson, P.Y. Ayala, Q. Cui, K. Morokuma, D.K. Malick, A.D. Rabuck, K. Raghavachari, J.B. Foresman, J. Cioslowski, J.V. Ortiz, B.B. Stefanov, G. Liu, A. Liashenko, P. Piskorz, I. Komaromi, R. Gomperts, R.L. Martin, D.J. Fox, T. Keith, M.A. Al-Laham, C.Y. Peng, A. Nanayakkara, C. Gonzalez, M. Challacombe, P.M.W. Gill, B.G. Johnson, W. Chen, M.W. Wong, J.L. Andres, M. Head-Gordon, E.S. Replogle, and J.A. Pople, *Gaussian 98. Revision A3* (Gaussian Inc., Pittsburgh PA, 1998).
13. L.P. Sukhanov, V.V. Zheleznyakov, N.L. Zakamskaya, and Sh.Sh. Nabiev, Proc. SPIE **4341**, 12–17 (2000).

316 Atmos. Oceanic Opt. /April 2002/ Vol. 15, No. 4 N.A. Zvereva and Yu.N. Ponomarev

Molecular complexes of water and hydrogen chloride in the atmosphere

N.A. Zvereva and Yu.N. Ponomarev

Institute of Atmospheric Optics,
Siberian Branch of the Russian Academy of Sciences, Tomsk

Received March 1, 2002

We present a study of structurally nonrigid molecular complexes formed by water and hydrogen chloride molecules being the products of emissions from some chemical and metallurgic plants using theoretical *ab initio* methods. Equilibrium configurations of the complexes $(H_2O)_n(HCl)_m$ (2:2; 3:3) and positions of vibration bands are determined based on *ab initio* calculations of the potential energy surfaces with application of second-order Möller–Plesset perturbation theory (MP2), split-valence basis set 6-31G (d,p), and correlation-consistent basis set aug-cc-pVDZ. The data obtained are needed for assignment of IR absorption spectra and in real-time remote monitoring of these complexes that are ecologically hazardous under atmospheric conditions.

Introduction

The problem of creation, stability, and optical activity of structurally nonrigid molecular complexes of water with chemically active and toxic molecules of anthropogenic origin is one of the most urgent problems in modern physics and chemistry of the atmosphere. Weakly bound molecular complexes may cause extra radiative losses in the atmosphere. Complexes of hydrogen chloride and water play an important role in the ozone depletion cycle.[1] *Ab initio* investigations of the structure and vibration spectra of weakly bound complexes characterized by several types of large-amplitude motions (LAMs) allow the contribution of these complexes to atmospheric absorption to be assessed. Several types of large-amplitude motions may lead to transformation of vibration spectra of monomers comprising a complex and to the appearance of new bands corresponding to intermolecular vibrations. This opens the possibility for detecting and estimating the concentrations of such complexes in the atmosphere with modern remote laser sensing instrumentation.

A considerable progress has been achieved recently in experimental investigation of intermolecular systems in the gas phase.[1–15] However, the complete set of intermolecular vibrations is known only for few complexes. The investigators' attention was mostly concentrated at the systems with rather high bond energies, for example, H_2O...HF (Ref. 9). Weak hydrogen bonds, such as in H_2O...HCl, are poorly studied, in spite of their chemical importance. The geometry of this complex was determined by the methods of rotational spectroscopy,[10] but the data on vibrational spectra are limited to intramolecular modes in solid matrices.[11–14] The geometry of the weakly bound trimer $HCl(H_2O)_2$ was found by Kisiel with co-authors[15] from rotational spectra observed at extension of a supersonic jet. The clusters $HCl(H_2O)_n$, n = 1–5, were studied in Refs. 16 and 17 from the viewpoint of their stability and protolytic dissociation of the HCl molecule in water clusters. *Ab initio* prediction of rovibrational spectra of $HCl(H_2O)_2$ complex with tunneling effects was reported in Ref. 18.

In this paper, we present the results of the quantum-mechanical study of the structure, stability, and vibration spectra of $(H_2O)_n(HCl)_m$ (2:2, 3:3) complexes.

Calculation methods

The potential energy surfaces (PESs) of the $(HCl)_n·(H_2O)_m$ complexes were calculated by the Hartree–Fock (HF) and Möller–Plesset (MP2) methods using the GAUSSIAN-98 program[19] adapted for use on Pentium PCs. In our approach we applied the Pople's split-valence double-zeta plus polarization basis set 6-31G (d, p). This basis set includes external polarized d- and p-functions at the Cl, O, and H atoms. Besides, the 6-31 ++ G(3df, 3pd) basis set with diffuse functions and the correlation-consistent basis set aug-cc-pVDZ were used.

Tables 1 and 2 present the results of *ab initio* calculations of the geometric and energy characteristics of the HCl and H_2O monomer molecules and their complex H_2O...HCl in the configuration of absolute PES minimum. Harmonic vibration frequencies of the monomers and of the complex are given in Tables 3 and 4.

For a comparison, the tables include both the experimental data and the data calculated with the allowance for the electron correlation by the Möller–Plesset perturbation theory.

The data presented in Table 1 evidence of a rather low sensitivity of the geometric parameters to extension of the basis set. The discrepancy with the experimental results for the length of the n–m bond is ~ 0.015 Å when using the HF method. The allowance for the electron correlation leads to better agreement with the experiment.

0235-6880/02/04 316-05 $02.00

Table 1. Molecular properties of the H_2n and HCl Holecules

Parameter	6-31G(d,p) HF	6-31++G (3df,3pd) HF	6-31G(d,p) MP2	6-31++G (3df,3pd) MP2	Aug-cc-pVDZ HF	Aug-cc-pVDZ MP2	Exp. Ref. 21
				H_2O			
r(O–H), Å	0.943	0.942	0.961	0.958	0.944	0.966	0.958
α(HOH), deg	106.0	106.3	103.7	103.8	106.0	103.9	104.5
μ, D	2.148	1.948	2.201	2.0	1.96	2.02	1.847
E, a.u.	−76.02361	−76.040899	−76.219785	−76.297593	−76.041843	−76.260910	–
				HCl			
r(Cl–H), Å	1.266	1.265	1.269	1.271	1.278	1.288	1.274
μ, D	1.471	1.178	1.475	1.184	1.244	1.256	1.093
E, a.u.	−460.066214	−460.074749	−460.205446	−460.269626	−460.09262	−460.251823	–

Table 2. Structure and energy paraHeters of the H_2O…HCl coHplex

Basis set	O–H, Å	O…H, Å	H–Cl, Å	HOH, deg	O…HCl, deg	HO…H, deg	Cl…O, Å	$-E$, a.u.	$-\Delta E$, a.u.
HF/6-31G(d,p)	0.944	1.975	1.278	106.8	178.5	120.7	3.25	536.098081	5.2
MP2/6-31G(d,p)	0.963	1.862	1.288	104.8	177.6	111.6	3.15	536.437692	7.8
HF/6-31++G(3df, 3pd)	0.942	2.096	1.274	106.7	178.1	122.5	3.37	536.121840	3.89
MP2/6-31++G(3df, 3pd)	0.960	1.855	1.287	104.3	177.8	110.7	3.14	536.576767	5.99
HF/aug-cc-pVDZ	0.944	2.067	1.286	106.5	178.6	124.5	3.35	536.141111	4.17
MP2/aug cc-pVDZ	0.967	1.856	1.307	104.5	178.8	114.3	3.16	536.522601	6.19

Table 3. Frequencies of harHonic vibrations ω_i and IR intensities A calculated for H_2n and HCl HonoHers

Assignment	HF/6-31G(d,p), ω_i, cm^{-1}, (A, km/mol)	HF/6-31++G (3df, 3pd), ω_i, cm^{-1}, (A, km/mol)	MP2/6-31G(d,p), ω_i, cm^{-1}, (A, km/mol)	MP2/6-31++G (3df, 3pd), ω_i, cm^{-1}, (A, km/mol)	Experiment Refs. 24 and 25, ω_i, cm^{-1}, (A, km/mol)
ν (Cl–H)	3176 (34)	3148 (54)	3121 (22)	3070 (51)	3042 (39)
ν_{as} (O–H)	4262 (58)	4269 (89)	4050 (34)	4010 (75)	3942 (40)
ν_s (O–H)	4145 (16)	4147 (20)	3912 (4)	3893 (8)	3832 (2)
δ (HOH)	1770 (104)	1728 (114)	1679 (78)	1655 (73)	1648 (67)

Notes: ν_s is symmetric stretching vibration; ν_{as} is antisymmetric stretching vibration; δ is bending vibration.

Table 4. Frequencies of harHonic vibrations ω_i and frequency shifts $\Delta\omega_i$ (cH^{-1}) for H_2O…HCl coHplex

Basis	Δω (n m)	Δω (n m)	Δω (ClH)	Δω (HOH)	ν (O…H)	δ_i (OH_bCl)	δ_0 (OH_bCl)	δ_i (HOH_b)	δ_0 (HOH_b)
HF/6-31G(d,p)	−6	−5	−161	−5	151	558	446	210	181
HF/6-31++G(3df,3dp)	−51	−17	−115	21	126	461	366	147	94
+VP^s(2d)^s (Ref. 14)	−3	−4	−105	1	118	459	351	143	94
Experiment	–	–	−216	–	100	460	–	157	64
			Ref. 11		Ref. 11	Ref. 11		Ref. 22	Ref. 22

Notes: ν are stretching vibrations; δ_i are bending vibration in a plane; δ_0 are out-of-plane bending vibrations of the H_2O molecule.

For the mn m valence angle, Δα is ~ 1.5° (HF), and allowance for the correlation effects decreases it down to ~ 0.6°. The length of the H–Cl bond is insensitive to extension of the split-valence basis set; the discrepancy Δr (H–Cl) from the experimental value is 0.008 Å, and with the aug-cc-pVDZ basis set it is only 0.003 Å as small. The allowance for the electron correlation with the use of MP2/6-31++G(3df, 3pd) gives Δr = 0.003 Å, while MP2/aug-cc-pVDZ gives the overestimated value Δr = 0.014 Å.

Table 2 presents the geometric parameters of the H_2O…HCl complex as obtained by use of different basis sets (HF, MP2). When using the HF and MP2 methods, the maximum discrepancy for intramolecular parameters is ~ 0.02 Å for Δr and Δα ~ 2° for the valence angle. For the intermolecular parameters ΔR ~ 0.2 Å and Δθ ~ 10°.

Recent experimental data obtained by Kisiel et al.[15] allow a comparison to be made with the cyclic $(H_2O)_2$HCl complex. It can be seen from Table 5,

which presents the intermolecular geometric parameters, that although the calculations with the use of HF/6-31G(d,p) give correct cyclic structure,[20] but the intermolecular lengths of bonds are overestimated as compared with the experimental values. When using MP2/aug-cc-pVDZ, ΔR is 0.02–0.07 Å.

Table 5. InterHolecular geoHetric paraHeters of $(H_2O)_2HCl$ coHplex

Parameter	HF/6-31G(d,p)	MP2/aug-cc-pVDZ	Exp. Ref. 15
Cl_1O_3	3.346	3.022	3.084
O_3O_6	3.099	2.79	2.815
Cl_1O_6	3.677	3.383	3.415
O_3H_2	2.111	1.778	1.831
O_6H_4	2.228	1.875	1.943
Cl_1H_7	2.946	2.610	2.810
$O_3H_4O_6$	150.9	154.1	149.1
$Cl_1H_2O_3$	160.9	165.9	164.0
$Cl_1H_7O_6$	135.3	137.4	122.0

As can be seen from the above results, to study weakly bound complexes, it is important to include dispersion forces into consideration through making allowance for the electron correlation at optimization of the geometry. The geometric parameters of the complexes $(H_2O)_2(HCl)_2$ and $(H_2O)_3(HCl)_3$ were optimized with the use of MP2/aug-cc-pVDZ and MP2/6-31G(d,p) basis sets, respectively.

The aim of this work was to obtain the geometric characteristics and $\Delta\nu$ corresponding to the shifts of the vibration frequencies ν at the formation of complexes.

Table 3 gives the corresponding harmonic frequencies ω_i of the H_2O and HCl monomers for different basis sets and calculation methods. Addition of the diffusion functions does not lead to a considerable change in the harmonic frequencies ω_i. The discrepancy between the calculated, ω_{icalc}, (HF) and experimental frequencies, ω_{iexp}, is 4–9%. The allowance for the electron correlation effects (MP2/6-31++G(3df, 3dp), MP2/6-31G(d,p)) decreased $\Delta\omega_i$ down to 1–2%. When comparing the calculated frequencies ω_i and the observed fundamental frequencies ν_i that effectively include the anharmonicity of vibrations, one should keep in mind the difference between ν_{iexp} and ω_{iexp}. For the considered H_2O and HCl monomers, ω_{iexp} differs from ν_{iexp} by 3–5%.

Table 4 gives the shifts $\Delta\omega_i$ for the heterodimer H_2O…HCl with respect to the monomers' frequencies along with the intermolecular harmonic frequencies obtained for different basis sets. For the relative values of the frequency shifts, the allowance for the electron correlation is not so important as for their absolute values.

The use of calibration functions with the coefficients determined by least-squares method can be one of the methods for effective consideration of vibration anharmonicity in complexes. We propose the use of a linear calibration function

$$\nu_{corr} = a + b \cdot \omega_{calc},$$

where a and b are the calibration parameters; ω_{calc} are the calculated (HF/6-31G(d,p)) harmonic frequencies; ν_{corr} are the corrected values of the vibration frequencies. The experimental values of the monomers' frequencies ν (exp.) presented in Table 6 are used to determine the parameters of the function.

Table 6. Calculated ω_i and corrected ν_{corr} frequencies in the H_2n and HCl HonoHers

HF/6-31G(d,p), ω_i, cm^{-1}	ν_{exp}, cm^{-1}	ν_{corr}, cm^{-1}
3176	2886	2850
4262	3756	3795
4145	3657	3693
1770	1595	1627

The parameters a and b determined with the use of the calibration function by least-squares method are equal to 87 cm^{-1} and 0.87, respectively, and the mean absolute discrepancy between ν_{corr} and ν_{exp} is 34 cm^{-1}. The coefficient of correlation between the experimental and calculated frequencies is 0.998.

Results and discussion

Energy stability of $(H_2O)_n(HCl)_n$ complexes and their structure peculiarities

The complex $(H_2O)_n(HCl)_n$ with the even number of molecules $n = 2$ is characterized by the cyclic structure (Fig. 1, Table 7) with $\Delta E = -22.4$ kcal·mol^{-1} and the total energy $e = -1073.061328$ a.u. (MP2/aug-cc-pVDZ). The complex $(H_2O)_n(HCl)_n$ with $n = 3$ forms a closed plane structure (Fig. 2, Table 8) with the energy of monomer interaction of −37.35 kcal·mol^{-1} and the total energy $e = -1609.335210$ a.u. (MP2/6-31G(d,p)).

For the complex $(H_2O)_2(HCl)_2$, the H–Cl bond becomes considerably longer (Δr is ~ 0.02–0.06 Å) as compared with the monomer HCl, while the n –m bond elongates less significantly (~ 0.001–0.003 Å). As compared with the $(H_2O)_2HCl$ complex, addition of one more HCl molecule leads to shortening of the intermolecular bonds: ΔR(O–O) is 0.05 Å and ΔR(Cl–O) is 0.04–0.08 Å. As compared with the heterodimer H_2O…HCl, where ΔR(Cl–O) is 0.215 Å, and ΔR(n – O) = 0.18 Å as compared with the water dimer $(m_2n)_2$.

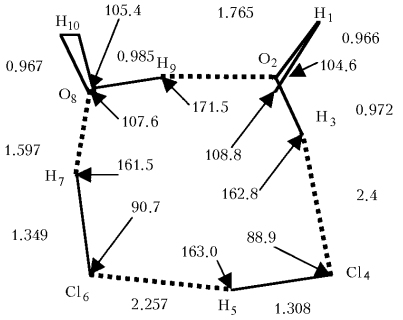

Fig. 1. Geometry of $(H_2O…HCl)_2$ complex.

Table 7. Cartesian coordinates (Å) for $(H_2O)_2...(HCl)_2$ coHplex (MP2/aug-cc-pVDZ)

—	Atomic number	*X*	*Y*	*Z*
1	1	1.273	2.690	0.888
2	8	0.937	2.277	0.082
3	1	1.431	1.443	0.009
4	17	1.970	−0.886	−0.204
5	1	0.702	−1.168	−0.053
6	17	−1.536	−1.336	0.188
7	1	−1.666	0.002	0.067
8	8	−1.718	1.594	−0.049
9	1	−0.790	1.925	−0.019
10	1	−2.077	1.912	−0.889

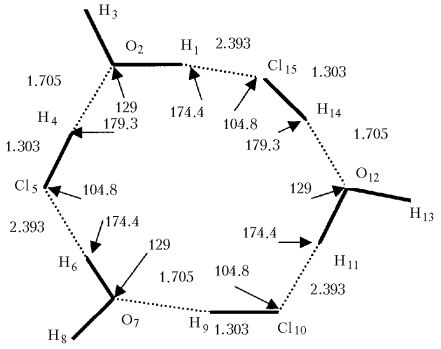

Fig. 2. Geometry of $(H_2O...HCl)_3$ complex.

Table 8. Cartesian coordinates (Å) for $(H_2O)_3...(HCl)_3$ coHplex (MP2/6-31G(d,p))

—	Atomic number	*X*	*Y*	*Z*
1	1	2.540	0.0	0.614
2	8	2.495	0.0	1.579
3	1	3.405	0.0	1.888
4	1	1.120	0.0	2.589
5	17	0.078	0.0	3.372
6	1	−1.802	0.0	1.891
7	8	−2.616	0.0	1.370
8	1	−3.338	0.0	2.005
9	1	−2.803	0.0	−0.325
10	17	−2.960	0.0	−1.619
11	1	−0.737	0.0	−2.504
12	8	0.121	0.0	−2.948
13	1	−0.066	0.0	−3.890
14	1	1.683	0.0	−2.263
15	17	2.882	0.0	−1.754

The complex $(H_2O)_3(HCl)_3$ is characterized by a decrease of the intermolecular Cl–O bond with ΔR(Cl–O) = 0.142 Å as compared with the heterodimer $H_2O...HCl$ and elongation of the Cl–O bond as compared with the complex $(H_2O)_2(HCl)_2$ by ΔR(Cl–O) = 0.06 Å. For the H–Cl intramolecular bond, the elongation with respect to the monomer HCl is 0.015 Å, and the elongation of the $(O–H)_b$ bond taking part in the hydrogen bonding is 0.003 Å.

Vibrational spectra of $(H_2O)_n(HCl)_n$ complexes

As was noted in the previous section, the calculated harmonic frequencies ω_i can differ significantly from the experimentally observed frequencies ν_i of the fundamental vibrational transitions. This discrepancy is caused, on the one hand, by the errors of HF method in calculating the ω_i and, on the other hand, with the contributions of anharmonic terms to ν_i when describing vibrational spectra of complexes with the hydrogen bonds. The shift $\Delta\omega = \omega_{monomer} - \omega_{complex}$ of the harmonic frequency of vibrations in the HCl molecule as calculated by the HF/6-31G(d,p) method is 161 cm^{-1} for the complex $H_2O...HCl$ (see Table 4), while the experimental[11] $\Delta\nu = \nu_{monomer} - \nu_{complex} = 216$ cm^{-1}. However, we should take into account that the use of N_2 matrix leads to a larger shift as compared with the gas phase (for similar systems in Ref. 11, the shift $\Delta\nu$ in the gas phase is 1.8 times smaller than $\Delta\nu$ with the use of the N_2 matrix). The anharmonic red shift obtained in Ref. 23 is 157 cm^{-1}. Thus, the frequency shift value determined as described above can be thought correct enough. The calculated ω_i and corrected ν_i frequencies of the complexes $(H_2O)_n(HCl)_n$ are given in Tables 9–11. The calculation predicts red shift of the frequency ν_{HCl} and the increase in the intensity of the corresponding spectral line.

Table 9. Frequencies of interHolecular vibrations in $(H_2O)_2...(HCl)_2$ coHplex (HF/6-31G(d,p))

ω_i, cm^{-1}, (*A*, km/mol)	$\nu_{i,corr}$, cm^{-1}	$\Delta\nu_i$, cm^{-1}
1776 (114)	1632	+5
1794 (73)	1648	+21
2825* (212)	2545	−305
3119* (254)	2801	−49
4014 (89)	3579	−114
4129 (62)	3679	−14
4226 (124)	3764	−31
4241 (139)	3777	−18

* ν is the stretching vibration of the H–Cl bond.

Table 10. Frequencies of interHolecular vibrations in $(H_2O)_3...(HCl)_3$ (HF/6-31G(d,p))

ω_i, cm^{-1}, (*A*, km/mol)	$\nu_{i,corr}$, cm^{-1}	$\Delta\nu_i$, cm^{-1}
1777 (107)	1633	+6
1777 (106)	1633	+6
1782 (0)	1637	+10
2859* (0)	2574	−276
2874* (1228)	2587	−263
2874* (1226)	2587	−15
4127 (0)	3678	−13
4130 (201)	3680	−13
4249 (0)	3680	−11
4249 (259)	3784	−11
4249 (260)	3784	−11

* ν is the stretching vibration of the H–Cl bond.

Table 11. Frequencies of interHolecular vibrations in $(H_2O)_n...(HCl)_n$ coHplexes (HF/6-31G(d,p))

ω_i, cm^{-1}, (A, km/mol) $(H_2O)_2...(HCl)_2$	ω_i, cm^{-1}, (A, km/mol) $(H_2O)_3...(HCl)_3$
23 (1)	8 (1)
44 (1)	13 (10)
83 (5)	13 (0)
85 (4)	31 (2)
140 (52)	31 (2)
174 (10)	57 (0)
212 (71)	73 (0)
221 (77)	87 (12)
244 (86)	87 (12)
268 (70)	109 (0)
290 (122)	109 (0)
389 (60)	192 (10)
431 (163)	192 (10)
558 (59)	197 (0)
680 (234)	278 (0)
799 (143)	279 (0)
	289 (0)
	312 (65)
	312 (65)
	315 (580)
	504 (0)
	504 (0)
	513 (295)
	669 (145)
	669 (145)
	702 (0)

Conclusion

The performed *ab initio* calculations of the complexes of water and hydrogen chlorine $(H_2O)_n...(HCl)_n$ {2:2; 3:3} refine the characteristics and improve the assignment of the IR spectra of water vapor mixed with hydrogen chloride under atmospheric conditions.

In all $(H_2O)_n...(HCl)_n$ {2:2; 3:3} complexes, the value of ν (HCl) shifts to lower frequencies. This shift for the considered complexes falls within the following frequency range $\Delta\omega$ (cm^{-1}): from −40 to −300. The other group of the low-frequency vibrations corresponds to the intermolecular vibrations of the $(H_2O)_n...(HCl)_n$ complexes and falls in the frequency range ~ 10–800 cm^{-1}.

The geometry of the considered complexes is characterized by manifestation of the cooperative nature of the intermolecular interactions, which results in a decrease of the length of the hydrogen bond between heavy atoms with respect to the heterodimer $H_2O...HCl$ and dimer $H_2O...H_2O$.

References

1. M.J. Molin, T.L. Tso, L.T. Molina, and F.C.Y. Wang, Science **238**, 1253–1257 (1987).
2. L.A. Surin, B.S. Dumesh, G. Winnewisser, and I. Pak, J. Chem. Phys. **113**, No. 20, 9351–9352 (2000).
3. I. Pak, L.A. Surin, B.S. Dumesh, D.A. Roth, F. Lewen, and G. Winnewisser, Chem. Phys. Lett. **304**, 145–149 (1999).
4. Z. Kisiel, A. Pietrewicz, P.W. Fowler, A.C. Legon, and E. Steiner, J. Phys. Chem. A **104**, No. 30, 6970–6978 (2000).
5. E. Isoniemi, M. Petterson, L. Khriachtchev, J. Lundell, and M. Rasanen, J. Phys. Chem. A **103**, No. 6, 679–685 (1999).
6. Y. Xu, W. Jäger, L.A. Surin, I. Pak, L.A. Panfilov, and G. Winnewisser, J. Chem. Phys. **111**, No. 23, 10476–10483 (1999).
7. S. Novick, *Bibliography of Rotational Spectra of Weakly Bound Complexes* (2001), http:// www.wesleyan.edu/ chem/faculty/novick/vdw.html
8. B.T.M. Willes, ed., *Chemical Applications of Thermal Neutron Scattering* (Oxford University, London, 1973), 300 pp.
9. R.K. Thomas, Proc. R. Soc. Lond. A **344**, 579–593 (1975).
10. A.C. Legon and L.C. Willoughby, Chem. Phys. Lett. **95**, 449–457 (1983).
11. B.S. Ault and G.C. Pimentel, J. Phys. Chem. **77**, No. 1, 57–61 (1973).
12. G.P. Ayers and A.D.E. Pullin, Spectrochim. Acta. Part A **32**, 1641–1650 (1976).
13. A. Schriver, B. Silvi, D. Maillard, and J.P. Perchard, J. Phys. Chem. **81**, 2095–2102 (1977).
14. Z. Latajka and S. Scheiner, J. Chem. Phys. **87**, No. 13, 5928–5936 (1987).
15. Z. Kisiel, E. Białkowska-Jaworska, L. Pszczółkowski, A. Milet, C. Struniewicz, R. Moszynski, and J. Sadlej, J. Chem. Phys. **112**, No. 13, 5767–5776 (2000).
16. S. Re, Y. Osamura, Y. Suzuki, and H.F. Schaefer, J. Chem. Phys. **109**, 973–977 (1998).
17. A. Milet, C. Struniewicz, R. Moszynski, and P.E.S. Wormer, J. Chem. Phys. **115**, No. 1, 349–356 (2001).
18. P.E.S. Wormer, G.C. Groenenboom, and A. Van der Avoird, J. Chem. Phys. **115**, No. 8, 3604–3613 (2001).
19. M.J. Frisch, G.W. Trucks, H.B. Schlegel, G.E. Scuseria, M.A. Robb, J.R. Cheeseman, V.G. Zakrzewski, J.A. Montgomery, R.E. Stratmann, J.C. Burant, S. Dapprich, J.M. Millam, A.D. Daniels, K.N. Kudin, M.C. Strain, O. Farkas, J. Tomasi, V. Barone, M. Cossi, R. Cammi, B. Mennucci, C. Pomelli, C. Adamo, S. Clifford, J. Ochterski, G.A. Petersson, P.Y. Ayala, Q. Cui, K. Morokuma, D.K. Malick, A.D. Rabuck, K. Raghavachari, J.B. Foresman, J. Cioslowski, J.V. Ortiz, B.B. Stefanov, G. Liu, A. Liashenko, P. Piskorz, I. Komaromi, R. Gomperts, R.L. Martin, D.J. Fox, T. Keith, M.A. Al-Laham, C.Y. Peng, A. Nanayakkara, C. Gonzalez, M. Challacome, P.M.W. Gill, B.G. Johnson, W. Chen, M.W. Wong, J.L. Andres, M. Head-Gordon, E.S. Replogle, and J.A. Pople, *Gaussian 98. Revision A.3.* (Gaussian, Inc., Pittsburgh PA, 1998).
20. N.A. Zvereva, Zh. Struktur. Khimii **42**, No. 5, 875–881 (2001).
21. K.P. Huber and G. Herzberg, *Molecular Spectra and Molecular Structure* (Van Nostrand Reinhold, New York, 1979), Vol. 4.
22. Z. Kisiel, A.C. Legon, and D.J. Millen, Proc. R. Soc. Lond. A **38**, 419–425 (1982).
23. Y. Hannachi, B. Silvi, and Y. Bouteiller, J. Chem. Phys. **94**, No. 4, 2915–2921 (1991).
24. R.M. Bentwood, A.J. Barnes, and W.J. Orville-Thomas, J. Mol. Spectrosc. **84**, 391–404 (1980).
25. D.R. Stull and J. Prophet, *JANAF Thermochemical Tables*, Natl. Stand. Ref. Data. Ser. Natl. Bur. Stand. (National Bureau of Standards, Washington, 1971), Vol. 17, 250 pp.

N.A. Zvereva Vol. 16, No. 3 /March 2003/ Atmos. Oceanic Opt. 203

Complexes with inorganic hydrides (NH_3, PH_3, AsH_3)

N.A. Zvereva

Institute of Atmospheric Optics,
Siberian Branch of the Russian Academy of Sciences, Tomsk

Received December 27, 2002

The optimal structures and harmonic vibrational frequencies of water complexes with NH_3, PH_3, AsH_3 have been determined by the Restricted Hartree–Fock (RHF) and second order Möller–Plesset perturbation theory (MP2) with augmented correlation consistent double zeta basis set for NH_3–H_2O, PH_3–H_2O complexes and 6-31++G(d, p) basis set for AsH_3–H_2O. At the MP2 level, this basis set yields very accurate results for the structure, dipole moment, and harmonic vibrational frequencies of water monomer. Analysis of the structural trends revealed that the separation between the neighboring oxygen atom and the X (N, P, As) atom increases in the row from N to As. The harmonic vibrational frequencies corresponding to OH_b ("bridge" hydrogen) stretches show large red shift by 224 cm^{-1} for the NH_3–H_2O complex, but for PH_3–H_2O and AsH_3–H_2O these shifts are about 20 cm^{-1}. The intensities corresponding to the OH_b stretches increase several orders of magnitude as a result of H-bonding. The intensity patterns are analyzed by means of electronic density redistribution, which reveals that intensification of the proton donor stretch is chiefly due to the increasing charge flux associated with H-bond formation.

Introduction

Ammonia is of greatest interest for ordinary atmospheric chemistry. Such hydrides as PH_3 and AsH_3 may present in trace amounts in the atmosphere. The structure of the $H_2O...NH_3$ was studied for the first time by the method of rotational spectroscopy in Refs. 1 and 2. The spectra in the microwave and far infrared regions (36–86 and 520–800 GHz, respectively) of the water–ammonia complex were studied in Ref. 3. Almost free rotation of the NH_3 molecule in the complex with the barrier of (10.5 ± 5.0) cm^{-1} were observed experimentally, as well as the H_2O tunneling effect leading to exchange of two protons in the water molecule with the barrier of 700 cm^{-1}. Fine spectral effects in the region of NH_3 umbrella mode at 1021 cm^{-1} were studied with a specialized IR spectrometer in Ref. 4. The observed set of vibrationally averaged rotational constants of the complex is better described by the presence of the "bent" intermolecular hydrogen bond in the complex (deviation of 10° from the linear configuration).

The $H_2O...NH_3$ complex in low-temperature matrices was studied by the IR spectroscopic method in the region of 4000–300 (Ref. 5) and 4000–10 cm^{-1} (Ref. 6). The longwave shift $\Delta\nu_{OH}$ of the ν_1 and ν_2 water bands in the $H_2O - NH_3$ complex as compared to the corresponding values of the free water molecule almost twice exceeds that for the water dimer.[7] Based on the almost linear dependence between enthalpy of complex formation ΔH_f and the value of $\Delta\nu_{OH}$ for the series of proton acceptors at the same donor, we can assume that ΔH_f for this complex will be roughly twice as large as that for the water dimer, that is, (–5.2 ± 1.5) kcal·mol^{-1} (Ref. 8). In Ref. 6 the principal attention was paid to analysis of low-frequency bands of intermolecular vibrations in the complex, and the bands nearby 19.5 cm^{-1} was assigned to the torsion vibration of the linearly (N...H–O) H-bonded water molecule around the symmetry axis of the complex, while the ammonia molecule remains fixed relative to the matrix. Stockman et al.[3] have assigned this band, taking into account the results of microwave and IR spectroscopic studies of this complex in the gas phase, to the rotation-torsion transitions of the water molecule lying between 20 and 22 cm^{-1}. In Refs. 9, 10, and 12–16 the potential surface of the $H_2O...NH_3$ complex and its vibrational spectrum were studied by quantum-chemistry methods.

The complexes of hydrides of elements belonging to the VA group of the low-lying periods (PH_3, AsH_3) with water in the gas phase are still almost unstudied. In Ref. 11 the comparative calculation of the structure and energy of the $H_2O...NH_3$ and $H_2O...PH_3$ complexes was performed (Table 1, where $R = |O...N|$; $r = |O–H|$; $\theta = \angle H–O...X$; ΔE is the bond energy with allowance for the electronic correlation calculated by the MP2 method; ΔH^0 is the enthalpy of the formation process). The strength of the complex with participation of phosphine is several times lower than that of the complex with participation of ammonia.

Table 1. Geometry and energy parameters of complexes

Complex	Basis set	R, Å	r, Å	θ, deg	ΔE, MP2, kcal/mol	ΔH^0, kcal/mol	Ref.
$H_2O...NH_3$	6-31G++(2d, 2p)	3.039	0.955	2.3	–6.6	–4.7	17
	6-31G**+VP*(2d)	3.096	0.930	4.6	–6.48	–4.16	18
$H_2O...PH_3$	6-31G++(2d, 2p)	3.918	0.949	3.0	–2.2	–0.8	19

0235-6880/03/03 203-08 $02.00

204 Atmos. Oceanic Opt. /March 2003/ Vol. 16, No. 3 N.A. Zvereva

In this paper we theoretically investigate the complexes of NH_3 and PH_3 in the augmented correlation consistent double zeta basis set aug-cc-pVDZ, calculate the structure and energy characteristics of the AsH_3 complex in the 6-31G(d, p) and 6-31++G(d, p) basis sets, determine the vibrational frequencies of the complexes considered, and analyze the main spectroscopic manifestations at H-bonding. Calculations are performed using Gaussiana-98, Restricted Hartree–Fock (RHF) and second order Möller–Plesset perturbation theory (MP2) (Ref. 24).

Theory

Vibrational analysis in *ab initio* calculations

Mass-weighted Hessian and diagonalization

Let us begin our study from the determination of the Hessian matrix $\mathbf{f}_{\mathrm{CART}}$, which includes second partial derivatives of the potential V with respect to displacement of atoms in the Cartesian coordinates (CART):

$$f_{\mathrm{CART}_{ij}} = \left(\frac{\partial^2 V}{\partial\xi_i \partial\xi_j}\right)_0 . \qquad (1)$$

It is the $3N \times 3N$ matrix (N is the number of atoms), where ξ_1, ξ_2, ξ_3, ..., ξ_{3N} are used for displacements in the Cartesian coordinates, Δx_1, Δy_1, Δz_1, ..., Δz_N. The designation $(\,)_0$ refers to the fact that the derivatives are taken at the equilibrium positions of the atoms, and that the first derivatives are zero. Then these force constants are converted to the mass-weighted Cartesian coordinates:

$$f_{\mathrm{MWC}_{ij}} = \frac{f_{\mathrm{CART}_{ij}}}{\sqrt{m_i m_j}} = \left(\frac{\partial^2 V}{\partial q_i \partial q_j}\right)_0 , \qquad (2)$$

where $q_1 = \sqrt{m_1}\xi_1 = \sqrt{m_1}\Delta x_1, q_2 = \sqrt{m_1}\xi_2 = \sqrt{m_1}\Delta y_1$, and so on are the mass-weighted Cartesian coordinates. The matrix $\mathbf{f}_{\mathrm{MWC}}$ is diagonalized, yielding a set of $3N$ eigenvectors and $3N$ eigenvalues. The eigenvectors, which are the normal modes, are discarded; they will be calculated again after the rotation and translation modes are separated. The roots of the eigenvalues are the fundamental frequencies of the molecule. They are converted to cm^{-1}. In general, the frequencies for rotation and translation modes should be close to zero. If there is a transition state or a higher order saddle point, then there will appear some negative frequencies.

Determination of the principal axes of inertia

The center of mass ($\mathbf{R}_{\mathrm{COM}}$) is found in the usual way:

$$R_{\mathrm{COM}} = \sum_\alpha m_\alpha r_\alpha \Big/ \sum_\alpha m_\alpha , \qquad (3)$$

where the sums are over the atoms α. The origin is then shifted to the center of mass $\mathbf{r}_{\mathrm{COM}_\alpha} = \mathbf{r}_\alpha - \mathbf{R}_{\mathrm{COM}}$. Next we have to calculate the moments of inertia (diagonal elements) and the products of inertia (off-diagonal elements) of the moment of inertia tensor (**I**):

$$\mathbf{I} = \begin{pmatrix} I_{xx} & I_{xy} & I_{xz} \\ I_{yx} & I_{yy} & I_{yz} \\ I_{zx} & I_{zy} & I_{zz} \end{pmatrix} =$$

$$= \begin{pmatrix} \sum\limits_\alpha m_\alpha (y_\alpha^2 + z_\alpha^2) & -\sum\limits_\alpha m_\alpha (x_\alpha y_\alpha) & -\sum\limits_\alpha m_\alpha (x_\alpha z_\alpha) \\ -\sum\limits_\alpha m_\alpha (y_\alpha x_\alpha) & \sum\limits_\alpha m_\alpha (x_\alpha^2 + z_\alpha^2) & -\sum\limits_\alpha m_\alpha (x_\alpha z_\alpha) \\ -\sum\limits_\alpha m_\alpha (z_\alpha x_\alpha) & -\sum\limits_\alpha m_\alpha (z_\alpha y_\alpha) & \sum\limits_\alpha m_\alpha (x_\alpha^2 + y_\alpha^2) \end{pmatrix} . \qquad (4)$$

This symmetric matrix is diagonalized, yielding the principal moments (the eigenvalues $\mathbf{I}'$) and a 3×3 matrix (**X**) which is made up of the normalized eigenvectors of **I**. The eigenvectors of the moment of inertia tensor are used to generate the vectors corresponding to translation and infinitesimal rotation of the molecule.

Separation of rotation and translation motion

Consider generation of the transformation of **D** from the mass-weighted Cartesian coordinates to a set of $3N$ coordinates, where rotation and translation of the molecule are separated, leaving $3N - 6$ or $3N - 5$ modes for vibrational analysis.

The three vectors ($\mathbf{D}_1$, $\mathbf{D}_2$, $\mathbf{D}_3$) of length $3N$ corresponding to translation are trivial to generate in the Cartesian coordinates (Sayvetz relationship). They are just $\sqrt{m_i}$ times the corresponding coordinate axis. For example, for $m_{\mathrm{H}} = 1$ and $m_{\mathrm{O}} = 16$ the translational vectors are

$$\mathbf{D}_1 = (1,0,0,4,0,0,1,0,0)^{\mathrm{T}},$$
$$\mathbf{D}_2 = (0,1,0,0,4,0,0,1,0)^{\mathrm{T}},$$
$$\mathbf{D}_3 = (0,0,1,0,0,4,0,0,1)^{\mathrm{T}}.$$

The vectors corresponding to rotational motion of atoms in the Cartesian coordinates can be written as

$$D_{4j,i} = [(P_y)_i X_{j,3} - (P_z)_i X_{j,2}]/(m_i)^{1/2},$$
$$D_{5j,i} = [(P_z)_i X_{j,1} - (P_x)_i X_{j,3}]/(m_i)^{1/2}, \qquad (5)$$
$$D_{6j,i} = [(P_x)_i X_{j,2} - (P_y)_i X_{j,1}]/(m_i)^{1/2},$$

where $j = x, y, z$; i is over all atoms, and P is the dot product of **R** (the coordinates of the atoms with respect to the center of mass) and the corresponding row of **X**. The next step is to normalize these vectors using the reciprocal square root of the scalar product.

A Schmidt orthogonalization is used to generate $N_{vib} = 3N - 6$ (or $3N - 5$) remaining vectors, which are orthogonal to the five or six rotational and translational vectors. The result is the transformation matrix **D**, which transforms from the mass-weighted Cartesian coordinates **q** to the internal coordinates **S** = **D q**, where rotation and translation have been separated.

Hessian transformation to internal coordinates and diagonalization

When transforming the Hessian $\mathbf{f}_{MWC}$ to the new internal coordinates (INT), only the N_{vib} coordinates corresponding to internal coordinates will be diagonalized, although the full $3N$ coordinates are used to transform the Hessian. The transformation is straightforward:

$$\mathbf{f}_{INT} = \mathbf{D}^{\dagger}\, \mathbf{f}_{MWC}\, \mathbf{D}. \qquad (6)$$

The $N_{vib} \times N_{vib}$ submatrix of $\mathbf{f}_{INT}$, which represents the force constants in internal coordinates, is diagonalized yielding N_{vib} eigenvalues $\lambda = 4\pi^2\nu$ and N_{vib} eigenvectors. If we call the transformation matrix composed of the eigenvectors **L**, then we have

$$\mathbf{L}^{\dagger}\, \mathbf{f}_{INT}\, \mathbf{L} = \mathbf{\Lambda}, \qquad (7)$$

where $\mathbf{\Lambda}$ is the diagonal matrix with eigenvalues λ_i.

Then the eigenvalues need to be converted into frequencies in units of wavenumbers. First we change from frequencies ν_i to wavenumbers $\tilde{\nu}_i$ via the relationship $\nu_i = \tilde{\nu}_i\, c$, where c is the speed of light. Solving $\lambda = 4\pi^2 \tilde{\nu}_i^2\, c^2$ for $\tilde{\nu}_i^2$, we obtain

$$\tilde{\nu}_i = \sqrt{\lambda_i / (4\pi^2 c^2)}\,. \qquad (8)$$

The rest is simply applying the appropriate conversion factors: from a single molecule to a mole, from hartrees to joules, and from atomic mass units to kilograms.

Combining Eqs. (6) and (7), we arrive at

$$\mathbf{L}^{\dagger}\, \mathbf{D}^{\dagger}\, \mathbf{f}_{INT}\, \mathbf{DL} = \mathbf{\Lambda} = \mathbf{l}_{MWC}{}^{\dagger}\, \mathbf{f}_{MWC}\, \mathbf{l}_{MWC}, \qquad (9)$$

where $\mathbf{l} = \mathbf{DL}$; $\mathbf{l}_{MWC}$ is determined from calculation of $\mathbf{l}_{CART}$. The elements of the matrix **M** are determined as

$$M_{i,i} = 1/\sqrt{m_i}\,, \qquad (10)$$

i runs over the x, y, and z coordinates for every atom. The individual elements are given by

$$\mathbf{l}_{CART_{k,i}} = \sum_{j}^{3N} \left(\frac{D_{k,j} L_{j,i}}{\sqrt{m_j}} \right). \qquad (11)$$

The column vectors of these elements, which are normal modes in the Cartesian coordinates, are used for calculating a number of spectroscopic properties, including IR intensities. First of all, once normalized by the procedure described below, they are displacements in the Cartesian coordinates. Each of the $3N$ elements of $\mathbf{l}_{CART_i}$ is scaled by normalization factor N_i for that particular vibrational mode. The normalization is defined by

$$N_i = \sqrt{\left(\sum_{k}^{3N} l^2_{CART_{k,i}} \right)^{-1}}\,. \qquad (12)$$

The reduced mass μ_i for the vibrational mode is calculated in a similar way:

$$\mu_i = \left(\sum_{k}^{3N} l^2_{CART_{k,i}} \right)^{-1} = \left[\sum_{k}^{3N} \left(\frac{l_{MWC_{k,i}}}{\sqrt{m_j}} \right)^2 \right]^{-1} =$$

$$= \left[\sum_{k}^{3N} \left(\frac{l^2_{MWC_{k,i}}}{m_j} \right) \right]^{-1} = N_i^2. \qquad (13)$$

Note that since **D** is orthonormal, and we can choose **L** to be orthonormal, then **l** is orthonormal as well (Since $\mathbf{D}^{\dagger}\,\mathbf{D} = 1$, $\mathbf{L}^{\dagger}\,\mathbf{L} = 1$ then $\mathbf{l}^{\dagger}\,\mathbf{l} = (\mathbf{DL})^{\dagger}\,\mathbf{DL} = \mathbf{L}^{\dagger}\,\mathbf{D}^{\dagger}\,\mathbf{DL} = \mathbf{L}^{\dagger}\,1\,\mathbf{L} = 1$).

There is a difference between the reduced mass calculated in the *ab initio* program and the one calculated using the formula usually used for diatomic molecules:

$$1/\mu = 1/m_1 + 1/m_2. \qquad (14)$$

Ab initio programs (like GAUSSIAN) use $l^2_{MWC_{k,i}}$ rather than 1. Using the elements of $\mathbf{l}_{MWC}$ gives consistent results for polyatomic cases, and automatically takes symmetry into consideration. Simple extending the formula (14) to $1/\mu = \Sigma 1/m_i$ would incorrectly yield the same reduced mass for every mode of a polyatomic molecule.

The coordinates used to calculate the force constants, the reduced mass and the Cartesian displacements all are self-consistent. The force constants k_i are written as $k_i = 4\pi^2\tilde{\nu}^2\mu_i$, since

$$\tilde{\nu} = \frac{1}{2\pi}\sqrt{\frac{k_i}{\mu_i}}\,.$$

The force constants are converted from atomic units to millidyne/angström.

Discussion

Energy stability of XH_3–H_2O (X = N, P, As) complexes

The geometry structure of the complexes XH_3–H_2O (X = N, P, As) (symmetry C_s) with the energy of interaction between monomer molecules (MP2/aug-cc-pVDZ): $\Delta E = -6.96$ kcal/mol (X = N); $\Delta E = -2.83$ kcal/mol (X = P), and (MP2/6-31++G(d,p): $\Delta E = -7.84$ kcal/mol (X = N); $\Delta E = -3.35$ kcal/mol (X = P); $\Delta E = -3.71$ kcal/mol (X = As), the

corresponding absolute minimum configuration on the potential energy surface (PES) has a bent intermolecular H-bond (for X = N, P the deviation from linearity is ~ 10°, which agrees with the data of Ref. 4). In the case of the AsH_3–H_2O complex, it is possible to speak about almost quasilinear H-bond (~ 2°). The complexes of elements of the VA-group of low-lying periods (PH_3, AsH_3) are less stable as compared to the complex with participation of ammonia.

In formation of complexes, we can notice the following structure changes in the monomers (Tables 2–4): for NH_3–H_2O the intramolecular parameters of NH_3 remain unchanged, while the water molecule is characterized by elongation of the OH_b bond (taking part in the formation of H-bonding) by 0.01 Å and increase of the valence angle by 1.5°; for the PH_3–H_2O complex one can see (Tables 2–4) insignificant elongation (0.003 Å) of the PH bond and increase of the HPH angle by 1°, for the water molecule in the complex no significant changes occur in the bond lengths and valence angles; for AsH_3–H_2O (Tables 2, 5, and 6) we can see increase in the valence angle HAsH by 1°, the AsH bond length remains almost unchanged, and for water molecule only OH_b changes by 0.01 Å.

Table 2. Geometry and energy parameters of H_2O

Parameter \ Method	RHF/ 6-31++G(d, p)	RHF/ aug-cc-pVDZ	MP2/ 6-31++G(d, p)	MP2/ aug-cc-pVDZ
$-E$, a.u.	76.031309	76.041843	76.233376	76.260910
μ, D	2.2259	1.9636	2.2774	2.0162
R(OH), Å	0.943	0.944	0.963	0.966
∠HOH, deg	107.2	106.0	105.3	103.9

Note. R(OH) = 0.957 Å; ∠HOH = 104.5°; μ = 1.854 (Ref. 23).

Table 3. Geometry and energy parameters of PH_3 and NH_3

Parameter \ Method	RHF/ aug-cc-pVDZ	MP2/ aug-cc-pVDZ	Parameter \ Method	RHF/ aug-cc-pVDZ	MP2/ aug-cc-pVDZ
PH_3 (C_{3V})			NH_3 (C_{3V})		
$-E$, a.u.	342.472369	342.614054	$-E$, a.u.	56.205590	56.404890
μ, D	0.7676	0.7125	μ, D	1.5822	1.6413
R(PH), Å	1.418	1.427	R(NH), Å	1.004	1.020
∠HPH, deg	95.5	93.7	∠HNH, deg	107.5	106.3
$\angle H_1H_3P_2H_4$, deg	96.17	94.0	$\angle H_1H_3N_2H_4$, deg	115.6	113.0
$R(PH)^{exp}$ = 1.412, Å			$R(NH)^{exp}$ = 1.02, Å		
$\angle HPH^{exp}$ = 93.6°			$\angle HNH^{exp}$ = 107.3°		

Table 4. Geometry and energy parameters of the complexes NH_3–H_2O and PH_3–H_2O

Parameter \ Method	RHF/ aug-cc-pVDZ	MP2/ aug-cc-pVDZ	Parameter \ Method	RHF / aug-cc-pVDZ	MP2/ aug-cc-pVDZ
NH_3–H_2O (C_s)			PH_3–H_2O (C_s)		
$-E$, a.u.	132.255238	132.676888	$-E$, a.u.	418.516763	418.879471
μ, D	3.4456	3.8783	μ, D	2.7326	2.6862
R(NH), Å	1.004	1.02	R(PH), Å	1.417	1.424
∠HNH, deg	107.4	106.4	∠HPH, deg	96.2	94.8
	105.4	106.3		96.0	94.7
	105.4	106.3		96.0	94.7
∠HOH, deg	106.1	104.5	∠HOH, deg	105.8	104.0
$R(OH_f)$, Å	0.943	0.965	$R(OH_f)$, Å	0.943	0.966
$R(OH_b)$, Å	0.951	0.979	$R(OH_b)$, Å	0.946	0.970
R(N…O), Å	3.087	2.939	R(P…O), Å	3.919	3.599
$\angle HNH_b$, deg	120.8	120.5	$\angle HPH_b$, deg	127.0	129.3
	106.6	108.2		117.3	116.1
	106.6	108.2		117.3	116.1
$\angle NH_bO$, deg	172.7	170.7	$\angle PH_bO$, deg	177.5	168.0
$\angle H_7NOH_f$, deg	−123.3	123.4	$\angle H_7POH_f$, deg	123.1	125.0

Note. $R(N…H)_{exp}$ = 2.983 Å (Ref. 21).

Table 5. Geometry and energy parameters of AsH_3

Method / Parameter	RHF / 6-31G(d, p)	RHF / 6-31++G(d, p)	MP2/ 6-31G(d, p)	MP2/ 6-31++G(d, p)
$-E$, a.u.	2233.718274	2233.734738	2233.718107	2233.854811
μ, D	0.5571	0.5943	0.5035	0.5462
R(AsH), Å	1.501	1.491	1.505	1.494
∠HAsH, deg	93.7	93.7	92.2	92.455
$\angle H_1H_3As_2H_4$, deg	93.9	94.0	92.3	92.565

Note. R(AsH) = 1.511 Å, ∠HAsH = 92.1° (Ref. 20).

Table 6. Geometry and energy parameters of AsH_3–H_2O

Method / Parameter	RHF / 6-31G(d, p)	RHF / 6-31++G(d, p)	MP2/ 6-31G(d, p)	MP2/ 6-31++G(d, p)
$-E$, a.u.	2309.745989	2309.770621	2310.062612	2310.094099
μ, D	2.6204	2.8194	2.3297	2.902
R(AsH), Å	1.499	1.489	1.501	1.492
∠HAsH, deg	94.6	94.3	92.1	93.1
	94.9	94.7	93.2	93.5
	94.9	94.7	93.2	93.5
∠HOH, deg	105.7	106.9	103.5	105.1
$R(OH_f)$, Å	0.943	0.943	0.962	0.963
$R(OH_b)$, Å	0.944	0.945	0.962	0.966
R(As…O), Å	4.037	3.960	3.902	3.781
$\angle HAsH_b$, deg	141.9	129.8016	175.0	130.8
	110.4	117.8	89.7	118.6
	110.4	117.8	89.7	118.6
$\angle AsH_bO$, deg	177.3	178.0	176.7	178.1
$\angle H_7AsOH_f$, deg	128.6	124.2	133.9	124.5

Intermolecular vibrations of XH_3–H_2O complexes

Analysis of normal modes of the NH_3–H_2O complex shows that the smallest vibrational frequency of 41 cm^{-1} (A″) can be assigned to the torsion vibration of the NH_3 group, while the frequency of 187 cm^{-1} (A″) can be assigned to the torsion vibration of the H_2O molecule. The frequency of 176 cm^{-1} (A′) corresponds to stretching of the H-bond (N…O). The vibrational frequency of 201 cm^{-1} (A′) is determined by bending mode of the NH_3 proton acceptor. The frequencies of 447 (A′) and 727 cm^{-1} (A″) can be assigned to bending vibrations of the H_2O proton donor.

Analysis of normal mode frequencies of the PH_3–H_2O complex shows that the frequency of 23 cm^{-1} (A″) can be assigned to the torsion vibration of the H_2O molecule, while the frequency of 78 cm^{-1} (A″) can be assigned to the torsion mode of the PH_3 group. The frequency of 93 cm^{-1} (A″) is connected with the bending mode of the PH_3 proton acceptor. Stretching of the H-bond (P…O) corresponds to the frequency of 106 cm^{-1} (A′). The frequencies of 245 (A′) and 397 cm^{-1} (A″) can be assigned to the bending modes of the H_2O proton donor.

For the AsH_3–H_2O complex, the frequency of 20 cm^{-1} (A″) can be assigned to the torsion vibration of the AsH_3 group, and the frequency of 122 cm^{-1} (A″) – to the torsion vibration of the water molecule. Stretching of the H-bond (As…O) corresponds to the frequency of 74 cm^{-1} (A′). The frequencies of 237 (A′) and 419 cm^{-1} (A″) can be assigned to bending vibrations of the H_2O proton donor.

Intramolecular vibrations of XH_3–H_2O complexes

Intramolecular bending vibrations of the NH_3 group in the NH_3–H_2O complex occur at the frequencies of 1110 (A′), 1645 (A′) and 1647 cm^{-1} (A″), and the stretching vibrations at 3476 (A′), 3627 (A″), and 3629 cm^{-1} (A′). The frequencies of 1662 (A′, bending vibration) and 3579 cm^{-1} (A′) can be assigned to intramolecular vibrations of the water molecule; 3895 cm^{-1} (A′) corresponds to the bending vibrations of OH.

The frequencies of 1007 (A′), 1152 (A′), and 1153 cm^{-1} (A″) are assigned to intramolecular bending vibrations of the PH_3 group of the PH_3–H_2O complex, while the frequencies of 2465 (A′), 2483 (A′), and 2486 cm^{-1} (A″) are assigned to stretches. The intramolecular vibrations of the water molecule are characterized by the frequencies of 1629 cm^{-1} (A′, bending vibration) and 3751 cm^{-1} (A′); 3908 cm^{-1} (A′) corresponds to OH stretches.

The intramolecular bending vibrations of the AsH_3 group in the AsH_3–H_2O complex have the frequencies of 1029 (A′), 1242 (A′), and 1243 cm^{-1} (A″), while the stretches have the frequencies of 2454 (A′), 2477 (A′), and 2459 cm^{-1} (A″). The frequencies of 1747 cm^{-1} (A″, bending) and 4130 cm^{-1} (A′) can be assigned to intramolecular modes of the water molecule; 4253 cm^{-1} (A′) corresponds to OH stretches.

Significant changes in the frequencies of intramolecular vibrations at H-bonding were observed in proton donor, namely, the OH_b bond (OH_b – X … O–H_b, O–H_f – free valence bond) of the water molecule: for the NH_3–H_2O complex the displacement $\Delta\omega = 224$ cm^{-1} with a considerable intensity increase (see Tables 7–9). With a decrease of the interaction energy in the PH_3–H_2O and AsH_3–H_2O complexes, these displacements are not so large (~ 20 cm^{-1}), but the increase in the band intensity is observed, though not so large as in the NH_3–H_2O complex.

Table 7. Vibrational frequencies of NH_3, PH_3, AsH_3

Molecule			ω, cm^{-1} (*A*, km/mol)					
			NH_3		PH_3		AsH_3	
Experiment[20]			RHF	MP2	RHF	MP2	RHF	
NH_3	PH_3	AsH_3	aug-cc-pVDZ		aug-cc-pVDZ		6-31G(d,p)	6-31++G(d,p)
950	992	906	1104 (172)	1046 (131)	1091 (25)	1008 (18)	1022 (46)	1103 (47)
1628	1122	999	1766 (18)	1649 (13)	1224 (17)	1152 (18)	1155 (21)	1241 (22)
1628	1122	999	1767 (18)	1650 (13)	1224 (17)	1152 (13)	1155 (21)	1241 (22)
3337	2323	2115	3686 (1)	3480 (5)	2525 (40)	2452 (34)	2428 (67)	2443 (156)
3444	2328	2126	3816 (5)	3634 (5)	2528 (87)	2469 (59)	2431 (141)	2444 (156)
3444	2328	2126	3820 (5)	3636 (5)	2528 (87)	2469 (59)	2431 (141)	2461 (85)

Table 8. Harmonic vibrational frequencies of the water molecule ω, in cm^{-1}

Method / Symmetry	RHF / /6-31++G(d, p)	RHF / /aug-cc-pVDZ	MP2/ /6-31++G(d, p)	MP2/ /aug-cc-pVDZ	Experiment[20]
A_1	1728 (114)	1744 (93)	1679 (78)	1622 (67)	1648
A_1	4145 (20)	4130 (14)	3912 (4)	3803 (4)	3832
B_2	4268 (90)	4237 (88)	4050 (34)	3938 (67)	3943

Table 9. Vibrational frequencies of NH_3–H_2O, PH_3–H_2O, AsH_3–H_2O complexes

ω, cm^{-1} (*A*, km/mol)					
NH_3–H_2O		PH_3–H_2O		AsH_3–H_2O	
RHF	MP2	RHF	MP2	RHF	
aug-cc-pVDZ		aug-cc-pVDZ		6-31G(d,p)	6-31++G(d,p)
Frequencies of intermolecular vibrations					
50 (82)	41 (71)	20 (98)	23 (86)	15 (88)	20 (125)
150 (6)	176 (19)	67 (1)	78 (14)	47 (9)	74 (0)
172 (39)	187 (40)	88 (21)	93 (16)	61 (8)	103 (10)
176 (50)	202 (35)	93 (5)	106 (7)	72 (0)	122 (9)
404 (94)	447 (83)	209 (75)	245 (79)	176 (103)	237 (109)
642 (141)	727 (90)	332 (106)	397 (52)	294 (169)	419 (142)
Frequencies of intramolecular vibrations					
1167 (183)	1110 (138)	1090 (35)	1007 (30)	1014 (58)	1029 (61)
1766 (20)	1645 (42)	1223 (15)	1152 (10)	1148 (19)	1243 (19)
1766 (50)	1647 (16)	1224 (17)	1153 (12)	1148 (23)	1243 (25)
1776 (38)	1662 (11)	1752 (67)	1629 (31)	1781 (85)	1747 (84)
3683 (0)	3476 (0)	2534 (41)	2465 (33)	2437 (76)	2454 (130)
3811 (10)	3579 (547)	2538 (69)	2483 (44)	2443 (107)	2459 (128)
3813 (9)	3627 (12)	2540 (70)	2486 (41)	2444 (119)	2477 (78)
4017 (332)	3629 (11)	4110 (87)	3751 (154)	4142 (51)	4130 (90)
4208 (111)	3895 (85)	4223 (154)	3908 (154)	4256 (112)	4253 (159)

Redistribution of electron density at H-bonding

Consideration of the electron density distribution at formation of complexes (Fig. 1) shows that for the NH_3–H_2O complex not only the intramolecular charge redistribution (charge flux of – 0.045e from the H atoms to the N atom of the NH_3 group, for the water molecule) from the H_b atom to the O and H_f atoms + 0.111e is observed, but also the intermolecular charge flux from NH_3 to H_2O $\Delta Q = 0.07$e.

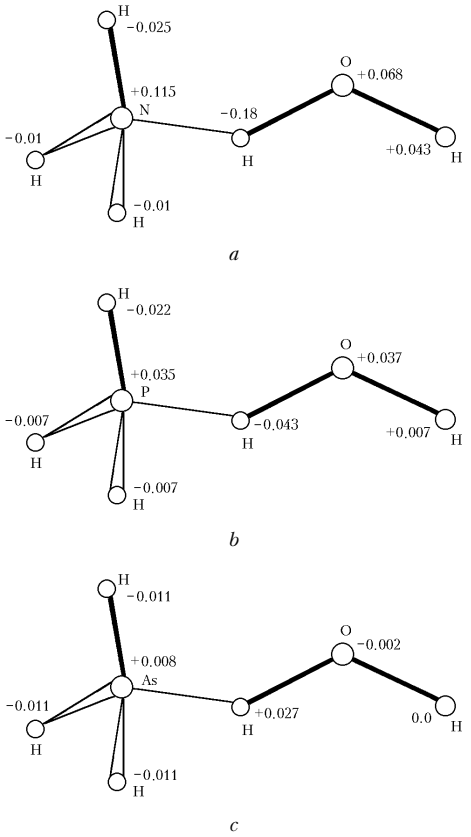

Fig. 1. Geometry structure and changes of the total charge Q at formation of NH_3–H_2O (*a*), PH_3–H_2O (*b*), and AsH_3–H_2O (*c*) complexes.

For the PH_3–H_2O complex the intermolecular charge flux is insignificant $\Delta Q = 0.001$e, and inside the PH_3 group the following charge redistribution occurs: charge flux of + 0.035e from the H atoms to the P atom, and for the water molecule – charge flux of + 0.044e from the H_b atom to the O and H_f atoms. The AsH_3–H_2O complex is also characterized by lower intermolecular charge flux as compared with the NH_3–H_2O complex – ΔQ = 0.025e, the charge is transferred from the AsH_3 group to H_2O, and intramolecular charge redistribution is the following: the electron density of + 0.008e is transferred from the H atoms of the AsH_3 group to the As atom and –0.002e is transferred from the oxygen atom of the water molecule to the H_b atom. The high charge flux in the NH_3–H_2O complex determines the largest increase in the intensity of OH_b vibration.

Conclusion

Harmonic vibrational frequencies corresponding to the OH_b (the H atom of the hydrogen bridge) stretch are characterized by the largest red shift – 224 cm^{-1} for the NH_3–H_2O complex, while for PH_3–H_2O and AsH_3–H_2O these shifts are about 20 cm^{-1}. The intensities corresponding to the OH_b stretch increase by several orders of magnitude at H-bond formation. Analysis of intensity variations through consideration of electron density redistribution reveals that the increase in the intensity of the stretching vibration of the proton donor is primarily determined by the increase in the charge flux at H-bond formation.

References

1. A.J. Fillery-Travis, A.C. Legon, and L.C. Willoughby, *The structure of* NH_3–H_2O, Proc. Roy. Soc. London. A **396**, 405–411 (1984).
2. P. Herbine, T.A. Hu, G. Johnson, and T.R. Dyke, *The structure of* NH_3–H_2S *and free internal rotational effects*, J. Chem. Phys. **93**, No. 8, 5485–5495 (1990).
3. P.A. Stockman, R.E. Bumgarner, S. Suzuki, and G.A. Blake, *Microwave and tunable far-infrared laser spectroscopy of the ammonia–water dimer*, J. Chem. Phys. **96**, No. 4, 2496–2510 (1992).
4. G.T. Fraser and R.D. Suenram, *Perturbations in the infrared spectrum of the* NH_3 *umbrella mode of* HOH–NH_3, J. Chem. Phys. **96**, No. 10, 7287–7297 (1992).
5. Engdahl and B. Nelander, *The intermolecular vibrations of the ammonia water complex. A matrix isolation study*, J. Chem. Phys. **91**, No. 11, 6604–6612 (1989).
6. Nelander and L. Nord, *Complex between water and ammonia*, J. Phys. Chem. **86**, No. 22, 4375–4379 (1982).
7. G.A. Yeo and T. Ford, Struct. Chem. **3**, 75–82 (1992).
8. G.C. Pimentel and A.L. McClellan, *Study of ammonia complex*, Ann. Rev. Phys. Chem. **22**, 349–353 (1971).
9. H.A. Gebbie, W.J. Burroughs, J. Chamberlain, J.E. Harries, and R.G. Jones, *Dimers of the water molecule in the earth's atmosphere*, Nature (Gr. Brit.) **221**, 143–145 (1969).
10. Z. Latajka and S. Scheiner, *Energetics, and vibrational spectrum of* NH_3...HOH, J. Phys. Chem. **94**, No. 1, 217–227 (1990).
11. H.S. Rzepa and Min Yan Yi, *Ab initio study of* H_2O...NH_3 *and* H_2O...PH_3, J. Chem. Soc. Perkin Trans. 2, 943–954 (1990).
12. C.S. Dykstra and L. Andrews, *Structures, stabilities, and intermolecular vibration frequencies of small ammonia complex by molecular mechanics for clusters analysis*, J. Chem. Phys. **92**, No. 10, 6043–6048 (1990).

13. E.L. Coitino, O.N. Ventura, and R.M. Sosa, J. Mol. Struct. **254**, 315–320 (1992).
14. G.A. Yeo and T.A. Ford, *Ab initio molecular orbital calculations of the infrared spectra of complexes of water, ammonia and hydroxylamine. Part 10. The intermolecular modes*, J. Mol. Struct. **266**, 183–204 (1992).
15. E.C. Vauthier, V. Barone, C. Minichino, and S. Fliszar, Can. J. Chem. **68**, 1233–1239 (1990).
16. J.E. Del Bene, *Ab Initio Molecular Orbital Study of the Structure and Energetics of Neutral and Changed Biomolecular Hidrides*, AH_n (*A* = N, O, F, P, S, *and* Cl), J. Phys. Chem. **92**, No. 10, 2874–2880 (1988).
17. R.C. Cohen and R.J. Saykally, *Extending the Collocation Method to Multidimensional Molecular Dynamics: Direct Determination of the Intermolecular Potential of* Ar–H_2O *from Tunable Far-Infrared Laser Spectrum*, J. Phys. Chem. **94**, No. 20, 7991–8000 (1990).
18. J.J. Novoa, B. Tarron, and L.M. Myung-Hwan Whangbo, *Interaction energies associated with short intermolecular contacts of* C–H *bonds. Ab initio computational study of the* C–H...O *contact interaction in* CH_4...OH_2, J. Phys. Chem. **95**, Iss. 7, 5179–5186 (1991).
19. J. Novoa and F. Mota, *Substituent effects in intermolecular* $C(sp^3)$–H...$O(sp^3)$ *contacts: how strong can a* $C(sp^3)$–H...$O(sp^3)$ *hydrogen bond be?* Chem. Phys. Lett. **266**, Iss. 1–2, 23–30 (1997).
20. K.S. Krasnov, ed., *Molecular Constants of Inorganic Compounds* (Khimiya, Leningrad, 1979), 446 pp.
21. P. Herbine and T.R. Dyke, *Rotational spectra and structure of the ammonia–water complex*, J. Chem. Phys. **83**, No. 8, 3768–3774 (1985).
22. W.S. Benedict, N. Gailar, and E.K. Plyler, J. Chem. Phys. **24**, 1139–1143 (1956).
23. S.S. Xantheas and T.H. Dunning, *Ab initio studies of cyclic water clusters* $(H_2O)_n$, $n = 1–6$. *I. Optimal structures and vibrational spectra*, J. Chem. Phys. **99**, No. 11, 8774–8792 (1993).
24. M.J. Frisch, G.W. Trucks, H.B. Schlegel, G.E. Scuseria, M.A. Robb , J.R. Cheeseman, V.G. Zakrzewski, J.A. Montgomery, Jr., R.E. Stratmann, J.C. Burant, S. Dapprich, J.M. Millam, A.D. Daniels, K.N. Kudin, M.C. Strain, O. Farkas, J. Tomasi, V. Barone, M. Cossi, R. Cammi, B. Mennucci, C. Pomelli, C. Adamo, S. Clifford, J. Ochterski, G.A. Petersson, P.Y. Ayala, Q. Cui, K. Morokuma, D.K. Malick, A.D. Rabuck, K. Raghavachari, J.B. Foresman, J. Cioslowski, J.V. Ortiz, B.B. Stefanov, G. Liu , A. Liashenko, P. Piskorz , I. Komaromi, R. Gomperts, R.L. Martin, D.J. Fox, T. Keith, M.A. Al-Laham, C.Y. Peng, A. Nanayakkara, C. Gonzalez, M. Challacombe, P.M.W. Gill, B.G. Johnson, W. Chen, M.W. Wong, J.L. Andres, M. Head-Gordon, E.S. Replogle, and J.A. Pople, *Gaussian 98, Revision A. 3* (Gaussian, Inc., Pittsburgh PA, 1998).

832 Atmos. Oceanic Opt. /November 2004/ Vol. 17, No. 11 N.A. Zvereva et al.

Database of structure-energy and spectral characteristics of $(H_2O)_mM_n$ complexes in gas phase

N.A. Zvereva, Yu.S. Gospodareva, and Yu.N. Ponomarev

Institute of Atmospheric Optics,
Siberian Branch of the Russian Academy of Sciences, Tomsk

Received September 1, 2004

The first version of the database of structure, energy and spectral characteristics of H_2O complexes with diatomic HX molecules, where X = F, Cl, and the number of molecules in a complex varies from two to six, is considered.

Introduction

Real-time monitoring of gaseous emissions from industrial enterprises is now carried out by remote sensing methods with IR lasers.[1] The efficient use of these lasers and the development of physical principles for new diagnostics methods requires systematically ordered information about the structure, physical-chemical and optical characteristics of such components of gaseous emissions as molecules and molecular complexes. Chemically active molecules of anthropogenic origin (fluorides, hydrides, and others) interact with water vapor yielding the formation of complexes of $(H_2O)_mM_n$ type, where $m, n \geq 1$.

In addition to the gas-phase reactions, whose probability is rather high at a relatively high concentration of reagent molecules, formation of stable molecular complexes of the donor-acceptor type is possible in the atmosphere. The binding energies in such complexes can amount up to several tens of kilocalories.[2,3] The complexes can show the optical activity high enough for their detection in the atmosphere by remote methods. As a rule, these complexes are characterized by several types of high-amplitude motions,[3–6] leading to the transformation of vibrational spectra of the molecular components and the appearance of new absorption bands, corresponding to intermolecular vibrations.

The characteristics of optical spectra of individual molecules can be found, in a systematized form, in databases, such as, for example, HITRAN.[7] For molecular complexes, no such a systematization is available, despite the urgent practical need.

This paper considers the structures of databases, compiled by analogy with HITRAN,[7] for the complexes of H_2O with diatomic molecules $(H_2O)_mM_n$, where $1 \leq m, n \leq 6$.

Characteristics of $(H_2O)_mM_n$ complexes

Consider a set of characteristics of the complexes and their spectra, which should be included into the database and determine the database structure, with the $(H_2O)_m(HF)_n$ complex taken as an example. For the simplest H_2O … HF complex, a rather detailed information on the structure, energy, and spectral characteristics is available.[7,8]

Tables 1 and 2 from Ref. 8 illustrate how the amount of information to be included into the database increases as the complex forms (Fig. 1).

Fig. 1. Geometric structure of H_2O…HF complex (C_s symmetry) calculated by the HFR/6-31G** method; $E_{tot} = -176.0497$ a.u., H–O–H angle of 107°, O–H_b–F angle of 176°; internuclear separations are given in Å; H_b is the bridge atom.

As the number of molecules in the complex increases up to three and more, the complex can exist in several configurations with significantly different structure, energy, and spectral characteristics. Thus, for the H_2O…$(HF)_2$ complex, two of all possible configurations (Fig. 2) are stable. They are characterized by the binding energies of 15 and 21 kcal·mol^{-1}, corresponding to the open (Fig. 2*a*) and closed (Fig. 2*b*) structures. The closed configuration of the H_2O…$(HF)_2$ complex is more stable. The frequencies and intensities of intramolecular vibrations for the H_2O…$(HF)_2$ complex with the open and closed structures are given in Table 3 on the basis of the data from Ref. 8, and the frequencies and intensities of intermolecular vibrations are given in Table 4.

As can be seen from Tables 3 and 4, the formation of complexes changes the frequencies of intramolecular vibrations and leads to appearance of the bands corresponding to low-frequency intermolecular vibrations.

0235-6880/04/11 832-05 $02.00

Table 1. Geometric and energy characteristics of HF, H_2O monomers, and H_2O...HF complex, calculated by different methods and obtained experimentally[a]

Molecule	Symmetry	Method	ΔE, kcal·mol^{-1}	R_e, Å			Angle, deg		
				H_b–F	O–H	O–F	H–O–H	α	H_b–F–O
HF	$C_{\infty v}$	HFR/6-31G**[b]	–	0.90	–	–	–	–	–
		Experiment, Ref. 9	–	0.92	–	–	–	–	–
H_2O	C_{2v}	HFR/6-31G**[b]	–	–	0.94	–	106	–	–
		Experiment, Ref. 10	–	–	0.96	–	105	–	–
H_2O...HF	C_s	HFR/6-31G**[b]	9	0.91	0.94	2.72	107	134	4
		MP2/6-31G**[b]	11	0.93	0.96	2.67	105	131	6
		MP2/6-311G** [Ref. 11]	11	0.92	0.96[c]	2.64	105[c]	129	5
		MP3/6-311G**[Ref. 11]	11	0.92	0.96[c]	2.65	105[c]	133	3
		Experiment, Refs. 11, 12	–	–	–	2.66	–	134	–
		MP4/6-311+G(2d,2p) [Ref. 13]	9[d]	0.92[d]	–	2.72[d]	–	–	5[d]
		Experiment, Ref. 14	10	–	–	–	–	–	–

[a] Atomic designations in the complex are shown in Fig. 1; ΔE is the binding energy between monomers in the complex; α is the angle between the axis O–F and the bisector of H–O–H angle. [b] Calculation from Ref. 6. [c] In the calculation of Ref. 11 by the Möller–Plesset perturbation theory of the second (MP2) and third (MP3) orders, the geometric parameters of the H_2O molecule had experimental values.[10] [d] Calculation by the Möller–Plesset perturbation theory of the fourth order (MP4) with the geometric parameters optimized by the HFR method in the 6-31G* basis.

Table 2. Harmonic frequencies (ω_i/cm^{-1}) of vibrations of HF and H_2O monomers and H_2O...HF complex

H_2O...HF			H_2O			HF		
Calc.[a]	Exp. [Ref. 15]	Assignment[b]	Calc.[a]	Exp. [Ref. 10]	Assignment[b]	Calc.	Exp. [Ref. 9]	Assignment[b]
4270	3608 ± 2	$\upsilon(H_bF)$	4265[a]	3939	υ^{as}(OH)	4493[a]	4138	υ(HF)
4258	3756	υ^{as}(OH)	4052[c]	–	–	4212[c]	–	–
4142	3657	υ^{s}(OH)	4010[d]	–	~	4119[d]	–	–
1765	1595	δ(HOH)	4148[a]	3835	υ^{s}(OH)	–	–	–
760	696 ± 30	$\delta_i(OH_bF)$	3909[c]	–	–	–	–	–
626	666 ± 30	$\delta_0(OH_bF)$	3863[d]	–	–	–	–	–
236	180 ± 30	$\upsilon(H_2O...H_bF)$	1770[a]	1648	δ(HOH)	–	–	–
206	145 ± 50	$\delta_0(HOH_b)$	1674[c]	–	–	–	–	–
194	170 ± 50	δ_i (HOH_b)	1620[d]	–	–	–	–	–

[a] Calculation of Ref. 6. [b] For the complex (see Fig. 1) the frequencies (υ) [Ref. 15] of fundamental transitions are presented. Designations: υ^s and υ^{as} are stretching symmetric and antisymmetric vibrations, respectively; δ are bending vibrations in the plane of the H_2O molecule (δ_i) and out of the plane (δ_0). [c] Calculation [Ref. 6] by the MP2 method in the 6-31G** basis. [d] Calculation [Ref. 16] by the MP2 method in the 6-31++G** basis.

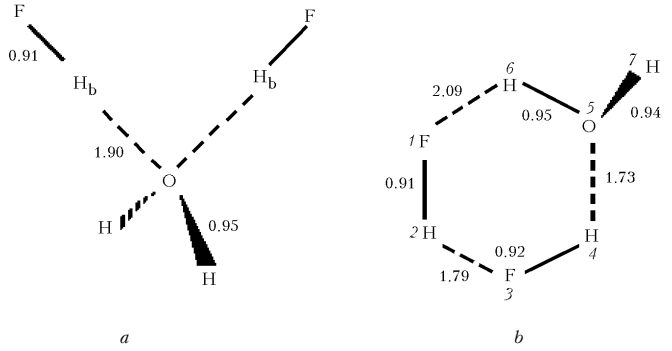

Fig. 2. Geometric structure of the complexes: H_2O–$(HF)_2$ of C_{2v} symmetry (*a*) and H_2O–$(HF)_2$ of C_1 symmetry (*b*), calculated by the HFR/6-31G** method. Internuclear separations are given in Å, the angles between bonds and binding energies are tabulated in Tables 1 and 7.

Table 3. Frequencies (ω_i; cm^{-1}) and intensities of IR vibrational bands (S_i; $km \cdot mol^{-1}$) of $H_2O...(HF)_2$ complexes with open (C_{2v}) and closed (C_1) structure

Complex (symmetry)	$\omega_i(S_i)$	Assignment
$H_2O \cdot (HF)_2$ (C_{2v})	1765(121)	δ(HOH) (A_1)
	4120(81)	υ(OH) (A_1)
	4230(152)	υ(OH) (B_1)
	4331 (839)	υ(H_bF) (B_2)
	4357(142)	υ(H_bF) (A_1)
$H_2O \cdot (HF)_2$ (C_1)	1777(112)	δ($H_6O_5H_7$)
	4024(555)	υ(H_4F_3)
	4103(190)	υ(O_5H_6)
	4228(154)	υ(O_5H_7)
	4268 (544)	υ(H_2F_1)

Table 4. Intermolecular harmonic vibrational frequencies of $H_2O \cdot (HF)_2$ complexes (cm^{-1}) and the corresponding intensities of IR bands

Complex (symmetry)	$\omega_i(S_i)$
$H_2O \cdot (HF)_2$ (C_{2v})	691 (65)
	690 (349)
	647 (238)
	592 (362)
	250 (114)
	199 (23)
	175 (0)
	167 (3)
	100 (0)
	32 (12)
$H_2O \cdot (HF)_2$ (C_1)	1055 (121)
	805 (409)
	669 (378)
	548 (91)
	522 (240)
	334 (60)
	266 (6)
	236 (103)
	223 (7)
	162 (11)

Architecture of the database on structure–energy and spectral characteristics of complexes

The developed version of the database on the characteristics of $(H_2O)_mM_n$ complexes assumes the input and systematization of the information about the following characteristics:

– geometry of a complex in the equilibrium state;

– binding energies of the component molecules;

– frequencies of intra- and intermolecular vibrations;

– intensities of vibrational IR bands;

– electro-optical characteristics (dipole moment, polarizability);

– concentrations of monomer molecules, forming the complex, and complexes in the gas medium (atmosphere);

– sources of information (in each column).

Table 5 summarizes the designations used in the database. A database string format is illustrated in Table 6.

Table 5. Designations of characteristics included in the database for $(H_2O)_m(HX)_n$, X = F, Cl, complexes

Symbol	Characteristic
R_e	Equilibrium bond length
ΔE	Binding energy between monomers
α	Angle between the axis O–F and the bisector of ∠H–O–H
ω_i	Frequencies of vibrational bands
υ_s	Stretching symmetric vibrations
υ_{as}	Stretching antisymmetric vibration
Δ	Bending vibrations
δ_i	Bending vibrations in the plane of the H_2O molecule
Δ_0	Bending vibrations out of the plane of the H_2O molecule
N	Equilibrium concentration of complexes
A	Intensity of absorption band
a	Calculation by the HFR/6-31G** method
b	Calculation by the MP2/6-31G** method
c	Calculation by the Möller–Plesset perturbation theory MP2/6-311G**
d	Calculation by MP3/6-311G**
e	Calculation by MP4/6-311+G(2d,2p)
f	Calculation by MP2/6-31++G**
g	Calculation by HFR/6-31G**+VP^s
h	Calculation by HFR/6-31G**+VP^s(2d)^s
j	Calculation by MP2/6-31G**+VP^s(2d)^s
μ, α	Dipole moment and polarizability

Table 6. String format

Parameter	Units
Type of the complex	
Equilibrium bond length	Å
Angles between bonds	deg
Binding energy of monomers in complex	$kcal \cdot mol^{-1}$
Frequencies of vibrational bands	cm^{-1}
Intensity of vibrational bands	$km \cdot mol^{-1}$
Equilibrium concentrations of complexes and monomer molecules	m^{-3}
Dipole moment	D

Every string corresponds to one or several columns. The first column gives the chemical formula of the complex. The string section "complex geometry in the equilibrium state" includes six columns, which contain the calculated and experimental values of equilibrium bond lengths and angles between bonds. The next column presents the calculated and experimental values of the energy of interaction between the molecules in the complex. The string section corresponding to the frequencies of intra- and intermolecular vibrations contains the number of columns equal to the number of the main types of vibrations (calculated and experimental values), and their assignment. The next string section, presenting the intensities of vibrational bands, is constructed similarly to the previous one, but the values in it are unfortunately absent because of the lack of reliable information. The string section "equilibrium configuration" includes three columns giving the information about the concentration of the monomer molecules and complexes formed by them in a gas at the standard temperature and pressure. The last column includes the data on the dipole moment and polarizability of the complex.

Table 7. Database string structure for H_2O…HF complexes taken as an example

Complex	Geometric structure											
	R_e, Å						Angles, deg					
	$H_{(2)}$–$F_{(2)}$		$O_{(1)}$–$H_{(1)}$		$O_{(1)}$–$F_{(2)}$		$H_{(1)}$–$O_{(1)}$–$H_{(1)}$		α		$H_{(2)}$–$F_{(2)}$–$O_{(1)}$	
	Calc.	Exp.	Calc.	Exp.	Calc.	Exp.	Calc.	Exp.	Calc.	Exp.	Calc.	Exp.
H_2O…HF	0.91[a]		0.94[a]		2.72[a]		107[a]		134[a]	134 (Ref. 15)	4[a]	
	0.93[b]		0.96[b]		2.67[b]		105[b]		131[b]		6[b]	
	0.92[c]		0.96[c]		2.64[c]		105[c]		129[c]		5[c]	
	0.92[d]		0.96[d]		2.65[d]		105[d]		133[d]		3[d]	
	0.92[e]				2.72[e]							

ΔE, kcal·mol^{-1}		Frequencies of vibrational bands, cm^{-1}								
		HF			H_2O			H_2O…HF		
Calc.	Exp	Calc.	Exp.	Assignment	Calc.	Exp.	Assignment	Calc.	Exp.	Assignment
9[a]	10 Ref. 10	4493[a]	4138 Ref.9	ν(HF)	4265[a]	3939 Ref. 10	ν_{as}(OH)	4270[a]	3608±2, Ref. 15	$\nu(H_{(2)}F_{(2)})$
11[b]		4212[b]			4052[b]			4258[a]	3756, Ref. 15	$\nu_{as}(O_{(1)}H_{(1)})$
11[c]		4119[f]			4010[f]			4142[a]	3657, Ref. 15	$\nu_s(O_{(1)}H_{(1)})$
11[d]					4148[a]	3835 Ref. 10	ν_s(OH)	1765[a]	1595, Ref. 15	$\delta(H_{(1)}O_{(1)}H_{(1)})$
9[e]					3909[b]			760[a]	696±30, Ref. 15	$\delta_f(O_{(1)}H_{(2)}F_{(2)})$
					3863[f]			626[a]	666±30, Ref. 15	$\delta_0(O_{(1)}H_{(2)}F_{(2)})$
					1770[a]	1648 Ref. 10	δ(HOH)	236[a]	180±30, Ref. 15	$\nu(H_2O$…HF)
					1674[b]			206[a]	145±50, Ref. 15	$\Delta_0(H_{(1)}O_{(1)}H_{(2)})$
					1620[f]			194[a]	170±50, Ref. 15	$\delta_f(H_{(1)}O_{(1)}H_{(2)})$

A, km·mol^{-1}		Equilibrium concentration, m^{-3}			μ, D
Calc.	Exp.	$n(H_2O)$	n(HF)	$n(H_2O$… HF)	
		$1.85 \cdot 10^{19}$ Refs. 17, 18	$6.66 \cdot 10^{20}$ Refs. 17, 18	$10.03 \cdot 10^{15}$ Refs. 17, 18	4.03[a]

Table 7 shows the string with the data for the H_2O…HF complex.

Conclusions

The first version of the database on the energy, structure and spectral characteristics of molecular complexes of H_2O with diatomic molecules has been proposed. Now the database contains the material on the $(H_2O)_m(HX)_n$ complexes, where X = F, Cl with $1 \le m,\ n \le 2$, based on the data of theoretical and experimental investigations.

This database can be used as information support in developing optical remote methods for monitoring of the gas composition of the atmosphere over industrial centers.

In the future it is planned to complement the database with the information about the complexes with $m,\ n > 2$, as well as on the complexes of water with triatomic molecules of natural and anthropogenic origin.

Acknowledgments

This work was supported, in part, by the Division of Physical Sciences RAS (project 2.10) and the Russian Foundation for Basic Research (grant No. NSh-373.2003.5).

References

1. V.E. Zuev, Yu.S. Makushkin, and Yu.N. Ponomarev, *Current Problems of Atmospheric Optics. 3. Atmospheric Spectroscopy* (Gidrometeoizdat, Leningrad, 1987), 247 pp.
2. Sh.Sh. Nabiev and Yu.N. Ponomarev, Atmos. Oceanic Opt. **11**, No. 12, 1093–1098 (1998).
3. Sh.Sh. Nabiev, P.G. Sennikov, and Yu.N. Ponomarev, in: *Abstracts of Papers Presented at V Colloq. on Atmospheric Spectroscopy Applications*, Reims, France (1999), p. CP2.
4. N.A. Zvereva, Sh.Sh. Nabiev, and Yu.N. Ponomarev, Atmos. Oceanic Opt. **12**, No. 9, 810–814 (1999).
5. Sh.Sh. Nabiev, Atmos. Oceanic Opt. **13**, No. 2, 109–118 (2000).
6. N.A. Zvereva, Sh.Sh. Nabiev, Yu.N. Ponomarev, and L.P. Sukhanov, Izv. Ros. Akad. Nauk, Ser. Khim., No. 1, 43–51 (2003).
7. L.S. Rothman, A. Barbe, D.C. Benner, L.R. Brown, C. Camy-Peyret, M.R. Carleer, K. Chance, C. Clerbaux, V. Dana, V.M. Devi, A. Fayt, J.-M. Flaud, R.R. Gamache, A. Goldman, D. Jacquemart, K.W. Jucks, W.J. Lafferty, J.-Y. Mandin, S.T. Massie, V. Nemtchinov, D.A. Newnham, and A. Perrin, J. Quant. Spectrosc. Radiat. Transfer **82**, Nos. 1–4, 5–44 (2003).
8. N.A. Zvereva, Sh.Sh. Nabiev, and Yu.N. Ponomarev, *Structure and Properties of Molecular Complexes of Water with Minor Gaseous Constituents of the Atmosphere* (Publishing House of the Institute of Atmospheric Optics SB RAS, Tomsk, 2003), 140 pp.

9. K.P. Huber and G. Herzberg, *Constants of Diatomic Molecules* (Van Nostrand Reinhold Company, Toronto, 1979).
10. K.S. Krasnov, ed., *Molecular Constants of Inorganic Compounds*. Handbook (Khimiya, Leningrad, 1979), 448 pp.
11. M.M. Szczesniak, S. Schemer, and Y. Bouteiller, J. Chem. Phys. **81**, Iss. 11, 5024–5030 (1984).
12. W. Bevan, Z. Kisiel, A.C. Legon, D.J. Millen, and S.C. Rogers, Proc. Roy. Soc. London A **372**, No. 1750, 441–451 (1980).
13. J.E. Del Bene, J. Phys. Chem. **92**, 2874–2880 (1988).
14. S.L.A. Adebayo, A.C. Legon, and D.J. Millen, J. Chem. Soc. Faraday Trans. **87**, Iss. 3, 443–447 (1991).
15. R.K. Thomas, Proc. Roy. Soc. London A **344**, 579–592 (1975).
16. C. Rovira, P. Constants, M.H. Whangbo, and J.J. Novoa, Int. J. Quantum Chem. **52**, Iss. 1, 177–189 (1994).
17. K. Nakamoto, *IR and Raman Spectra of Inorganic and Coordination Compounds* (John Wiley&Sons, 1978).
18. A.D. Bykov, L.N. Sinitsa, and V.I. Starikov, *Experimental and Theoretical Methods in Spectroscopy of Water Vapor* (SB RAS Publishing House, Novosibirsk, 1999), 376 pp.

0235-6880/04/11 832-05 $02.00

Chapitre 7

Un complexe d'intérêt astrophysique, $CH_4 - N_2$

Publication : P25

7.1 Introduction

$CH_4 - N_2$ est un complexe de van der Waals dont l'étude est importante pour la connaissance des atmosphères planétaires, telles que celles des planètes géantes, ou encore de Titan. Le spectre de ces atmosphères et de leurs différents composés (molécules, complexes, aérosols,...) est en effet largement dominé par les fortes bandes d'absorption du méthane, du fait de son abondance. La détermination des autres composés minoritaires, comme les molécules organiques complexes, nécessite de pouvoir «soustraire» du spectre des atmosphères planétaires celui de CH_4 ou de ses complexes comme $CH_4 - N_2$, pour disposer d'un modèle fiable. Un tel modèle doit de plus être valide sur une large gamme de longueurs d'onde.

L'équipe Spectroscopie Moléculaire et Applications (SMA) de l'Institut Carnot de Bourgogne (ICB) est reconnue au niveau international depuis de nombreuses années comme l'équipe spécialiste de l'analyse et de la modélisation du spectre du méthane [56, 57, 58]. De fait, si de nombreux groupes à travers le monde étudient CH_4 du point de vue expérimental (en enregistrant des spectres en laboratoire), l'équipe SMA est la seule à analyser ce type de spectres et se trouve donc au centre de la plupart des travaux concernant la spectroscopie du méthane. En particulier, elle a pu récemment collaborer étroitement et de manière constructive avec des équipes de planétologues pour contribuer à l'interprétation de spectres de l'atmosphère de Titan.

Cette étude se place donc ainsi dans le cadre du projet ANR $CH_4@Titan$. Il s'agit de mettre en œuvre des calculs *ab initio* pour le complexe $CH_4 - N_2$. Le thème, déjà bien avancé, fait l'objet d'une thèse (Yulia Kalugina). Un article où est définie la surface potentielle est vient d'être publié [P25].

7.2 Résultats obtenus

La surface de potentiel pour l'énergie d'interaction du complexe de van der Waals pour un large domaine de séparation et des configurations différentes a été calculée par les méthodes CCSD(T) et MP2, en appliquant une base de fonctions aug-cc-pVTZ. La correction BSSE a été prise en compte pendant tous les calculs. La configuration la plus stable a été déterminée. Les énergies de liaison ont été calculées pour une base limite complète (limit CBS (Complete Basis Set)), en considérant les déformations des molécules CH_4 et N_2. Les fréquences harmoniques et anharmoniques ont été calculées pour la configuration la plus stable ; les constantes rotationnelles ont été obtenues pour l'état de base et le premier état excité vibrationnel, en utilisant la méthode MP2 et la correction BSSE. Les paramètres

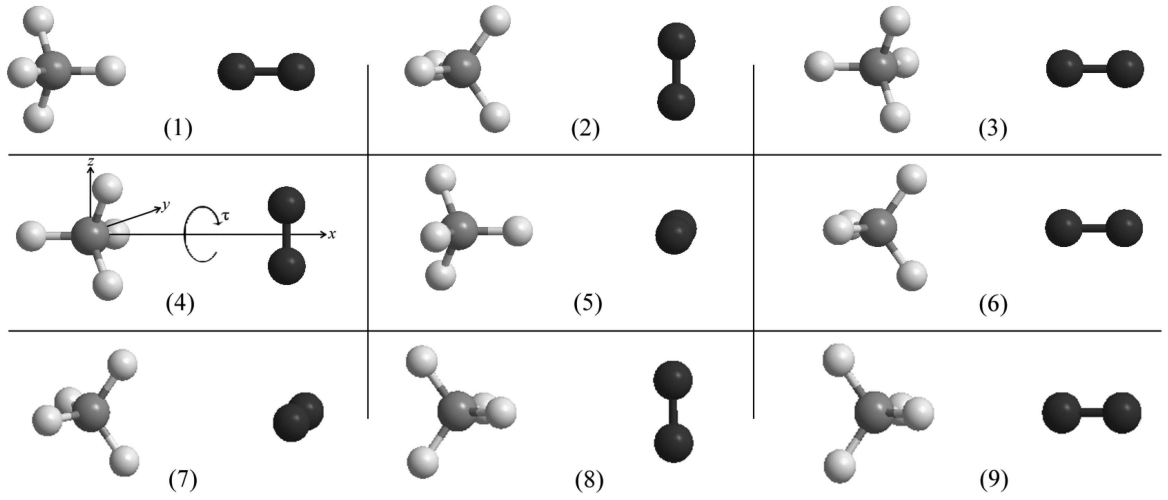

FIG. 7.1 – Géometries du complexe CH_4-N_2.

d'ajustement de la surface potentielle ont été déterminés en utilisant les potentiels de Lennard-Jones et Esposti-Werner.

L'analyse de la surface de potentiel du complexe $CH_4 - N_2$ met en évidence une famille dans laquelle les configurations sont les plus stables. La géometrie de ces configurations peut être obtenue par rotation de la molécule N_2 autour de l'axe x d'un angle τ qui correspond à deux angles d'Euler : θ_b et ϕ_b (b correspond à l'angle d'Euler de la molécule N_2) en prenant comme géométrie de référence la configuration stable 4 (Fig.7.1).

Ces calculs *ab initio* de la surface de potentiel et la description analytique qui en a été déduite peuvent être considérés comme une bonne base en vue de la description complète de la surface d'énergie d'interaction du complexe de van der Waals CH_4-N_2.

7.3 Article-clé : P25

THE JOURNAL OF CHEMICAL PHYSICS **131**, 134304 (2009)

Theoretical investigation of the potential energy surface of the van der Waals complex CH_4-N_2

Yulia N. Kalugina,[1,2,a)] Victor N. Cherepanov,[1] Mikhail A. Buldakov,[3] Natalia Zvereva-Loëte,[2,b)] and Vincent Boudon[2]
[1]*Department of Optics and Spectroscopy, Tomsk State University, 36, Lenin Avenue, Tomsk 634050, Russia*
[2]*Institut Carnot de Bourgogne, CNRS UMR 5027, 9, Avenue Alain Savary, B.P. 47 870, Dijon Cedex F-21078, France*
[3]*Institute of Monitoring of Climatic and Ecological Systems, SB RAS, Akademicheskii Ave. 10/3, Tomsk 634055, Russia*

(Received 2 June 2009; accepted 12 September 2009; published online 2 October 2009)

The interaction potential energy surface of the van der Waals CH_4-N_2 complex has been calculated for a broad range of intermolecular separations and configurations in the approximation of rigid interacting molecules at the CCSD(T) and MP2 levels of theory using the correlation consistent aug-cc-pVTZ basis set. The BSSE correction was taken into account for all the calculations. The most stable configurations of the complex were found. Binding energies were calculated in the CBS limit with accounting for the molecular deformations. The harmonic and anharmonic fundamental vibrational frequencies and rotational constants for the ground and first excited vibrational states were calculated for the most stable configurations at the MP2 level of theory with BSSE correction. Fitting parameters were found for the most stable configuration for the Lennard-Jones and Esposti–Werner potentials. © *2009 American Institute of Physics*. [doi:10.1063/1.3242080]

I. INTRODUCTION

In gaseous media containing N_2 and CH_4 molecules there are both collisional and weakly bound van der Waals complexes. At present, collisional CH_4-N_2 complexes have been investigated in some experimental[1,2] and theoretical[3–8] works, but there is comparatively little information about the weakly bound van der Waals complexes.[9,10] The CH_4-N_2 complex is of particular interest in astrophysical applications. For example, the most abundant compounds in the atmosphere of Saturn's satellite Titan are N_2 (94%) and CH_4 (2%–5%) molecules.[3,4,8,11–21] Due to the low temperature of Titan [the temperature ranges from 70 to 100 K (Ref. 13)], there may exist both collisional and van der Waals complexes in stable configurations.

One of the most important characteristics of the complex is its potential energy surface (PES). Earlier, the PES of the CH_4-N_2 complex was investigated only in two works.[9,10] In pioneering work[9] this PES was obtained by self-consistent field calculations and Monte Carlo simulations. But it is worth noting that the basis sets employed are not large enough for the description of the interactions in van der Waals systems. Moreover, the basis set superposition error (BSSE) and the basis set incompleteness error (BSIE) were not taken into account. The calculations in Ref. 9 were carried out for six geometries of the complex and among them the most stable geometry was found. Recently, Shadman *et al.*[10] obtained PES of the complex calculated at the second-order Møller–Plesset (MP2) level of theory with BSSE and BSIE corrections. The BSIE correction in this work was accounted by means of calculations with aug-cc-pV*X*Z ($X=2,3,4$) (Ref. 22) basis sets. But it should be noted that aug-cc-pVQZ basis set gives results which are generally still too far from convergence for many weakly bound complexes. The MP2 method employed accounts for the electron correlation and is the most simple one required for the description of such systems. The calculations in Ref. 10 were carried out for a wide range of intermolecular distances R (5.0–20.0 a.u.) for 12 geometries of the complex. The large step (0.5 a.u.) used in the vicinity of equilibrium separation results in significant errors in the evaluation of the binding energy (BE) of the complex. In Ref. 10 the authors also found (among the investigated geometries) the geometry corresponding to the deepest potential well. But it draws attention that the stable configurations found in Refs. 9 and 10 are different. It should be noted that all these calculations[9,10] were carried out in the approximation of rigid interacting molecules. But, in reality, the molecules in the complex undergo distortions while interacting with each other.

At present, it is known that the most suitable method for calculating the energy of complexes is the coupled cluster method with singles and double excitations and noniterative correction to triple excitations [CCSD(T)]. But the MP2 method can also be used as a compromise between accuracy and computational costs. However, there is no calculation for this complex at the CCSD(T) level of theory. In this work we carried out the PES calculations both at the MP2 and more advanced CCSD(T) levels of theory. The main object of investigation in this work is the van der Waals CH_4-N_2 complex and its stable configurations.

We give the description of the computational methods used in the present work and the coordinate system of the methane-nitrogen complex in Sec. II. In Sec. III we present

a)Electronic mail: kalugina@phys.tsu.ru.
b)Electronic mail: natalia.loete@u-bourgogne.fr.

the results of the computation of the PES and the investigation of the stable geometries of the complex. The calculation of the harmonic and anharmonic frequencies is also shown in Sec. III. Section IV gives the conclusions. Conversion factors to SI units are: energy, 1 hartree=4.359 748 2 $\times 10^{-18}$ J, and length, $1a_0$=0.529 177 2$\times 10^{-10}$ m.

II. COMPUTATIONAL DETAILS

A. Methods and basis sets

For the accurate evaluation of intermolecular interactions in van der Waals complexes, one should use a high level treatment of electron correlation effects. It is known[23–25] that the HF and DFT methods cannot evaluate dispersion interactions, which is why all van der Waals systems are predicted to be nonbound at these levels of theory. However, there are works (see, for example, Refs. 24 and 25) devoted to the determination of the PES of van der Waals complexes by adding to the HF and DFT potentials the dispersion energy correction in order to improve them. Nevertheless, the accuracy of the energy calculations using these methods is not high enough relative to the typically required advanced CCSD(T) calculations, which more accurately evaluate the interactions of van der Waals systems. Detailed description of *ab initio* methods mentioned above can be found in standard textbooks.[26]

Moreover, it is essential to use a correlation consistent basis set, for example, aug-cc-pV*X*Z basis set containing diffuse functions, which are very important for the description of dispersion interactions. When calculating the energy of van der Waals systems, one should also take into account the BSSE. Note that due to the BSSE, computed interaction energies become too large. In the present work, the BSSE is taken into account within the Boys–Bernardi counterpoise correction scheme,[27] which is fully automated in the GAUSSIAN 03 (Ref. 28) package used in this work.

For the most stable structure obtained in this work, we also calculated the interaction energy in the complete basis set (CBS) limit. If to use the CBS extrapolation for the BSSE-uncorrected energies, there is generally no monotonic convergence as is observed for BSSE-corrected ones.[29] Therefore, in present work the BSSE-corrected energies were employed to obtain the CBS limit. Moreover, for the good convergence of energies to the CBS limit, we have to use also rather large basis sets. For this purpose the aug-cc-pV*X*Z $[X=2(\mathrm{D}),3(\mathrm{T}),4(\mathrm{Q}),5]$ basis sets of Dunning[22] were employed. We used the CBS extrapolation schemes of Feller,[30]

$$E_X^{\mathrm{tot}} = E_{\mathrm{CBS}}^{\mathrm{tot}} + B\exp(-\alpha X), \tag{1}$$

Truhlar,[31]

$$E_X^{\mathrm{tot}} = E_{\mathrm{CBS}}^{\mathrm{tot}} + AX^{-\alpha}, \tag{2}$$

Martin,[32]

$$E_{\mathrm{CBS}}^{\mathrm{tot}} = \frac{(X+3/2)^4}{(X+3/2)^4-(X+1/2)^4}E_{X+1}^{\mathrm{tot}} - \frac{(X+1/2)^4}{(X+3/2)^4-(X+1/2)^4}E_X^{\mathrm{tot}}, \tag{3}$$

and Helgaker,[33]

$$E_X^{\mathrm{HF}} = E_{\mathrm{CBS}}^{\mathrm{HF}} + B\exp(-\alpha X),$$
$$E_X^{\mathrm{corr}} = E_{\mathrm{CBS}}^{\mathrm{corr}} + AX^{-3}, \tag{4}$$
$$E_{\mathrm{CBS}}^{\mathrm{tot}} = E_{\mathrm{CBS}}^{\mathrm{HF}} + E_{\mathrm{CBS}}^{\mathrm{corr}}.$$

Here X is the cardinal number of the correlation-consistent aug-cc-pV*X*Z basis set, E_X^{HF}, E_X^{corr}, and E_X^{tot} are the Hartree–Fock, and correlation and total energies, accordingly; B, A, and α are the parameters to be optimized. The subscripts "X" and "CBS" correspond to the energy calculated using aug-cc-pV*X*Z basis set and the energy obtained in the CBS limit. It should be noted that Helgaker's extrapolation scheme is a three-point one for the Hartree–Fock energy and a two-point for the correlation energy. The calculation was carried out for the Hartree–Fock energy and it was found that α in our case is constant for the given sequence of X. For $X=2,3,4$ $\alpha=1.38$ and for $X=3,4,5$ $\alpha=1.50$. So we reduced the number of points for the extrapolation of the HF energy to two. The notation for the Helgaker's extrapolation scheme, for example, "$X=(3),4,5$" means that α for the extrapolation of the Hartree–Fock energy was previously calculated with aug-cc-pV*X*Z ($X=3,4,5$) basis sets ($\alpha=1.50$) and the correlation energy was extrapolated using energies calculated with aug-cc-pV*X*Z ($X=4,5$) basis sets.

B. Molecules CH_4 and N_2

The geometries of the monomers CH_4 and N_2 were optimized at the CCSD(T) level of theory using the aug-cc-pVTZ correlation consistent basis set. The bond lengths and bond angles for the CH_4 molecule were found to be r_{CH} =2.0596 a.u. and θ_e=109.4712° (the angle for a tetrahedral molecule), and the bond length for the N_2 molecule is r_{NN} =2.0864 a.u., which are in a good agreement with the experimental values [r_{CH}=2.0580 a.u.,[34] r_{NN}=2.0742 a.u. (Ref. 35)]. When calculating the PES of the CH_4–N_2 complex, the methane and nitrogen molecules were kept rigid with the monomer geometric parameters mentioned above. However, for the calculation of the BE and vibrational frequencies of the most stable configuration, the molecules in the CH_4–N_2 complex were considered as nonrigid.

C. CH_4–N_2 complex

In the present work, for the description of the complex a Cartesian coordinate system was used (see Fig. 1). The origin of this coordinate system is placed on the carbon atom of the methane molecule. The vector $\boldsymbol{R}$ is directed from the carbon atom to the center of N_2 bond length and has the components $(R,0,0)$. The rotation of the methane molecule in this coordinate system is determined by three Euler angles: (1) rotation of angle χ_a around the z-axis, (2) rotation

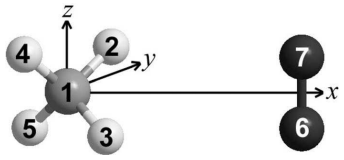

FIG. 1. Coordinate system of the CH_4–N_2 complex.

of angle θ_a around the y-axis, and (3) rotation of angle φ_a around the z-axis. The rotation of the nitrogen molecule can be described by two additional Euler angles: (1) rotation of angle θ_b around the y-axis and (2) rotation of angle φ_b around the z-axis. The initial position of the molecules in the CH_4–N_2 complex, corresponding to the Euler angles $\chi_a = \theta_a = \varphi_a = \theta_b = \varphi_b = 0°$, is presented in Fig. 1. In this figure the axis of the N_2 molecule is parallel to the z-axis in the coordinate system of the complex and the CH_4 molecule has the standard orientation: The carbon atom is at the origin (0, 0, 0) and hydrogen atoms have the coordinates (c,c,c), $(c,-c,-c)$, $(-c,-c,c)$, and $(-c,c,-c)$, where $c = r_{CH}/\sqrt{3}$.

III. RESULTS AND DISCUSSIONS

A. Potential energy surface

The calculations were carried out for the set of geometries of the CH_4–N_2 complex (some general geometries are presented in Fig. 2), which can be characterized by five Euler angles $\chi_a, \theta_a, \varphi_a, \theta_b$, and φ_b. For these geometries the value of R has been varied within the range of 5.67–189.0 a.u. This choice of distances covers both the long range attractive and short range repulsive regions of interaction in the CH_4–N_2 complex.

In general, we calculated 700 points on the PES at the CCSD(T) level of theory and 1000 points at the MP2 level. The data calculated at the CCSD(T) level of theory are available as electronic supplementary material.[36] The interaction energy ΔE as a function of the intermolecular distance R for nine geometries of the complex (Fig. 2) is plotted in Fig. 3. In Table I we present the equilibrium distance R_e and interaction energy $\Delta E(R_e)$ for these geometries calculated at the CCSD(T)/aug-cc-pVTZ level of theory with BSSE correction. It is seen from the Fig. 3 and Table I that the potential well corresponding to geometry 4 is the deepest one, which is in a good agreement with the work.[9] But there is a discrepancy with the work[10] where it was found that the most profound potential well corresponds to the geometry 1-C,

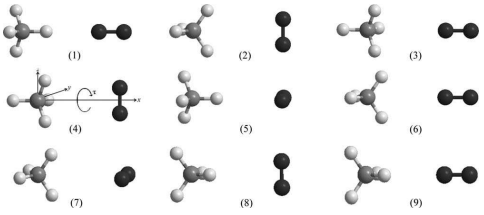

FIG. 2. Geometries of the CH_4–N_2 complex.

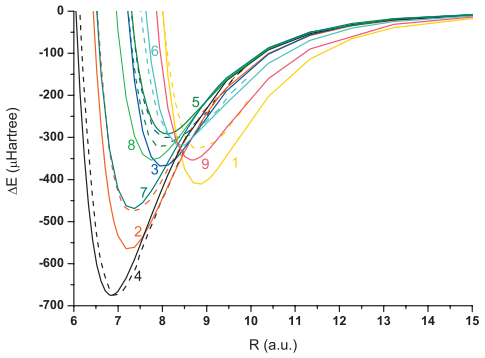

FIG. 3. Interaction energies of the CH_4–N_2 complex in different geometries. Solid lines: *ab initio* calculation at the CCSD(T)/aug-cc-pVTZ level of theory with BSSE correction (the numbers 1–9 are the numbers of the geometries from Fig. 2). Dashed lines: work (Ref. 9).

which can be obtained from the geometry 4 by rotation of the N_2 molecule of angle 30° around the x-axis. Thus, to clarify the situation we investigated the most stable configurations of the CH_4–N_2 complex in more details (see Sec. III B).

Moreover, some additional analytical calculations of the interaction energy surface of the complex for large R have been carried out for the comparison of *ab initio* theoretical methods used in this study. According to Ref. 37 the contribution to the interaction energy ΔE of the complex CH_4–N_2 at large intermolecular separations up to R^{-7} is determined by electrostatic and dispersion interactions:

$$\Delta E = E_{\text{elect}} + E_{\text{disp}}, \tag{5}$$

with the electrostatic energy

$$E_{\text{elec}} = -\tfrac{1}{45} Q^b_{\alpha\beta} \Omega^a_{\gamma\delta\nu} T_{\alpha\beta\gamma\delta\nu} + \tfrac{1}{315} Q^b_{\alpha\beta} \Phi^a_{\gamma\delta\nu\varepsilon} T_{\alpha\beta\gamma\delta\nu\varepsilon}, \tag{6}$$

and dispersion energy

TABLE I. Equilibrium distance R_e and interaction energy $\Delta E(R_e)$ for different geometries calculated at the CCSD(T)/aug-cc-pVTZ level of theory with BSSE correction. All angles are in deg. (Here $t = \arcsin(1/\sqrt{3})$.)

Geometry	χ_a	θ_a	φ_a	θ_b	φ_b	R_e (a.u.)	$\Delta E(R_e)$ (μhartree)
1	90	45	t	90	0	8.81	−412.251
2	0	45	90	0	0	7.26	−566.445
3	0	45	t	90	0	8.01	−369.226
4	0	45	t	0	0	6.84	−675.375
5	90	45	t	0	0	8.11	−291.741
6	0	45	90	90	0	8.43	−319.591
7	0	45	90	90	90	7.31	−469.805
8	90	45	90	0	0	7.77	−354.014
9	90	45	90	90	0	8.67	−353.620

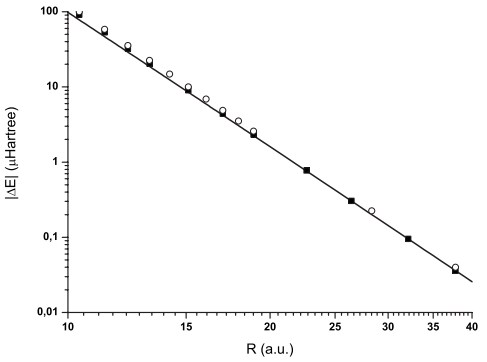

FIG. 4. R-dependence of the interaction energy (in logarithmic scale) of the CH_4–N_2 complex in the geometry 4. Solid line: calculation using analytic formula (6). Squares: *ab initio* calculation at the CCSD(T)/aug-cc-pVTZ level of theory with BSSE correction. Circles: *ab initio* calculation at the MP2/aug-cc-pVTZ level of theory with BSSE correction.

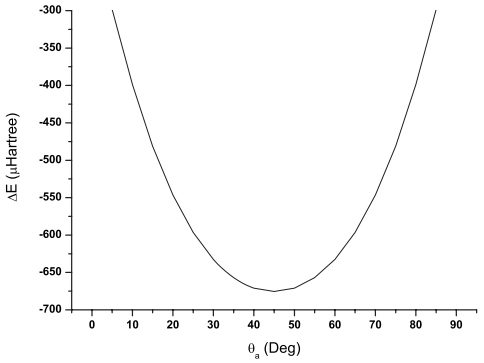

FIG. 5. θ_a-dependence of the interaction energy of the CH_4–N_2 complex (the values of other Euler angles and distances r_{CH}, r_{NN}, R_e correspond to the equilibrium geometry 4).

$$E_{\text{disp}} = -\frac{1}{2\pi} T_{\alpha\beta} T_{\gamma\delta} \int \tilde{\alpha}^a_{\alpha\gamma}(i\omega)^* \tilde{\alpha}^b_{\beta\delta}(i\omega) d\omega$$
$$- \frac{U_a U_b}{6(U_a + U_b)} T_{\alpha\beta} T_{\gamma\delta\nu} (\alpha^a_{\alpha\gamma} A^b_{\beta,\delta\nu} - A^a_{\beta,\delta\nu} \alpha^b_{\alpha\gamma}). \quad (7)$$

Here $T_{\alpha\beta\gamma\cdots\nu} = \nabla_\alpha \nabla_\beta \nabla_\gamma \cdots \nabla_\nu R^{-1}$ is a tensor symmetric relative to the permutation of any pair of subscripts and $\tilde{\alpha}^i_{\beta\delta}(i\omega)$ is the imaginary polarizability of the ith molecule. The Greek subscripts denote Cartesian components and the repeated subscripts imply summation over x, y, and z. The imaginary polarizabilities for the CH_4 and N_2 molecules were taken from Refs. 38 and 39, correspondingly. The values of the molecular parameters used for the analytical calculation of the interaction energy ΔE by Eqs. (6) and (7) are listed in Table IX (see Appendix). Particularly, for geometry 4, which has the deepest potential well, the interaction energy of the CH_4–N_2 complex takes the form:

$$\Delta E = -\frac{107.61}{R^6} + \frac{95.73}{R^7}. \quad (8)$$

The analysis of Eqs. (5)–(7) shows that the contribution of dispersion interaction to ΔE is the most important. More precisely, the contribution to the leading term in Eq. (8) of dispersion interaction is $-91.95/R^6$, while the contribution of electrostatic interaction is only $-15.66/R^6$. It should be noted that analytical Eqs. (5)–(7) describe very well the interaction energy of the complex at large R. Indeed, the analytically calculated averaged value of the dispersion coefficient C_6 =97.26 a.u. is very close to the calculated one C_6 =96.92 a.u. in Ref. 38. The calculated *ab initio* interaction energies ΔE at the CCSD(T) and MP2 level of theory and the analytical ΔE are plotted in Fig. 4. The figure shows that the CCSD(T) level of theory provides better agreement with the theoretical dependence of the interaction energy at long-range intermolecular separation R than the MP2 one.

Generally, the interaction energy not only depends on the intermolecular separations R but also on the mutual orientation of the CH_4 and N_2 molecules in the complex. Figures 5 and 6 illustrate the dependence of the interaction energy of the complex on the angles θ_a and θ_b. While computing, all other parameters were kept constant as in the equilibrium geometry 4.

B. Most stable configuration

In this section, to solve the problem of finding the most stable configuration, we accurately investigated geometry 4 from Ref. 9 and geometry 1-C from Ref. 10. For this purpose we carried out the calculations of the interaction energy of the CH_4–N_2 complex versus the angle τ (Fig. 2) of which the N_2 molecule rotates around x-axis in the CH_4–N_2 complex. The geometries of the complex obtained by rotation of the angle τ will be designated by C_τ. Note that at τ=0° we have geometry 4 (or geometry C_0) and the rotation of N_2 of the angle τ=30° corresponds to the geometry 1-C (or geometry C_{30}). There is the following relation between the new angle τ and Euler angles: The rotation of angle τ corresponds to the rotation of Euler angles $\theta_b = \tau$ and φ_b=90°.

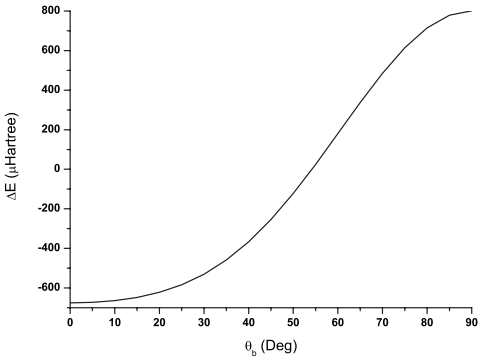

FIG. 6. θ_b-dependence of the interaction energy of the CH_4–N_2 complex (the values of other Euler angles and distances r_{CH}, r_{NN}, R_e correspond to the equilibrium geometry 4).

TABLE II. Interaction energies ΔE (in μhartree) calculated at the CCSD(T) level with aug-cc-pVTZ basis set with BSSE correction for the geometry C_τ (τ=0°–30°).

R (a.u.)	τ (deg) 0	5	10	15	20	25	30
6.43	−544.22	−544.21	−544.19	−544.15	−544.11	−544.08	−544.06
6.61	−641.73	−641.72	−641.70	−641.68	−641.65	−641.63	−641.61
6.71	−664.45	−664.44	−664.43	−664.41	−664.38	−664.37	−664.35
6.80	−674.40	−674.39	−674.38	−674.36	−674.34	−674.33	−674.31
6.90	−674.37	−674.37	−674.35	−674.34	−674.32	−674.31	−674.30
6.99	−666.58	−666.57	−666.56	−666.54	−666.53	−666.51	−666.51
7.18	−634.68	−634.68	−634.67	−634.66	−634.65	−634.63	−634.63
7.34	−589.71	−589.71	−589.70	−589.69	−589.67	−589.67	−589.68
7.56	−538.87	−538.87	−538.86	−538.85	−538.84	−538.84	−538.84
8.50	−305.27	−305.27	−305.27	−305.27	−305.27	−305.27	−305.27
9.45	−164.84	−164.84	−164.84	−164.84	−164.84	−164.85	−164.85
10.39	−91.51	−91.51	−91.51	−91.51	−91.51	−91.51	−91.51
11.34	−53.21	−53.21	−53.21	−53.21	−53.21	−53.21	−53.21
13.23	−20.45	−20.45	−20.45	−20.45	−20.45	−20.46	−20.46
15.12	−9.00	−9.00	−9.00	−9.00	−9.00	−9.00	−9.00
17.00	−4.37	−4.37	−4.37	−4.37	−4.37	−4.37	−4.37
18.90	−2.29	−2.29	−2.29	−2.29	−2.29	−2.29	−2.29

Calculations of ΔE for geometries C_τ (τ was varied from 0° to 30° by 5°) of the CH_4–N_2 complex at the MP2 and CCSD(T) levels of theory were carried out. The chosen range of angles τ is enough to describe the nonequivalent configurations of the complex in accordance with its symmetry. The calculated interaction energies ΔE at the CCSD(T) level of theory with the aug-cc-pVTZ basis set using the BSSE correction are presented in Table II. It is seen from the table that for all R and τ the difference in ΔE does not exceed 0.16 μhartree (~0.04 cm^{-1}). As the difference in ΔE is less then any energy in the ground vibrational state of the CH_4–N_2 complex, all configurations C_τ should be considered as a family of the most stable configurations of the complex. From this point of view, geometry 4 from Ref. 9 and geometry 1-C from Ref. 10, which belong to the family of geometries C_τ, are both the most stable.

Note also that the difference in interaction energies for the geometry 1-B (in our notation, geometry C_0) and the geometry 1-C (or geometry C_{30}) obtained in Ref. 10 at R =6.5 a.u. is 203.03 μhartree, which is in disagreement with our previous statement. That is why we carried out additional calculations of the interaction energy of the CH_4–N_2 complex being in these geometries with the same geometric parameters and level of theory (MP2 level with BSSE and BSIE corrections) as in Ref. 10. The results of the calculation are presented in Table III. It is seen from the table that in this case the values of ΔE for the both geometries practically coincide for Martin's and Helgaker's methods accounting for BSIE when the larger basis set is used. The larger the basis set, the closer the extrapolated interaction energies using different extrapolation methods.

It should be noted that the same behavior of the interaction energy ΔE is obtained when calculating it with the use of analytical Eqs. (5)–(7) described in Sec. III A. The analysis of these expressions shows that the coefficients in Eq. (8) are constant for all angles τ, and, as a result, analytical interaction energy does not depend on angle τ.

One of the important criteria of the complex stability is its BE. In order to accurately evaluate BE, one should account for the BSSE, BSIE corrections and correction of the nonrigidity of the molecules in the complex. To obtain the BSIE correction, the calculations were carried out at the MP2 and CCSD(T) levels of theory (with BSSE correction) using four CBS extrapolation schemes (1–4). The nonrigidity correction ΔE_{nr} was accounted by subtracting the BE calculated in the CBS limit for the geometry C_{30} with the rigid molecules from the BE in CBS limit for the fully optimized (at the MP2/aug-cc-pVTZ level of theory) geometry C_{30}. The parameters of the rigid and nonrigid complexes being in geometry C_{30} are given in Table IV. The total BE of the complex can be calculated as follows:

TABLE III. Interaction energy ΔE_{CBS} (in μhartree) at R=6.5 a.u. with BSIE correction [see Eqs. (1)–(4)] for the geometry C_τ (τ=0°,30°) (the geometric parameters were chosen as in Ref. 10) of the CH_4–N_2 complex calculated at the MP2 level of theory with BSSE correction.

τ (deg)	ΔE_{CBS} (Feller's scheme) X=2,3,4	X=3,4,5	ΔE_{CBS} (Truhlar's scheme) X=2,3,4	X=3,4,5	ΔE_{CBS} (Martin's scheme) X=3,4	X=4,5	ΔE_{CBS} (Helgaker's scheme) X=(2),3,4	X=(3),4,5	ΔE_{CBS} Ref. 10
0	−817.089	−833.279	−849.831	−848.826	−826.525	−836.776	−835.999	−842.480	−844.47
30	−817.215	−833.181	−849.970	−848.598	−826.642	−836.730	−836.278	−841.755	−1047.50

TABLE IV. Optimized bond lengths (in a.u.) and angles (in deg) for the geometry C_{30} with and without nonrigidity of the molecules (the optimization has been carried out using the MP2/aug-cc-pVTZ level of theory with BSSE correction).

Parameters	Nonrigid molecules	Rigid molecules
$r_{(C1-H2)}$	2.0534	2.0577
$r_{(C1-H3)}$	2.0577	2.0577
$r_{(C1-H4)}$	2.0577	2.0577
$r_{(C1-H5)}$	2.0526	2.0577
$r_{(N6-C1)}$	6.8259	6.8336
$r_{(N7-N6)}$	2.1057	2.0864
∠H2–C1–H3	109.4347	109.4712
∠H2–C1–H4	109.4347	109.4712
∠H2–C1–H5	109.5013	109.4712
∠H2–C1–N6	79.2385	79.3095
∠C1–N6–N6	81.6445	81.2193
∠H3–H2–C1–H4	109.6170	109.4712
∠H3–H2–C1–H5	109.4199	109.4712
∠H3–H2–C1–N6	66.4122	66.3350
∠H2–C1–N6–N7	0.0000	0.0000

$$BE = BE_r + \Delta BSIE_r + \Delta E_{nr}, \quad (9)$$

where BE_r is the BE of the complex with rigid molecules, calculated without the BSIE correction, $\Delta BSIE_r$ is the BSIE correction for the case of rigid molecules, ΔE_{nr} is the correction on the nonrigidity of the molecules in complex to the BE. In Table V the contribution of different corrections to the total BE of the complex being in the geometry C_{30} is presented. As seen from the Table V, the BSSE correction gives the biggest contribution to the BE and the nonrigidity correction is higher than the BSIE one. Tables III and V show that the closest energies are obtained when Martin's and Helgaker's extrapolation schemes are used. But the convergence of the interaction energies to the CBS limit is better for the Helgaker's extrapolation scheme due to the separate extrapolation of the HF and correlation energies. Finally, the calculated values of BE at the MP2 level of theory with aug-cc-pVXZ (X=3,4,5) basis sets are the following: −938.520 μhartree for Martin's extrapolation scheme [Eq. (3)] and −942.373 μhartree for Helgaker's scheme [Eq. (4)]. These values can be improved by replacing $BE_r^{CBS}=BE_r+\Delta BSIE_r$ in Eq. (9) calculated at the MP2 level of theory by BE_r^{CBS} calculated at the CCSD(T) level (with aug-cc-pVXZ basis set, where X=2,3,4). Thus, the recommended values of the BE of the complex are: −820.536 μhartree for CBS extrapolation scheme of Martin and −827.143 μhartree for CBS extrapolation scheme of Helgaker.

TABLE V. The BE and contributions of the corrections to the BE (in μhartree) for the geometry C_{30} of the CH_4–N_2 complex.

Extrapolation scheme	Total BE	BE_r [a]	ΔBSSE	$\Delta BSIE_r$	ΔE_{nr}
Feller[b]	−979.143	−776.818	374.011	−62.807	−139.519
Truhlar[c]	−1014.007	−776.818	374.011	−88.029	−149.160
Martin[d]	−938.520	−776.818	374.011	−76.126	−85.576
Helgaker[e]	−942.373	−776.818	374.011	−79.985	−85.570

[a]BE_r is calculated at the MP2 level of theory with the aug-cc-pVTZ basis set only with BSSE correction.
[b]Reference 30.
[c]Reference 31.
[d]Reference 32.
[e]Reference 33.

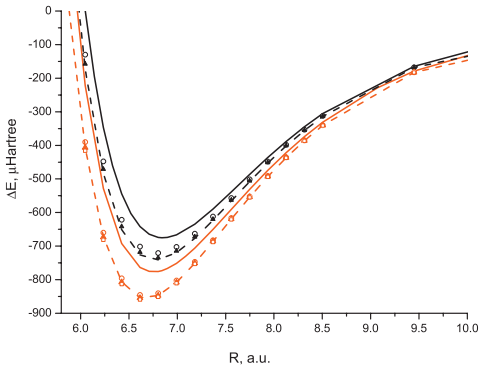

FIG. 7. Interaction energies ΔE of the CH_4–N_2 complex for geometry 4. Black color: calculation at the CCSD(T) level of theory. Red color: calculation at the MP2 level of theory. Solid line: calculation using aug-cc-pVTZ basis set. Circles: CBS extrapolation scheme of Martin [Eq. (3)] with aug-cc-pVXZ [X=2,3 for the CCSD(T) level and X=3,4 for the MP2 one]. Triangles: CBS extrapolation scheme of Martin [Eq. (3)] with aug-cc-pVXZ [X=3,4 for the CCSD(T) level and X=4,5 for the MP2 one]. Dash line: CBS extrapolation scheme of Helgaker [Eq. (4)] with aug-cc-pVXZ (X=(2),3,4). Squares: CBS extrapolation scheme of Helgaker [Eq. (4)] with aug-cc-pVXZ (X=(3),4,5).

It is also of interest to investigate the BSIE effect on the interaction energy $\Delta E(R)$ of the complex being in the most stable configuration, for example, for the geometry 4. In the calculations, the BSIE correction was carried out using the CBS extrapolation schemes of Martin and Helgaker (3–4) as we believe them to be more reliable. The results of the calculations at the MP2 and CCSD(T) levels of theory are presented at Fig. 7. We investigated the convergence of interaction energies to the CBS limit for the MP2 (X=2,3,4,5) and CCSD(T) (X=2,3,4) levels and found out that the CCSD(T) level with aug-cc-pVXZ up to X=4 is enough for the evaluation of the interaction energy as there is good convergence to the CBS limit; as for the calculation at the MP2 level with aug-cc-pVXZ up to X=5, there is high convergence to the CBS limit. Figure 7 shows that the CBS limit for the MP2 level is too far from the CBS limit for the CCSD(T) level of theory and it overestimates the interaction energy.

C. Analytical representation of the interaction potential of the most stable configuration

For some applications there is a particular interest in the analytical representation of the interaction energy ΔE. In the present work, for the most stable geometries C_7, we used the simple but popular Lennard-Jones potential and more correct Esposti–Werner potential.[40] In our work all parameters for these potentials were fitted using the homemade program with the modified Levenberg–Marquardt algorithm from the MINPACK set of routines for nonlinear least-squares fitting.[41]

The fitting was done for the Lennard-Jones potential

TABLE VI. Fitted parameters for geometry 4. All values are in a.u.

g_0	g_1	g_2	g_3	g_4	g_5
−829 655.40	415 403.22	−155 060.74	36 518.590	−5428.7009	506.308 20
g_6	g_7	g_8	a_1	a_2	t
−29.136 743	0.950 265 1	−0.013 815 3	0.996 920 8	10.004 532	2.442 4463
C_6	C_7	C_8	C_9	C_{10}	
−143.892 55	18 655.527	−394 872.85	1 920 880.0	−2 861 433.0	

$$\Delta E(R) = 4\epsilon\left[\left(\frac{\sigma}{R}\right)^{12} - \left(\frac{\sigma}{R}\right)^{6}\right] \quad (10)$$

to *ab initio* points, calculated at the CCSD(T)/aug-cc-pVTZ level of theory (with the BSSE and without the BSIE correction), with a satisfactory agreement (standard deviation $=0.3\times10^{-4}$ a.u. for 34 points in the region of $R=5.67-37.8$ a.u.). In Eq. (10) ϵ and σ are the depth of the potential well and the effective interaction diameter (the distance at which the potential is zero), respectively. The fitting parameters are defined as $\sigma=6.002\ 372$ a.u. and $\epsilon=660.306$ μhartree.

A better agreement (standard deviation of 0.5×10^{-7} a.u.) was obtained by fitting to the same *ab initio* data for the one-dimensional function of Esposti–Werner type:

$$\Delta E(R) = \left[G(R)\exp(-a_1R - a_2) - T(R)\sum_{i=6}^{10}\left(\frac{C_i}{R^i}\right)\right], \quad (11)$$

where

$$G(R) = \sum_{i=0}^{8}(g_iR^i), \quad (12)$$

and

$$T(R) = \tfrac{1}{2}[1 + \tanh(1 + tR)] \quad (13)$$

is a switching function. In this potential the position of the minimum is at $R_e=6.84$ a.u. with a well depth of −675.375 μhartree. All fitting parameters a_i, g_i, t, C_i for the potential of Esposti–Werner are presented in Table VI.

Figure 8 illustrates the efficiency of the analytical interaction potentials (10) and (11) in comparison with the *ab initio* interaction potential. It is seen that potential (11) better describes *ab initio* calculations. It should be noted that in spite of the good agreement of analytical (11) and *ab initio* interaction potentials, at large intermolecular separations R, Eq. (11) gives bigger values of the interaction energy due to the fact that fitted parameter C_6 (143.89 a.u.) is bigger then C_6 (107.61 a.u.) calculated accurately by Eq. (5).

D. Frequency calculation

In this study we calculated at the MP2/aug-cc-pVTZ level of theory the harmonic frequencies (Table VII) for a set of the most stable geometries C_τ. It is seen from the table that the frequencies, except for the lowest one, are changing slightly for these geometries. Here, the modes from 1 to 5 are intermolecular, the modes 6–10 and 12–15 are the vibrational modes for the CH_4 molecule and the 11th mode is the vibration of the N_2 molecule. As the symmetry of the CH_4 molecule in the complex becomes lower due to the deformations, its degenerate vibrational energy levels are split. For this reason all vibrational modes of CH_4 and N_2 molecules in the complex are IR active. In the CH_4–N_2 complex there are vibrational frequency shifts $\Delta\omega=\omega^{\text{mon}}-\omega^{\text{com}}$ (here, ω^{mon} and ω^{com} are the harmonic frequencies of the monomer and of the complex, respectively, calculated at the MP2/aug-cc-pVTZ level) which are presented in Table VIII for geometry 4. As follows from Table VIII, there is a small tendency of the intramolecular vibrational frequencies of CH_4 and N_2 to a redshift. Analogous shift tendency is observed for all geometries C_τ. The fully automated code to build the anharmonic constants used in a second-order perturbative method of Barone[42] implemented in GAUSSIAN 03 was employed to calculate the anharmonic frequencies of the CH_4–N_2 complex. The calculated anharmonic frequencies for the fundamental bands of the complex being in the geometry 4 are presented in Table VIII. Due to the large error of intermolecular anharmonic frequency calculations, these frequencies are not given in Table VIII. The calculated rotational constants are also presented in this table. It is noteworthy that the CH_4–N_2 complex is almost a prolate symmetric top as follows from the analysis of rotational constants. Indeed, the asymmetry

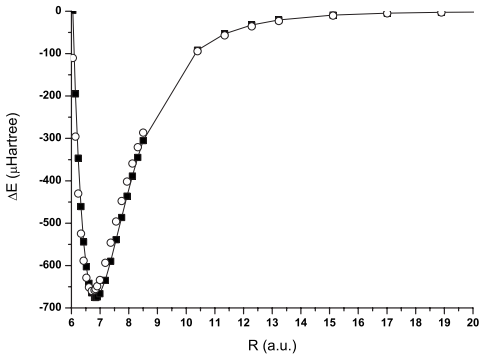

FIG. 8. R-dependence of the interaction energy of the CH_4–N_2 complex for the equilibrium geometry 4. Solid line: *ab initio* calculation at the CCSD(T)/aug-cc-pVTZ level of theory with BSSE correction. Circles: Lennard-Jonnes potential [Eq. (7)]. Squares: Esposti–Werner potential [Eq. (8)].

TABLE VII. Harmonic (ω) vibrational wave numbers (cm^{-1}) calculated at the MP2/aug-cc-pVTZ level with BSSE correction for the CH_4–N_2 complex being in the geometry C_τ (τ=0°–30°).

	τ (deg)						
Normal mode	0	5	10	15	20	25	30
1	19.6				7		9.5
2	23.3	26.2	25.8	28.6	26.6	26.3	28.2
3	48.2	50.8	50.8	54.0	50.6	50.6	54.3
4	65.7	67.3	66.3	70.2	66.8	66.8	74.4
5	71.8	75.3	76.0	79.9	77.6	76.4	78.5
6	1355.4	1355.4	1355.4	1355.5	1355.4	1355.4	1355.5
7	1356.0	1356.9	1355.9	1355.9	1355.9	1355.9	1356.0
8	1356.1	1356.1	1356.1	1356.1	1356.1	1356.1	1356.2
9	1587.7	1587.6	1587.6	1587.6	1587.7	1587.6	1587.6
10	1588.3	1588.4	1588.4	1588.4	1588.4	1588.4	1588.4
11	2185.0	2184.8	2184.9	2184.8	2184.8	2184.8	2184.8
12	3066.8	3067.0	3067.1	3067.0	3066.9	3067.0	3066.8
13	3201.6	3201.9	3202.0	3201.9	3201.9	3201.9	3201.4
14	3201.6	3202.1	3202.1	3202.0	3202.0	3202.0	3202.1
15	3204.0	3203.9	3204.0	3204.0	3203.8	3203.9	3203.8

parameter $K=(2B-A-C)/(A-C)=-0.99$ almost equals to -1, which corresponds to a prolate symmetric top.

IV. CONCLUSION

The analysis of the PES of the CH_4–N_2 complex calculated both at the MP2 and CCSD(T) level of theory employing aug-cc-pVTZ basis set showed that there is a family of the most stable geometries C_τ. These geometries are obtained by the rotation of the N_2 molecule around the x-axis of an angle τ, where the initial geometry C_0 of the complex corresponds to geometry 4. The recommended BE of the most stable configuration at R_e=6.8 a.u. almost does not depend on the method used for CBS limit calculations: ΔE =−820.536 μhartree when Martin's extrapolation scheme (the cardinal number X=4,5) for total energy is used and ΔE=−827.143 μhartree for Helgaker's scheme (X=(3),4,5) separately extrapolating Hartree–Fock and correlation energy. The present *ab initio* calculations of the PES together with its analytical description [Eqs. (5)–(7)] for long-range intermolecular separations can serve as a good basis for the full description of interaction energy surface of the van der Waals CH_4–N_2 complex.

ACKNOWLEDGMENTS

This work was supported by the CH_4@Titan.

APPENDIX: MOLECULAR PARAMETERS FOR THE CH_4 AND N_2 MONOMERS

See Table IX.

TABLE VIII. Harmonic (ω) and anharmonic (ν) vibrational wavenumbers, shifts $\Delta\omega=\omega^{mon}-\omega^{com}$, and rotational constants (A,B,C) [rotational constants in the equilibrium geometry: A_e=1.420 734, B_e=0.123 238, and C_e=0.115 954; in the ground state: A=1.522 647, B=0.106 818, and C=0.100 360 (cm^{-1})] calculated at the MP2/aug-cc-pVTZ level with BSSE correction for geometry 4 of the CH_4–N_2 complex. All values are in cm^{-1}.

Mode	Sym.	ω	$\Delta\omega$	ν	A	B	C
1	A''	19.6			1.533 416	0.106 836	0.100 632
2	A''	23.3			1.706 804	0.109 399	0.100 219
3	A'	48.2			1.522 507	0.096 197	0.091 039
4	A'	65.7			1.538 965	0.094 149	0.089 516
5	A''	71.8			1.537 200	0.094 502	0.089 132
6	A'	1355.4	0.6	1317.4	1.523 007	0.106 739	0.100 339
7	A''	1356.0	0.0	1317.9	1.515 098	0.106 811	0.100 339
8	A'	1356.1	−0.1	1317.4	1.516 464	0.106 803	0.100 312
9	A''	1587.7	0.9	1549.5	1.528 913	0.106 856	0.100 418
10	A'	1588.3	0.3	1549.3	1.528 894	0.106 879	0.100 388
11	A'	2185.0	1.9	2148.0	1.511 501	0.107 070	0.100 509
12	A'	3066.8	2.8	2950.1	1.520 032	0.106 795	0.100 339
13	A''	3201.6	3.4	3070.2	1.520 209	0.106 792	0.100 334
14	A'	3201.6	3.4	3069.9	1.520 202	0.106 799	0.100 345
15	A'	3204.0	1.0	3070.2	1.520 327	0.106 799	0.100 344

TABLE IX. Molecular parameters used in the analytical calculation. Subscripts a and b refer to CH_4 and N_2, respectively.

Parameter	Definition	Value	Ref.
U_a	First ionization potential	0.4770 hartree	43
U_b	First ionization potential	0.5725 hartree	43
Q^b	Quadrupole moment	$-1.1258ea_0^2$	44
Ω^a	Octupole moment	$2.4095ea_0^3$	45
Φ^a	Hexadecapole moment	$-8.27ea_0^4$	46
Φ^b	Hexadecapole moment	$-6.75ea_0^4$	44
α^a	Polarizability	$16.39a_0^3$	45
α^b	Polarizability	$\alpha_{xx}=\alpha_{yy}=10.2351a_0^3$, $\alpha_{zz}=14.8425a_0^3$	44
A^a	Dipole-quadrupole polarizability	$9.01a_0^4$	47
E^a	Dipole-octupole polarizability	$-18.9a_0^5$	47

[1] G. Birnbaum, A. Borysow, and A. Buechele, J. Chem. Phys. **99**, 3234 (1993).
[2] I. R. Dagg, A. Anderson, S. Yan, W. Smith, C. G. Joslin, and L. A. A. Read, Can. J. Phys. **64**, 1467 (1986).
[3] R. Courtin, Icarus **51**, 466 (1982).
[4] R. Courtin, Icarus **75**, 245 (1988).
[5] X. Li, M. H. Champagne, and K. L. C. Hunt, J. Chem. Phys. **109**, 8416 (1998).
[6] M. Buser, L. Frommhold, M. Gustafsson, M. Moraldi, M. H. Champagne, and K. L. Hunt, J. Chem. Phys. **121**, 2617 (2004).
[7] M. Buser and L. Frommhold, J. Chem. Phys. **122**, 024301 (2005).
[8] D. E. Jennings, F. M. Flasar, V. G. Kunde, R. E. Samuelson, J. C. Pearl, C. A. Nixon, R. C. Carlson, A. A. Mamoutkine, J. C. Brasunas, E. Guandique, R. K. Achterberg, G. L. Bjoraker, P. N. Romani, M. E. Segura, S. A. Albright, M. H. Elliott, J. S. Tingley, S. Calcutt, A. Coustenis, and R. Courtin, Astrophys. J. **691**, L103 (2009).
[9] H. Schindler, R. Vogelsang, V. Staemmler, M. A. Siddiqi, and P. Svejda, Mol. Phys. **80**, 1413 (1993).
[10] M. Shadman, S. Yeganegi, and F. Ziaie, Chem. Phys. Lett. **467**, 237 (2009).
[11] O. B. Toon, C. P. McKay, R. Courtin, and T. P. Ackerman, Icarus **75**, 255 (1988).
[12] G. F. Lindal, G. E. Wood, H. B. Hotz, D. N. Sweetnam, V. R. Eshleman, and G. L. Tyler, Icarus **53**, 348 (1983).
[13] W. Reid Thompson, J. A. Zollweg, and D. H. Gabis, Icarus **97**, 187 (1992).
[14] A. Borysow and C. Tang, Icarus **105**, 175 (1993).
[15] R. Courtin, D. Gautier, and C. P. McKay, Icarus **114**, 144 (1995).
[16] C. P. McKay, Planet. Space Sci. **44**, 741 (1996).
[17] R. E. Samuelson, N. R. Nath, and A. Borysow, Planet. Space Sci. **45**, 959 (1997).
[18] F. M. Flasar, R. K. Achterberg, B. J. Conrath, P. J. Gierasch, V. G. Kunde, C. A. Nixon, G. L. Bjoraker, D. E. Jennings, P. N. Romani, A. A. Simon-Miller, B. Bezard, A. Coustenis, P. G. J. Irwin, N. A. Teanby, J. Brasunas, J. C. Pearl, M. E. Segura, R. C. Carlson, A. Mamoutkine, P. J. Schinder, A. Barucci, R. Courtin, T. Fouchet, D. Gautier, E. Lellouch, A. Marten, R. Prange, S. Vinatier, D. F. Strobel, S. B. Calcutt, P. L. Read, F. W. Taylor, N. Bowles, R. E. Samuelson, G. S. Orton, L. J. Spilker, T. C. Owen, J. R. Spencer, M. R. Showalter, C. Ferrari, M. M. Abbas, F. Raulin, S. Edgington, P. Ade, and E. H. Wishnow, Science **308**, 975 (2005).
[19] S. J. Kim, T. R. Geballe, K. S. Noll, and R. Courtin, Icarus **173**, 522 (2005).
[20] A. Coustenis, R. K. Achterberg, B. J. Conrath, D. E. Jennings, A. Marten, D. Gautier, C. A. Nixon, F. M. Flasar, N. A. Teanby, B. Bézard, R. E. Samuelson, R. C. Carlson, E. Lellouch, G. L. Bjoraker, P. N. Romani, F. W. Taylor, P. G. J. Irwin, T. Fouchet, A. Hubert, G. S. Orton, V. G. Kunde, S. Vinatier, J. Mondellini, M. M. Abbas, and R. Courtin, Icarus **189**, 35 (2007).
[21] H. Seo, S. J. Kim, J. H. Kim, T. R. Geballe, R. Courtin, and L. R. Brown, Icarus **199**, 449 (2009).
[22] T. H. Dunning, Jr., J. Chem. Phys. **90**, 1007 (1989).
[23] S. Tsuzuki, T. Uchimaru, and K. Tanabe, Chem. Phys. Lett. **287**, 202 (1998).
[24] E. R. Johnson and A. D. Becke, J. Chem. Phys. **123**, 024101 (2005).
[25] E. R. Johnson and A. D. Becke, J. Chem. Phys. **124**, 174104 (2006).
[26] F. Jensen, *Introduction to Computational Chemistry* (Wiley, New York, 2007).
[27] S. F. Boys and F. Bernardi, Mol. Phys. **19**, 553 (1970).
[28] M. J. Frisch, G. W. Trucks, H. B. Schlegel, *et al.*, GAUSSIAN 03, Revision D.02, Gaussian, Inc., Wallingford CT, 2004.
[29] B. Paizs, P. Salvador, A. G. Csaszar, M. Duran, and S. Suhai, J. Comput. Chem. **22**, 196 (2001).
[30] D. Feller, J. Chem. Phys. **96**, 6104 (1992).
[31] D. G. Truhlar, Chem. Phys. Lett. **294**, 45 (1998).
[32] J. M. L. Martin, Chem. Phys. Lett. **259**, 669 (1996).
[33] A. Halkier, T. Helgaker, P. Jørgensen, W. Klopper, and J. Olsen, Chem. Phys. Lett. **302**, 437 (1999).
[34] A. Mourbat, A. Aboumajd, and M. Loete, J. Mol. Spectrosc. **190**, 198 (1998).
[35] J. Bendtsen, J. Raman Spectrosc. **2**, 133 (1974).
[36] See EPAPS supplementary material at http://dx.doi.org/10.1063/1.3242080 for the energies calculated at the CCSD(T)/aug-cc-pVTZ level of theory with BSSE correction.
[37] A. D. Buckingham, *Intermolecular Interaction: From Diatomic to Biopolymers* (Wiley, New York, 1978).
[38] D. J. Margoliash and W. J. Meath, J. Chem. Phys. **68**, 1426 (1978).
[39] D. Spelsberg and W. Meyer, J. Chem. Phys. **111**, 9618 (1999).
[40] A. D. Esposti and H. W. Werner, J. Chem. Phys. **93**, 3351 (1990).
[41] MINPACK, available online at http://www.netlib.org/minpack/.
[42] V. Barone, J. Chem. Phys. **122**, 014108 (2005).
[43] A. A. Radtsig and B. M. Smirnov, *Reference Book on Atomic and Molecular Physics* (Atomizdat, Moscow, 1980).
[44] G. Maroulis, J. Chem. Phys. **118**, 2673 (2003).
[45] G. Maroulis, Chem. Phys. Lett. **226**, 420 (1994).
[46] R. D. Amos, Mol. Phys. **38**, 33 (1979).
[47] G. Maroulis, J. Chem. Phys. **105**, 8467 (1996).

Chapitre 8

Etude du piégeage des molécules dans les zéolithes

Publication : P24

8.1 Présentation de l'étude

Ce travail a son origine dans une collaboration de l'équipe «Spectroscopie Moléculaire et Applications» avec l'équipe «Adsorption sur Solides Poreux» au sein de l'ICB. Cette dernière équipe a développé des techniques expérimentales d'approche moléculaire, y compris la spectroscopie infrarouge *in situ*, qui fournissent de riches informations sur les systèmes adsorbat (molécules physisorbées)/adsorbant (solide). La modélisation moléculaire est nécessaire pour aider à la compréhension et l'interprétation des données expérimentales. Les études *ab initio* des structures micro- et nanoporeuses sont une composante importante de ces études théoriques. Elle pemettent l'analyse des modifications des spectres vibrationnels de l'adsorbat et/ou de l'adsorbant lors de l'adsorption ainsi que l'interprétation des spectres expérimentaux, et fournissent un support pour améliorer la compréhension de ce phénomène.

8.1.1 Le matériau considéré

La zéolithe de type ZSM-5 (acronyme de Zeolite Socony Mobil type 5) et la silicalite-1, qui est l'homologue structural de la zéolithe ZSM-5, ont été choisies comme adsorbant modèle. Elles sont représentées par la formule $M_nAl_nSi_{96-n}O_{192}$, mH_2O, n=3 dans le cas de ZSM-5, et n=0 dans le cas de la silicalite. Les zéolithes sont des adsorbants de la famille des aluminosilicates, minéraux microporeux et nanoporeux avec une charpente ouverte. Elles sont construites sur la base d'une charpente tridimensionnelle de TO_4 (T = Al, Si) (Fig.8.1a) sous forme de tétraèdres, chaque atome d'oxygène étant partagé entre deux tétraèdres (Fig.8.1b).

L'ensemble de ces tétraèdres produit une structure poreuse avec des ouvertures régulières, canaux et cavités où des molécules de dimensions variées peuvent être piégées. La structure ouvre des possibilités pour de nombreuses applications, comme la séparation de gaz, la récupération de polluants, la catalyse. Les domaines d'utilisation sont donc dans l'industrie (notamment la pétrochimie) et la protection de l'environnement. L'optimisation des procédés de séparation par adsorption nécessite une compréhension fondamentale du processus d'adsorption à une l'échelle micro- et nano-scopique.

Il faut pour cela interpréter les spectres expérimentaux, ce qui nécessite de déterminer les spectres vibrationnels de la molécule dans l'état adsorbé et aussi d'une cellule de silicalite en présence des interactions avec la molécule adsorbée. Ces spectres ont été également calculés, en utilisant un modèle théorique de canal droit et de canal sinusoïdal d'une zéolithe ZSM-5.

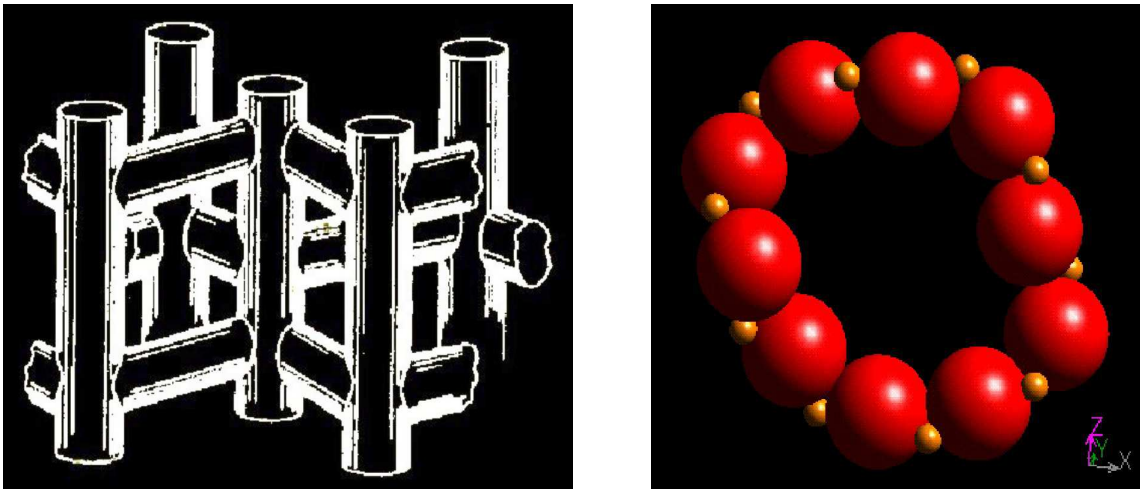

(a) (b)

FIG. 8.1 – Structure des zéolithes, (a) leur charpente tridimensionnelle, (b) position des atomes

8.1.2 Propriétés physiques

L'adsorption est un phénomène de surface par lequel des molécules de gaz ou de liquides se fixent sur les surfaces solides des adsorbants selon divers processus plus ou moins intenses.

La physisorption, ou l'adsorption physique met en jeu des liaisons faibles, du type forces de van der Waals, et se produit sans formation de liaisons chimiques. Elle se produit bien avant que le gaz n'atteigne une pression égale à sa pression de vapeur saturante, à des températures assez basses et voisines du point d'ébullition de la phase adsorbée. Elle est en général réversible et on peut la comparer au dépôt de buée sur une paroi froide. L'équilibre est obtenu lorsque les vitesses d'évaporation et de condensation sont égales. L'adsorption physique est donc favorisée par une baisse de la température.

Dans le cas des forces d'adsorption, les forces mises en jeu dans les zéolithes correspondent d'une part à l'interaction entre les molécules adsorbées et la charpente zéolithique (interactions adsorbat/adsorbant), et d'autre part entre les molécules adsorbées (interactions adsorbat/adsorbat). On définit :

- *les interactions non spécifiques* : elles sont universelles bien que leurs grandeurs soient fonction de l'environnement local de l'adsorbant. Leur origine est dans les forces de dispersion, qui sont des forces d'attraction, et de répulsion à courte distance entre les atomes. Parmi les modèles théoriques décrivant ces interactions, un des modèles les plus utilisés est celui de Lennard-Jones ;
- *les interactions spécifiques* : elles correspondent aux forces électrostatiques consécutives à une répartition singulière des charges dans l'adsorbant solide ainsi que dans les molécules adsorbées.

La contribution relative de ces deux types d'interaction a été analysée suivant la nature des molécules adsorbables et de l'adsorbant par Kiselev [59]. Une classification a été proposée sur la base des différences spécifiques de la répartition de la densité électronique autour des atomes ou des groupes des atomes de la molécule adsorbée, ainsi que la répartition des charges à la surface du solide. Selon cette classification, les zéolithes aluminosiliques (zéolithes classiques) sont des adsorbant du type II (adsorbant spécifique de charge positive) et les zéolithes siliciques non cationiques sont de type I (adsorbant neutre non spécifique). Les expérimentateurs utilisent très souvent la valeur numérique de l'énergie d'absorption en tant que critère discriminant entre physisorption et chimisorption (pour la physisorption, l'énergie d'adsorption vaut moins de 0.30 eV [60]). On peut également tester la dépendance de la distance du potentiel d'interaction [61] : on parle alors d'une contribution «physique» si le potentiel d'interaction varie comme une puissance négative de la distance R entre l'adsorbat et la surface, tandis que l'interaction «chimique» montre un comportement exponentiel. Il y a trois contributions à

l'interaction adsorbat/adsorbant qui sont essentiellement de nature physique, et deux contributions de nature chimique :

- *interaction électrostatique* : cette contribution est causée par l'interaction coulombienne entre la distribution des charges du solide et la molécule adsorbée : une molécule adsorbée possède une énergie potentielle dans le champ électrostatique du solide. Cette interaction peut être présentée comme le développement multipolaire : $V_{el}(R) = \sum \left(Q_{l_A} * Q_{l_B} / R^{l_A+l_B+1}\right)$, où Q_{l_A} et Q_{l_B} sont les tenseurs des moments multipolaires électriques permanents à l'ordre l_A et l_B des fragments A et B. L'interaction électrostatique peut être répulsive ou attractive, ceci dépend du signe des moments multipolaires et de l'orientation de la molécule par rapport à la surface ;
- *induction (interaction de polarisation)* : les moments multipolaires de la molécule adsorbée peuvent induire des moments électriques dans le confinement zéolithique et interagir avec eux, et réciproquement. Cette interaction de polarisation est toujours attractive ;
- *interaction de dispersion de London* : les forces de dispersion de London sont des forces faibles intermoléculaires créées par des dipôles induits. Elles représentent en général la composante la plus importante des forces de Van der Waals. Si les systèmes n'ont pas de moments multipolaires permanents, cette interaction joue effectivement le rôle principal. Les termes dominants de cette interaction sont donnés par :

$$V_{disp}(R) = -\frac{C_6}{R^6} - \frac{C_8}{R^8} - ... \tag{8.1}$$

avec les coefficients de dispersion C_6, C_8. Le coefficient C_6 peut être exprimé comme

$$C_6 = \frac{3h}{2\pi h^2} \int \alpha_A(iw) * \alpha_B(iw)\, dw \tag{8.2}$$

où $\alpha_A(iw)$ et $\alpha_B(iw)$ sont les polarisabilités dynamiques de deux systèmes en interaction. Si on remplace la polarisabilité par une constante diélectrique du solide et qu'on fait l'intégration sur tous les atomes, on va obtenir comme terme principal :

$$V_{disp}(R) = -\frac{C_3}{R^3} - ... \tag{8.3}$$

avec un terme d'interaction de dispersion de van der Waals entre molécule adsorbée et surface de solide :

$$C_3 = \frac{h}{8\pi^2} \int \frac{\alpha_A(iw) * (\varepsilon(iw) - 1)}{\varepsilon(iw) + 1}\, dw \tag{8.4}$$

- *répulsion de Pauli* : une de deux parties «chimiques» de l'énergie d'interaction totale est une répulsion entre couches fermées (principe de Pauli) appelée répulsion d'échange (XR). Cette interaction est à courte-portée et peut s'exprimer comme $V_{XR}(R) = A*\exp(-\alpha R)$;
- *liaison chimique* : il existe une seconde partie «chimique» dans la contribution à l'énergie d'interaction totale s'il y a une liaison ionique ou une liaison chimique covalente entre une molécule adsorbée et la surface. Cette interaction montre aussi une dépendance exponentielle, car les liaisons covalentes dépendent du chevauchement entre les fonctions d'ondes des sous-systèmes. En général, les liaisons covalentes ne sont possibles que si au moins l'un des partenaires de l'interaction possède des valences orbitales partiellement occupées.

  Il faut noter que l'interaction de van der Waals et la répulsion de Pauli sont toujours présentes. Le traitement théorique de l'interaction de van der Waals demande l'application des méthodes les plus sophistiquées telles que la théorie de perturbation (Møller-Plesset, MP), l'interaction de configuration (CI) ou les clusters couplés (CC)), dont on a vu la description au chapitre 2.

8.2 Les éléments de la modélisation

8.2.1 Modélisation du solide : les clusters

Pour traiter des solides micro- ou nanoporeux par méthodes de chimie quantique, il est nécessaire de choisir un modèle qui représente une partie du solide. Il y a essentiellement trois types de modèles de cluster qui sont actuellement utilisés pour le calcul des propriétés locales du solide et la description de l'adsorption à la surface : cluster libre («free»), cluster saturé, et «embedded» cluster. Le cluster libre est simplement une partie tridimensionnelle du solide sans modification. Le cluster saturé est quant à lui totalement rempli par des atomes fictifs. Il s'agit d'un petit cluster, si bien que, pour compenser sa taille et ne pas être trop perturbé par les conditions aux limites, on doit saturer les sites du cluster de façon raisonnable. Dans la plupart des applications, la saturation est apportée par des atomes d'hydrogène. Un modèle typique de «embedded» cluster est un petit cluster traité par des méthodes de chimie quantique, telles que SCF, DFT, CI ou CC. Ce cluster se trouve dans un champ de charges ponctuelles étendu «extended point charge field (PCF)», qui doit reproduire le potentiel de Madelung sur la surface et au-dessus de la surface. Mais il n'est pas toujours facile de déterminer les charges effectives, surtout pour les systèmes à haut degré de covalence, lorsque les valeurs des charges calculées sont très sensibles aux méthodes théoriques appliquées. On a choisi dans ce travail deux types de cluster pour modéliser la zéolithe : un cluster libre avec un nombre d'atomes assez important, et un petit cluster saturé avec des atomes d'hydrogène, qui représente un fragment du cluster précédent. Le premier cluster donne une possibilité d'entourer la molécule adsorbée pour mieux reproduire le confinement zéolithique, tandis que son fragment a pu être traité avec des méthodes *ab initio* plus sophistiquées.

8.2.2 L'adsorbat : la silicalite.

La silicalite est répresentive des zéolithes de topologie MFI (Mobil type FIve) [62], qui se distingue des zéolithes de type ZSM-5 (Zeolite Socony Mobil type 5) [63] par son rapport Si/Al infini. C'est un système purement silique de formule chimique $Si_{96}O_{192}$. Sa maille élémentaire est construite à partir de 96 tétraèdres [SiO_4], qui sont liés entre eux par leurs atomes d'oxygène. Le cristal de silicalite a une structure cristalline orthorhombique Pnma d'après des données cristallographiques expérimentales de van Koningsveld et al. [64]. La zéolithe ZSM-5 et la silicalite possèdent des structures identiques décrites par la formule empirique suivante [63] : $M_nAl_nS_{96-n}O_{192}$, mH_2O, où $n \leqslant 27$ avec n=3 dans le cas de la zéolithe ZSM-5 et n=0 dans le cas de la silicalite [65]. L'unité de construction secondaire (SBU, acronyme de Secondary Building Units) qui permet de décrire la structure des zéolithes de topology MFI est basée sur l'agencement de six tétraèdres TO_4, où T est un atome d'aluminium ou de silicium, suivant un modèle de type SBU 5-1 (Fig.8.1). L'accolement de huit de ces éléments fournit l'unité structurale de base : le pentasil. Les pentasils sont reliés entre eux par l'intermédiaire de liaisons T-O-T et forment les chaînes, qui sont elles-mêmes agencées entre elles, et qui génèrent des couches de tétraèdres (Fig.8.1). Les tétraèdres s'arrangent dans les trois directions de l'espace et génèrent une microporosité, qui est constituée de canaux droits parallèles à l'axe [010] (OY) et interconnectés à des canaux sinusoïdaux orientés suivant les axes [100] (OX) et [001] (OZ). La forme des canaux et leur diamètre d'ouverture dépendent du rapport Si/Al de la zéolithe. Dans le cas de ZSM-5, les canaux droits et les canaux sinusoïdaux sont elliptiques. Pour la silicalite (rapport Si/Al supérieur à 1000) les canaux droits sont quasi-cylindriques et les canaux sinusoïdaux gardent leur forme elliptique. Trois sites géométriques ont été définis au sein de la charpente zéolithique de topologie MFI pour mieux caractériser la localisation des molécules adsorbées [65, 66] :

- site I : d'une dimension de l'ordre de 0,51 nm$\times$0,55 nm$\times$0,66 nm (4 par maille, canaux sinusoïdaux) ;
- site II : d'une dimension de l'ordre de 0,54 nm$\times$0,56 nm$\times$0,45 nm (4 par maille, canaux droits) ;
- site III : d'un diamètre de l'ordre de 0,9 nm (4 par maille, intersections).

La maille élémentaire de la zéolithe a donc au total douze sites potentiels d'adsorption. La structure cristalline des zéolithes de topologie MFI est relativement sensible à l'influence du rapport Si/Al, à l'influence de la température et à l'influence du remplissage [67]. Trois variétes polymorphiques sont définies dans la littérature [64] :

- la structure monoclinique (MONO), de symétrie $P2_1/n.1.1$;
- la structure orthorhombique (ORTHO), de symétrie Pnma ;
- la structure orthorhombique (PARA), qui se différencie de la structure ORTHO par sa symétrie de type $P2_12_12_1$.

8.2.3 L'éthylène

L'éthylène dans l'état de base électronique est une molécule plane du groupe de symétrie D_{2h}. La double liaison de cette molécule apolaire lui confère la coplanarité de ses six atomes. La hauteur de la barrière de rotation interne est d'environ 20000 cm^{-1} [68] et l'effet tunnel ne s'observe pas dans cet état électronique. Ses principales caractéristiques physico-chimiques sont les suivantes [69] :

Masse molaire	28,04 g/mol
Dimensions L x l x e	0,49 nm × 0,42 nm × 0,28 nm
Moment dipolaire (D)	0
Masse volumique à 273 K, 1 bar	1,23 $kg.m^{-3}$
Point d'ébullition à 1 bar	169,44 K
Point de fusion à 1 bar	104,04 K

Les caractéristiques spectroscopique infrarouge de l'éthylène sont également bien connues ; elles sont présentées dans l'article principal [P24].

8.2.4 Etude des zéolithes par spectroscopie infrarouge

La spectroscopie infrarouge[1] est une des techniques de base pour la caractérisation des zéolithes. Les spectromètres à transformées de Fourier ont largement amélioré la sensibilité de la technique et la qualité des spectres. Les sources sont en général des GloBar (Glowing Bar) : barre de carbure de silicium chauffée par un courant électrique à 800 (4500 - 300 cm^{-1}) ou 1200 K (8000 - 50 cm^{-1}) selon le refroidissement. Deux sortes de détecteurs sont couramment utilisés : détecteur thermique (sensible à la chaleur dégagée par une cible) ou détecteur quantique (compteur des photons). Les détecteurs thermique sont de type DTGS (Deuterated TriGlycide Sulfate). Les détecteurs quantiques sont de type MCT (Mercure, Cadmium, Tellure) ; ils sont refroidis à l'azote, et sont beaucoup plus sensibles et beaucoup plus rapides, mais aussi plus chers. La séparatrice de l'interféromètre est en KBr pour le système infrarouge. Pour le proche et le lointain infrarouge, il faut utiliser des séparatrices particulières (quartz, mylar, CaF2 et CsI). Une des procédures utilisées pour obtenir un spectre infrarouge de zéolithe consiste à mettre la poudre en suspension dans le Nujol ou bien à la disperser (à 0.5 ou 1%) dans du bromure de potassium (KBr). Cette poudre est ensuite pressée pour former une pastille placée dans le faisceau infrarouge. Les bandes principales de la structure zéolithique que l'on peut observer se trouvent entre 400 et 1300 cm^{-1}. Ces bandes ont été attribués à des vibrations ν(T-O) [70], qui peuvent être (i) symétriques (800–750 cm^{-1}), (ii) asymétriques (1000–1200 cm^{-1}). Ces vibrations sont séparées en vibrations internes et externes aux tétraèdres. La modélisation montre que ces bandes sont le produit de l'ensemble des vibrations du réseau.

[1] L'infrarouge moyen couvre la zone de longueurs d'ondes de 25 à 2,5 μm, soit, en nombre d'ondes, de 400 à 4000 cm^{-1} ($\tilde{\nu} = 1/\lambda = \nu/c$, ν est une fréquence, λ est une longeur d'onde, c est la vitesse de la lumière). Dans le domaine de l'infrarouge, l'énergie des rayonnements correspond aux changements d'énergie de vibration et de rotation des molécules.

8.3 Principaux résultats [P24]

Le but de ce travail est donc l'étude par spectroscopie infrarouge (IR) et au moyen de méthodes *ab initio* de l'interaction de la molécule d'éthylène avec une zéolithe hydrophobique, la silicalite-1. Plusieurs méthodes de chimie quantique ont été utilisées (RHF, MP2 et DFT) simultanément au cours de l'experience IR, à la température ambiante. Les calculs ont été effectués en considérant une partie du canal droit et le canal sinusoïdal de la silicalite-1, un cluster $Si_{20}O_{50}$, et également un fragment hydrogénique du cluster, de forme $Si_4O_{12}H_8$. L'étude s'est concentrée sur l'évolution des spectres IR :

- pour l'éthylène, à partir de la phase gazeuse vers la phase adsorbée ;
- pour l'adsorbant, de l'état déchargé vers un état chargé.

On a choisi une méthode *ab initio* appropriée pour décrire avant tout les spectres de l'éthylène et du cluster libre d'adsorbant. Pour le cluster $Si_{20}O_{50}$, les calculs ont été effectués à l'aide de la méthode $RHF/3-21G**$. Dans ce cas, le spectre IR calculé est en bon accord avec les positions des bandes vibrationnelles expérimentales pour la zéolithe déchargée. En ce qui concerne la molécule d'éthylène, les calculs ont été exécutés par différentes méthodes. Le meilleur accord entre les spectres calculés et expérimentaux est obtenu par la méthode MP2.

La deuxième étape de ce travail a consisté à calculer le spectre infrarouge de la zéolithe en interaction avec une molécule d'éthylène afin de tenir compte des modifications expérimentales des bandes de vibration de l'adsorbant et l'adsorbat. Dans le cas du cluster, l'adsorption provoque un déplacement vers le rouge avec un glissement de 8 et 10 cm^{-1} par rapport à l'éthylène isolé pour les bandes de vibration ν_{11} et ν_9 respectivement. Ces déplacements sont dus à l'affaiblissement de la liaison C-H et ils sont proches des valeurs de l'expérience, qui sont respectivement 12 et 11 cm^{-1}. Toutefois, pour le mode de vibration ν_{12}, la simulation montre un déplacement vers le bleu alors que l'expérience donne un déplacement vers le rouge. En utilisant la méthode MP2 pour le fragment $Si_4O_{12}H_8$, cette anomalie est corrigée. Toutefois, avec ce cluster réduit, les bandes ν_{11} et ν_9 de la molécule d'éthylène ne sont pas modifiés par le processus d'adsorption. Ces résultats montrent l'importance qu'il y a à bien choisir à la fois la zéolithe modèle et le niveau de la théorie pour obtenir la bonne réponse spectroscopique. Concernant le choix du niveau de la théorie, il faut remarquer que la courbe d'énergie potentielle calculée par la méthode MP2, contrairement aux méthodes DFT, montre un potentiel avec un minimum prononcé en raison de l'interaction de van der Waals. En conséquence, la méthode MP2 est adaptée à l'étude de la physisorption de l'éthylène dont la molécule est non-polaire.

A cette étape de l'étude, les calculs quantiques apportent les éléments de compréhension suivants concernant la réponse spectroscopique des zéolithes en présence du phénomène d'adsorption d'éthylène :

- la méthode MP2 doit être utilisée pour le cluster $Si_{20}O_{50}$ représentant des canaux droits et sinusoïdaux, et pour l'intersection de ces canaux. La contribution des intersections correspond au tiers de celle de tous les sites d'adsorption ;
- la silicalite-1 peut adsorber jusqu'à 11 molécules par cellule élémentaire. Par conséquent, à haute charge, les interactions entre molécules jouent un rôle important. Ceci signifie que l'on doit simuler l'adsorption de deux ou plusieurs molécules d'éthylène ;
- la simulation MD (Molecular Dynamics) a montré que les molécules d'éthylène ne sont pas prises au piège sur des sites donnés à 298 K. Elles sont très mobiles, et présentent une large distribution de leur orientation. En conséquence, les calculs devraient être effectués sur des orientations différentes.

8.4 Article-clé : P24

Molecular Physics
Vol. 107, No. 19, 10 October 2009, 2081–2093

RESEARCH ARTICLE

Experimental IR study and *ab initio* modelling of ethylene adsorption in a MFI-type host zeolite

N. Zvereva-Loëte*, A. Ballandras, G. Weber, M. Rotger†, V. Boudon and J.-M. Simon

Institut Carnot de Bourgogne – UMR 5209 CNRS-Université de Bourgogne, 9, av. Alain Savary, B.P. 47870, F-21078 Dijon Cedex, France

(*Received 8 April 2009; final version received 25 June 2009*)

Different *ab initio* methods and experimental results are used to investigate the effect of the adsorption of one ethylene molecule on silicalite-1, a MFI-type zeolite. We used simplified models to simulate a portion of a straight or sinusoidal channel of silicalite-1 at a quantum level. The calculated absorption spectra of the models are qualitatively in good agreement with the experimental FTIR spectrum of silicalite-1. Additionally we simulate the FTIR spectrum of the isolated ethylene molecule and that of an ethylene molecule in interaction with the above-mentioned zeolite models. Results are discussed depending on the method and specific basis set and compared with experiments and previous molecular dynamics simulations.

Keywords: *ab initio*; FTIR spectroscopy; modelling; vibrational analysis

1. Introduction

Zeolites are adsorbents that belong to a class of microporous aluminosilicates with an open framework structure. They are built based on a three-dimensional framework of TO_4 (T = Al, Si) tetrahedra, each oxygen atom being shared between two tetrahedra. The assemblage of these tetrahedra creates a porous structure with regular arrays of openings, channels and/or cavities in which molecules of various sizes can be trapped. Their catalytic and adsorption properties are the basis of the use of zeolites in gas separation [1], catalysis [2–4], and environmental protection [5,6]. Many experimental and theoretical investigations have been carried out to study physicochemical properties of zeolites [7–27].

Fourier Transform Infrared (FTIR) spectroscopy is a powerful technique to investigate adsorption processes and particularly the state of physisorbed molecules [8,9,18,28,29]. Modifications of the spectra of both the adsorbent and the adsorbate are observed experimentally during physisorption processes. The interpretation of these modifications is still challenging and needs a theoretical support. Infrared experimental and molecular dynamics (MD) simulation studies were previously jointly performed to characterize the interaction of ethylene on silicalite-1 at room temperature [5,8,29]. The three main results are: (i) a good agreement between experiment and simulation, (ii) the vibrational response accounts for a global interaction between the whole structure of the zeolite and ethylene, indicating that the adsorbed ethylene molecule is not localized on a preferable silicalite site and (iii) the ν_{12} vibrational band of ethylene exhibits a small split at high loading attributed to a condensation effect of the adsorbed phase. It can be underlined that at very low temperature or/and using cumbersome adsorbates, molecules can be preferentially located at specific sites. In these cases, contrary to what occurs with ethylene, the spectroscopic response will be the signature of the specific interaction between a site and the molecule.

In this paper we report the experimental results of ethylene adsorption on silicalite-1 obtained by means of a new FTIR chamber. Additionally, we extended our studies to a quantum approach that is supposed to give a better description of infrared spectra compared to classical MD simulation. However, *ab initio* quantum calculations are computationally expensive for systems including a lot of electrons as it is for a unit cell of zeolite. As a consequence, authors considered only a part of a zeolite unit cell representative of the geometric and electronic environment [30].

*Corresponding author. Email: Natalia.Loete@u-bourgogne.fr
†Present address: GSMA, CNRS UMR 6089 Moulin de la Housse B.P. 1039 Cases 16-17 F-51687 REIMS Cedex 2, France.

ISSN 0026–8976 print/ISSN 1362–3028 online

DOI: 10.1080/00268970903153683

In this study a double ring (based on 20 T atoms with oxygen atoms linking two single rings to form a double ring) and a hydrogenated fragment of it were chosen as models. Previous *ab initio* calculations on different types of zeolites have used smaller fragments than double rings to model the framework [14,18, 19,21–28]. Different levels of theory are used in this study: RHF (Restricted Hartree Fock), DFT (Density Functional Theory) and MP2 (second-order Møller–Plesset) methods and compared to experimental and MD data. Section 2 is dedicated to the experimental technique. Section 3 deals with the *ab initio* calculating methods and results are discussed in Section 4.

2. Experiment

2.1. *Material*

Silicalite-1, the aluminium-free end number of MFI-type zeolites, was used. It was prepared using tetra-propylammonium bromide as template in a fluoride medium at low temperature (<373 K) by the Institut de Sciences des Matériaux de Mulhouse (France). As synthesized, the zeolite was calcined in air at 873 K for 6 h to ensure that the template was removed and therefore, that the microporous structure was opened up. Nitrogen adsorption performed on the calcined sample characterized a micropore volume of $0.19\,cm^3\,g^{-1}$. Silicalite-1 crystals exhibit plate-like coffin shape morphologies of homogeneous size of around $7 \times 3.5 \times 0.05\,\mu m^3$. Ethylene N35 quality gas was purchased from Air Liquide/Alphagaz Company and used as adsorptive without further purification.

2.2. *Apparatus and procedures*

A home-built infrared cell was used to investigate *in situ* the interaction of ethylene with silicalite-1. This stainless steel cell is operating at room temperature and for pressures ranging from 10^{-5} up to 10^3 hPa. It is composed of two main parts: (i) an optical chamber equipped with two KBr windows and (ii) a heat chamber where the sample can be activated up to 573 K under vacuum (10^{-5} hPa). A linear vertical transfer allows the transport of the sample held in the sample holder from the heat chamber to the optical cell. The cell was mounted inside a BRUKER Equinox 55 Fourier transform infrared spectrometer equipped with a Globar light source, a KBr beam splitter and a DTGS detector. All FTIR absorption spectra were collected at room temperature over the wavenumber range 400–4000 cm^{-1} and were recorded by averaging 100 scans with a resolution of 4 cm^{-1}.

Infrared spectra of the adsorbent (silicalite-1) were performed using both the KBr and self-supporting wafer techniques in order to characterize accurately strong and weak lattice zeolite vibrational bands, respectively. All sample and background (collected without zeolite sample) spectra were recorded at room temperature and pressure.

The infrared spectrum of the gas adsorptive was collected after 218 hPa of ethylene was introduced in the cell previously evacuated under 10^{-5} hPa at room temperature. The pressure value was chosen in order to measure a well-defined, unsaturated spectrum within the wavenumber range 400–4000 cm^{-1}. The infrared spectrum of ethylene was ratioed with a reference spectrum of the empty, evacuated optical cell.

Infrared spectra of zeolite in contact with ethylene were performed in the cell using the powder sample pressed into thin self-supporting wafers. Before adsorption, the zeolite sample held in the sample holder was degassed under vacuum (10^{-5} hPa) at room temperature. Adsorption (and desorption) measurements were carried out by exposing the dehydrated sample to increasing (or decreasing) equilibrium pressures of ethylene from 15 to 10^3 hPa (or inversely), at room temperature. The amounts of ethylene adsorbed at a given pressure, at the equilibrium, were determined from the sorption isotherm obtained by thermogravimetry. All spectra of the zeolite in equilibrium with gaseous ethylene at a given pressure were ratioed to background spectra of the cell without sample at the same pressure. The schematic diagram of the experimental set-up is shown in the Figure 1.

3. Computational procedures

All *ab initio* calculations were performed using the Gaussian03 package [31] on a Linux system. We performed three different types of calculations.

- The RHF method with a split-valence 3-21G** basis set, that includes d- and p-polarization functions, was applied to a $Si_{20}O_{50}$ cluster of silicalite. This method has been shown to produce good results for silicate structures [32]. The compromise between the reliability of the results and the computational cost is optimized with this basis set. It is important to notice that quantum chemical calculations at this level of theory overestimate the strength of the chemical bonds. Therefore, a scaling factor is commonly applied to correct the calculated vibrational harmonic wavenumbers [33]. This method was successfully applied in the

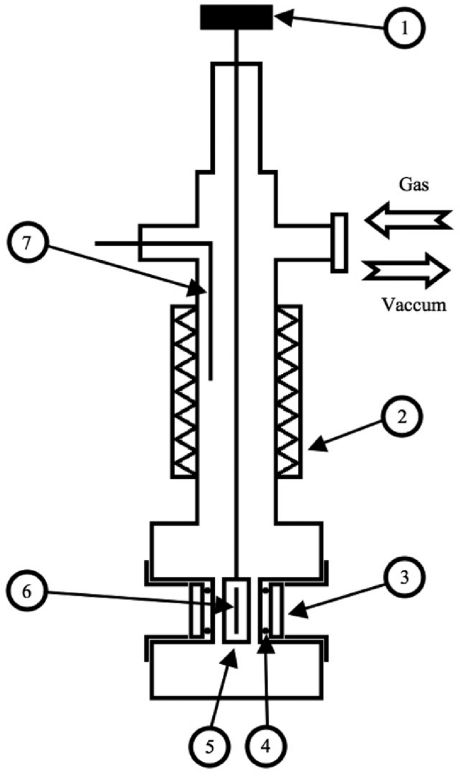

Figure 1. Schematic diagram of the experimental set-up: 1 – sample handler; 2 – oven; 3 – KBr window; 4 – indium o-ring; 5 – sample holder; 6 – sample; 7 – thermocouple.

development of the *ab initio* force field for aluminosilicate structures [20]. In our study we consider a $Si_{20}O_{50}$ cluster consisting in two $Si_{10}O_{20}$ rings linked by oxygen atoms. The geometry of the $Si_{20}O_{50}$ structure was fully optimized in the C_1 point group without any constraint. This is a simplified representation of a portion of a straight or sinusoidal channel of silicalite-1. The normal modes of the $Si_{20}O_{50}$ cluster were obtained from vibrational harmonic analysis (anharmonicity correction is negligible for these atoms). This structure was used to simulate the adsorption of ethylene within the zeolite framework.

- In the case of ethylene interaction with silicalite-1, adsorption is mainly due to van der Waals dispersion interactions. The use of post-Hartree–Fock levels of theory that account for electron correlation leads to more accurate *ab initio* calculations. The choice of the basis sets is also important. Møller–Plesset perturbation theory (MP2–MP4) and coupled-cluster methods with all single and double excitations followed by a perturbative treatment of triple excitations (CCSD(T)) are known to be appropriate for studying van der Waals complexes and molecular systems. But it should be noticed that these methods require significant computational resources for large systems. They are presently intractable for the double ring system. Therefore, the second-order Møller–Plesset perturbation theory MP2 and a more extended split-valence 6-31++G(2d) basis set with diffusion functions on heavy and hydrogen atoms and polarization functions on heavy atoms was applied to only a small part of the $Si_{20}O_{50}$ model, namely, $Si_4O_{12}H_8$ (hydrogen atoms are added to saturate the dangling bonds).
- Density Functional Theory (DFT) methods with a hybrid functional in which the exchange energy is combined with the exact energy from Hartree–Fock theory, provide a reasonable alternative to *ab initio* methods in predicting geometries, frequencies and energies of van der Waals systems. For zeolites, DFT methods produce ground state interaction energies that are often correct. The following DFT methods have been used in our study for the $Si_4O_{12}H_8$ fragment: B3LYP/6-31++G(2d), MPW1PW91/6-31++G(2d), PBE1PBE/6-31++G(2d) with three, one and without any parameters ('*ab initio*' functional), that define the hybrid functional, respectively. One of the Generalized Gradient Approximation methods, where the energy functional depends not only on the electron density but also on its gradient, namely TPSS, also has been used. The optimization of the $Si_4O_{12}H_8$ structure has been performed at these levels of theory. The potential energy as a function of the distance R between this fragment and the ethylene molecule was also examined and the results were compared with calculations performed at the MP2/6-31++G(2d) level of theory.

Ab initio calculations were also performed for the ethylene molecule alone. The harmonic and

anharmonic wavenumbers, overtones and combination bands were calculated by RHF/3-21G**, RHF/6-31++G(2d) and MP2/6-31++G(2d) methods.

The relative intensities of vibrational bands calculated at harmonic level using the Gaussian03 package have been applied for all simulated spectra presented below.

4. Results and discussion

Geometry optimization and frequency calculations were performed for the $Si_{20}O_{50}$ and $Si_4O_{12}H_8$ models. The comparison between frequency analysis based on *ab initio* calculations and experimental infrared spectroscopy allows one to test the validity of the different quantum models and approaches. This is a starting point of a more general investigation concerning the physisorption of a non-polar molecule on a microporous solid.

4.1. *Silicalite-1 framework modelling*

The structure of silicalite-1 is based on two interlinked channel systems formed by ten oxygen rings with sinusoidal channels (free circular cross-section diameter of 0.54 nm) running in the (010) plane and straight channels (free elliptic cross-section of $0.575 \times 0.515\,nm^2$) running in the [010] direction [10,34]. The minimal and maximal distances between two opposite oxygen atoms of the ten-membered rings are ranging from 0.7985 to 0.8406 nm for straight channels and from 0.8061 to 0.8308 nm for sinusoidal channels [10,34]. The two different channels are perpendicular to each other and generate intersection areas, which have a diameter of around 0.9 nm. In the orthorhombic framework geometry (Pnma) of silicalite-1 [10,34], each silicon atom is surrounded by four oxygen atoms in a tetrahedral conformation; the Si–O bond lengths are on average of about 0.1587 nm and the Si–O–Si and O–Si–O bending angles range from 145.7° to 177.7° and from 107.1° to 111.5°, respectively. In the present study, a double ring model with 20 Si atoms and 50 O atoms (20T) is first chosen to represent a portion of a straight or sinusoidal channel of silicalite-1 (Figure 2).

The geometry optimization has been performed using the RHF/3-21G** level of theory. The structure optimization of the silicalite model was done without any constraints (C_1 symmetry) and for the equilibrium geometry (S_e), i.e. at the minimum potential energy surface, without vibrational average structure (S_z). The thermal vibration of the atoms might give a deviation from the equilibrium (S_e) structure. The calculated

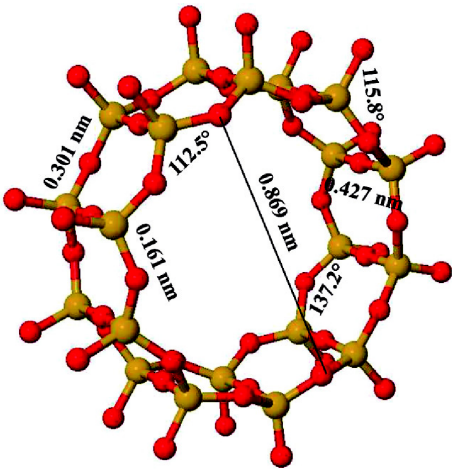

Figure 2. RHF/3-21G** optimized geometry of the $Si_{20}O_{50}$ double ring cluster representative of a portion of a straight or sinusoidal channel of silicalite-1 (red: oxygen atoms; yellow: silicon atoms).

R(Si–O) bond lengths are ranged between 0.161 and 0.162 nm: these values are close to the experimental average Si–O bond length [10,34]. The calculated O–Si–O bending angles are 112.5° and 115.8° and are slightly higher than the ones observed by van Koningsveld *et al.* [10,34]. The calculated Si–O–Si bending angles are 137.2° (angle within the ten-membered rings) and 174.0° (angle between the two ten-membered rings): these values are also not so far different from the ones given in [10,34]. The distances between two opposite oxygen atoms of the ten-membered rings equal 0.869 nm. This value is a little higher than the experimental value given in [10,34]. The distance between neighbour Si atoms of a single ring is 0.301 nm, which is close to published values [10,34]. It is the same for the distance between two opposite oxygen atoms of the double ring that is 0.427 nm. The differences may be ascribed to the optimization method for the structure of the silicalite model. As a remark, the DFT method was not used on the $Si_{20}O_{50}$ cluster because of a convergence problem.

4.2. *IR spectra of the unloaded MFI zeolite*

Vibrations of the zeolite framework give rise to characteristic bands in the mid and far infrared regions. The infrared spectrum of silicalite-1 obtained

from self-supporting and KBr pellet techniques exhibited fundamental bands assigned, according to the classification of Flanigen *et al.* [35], to: (i) the stretching vibrational bands ν_{as}(O–Si–O), ν_{as}(Si–O–Si), ν_s(Si–O–Si) and the bending vibrational band δ(O–Si–O) located at 1240, 1089, 806 and 442 cm^{-1}, respectively, (ii) two overtones of fundamental bands located at 2023 and 1892 cm^{-1}, and (iii) a system of complex bands located at 686, 629, 588, 569 and 548 cm^{-1}.

Figure 3 shows the experimental infrared spectrum of silicalite-1 in comparison with the simulated spectrum of the $Si_{20}O_{50}$ zeolite model based on the *ab initio* calculations. The calculated wavenumbers give the position of six vibrational band centres. The first three band centres located at 1129, 839 and 391 cm^{-1} correspond to ν_{as}(Si–O–Si), ν_s(Si–O–Si) and δ(O–Si–O), respectively. The three others located at 710, 654 and 563 cm^{-1} correspond to vibrations of the ten-membered double ring of the framework structure. The first two bands are of very weak intensity. Normal mode vibrational analysis performed in the harmonic approximation gives only the positions of fundamental wavenumbers. Overtones cannot be obtained at this level of theory. The ν_{as}(O–Si–O) fundamental asymmetrical stretching vibrational band is nevertheless not reproduced by this model, which may be owing to the fact that it belongs to another part of the zeolite framework and it will be interesting to check it using a more high level of theory. However, additional bands, in particular one located at 1017 cm^{-1}, of rather low intensities in comparison with those of the four strongest vibrational bands located at 1129, 839, 563 and 391 cm^{-1} (Table 1), are observed for the $Si_{20}O_{50}$ cluster. The simulated spectrum is in rather good agreement, with respect to the vibrational band positions, with the experimental spectrum (Figure 3). Nevertheless, it shows: (i) a blue-shift by 33 and 40 cm^{-1} of the ν_s(Si–O–Si) symmetric and ν_{as}(Si–O–Si) asymmetric stretching vibrational bands, respectively, and (ii) a red-shift by 51 cm^{-1} of the δ(O–Si–O) bending vibrational band (Table 1). Such a change in position of vibrational bands was also observed from MD simulation calculations [8] (Table 1). However, although calculations may be improved to get better absolute results, what is important to consider is the qualitative spectrum differences between the unloaded zeolite and the zeolite containing an amount of adsorbed ethylene. We assume that the shifts do not qualitatively modify the overall evolution of the system.

From these results, we estimated that the $Si_{20}O_{50}$ double ring model can be used to reproduce qualitatively the main vibrational band positions of silicalite-1.

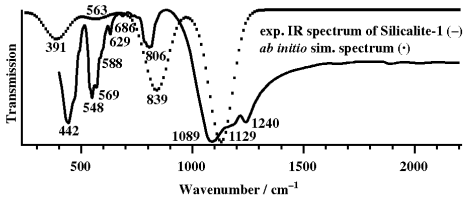

Figure 3. Experimental infrared spectrum of silicalite-1 (KBr-supported sample wafer) recorded under ambient conditions (continuous curve). Comparison with the infrared spectrum of the $Si_{20}O_{50}$ cluster calculated at the RHF/3-21G** level of theory (dotted lines).

4.3. *Infrared spectra of ethylene molecule*

The theoretical study of the infrared spectrum of an isolated ethylene molecule was carried out using different *ab initio* methods as described in Section 3. A large number of theoretical and experimental studies including high quality *ab initio* calculations have been already performed on the subject [36–43]. All known vibrational energies in C_2H_4 (X^1A_g) were reported in [43]. These data were deduced from high resolution investigations including the rotational structure. Our objective is to explain the experimental low resolution infrared spectrum of the ethylene molecule when it is

Table 1. Positions of silicalite vibration bands in cm^{-1}: experimental (Exp.) measurements and comparison with Molecular Dynamics (MD) and Restricted Hartee-Fock (RHF/3-21G**) calculations (Calc.) with scaling factor.

Vibr. type[a]	Overtones bands	ν_{as}(O–Si–O)	ν_{as}(Si–O–Si)	δ(O–Si–O)/(Si–O)$_{edge}$	ν_s(Si–O–Si)	Complex bands	δ(O–Si–O)
Exp. (this work)	2023 1892	1240	1089	–	806	686 629 588 569 548	442
Calc. (RHF/3-21G**)			1129	1017^{weak}	839	710 654 563	391
Calc. (MD)		1203	1203	–	815	582	499

[a]According to the classification of Flanigen [35].

Table 2. Harmonic (ω_i) and anharmonic (ν_i) wavenumbers in cm^{-1} and calculated related intensities I_i in $km\,mol^{-1}$ (in parentheses) cof the ethylene molecule: RHF/6-31++G(2d) and Møller–Plesset (MP2/6-31++G(2d)) calculations (Calc.) and comparison with experimental (Exp.) measurements.

		RHF/6-31++G(2d)	MP2/6-31++G(2d)	Exp.
Mode	Symmetry	ω_i (I_i)/ν_i	ω_i (I_i)/ν_i	ω_i [37]/ω_i [38]/ν_i [43]
1	A_g symm. CH stretch	3277 (0)/3160	3156 (0)/3024	3153/3156/3022
2	A_g CC stretch	1821 (0)/1792	1678 (0)/1617	1655/1656/1625
3	A_g symm. HCH bend	1480 (0)/1456	1390 (0)/1362	1370/1372/1344
4	A_u H_2C-CH_2 twist	1136/(0) 1113	1065 (0)/1042	1044/1045/1026
5	B_{3g} CH trans. stretch	3332 (0)/3213	3230 (0)/3094	3232/3207/3083
6	B_{3g} HCH anti. wag.	1342 (0)/1320	1261 (0)/1236	1245/1249/1222
7	B_{3u} sym. HCH bend out of plane	1072 (123)/1055	985 (118)/962	969/968/949
8	B_{2g} anti. HCH bend out of plane	1077 (0)/1056	945 (0)/938	959/960/940
9	B_{2u} *cis* CH stretch	3362 (25)/3234	3257 (10)/3118	3234/3239/3105
10	B_{2u} sym. HCH in plane	889 (0)/888	844 (1)/839	843/844/826
11	B_{1u} anti. CH stretch	3254 (19)/3126	3139 (7)/2926	3147/3130/2989
12	B_{1u} anti. HCH bend in plane	1593 (9)/1559	1484 (10)/1448	1473/1472/1443

Table 3. Position of ($\nu_i+\nu_j$) combination and $2\nu_i$ overtones bands in cm^{-1} for the ethylene molecule: Møller–Plesset (MP2/6-31++G(2d)) calculations (Calc.) and comparison with experimental (Exp.) measurements.

Band	MP2/6−31++G(2d)	Exp. [43]	Band	MP2/6−31++G(2d)	Exp. [43]
$\nu_8+\nu_{10}$	1776	1767	$2\nu_{10}$	1702	1662
$\nu_7+\nu_{10}$	1806	1781	$2\nu_8$	1893	1881
$\nu_4+\nu_{10}$	1882	1854	$2\nu_7$	1923	1900
$\nu_7+\nu_8$	1897	1889	$2\nu_4$	2082	2046
$\nu_4+\nu_8$	1976	1958	$2\nu_3$	2721	2685
$\nu_4+\nu_7$	1996	1965	$2\nu_{12}$	2891	2877
$\nu_6+\nu_{10}$	2067	2048	$2\nu_2$	3231	3239
$\nu_3+\nu_{10}$	2202	2173	$2\nu_{11}$	5826	5939
$\nu_3+\nu_7$	2321	2292	$2\nu_9$	6205	6197
$\nu_2+\nu_{10}$	2418	2439	$\nu_5+\nu_6$	4329	4310
$\nu_2+\nu_7$	2572	2571	$\nu_6+\nu_9$	4347	4322
$\nu_2+\nu_3$	2970	2962	$\nu_3+\nu_{11}$	4282	4329
$\nu_2+\nu_{12}$	3146	3079	$\nu_{11}+\nu_{12}$	4278	4408
$\nu_{10}+\nu_{11}$	3761	3809	$\nu_3+\nu_9$	4472	4440
$\nu_1+\nu_{10}$	3860	3842	$\nu_1+\nu_{12}$	4470	4460
$\nu_8+\nu_{11}$	3856	3921	$\nu_5+\nu_{12}$	4531	4515
$\nu_9+\nu_{10}$	3954	3928	$\nu_2+\nu_{11}$	4451	4597
$\nu_7+\nu_{11}$	3883	3931	$\nu_1+\nu_2$	4622	4632
$\nu_1+\nu_8$	3955	3954	$\nu_2+\nu_9$	4733	4730
$\nu_7+\nu_9$	4071	4047	$\nu_1+\nu_{11}$	5898	5995
$\nu_6+\nu_{11}$	4156	4207	$\nu_5+\nu_9$	6150	6151

adsorbed in the micropores and on the external surface of silicalite-1. Therefore, the fundamental, combination and overtone vibrational band wavenumbers were first calculated at the MP2/6-31++G(2d) level of theory. The effect of anharmonicity was taken into account by the method suggested by Barone that is implemented in the Gaussian03 program [6]. Computed harmonic ω and anharmonic ν wavenumbers are given in Table 2 together with the experimental data obtained by Duncan *et al.* [37,38] and Georges *et al.* [43]. It should be noticed that only ν_7, ν_9, ν_{10}, ν_{11} and ν_{12} vibrational modes are IR active for the ethylene molecule. The averaged absolute deviation (AAD) between the calculated ω_{calc} harmonic wavenumbers and experimental ones [37,38] is about $14\,cm^{-1}$ and averaged deviation (AD) is $+11\,cm^{-1}$ (Table 2). The AAD between the calculated and experimental [43] anharmonic wavenumbers is found to be about $15\,cm^{-1}$ and the AD is about $+3\,cm^{-1}$. These results show an overestimation of both ω and ν by the MP2 method for most of the vibrational modes (Table 2). The deviations with respect to the

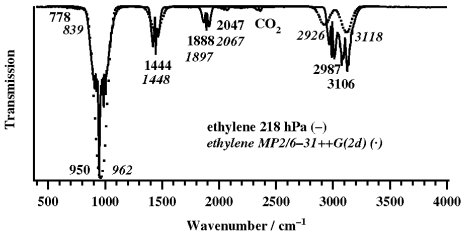

Figure 4. Experimental infrared spectrum of ethylene recorded under a pressure of 218 hPa at room temperature (continuous curve). Comparison with the spectrum of ethylene calculated at MP2/6-31++G(2d) level of theory.

experimental values do not exceed 23 cm^{-1} except for the ν_{11} vibrational mode that is largely red-shifted by 63 cm^{-1} (Table 2). Therefore, we can conclude that the calculated values are in good agreement with the experimental ones. However, anharmonic correction for ν_{11} is rather overestimated at this level of theory that results in a quite big red-shift with respect to the experimental value (Table 2). The calculated and experimental [43] values of the combination and overtone wavenumbers are reported in Table 3. The AAD is about 34 cm^{-1} and the AD is -4 cm^{-1}. However, most of vibrational band positions are overestimated. As far as the ethylene molecule is concerned, we note that this level of theory gives the position of vibrational bands with an accuracy that is not adapted to high resolution spectroscopy, but it can provide correct shifts between isolated and adsorbed molecules.

The infrared spectrum of ethylene simulated by the MP2 method is shown in Figure 4 along with the experimental spectrum obtained under a pressure of 218 hPa at room temperature. The assignment and location of ethylene vibrational bands are reported in Table 4, in comparison with previous molecular dynamics results [8]. Both quantum and classical calculations show deviations from experimental data, depending on the vibrational modes. In general the values of the calculated wavenumbers are slightly higher (blue-shifts) than the experimental ones. However, we considered that the simulated spectrum is in rather good agreement with the experimental one. Concerning MD simulation, it is worth noticing that the method is not suited to obtain combination bands.

4.4. *Infrared spectra of ethylene adsorbed in silicalite*

4.4.1. *For the $Si_{20}O_{50}/C_2H_4$ system*

In a first approach, we modelled the effect of the adsorption of one ethylene molecule on the vibrational

Table 4. Assignment and position of fundamental and combination vibration bands in cm^{-1} for ethylene: Møller–Plesset (MP2/6-31++G(2d)) and Molecular Dynamics (MD) calculations (Calc.) comparison with experimental (Exp.) data for the gas phase at 218 hPa.

Vibration modes	MP2/6-31++G(2d)	Exp. (this work)	MD [8]
ν_7	962	950	981
$\nu_7+\nu_8$	1897	1888	–
$\nu_6+\nu_{10}$	2067	2047	–
ν_9	3118	3106	3129
ν_{10}	839	778 (*P*-branch)	–
ν_{11}	2926	2987	3020
ν_{12}	1448	1444	1467

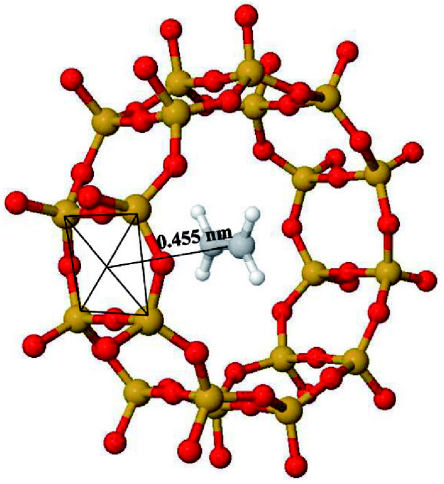

Figure 5. RHF/3-21G** optimized geometry of the $Si_{20}O_{50}/C_2H_4$ structure (red: oxygen atoms; yellow: silicon atoms; grey: carbon atoms; pale grey: hydrogen atoms).

bands of the $Si_{20}O_{50}$ zeolite fragment using the *ab initio* RHF/3-21G** method. The optimization of the $Si_{20}O_{50}/C_2H_4$ structure based on minimization of energy at 0 K, was carried out for a relaxed ethylene molecule and a rigid zeolite framework. The optimized configuration is shown in Figure 5. In this case the molecule is localized at the centre of the channel and the CC bond axis is oriented along the channel axis. As represented in Figure 5, the distance between the mass centre of the molecule and the surface of the double ring amounts to 0.455 nm. This result is

in agreement with molecular dynamics simulation calculations [8].

The calculated wavenumbers and intensities of the $Si_{20}O_{50}$ zeolite cluster and the $Si_{20}O_{50}/C_2H_4$ system were introduced in the XTDS software program [44] to further simulate the corresponding vibrational spectra at room temperature. The comparison of the simulated spectra shows that the adsorption of one molecule in the double ring induces a red-shift of about 1 or $2\,cm^{-1}$ and a very small decrease in intensity of the zeolite vibrational bands, over the wavenumber range 250–1500 cm^{-1} (Figure 6). Such an evolution is in agreement with the experimental results in so far as a red-shift of the fundamental zeolite vibrational bands is also observed during micropore filling (Figure 7). It can be noticed that the vibrational bands of silicalite-1 at zero loading are slightly shifted compared to Figure 3 because of different constraints for the two sample preparations.

Additional information about the vibrational bands of the ethylene adsorbed in silicalite-1 were obtained from the simulation. The adsorption induces a red-shift from 3 to $10\,cm^{-1}$ for the stretching and rocking vibrational bands and a blue-shift from 2 to $17\,cm^{-1}$ for the bending vibrational bands (except for the ω_3 and ω_6 vibrational bands) (Table 5). The interaction of the ethylene molecule with the $Si_{20}O_{50}$ cluster induces the splitting of the cluster vibrational band located at $1017\,cm^{-1}$ (Table 1) into two components at 1011 and $1016\,cm^{-1}$. The contribution at $1011\,cm^{-1}$ is due to a collective mode of the cluster

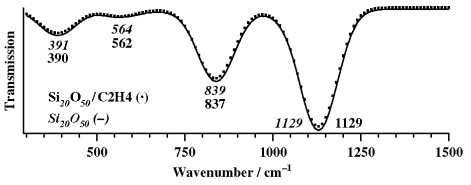

Figure 6. Infrared spectra of the $Si_{20}O_{50}$ cluster free of adsorbate (solid curve) and with one adsorbed ethylene molecule (dotted curve), calculated at the RHF/3-21G** level of theory.

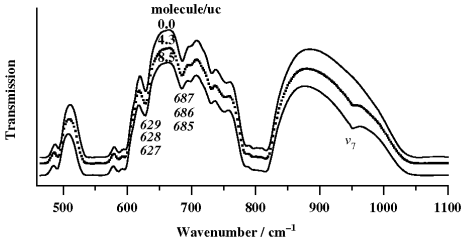

Figure 7. Dependence of the experimental infrared spectrum of silicalite-1 (self-supported sample wafer) on ethylene loading: (from bottom to top) 0.0, 4.3 and 8.5 molecules/uc, at room temperature. In italic also reported the position of two weak vibrational bands of silicalite-1 and their dependence on loading (values from top to bottom).

Table 5. Harmonic (ω_{ads}) wavenumbers in cm^{-1}, harmonic ($\Delta\omega = \omega_{ads} - \omega_{gas}$) wavenumber shifts in cm^{-1} and related intensities in $km\,mol^{-1}$ (in parentheses) for the ethylene molecule adsorbed (ads) in the $Si_{20}O_{50}$ cluster and the ethylene molecule alone (gas), calculated at the RHF level of theory using the 3-21G** basis set (with scaling factor), and for the ethylene molecule adsorbed on the $Si_4O_{12}H_8$ fragment and the molecule ethylene alone (gas), calculated at the MP2 level of theory using 6-31++G(2d) basis set.

		RHF/3-21G** $Si_{20}O_{50}$			MP2/6-31G++G(2d) $Si_4O_{12}H_8$		
Mode	Sym.	ω_{ads}	$\Delta\omega_{calc}/\Delta\nu_{exp}$	I_{gas} (I_{ads})	ω_{ads}	$\Delta\omega_{calc}/\Delta\nu_{exp}$	I_{gas} (I_{ads})
1	A_g	3075	−8	0(0)	3156	0	0(0)
2	A_g	1650	−10	0(0)	1673	−5	0(0)
3	A_g	1360	−6	0(0)	1386	−4	0(0)
4	A_u	1056	2	0(0)	1066	−1	0(136)
5	B_{3g}	3123	−10	0(2)	3231	0.5	0(0)
6	B_{3g}	1228	−7	0(0)	1256	−5	0(0)
7	B_{3u}	1022	17	116(81)	984	−1	118(46)
8	B_{2g}	1042	12	0(0)	941	−4	0(129)
9	B_{2u}	3150	−10/*−12*	29(29)	3258	1/*−12*	10(8)
10	B_{2u}	836	−3	1(779)	838	−6	1(4)
11	B_{1u}	3056	−8/*−11*	13(2)	3139	0/*−11*	7(6)
12	B_{1u}	1466	4/*−8*	10(9)	1478	−6/*−8*	10(10)

and ω_7 ethylene vibrations. It is interesting to note that the calculated red-shifts for the ν_9 and ν_{11} vibrational bands (we assume that $\Delta\omega$ is the same as $\Delta\nu$ in the first approximation) are in good agreement with the ones experimentally observed (Figure 8). The position of the ν_9 and ν_{11} vibrational bands does not change with loading up to 8.5 molecules per unit cell (uc). As a remark, the $Si_{20}O_{50}/C_2H_4$ system can be compared with silicalite-1 containing about eight molecules per unit cell. For the ν_{12} in plane bending vibrational band the simulated band is blue-shifted by $4\,cm^{-1}$ whereas the experimental one is red-shifted by $8\,cm^{-1}$ (Figure 9). Such a discrepancy may be corrected by using methods including electron correlation. The ν_7 vibrational band of the adsorbed phase is also experimentally observed during micropore filling. However, the evolution of this band is not analysed in the present study because it appears as a shoulder of the strongest vibrational bands of silicalite located at 1089 and $1240\,cm^{-1}$ (Figure 7). Indeed, these two bands cannot be observed because of detector saturation.

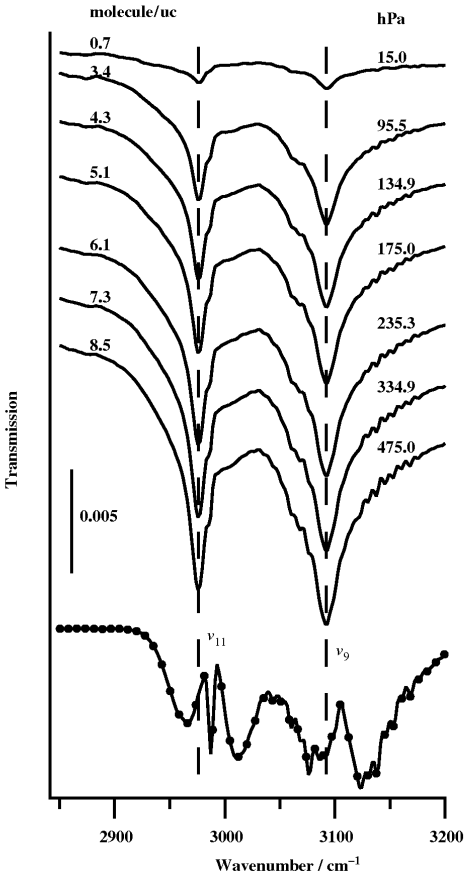

Figure 8. Dependence of the experimental of the ν_{11} and ν_9 vibrational bands of ethylene adsorbed on silicalite-1 on loading: (from top to bottom) 0.7, 3.4, 4.3, 5.1, 6.1, 7.3 and 8.5 molecules/uc (left), the corresponding equilibrium pressure in hPa (right). Comparison with the experimental gas ethylene spectrum (dotted curve).

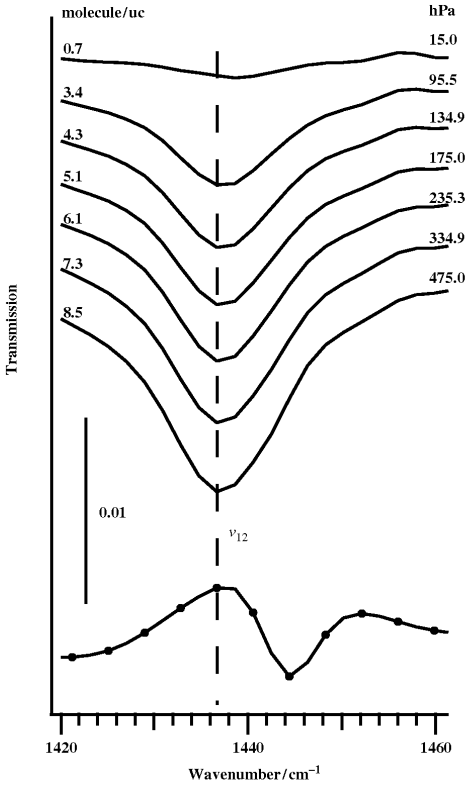

Figure 9. Dependence of the experimental of the ν_{12} vibrational band of ethylene adsorbed on silicalite-1 on loading: (from top to bottom) 0.7, 3.4, 4.3, 5.1, 6.1, 7.3 and 8.5 molecules/uc (left), the corresponding equilibrium pressure in hPa (right). Comparison with the experimental gas ethylene spectrum (dotted curve).

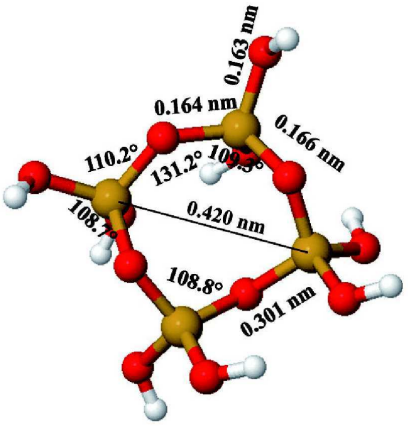

Figure 10. MP2/6-31++G(2d) optimized geometry of the $Si_4O_{12}H_8$ fragment (red: oxygen atoms; yellow: silicon atoms; pale grey: hydrogen atoms).

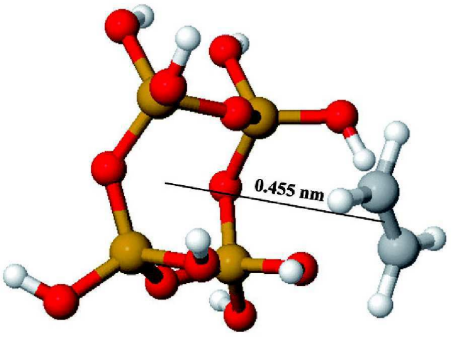

Figure 11. Geometry of the $Si_4O_{12}H_8/C_2H_4$ structure at the energy minimum calculated at the MP2/6-31++G(2d) level of theory (red: oxygen atoms; yellow: silicon atoms; grey: carbon atoms; pale grey: hydrogen atoms).

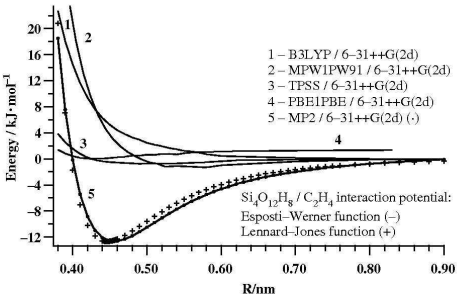

Figure 12. Interaction potential between ethylene molecule and $Si_4O_{12}H_8$ fragment as a function of the distance between the geometric centres. Comparison between different calculated models.

4.4.2. *For the $Si_4O_{12}H_8/C_2H_4$ system*

In a second approach, MP2 calculations were performed in order to include the effects of electron correlations. The MP2 method is known to well describe van der Waals dispersion interactions but calculations are in practice too expensive to be applied to large systems. Therefore, the $Si_4O_{12}H_8$ fragment (Figure 10) was chosen to calculate the interaction potential energy of the fragment with one ethylene molecule. The $Si_4O_{12}H_8$ and the ethylene molecule structures were separately optimized at the MP2/6-31++G(2d) level of theory. The optimized structure is shown in Figure 11, the obtained values of the bond lengths and angles are close to those of the $Si_{20}O_{50}$ cluster. As we observed for the $Si_{20}O_{50}$ cluster, the carbon–carbon double bond of the ethylene molecule is parallel to the plane built by the four silicon atoms of the $Si_4O_{12}H_8$ fragment. The curve of the interaction potential energy versus the distance R between the fragment and the ethylene molecule shows a pronounced energy minimum ($D_e = 12.56\,kJ\,mol^{-1}$) at $R = 0.455\,nm$ (Figure 12). R is defined as the distance between the middle of the carbon–carbon double bond of ethylene and the middle of the plane built by the four silicon atoms. It may be surprising that its value is the same as the one calculated at the RHF/3-21G** level of theory for the $Si_{20}O_{50}$ cluster. However, it is not worth putting emphasis on this result, which is a coincidence. The distance dependence of the interaction potential energy can be well fitted by the one-dimensional Esposti–Werner function or the Lennard-Jones potential (see Appendix 1) as shown in Figure 12. This is in agreement with the classical MD simulation results, where no electrostatic potential was used because the ethylene molecule is a non-polar molecule and the Lennard-Jones type of potential was applied, which is well suited to simulate this kind of system [8]. On the other hand, the energy curves calculated by the DFT methods do not show any potential minimum and as a consequence, these methods are not suited to investigate physisorption of non-polar molecules.

Wavenumber calculations and analyses were then carried out only for the $Si_4O_{12}H_8/C_2H_4$ system at the MP2/6-31++G(2d) level of theory. Calculated data are

Table 6. Harmonic (ω_i) wavenumbers in cm^{-1} and related intensities I_i in $km\,mol^{-1}$ (in parentheses) corresponding to T–O stretching and bending for the $Si_4O_{12}H_8$ fragment with and without ethylene molecule, calculated at the MP2 level of theory using the 6-31++G(2d) basis set.

Mode	ω ($Si_4O_{12}H_8$)	ω ($Si_4O_{12}H_8 + C_2H_4$)
O–Si–O(asym.)	1092 (1150)	1089 (1088)
O–Si–O(sym.)	1051 (219)	1051 (212)
O–Si–O(asym.)	1044 (161)	1042 (103)
O–Si–O(asym.)	1018 (319)	1017 (314)
O–Si–O(asym.)	928 (157)	926 (150)
O–Si–O(sym.)	808 (8)	808 (12)
Si–O–Si(sym.)	777 (93)	776 (107)
O–Si–O bend.	389 (112)	389 (102)
O–Si–O bend.	400 (87)	396 (72)
O–Si–O bend.	415 (87)	413 (109)
O–Si–O bend.	424 (44)	424 (41)
O–Si–O bend.	437 (58)	436 (66)
Ring	667 (121)	667 (119)
Ring	662 (91)	662 (89)
Ring	590 (18)	589 (16)
Ring	508 (94)	499 (73)
Ring	472 (48)	472 (44)

given in Table 5. The adsorption process induces modifications of some ethylene molecule vibrational bands: (i) the intensity of the ν_7 vibrational band is two times decreased, (ii) the appearance of ν_4 and ν_8 vibrational bands which are not infrared active in the gas phase, (iii) the ν_{10} and ν_{12} vibrational bands are red-shifted by $6\,cm^{-1}$ whereas the other vibrational bands are slightly or not red-shifted. It is interesting to note that the red-shift calculated for ν_{12} vibrational band is very close to the one experimentally observed ($8\,cm^{-1}$) and to the value calculated by MD simulation ($4\,cm^{-1}$). Concerning the appearance of ν_4 and ν_8 vibrational bands, we can notice that these bands are not experimentally observed. This result indicates that the $Si_4O_{12}H_8$ fragment, which is part of the $Si_{20}O_{50}$ cluster, is not well suited to reproduce all interactions that occur during the adsorption of ethylene in silicalite. On the other hand, the ν_9 and ν_{11} stretching modes were almost not changed, meaning that chemical bonds are weakly perturbed by the presence of the $Si_4O_{12}H_8$ fragment. Concerning the effect of ethylene adsorption on the vibrational bands of the $Si_4O_{12}H_8$ structure, the wavenumbers are also shifted to lower values and the intensities are slightly modified in agreement with experimental results (Table 6).

5. Conclusion

The aim of this study was to investigate by infrared spectroscopy the interaction of ethylene with a hydrophobic zeolite, silicalite-1. This study was carried out using quantum calculations at different levels of theory (RHF, MP2, DFT/B3LYP-PBE1PBE-MPW1PW91) conjointly to infrared experiments at room temperature. Calculations were performed considering a part of a straight or sinusoidal channel of silicalite-1, either a $Si_{20}O_{50}$ cluster or a hydrogenated fragment of it, $Si_4O_{12}H_8$. Particularly, we focused on the evolution of the infrared spectra of: (i) ethylene from the gaseous phase to the adsorbed phase and (ii) the adsorbent from the unloaded to a loaded state. The first step of this work was to choose the appropriate *ab initio* method that accounts for the infrared spectrum of ethylene and that of the cluster free of adsorbate. For the $Si_{20}O_{50}$ cluster, calculations were carried out using only the RHF/3-21G** level of theory. In this case, the calculated infrared spectrum is in a rather good agreement, with respect to the position of vibrational bands, with the experimental infrared spectrum of the unloaded zeolite. Considering the ethylene molecule, *ab initio* calculations were performed by using different methods. The best agreement between the calculated and experimental spectra is obtained with the MP2 method. The second step of this work was to calculate the infrared spectrum of the zeolite in interaction with one ethylene molecule in order to account for the experimental modifications of the vibrational bands of both the adsorbent and the adsorbate. In the case of the $Si_{20}O_{50}$ cluster (RHF/3-21G**), the adsorption induces a red-shift by 8 and $10\,cm^{-1}$ for the ν_{11} and ν_9 ethylene vibrational bands, respectively. These red-shifts are due to a weakening of the CH bonds and are close to the experimental values that are 12 and $11\,cm^{-1}$, respectively. However, for the ν_{12} in plane bending vibrational mode, the simulated band is blue-shifted whereas the experimental one is red-shifted. By using the MP2/6-31++G(2d) method for the $Si_4O_{12}H_8$ fragment this discrepancy is corrected to a red-shift. However, with this reduced cluster, the ν_{11} and ν_9 stretching modes of the ethylene molecule are not modified by the adsorption process. These results show the importance of the choice of both the zeolite model and the level of theory on the spectroscopic response. Concerning the choice of the level of theory, it should be noticed that the potential energy curve calculated by the MP2 method, contrary to RHF and DFT methods, shows a pronounced minimum potential due to van der Waals interactions. As a consequence, this method is suited to study physisorption of ethylene which is a non-polar molecule. At this step of the study, the quantum calculations give new insight into the understanding of the spectroscopic response due to adsorption phenomena. However, to be more realistic, additional calculations should be

done by exploring in the future the following new ideas.

- the MP2 level of theory should be used for (i) the $Si_{20}O_{50}$ cluster and (ii) a cluster representative of the intersections of straight and sinusoidal channels. This last point is important since the structure of intersections is different from that of the channels. Moreover, it contributes to one third of all adsorption sites.
- experimentally, silicalite-1 can adsorb up to around 11 molecules per unit cell. Therefore, at high loading, intermolecular interactions between ethylene molecules play a significant role. This key point means that we should simulate the adsorption of two or more ethylene molecules.
- from MD simulations we have shown that the ethylene molecules [8] are not trapped on specific sites at 298 K. They are very mobile: the self-diffusion coefficient is of the same order of magnitude as in the liquid. Moreover, they exhibit a wide distribution of orientations, however, narrower than in the liquid because of the porous texture. As a consequence, *ab initio* calculations should be done on different orientations to account for the adsorption process of ethylene on silicalite-1 at room temperature.

Acknowledgements

We acknowledge C. Adamo and L. Joubert for useful discussion and for the computer equipment support of the Ecole Nationale Supérieure de Chimie de Paris (ENSCP, UMR 7575 – Laboratoire d'Electrochimie, chimie des interfaces et modélisation pour l'énergie). We also thank L. Manceron for constructive discussions (LADIR, Paris). Support from the Région Bourgogne for the computer equipment of the Institut Carnot de Bourgogne is gratefully acknowledged. We also wish to thank the GDR 3152 'SpecMo' and the GDR 2997 'COMOVI' of the CNRS.

References

[1] V. Cottier, J.-P. Bellat, and M.-H. Simonot-Grange, J. Phys. Chem. B **101**, 4798 (1997).
[2] R. Barrer, *Zeolites and Clay Minerals as Sorbents and Molecular Sieves* (Academic Press, London, 1978).
[3] D.W. Breck, *Zeolite Molecular Sieves* (John Wiley & Sons, New York, 1974).
[4] M. Guisnet and J.-P. Gilson, *Zeolites for Cleaner Technologies* (Imperial College Press, London, 2002).
[5] G. Weber, J.-P. Bellat, F. Benoit, C. Paulin, S. Limborg-Noetinger, and M. Thomas, Adsorption **11**, 183 (2005).
[6] V. Barone, J. Chem. Phys. **122**, 014108 (2005).
[7] R.A. van Santen, B. van de Graaf, and B. Smit, in *Introduction to Zeolite Science and Practice*, edited by H. van Bekkum, E.M. Flanigen, P.A. Jacobs, and J.C. Jansen (Elsevier Science, New York, 2001), Vol. 137, p. 419.
[8] V. Bernardet, A. Decrette, J.-M. Simon, O. Bertrand, G. Weber, and J.-P. Bellat, Mol. Phys. **102**, 1859 (2004).
[9] G. Hübner, G. Rauhut, H. Stoll, and E. Roduner, Phys. Chem. Chem. Phys. **4**, 3112 (2002).
[10] H. van Koningsveld, H. van Bekkum, and J.C. Jansen, Acta Cryst. **B43**, 127 (1987).
[11] M. Boronat, C.M. Zicovich-Wilson, A. Corma, and P. Viruela, Phys. Chem. Chem. Phys. **1**, 537 (1999).
[12] E. Kassab and M. Castellá-Ventura, J. Phys. Chem. B **109**, 13716 (2005).
[13] J.T. Fermann, T. Moniz, O. Kiowski, T.J. McIntire, S.M. Auerbach, T. Vreven, and M.J. Frish, J. Chem. Theory. Comput. **1**, 1232 (2005).
[14] J. Limtrakul, T. Nanok, S. Jungsuttiwong, P. Khongpracha, and T.N. Truong, Chem. Phys. Lett. **349**, 161 (2001).
[15] R.A. van Santen, Catal. Today **38**, 377 (1997).
[16] A. Khodakov, S.P. Bates, J. Dwyer, C.M. Windsor, and N.A. Burton, Phys. Chem. Chem. Phys. **1**, 507 (1999).
[17] W. Panjan and J. Limtrakul, J. Mol. Struct. **654**, 35 (2003).
[18] G. Hübner, G. Rauhut, H. Stoll, and E. Roduner, J. Phys. Chem. B **107**, 8568 (2003).
[19] K. Bobuatong and J. Limtrakul, Appl. Catal., A **253**, 49 (2003).
[20] K.S. Smirnov and D. Bougeard, Catal. Today **70**, 243 (2001).
[21] G. Cantele, F. Trani, D. Ninno, M. Cossi, and V. Barone, J. Phys.: Condens. Matter **18**, 2349 (2006).
[22] J.M. Vollmer, E.V. Stefanovich, and T.N. Truong, J. Phys. Chem. B **103**, 9415 (1999).
[23] D. Zhou, N. He, Y. Wang, G. Yang, X. Liu, and X. Bao, J. Mol. Struct. (THEOCHEM) **756**, 39 (2005).
[24] J. Limtrakul, P. Khongpracha, S. Jungsuttiwong, and T.N. Truong, J. Mol. Catal. A: Chem. **153**, 155 (2000).
[25] H. Soscún, O. Castellano, and J. Hernández, J. Phys. Chem. B **108**, 5620 (2004).
[26] I.P. Zaragoza, J.M. Martínez-Magadán, R. Santamaria, D. Dixon, and M. Castro, Int. J. Quantum Chem. **80**, 125 (2000).
[27] J.M. Vollmer and T.N. Truong, J. Phys. Chem. B **104**, 6308 (2000).
[28] R.Z. Khaliullin, A.T. Bell, and V.B. Kazansky, J. Phys. Chem. A **105**, 10454 (2001).
[29] O. Bertrand, G. Weber, S. Maure, V. Bernardet, J.P. Bellat, and C. Paulin, J. Phys. Chem. B **109**, 13312 (2005).

[30] P. Sherwood, A.H. de Vries, S.J. Collins, S.P. Greatbanks, N.A. Burton, M.A. Vincent, and I. H. Hillier, Faraday Discuss. **106**, 79 (1997).
[31] M.J. Frisch, G.W. Trucks, H.B. Schlegel, G.E. Scuseria, M.A. Robb, J.R. Cheeseman, J.A. Montgomery Jr, T. Vreven, K.N. Kudin, J.C. Burant, J.M. Millam, S.S. Iyengar, J. Tomasi, V. Barone, B. Mennucci, M. Cossi, G. Scalmani, N. Rega, G.A. Petersson, H. Nakatsuji, M. Hada, M. Ehara, K. Toyota, R. Fukuda, J. Hasegawa, M. Ishida, T. Nakajima, Y. Honda, O. Kitao, H. Nakai, M. Klene, X. Li, J.E. Knox, H.P. Hratchian, J.B. Cross, V. Bakken, C. Adamo, J. Jaramillo, R. Gomperts, R.E. Stratmann, O. Yazyev, A.J. Austin, R. Cammi, C. Pomelli, J.W. Ochterski, P.Y. Ayala, K. Morokuma, G.A. Voth, P. Salvador, J.J. Dannenberg, V.G. Zakrzewski, S. Dapprich, A.D. Daniels, M.C. Strain, O. Farkas, D.K. Malick, A.D. Rabuck, K. Raghavachari, J.B. Foresman, J.V. Ortiz, Q. Cui, A.G. Baboul, S. Clifford, J. Cioslowski, B.B. Stefanov, G. Liu, A. Liashenko, P. Piskorz, I. Komaromi, R.L. Martin, D.J. Fox, T. Keith, M.A. Al-Laham, C.Y. Peng, A. Nanayakkara, M. Challacombe, P.M.W. Gill, B. Johnson, W. Chen, M.W. Wong, C. Gonzalez, and J.A. Pople, *Gaussian 03, Revision C.02* (Gaussian, Inc., Wallingford, CT, 2004).
[32] L.J. Criscenti, S.L. Brantley, K.T. Mueller, N. Tsomaia, and J.D. Kubicki, Geochim. Cosmochim. Acta **69**, 2205 (2005).
[33] A.P. Scott and L. Radom, J. Phys. Chem. **100**, 16502 (1996).
[34] H. van Koningsveld, Acta Cryst. **B46**, 731 (1990).
[35] E.M. Flanigen, H. Khatami, and H.A. Szymanski, Adv. Chem. Ser. **101**, 201 (1971).
[36] W. Raballand, M. Rotger, V. Boudon, M. Loëte, J. Breidung, and W. Thiel, J. Mol. Struct. **780-781**, 70 (2006).
[37] J.L. Duncan, D.C. McKean, and P.D. Mallinson, J. Mol. Spectrosc. **45**, 221 (1973).
[38] J.L. Duncan and E. Hamilton, J. Mol. Struct. (Theochem) **76**, 65 (1981).
[39] N. Dam, R. Engeln, J. Reuss, A.S. Pine, and A. Fayt, J. Mol. Spectrosc. **139**, 215 (1990).
[40] I. Cauuet, J. Walrand, G. Blanquet, A. Valentin, L. Henry, C. Lambeau, M. de Vleeschouwer, and A. Fayt, J. Mol. Spectrosc. **139**, 191 (1990).
[41] D.V. Lerberghe, I.J. Wright, and J.L. Duncan, J. Mol. Spectrosc. **42**, 251 (1972).
[42] J.M.L. Martin, T.J. Lee, P. Taylor, and J.-P. François, J. Chem. Phys. **103**, 2589 (1995).
[43] R. Georges, M. Bach, and M. Herman, Mol. Phys. **97**, 279 (1999).
[44] C. Wenger, V. Boudon, M. Rotger, M. Sanzharov, and J.-P. Champion, J. Mol. Spectrosc. **251**, 102 (2008).
[45] A.D. Esposti and H.J. Werner, J. Chem. Phys. **93**, 3351 (1990).

Appendix 1. Analytical representation of the $Si_4O_{12}H_8/C_2H_4$ potential

The interaction potential between the ethylene molecule and the $Si_4O_{12}H_8$ fragment is plotted in Figure 12 as a function of R, that is the distance between the mass centres of C_2H_4 and $Si_4O_{12}H_8$. *Ab initio* data were fitted first to an one-dimensional function of the Esposti–Werner type [45]:

$$V(R) = \left[G(R)\exp(-a_1 R - a_2) - T(R)\sum_{i=3}^{8}\left(\frac{C_i}{R^i}\right)\right],$$

where

$$G(R) = \sum_{i=0}^{8}\left(g_i R^i\right)$$

and

$$T(R) = \frac{1}{2}[1 + \tanh(1 + tR)]$$

is a switching function. The parameters a_i, g_i, t, C_i are fitted using the modified Levenberg–Marquardt algorithm from the MIN-PACK set of routines for nonlinear least-squares fitting. The quality of the one-dimensional fit is very good. In our potential the position of minimum is $R_e = 0.455\,\text{nm}$ with a well depth (D_e) of $1049\,\text{cm}^{-1}$ ($12.56\,\text{kJ mol}^{-1}$).

Ab initio points were also fitted to a function of the Lennard-Jones potential with very good agreement:

$$V(R) = 4\epsilon\left[\left(\frac{\sigma}{R}\right)^{12} - \left(\frac{\sigma}{R}\right)^{6}\right],$$

where ϵ and σ are the depth of the potential well and effective interaction diameter (the distance at which the potential is zero), respectively. The fitted parameters are $\sigma = 0.3967\,\text{nm}$ and $\epsilon = 12.7\,\text{kJ mol}^{-1}$ (D_e).

Chapitre 9

Conclusion et perspectives

9.1 Conclusion

J'ai décrit dans ce mémoire mes activités de chercheur aussi bien à Tomsk, avant 2003, successivement à l'Université d'Etat de Tomsk à la faculté de Physique, à l'Institut de Physique de Sibérie, puis à l'Institut d'Optique Atmosphérique, qu'en France depuis cette date, essentiellement à l'Université de Bourgogne (ICB), mais également à l'Université de Lille I (PhLAM) et à l'Université de Marne-la-Vallée (LCT).

Après l'introduction, les chapitres suivants du document peuvent se classer comme suit :

- les chapitres (2) et (3) ont pour rôle de fournir un socle théorique adapté à la compréhension des simulations numériques qui sont faites par la suite ;
- les chapitres (4) et (5) presentent des calculs sur des molécules, qu'il s'agisse de travaux *ab initio* pour la spectroscopie rovibrationnelle de molécules stables ou de recherches sur la détection de molécules organiques dans l'atmosphère ;
- les chapitres (6) et (7) ont trait à des calculs de complexes de l'atmosphère, et à la caractérisation d'un complexe de van der Waals, $CH_4 - N_2$, qui est abondant dans l'atmosphère de Titan ;
- le chapitre (8) contient les résultats de mes recherches sur l'adsorption de la molécule d'éthylène sur la silicalite-1.

Une partie de mon travail a donc été dédiée à l'évaluation par calcul *ab initio* (avec Gaussian) de constantes rovibrationnelles pour des molécules quasi-sphériques. J'ai donné les constantes de distorsion centrifuge et le moment dipolaire de la molécule SO_2F_2 pour valider la théorie tensorielle développée à l'ICB et interpréter le spectre. On peut constater que les calculs *ab initio* peuvent fournir les constantes rovibrationnelles avec une précision satisfaisante pour les besoins de la spectroscopie à haute résolution. Les calculs *ab initio* sont *a priori* une source intéressante de données supplémentaires.

J'ai présenté aussi des résultats de calculs *ab initio* pour le champ de force anharmonique et la structure à l'équilibre de la molécule C_2H_3Br. La structure calculée par moindres carrés des moments d'inertie semi-expérimentaux avec les constantes d'interaction de rotation-vibration déduites de calculs *ab initio* combinées avec les constantes de rotation expérimentales révèle une très bonne précision. Cette stratégie de recalage, dans laquelle le champ de force fourni par le calcul *ab initio* est utilisé pour corriger les constantes de rotation obtenues à partir des données expérimentales s'affirme donc bien comme une méthode intéressante pour calibrer des constantes physiques.

Comme nous avons pu le voir dans ce document, une grande partie de mon activité a consisté à rechercher et à exploiter de nouvelles ouvertures pour la détection de molécules et de complexes en phase gazeuse. Dans ce cadre, les différents états électroniques et vibrationnels des molécules et des complexes ont été étudiés par méthodes *ab initio*. Nous avons tenté de mieux comprendre la photophysique induite par les radiations et la possibilité d'application de la méthode de photofragmentation. Les longueurs d'ondes pour certains processus de photofragmentation ont été proposées.

Les résultats des études sur les complexes formés avec la molécule d'eau en vue de la détermination

de leur stabilité et de la caractérisation de leur activité optique ont été exposés également. On peut noter les tendances structurales et spectroscopiques pour les complexes avec la molécule d'eau :

- le minimum global de la surface d'énergie potentielle correspond à la structure cyclique pour les complexes $(H_2O)_n$ - $(HX)_m$ (X = F, Cl) avec $n, m \geqslant 2$.
- les complexes ont une structure avec liaisons hydrogène R($O \ldots H$) de 1,6 à 2,4 Å.
- les atomes d'hydrogène participant à la liaison hydrogène sont quasi-coplanaires avec les atomes lourds, alors que les atomes H libres sont hors du plan ;
- les liaisons H_b - X (X = F, Cl) sont allongées par rapport aux molécules isolées, ce qui conduit à un déplacement vers le rouge des fréquences associées $\Delta\nu$.
- Lors de l'excitation électronique, la transition dans l'état électronique de basse énergie est localisée sur les liaisons O-H d'une des molécules d'eau, ce qui assure la préservation du caractère dissociatif de la bande d'absorption comme dans la molécule d'eau isolée, avec cependant un déplacement vers le domaine des ondes courtes.

Les résultats obtenus sont importants pour la détection des composants mineurs dans l'atmosphère et peuvent contribuer à la modélisation de la balance thermique de l'atmosphère.

La partie concernant le complexe $CH_4 - N_2$ a consisté à obtenir la surface de potentiel du complexe pour des configurations différentes par calculs *ab initio* et à étudier des propriétés telles que le moment dipolaire, la polarisabilité et l'hyperpolarisabilité du complexe. Ce travail donne lieu à une thèse (Yulia Kalugina, depuis octobre 2007). La surface de potentiel est obtenue en s'appuyant sur le calcul *ab initio* au niveau «Coupled Cluster CCSD(T)» et sur une base de type aug-cc-pV(X)Z. La forme analytique du potentiel correspondant a été proposée. L'analyse de la surface de potentiel détermine la famille des configurations les plus stables correspondant à la rotation de la molécule N_2 autour de l'axe x . Les fréquences harmoniques et anharmoniques sont calculées pour la configuration la plus stable. Le paramètre d'asymétrie $K = (2B - A - C)/(A - C) = -0.99$ est très proche de -1, ce qui correspond à une toupie quasi-symétrique allongée. Ce travail peut contribuer aux études sur l'élargissement des bandes rovibrationnelles et présente une contribution à la compréhension fondamentale de l'interaction des molécules sphériques comme le méthane avec des molécules constituant des atmosphères planétaires.

Le chapitre concernant l'adsorption sur la zéolithe contient mes résultats sur la modélisation de la silicalite-1 et le processus d'adsorption de l'éthylène. Ces résultats montrent l'importance qu'il y a à bien choisir à la fois la zéolithe modèle et le niveau de la théorie pour obtenir la bonne réponse spectroscopique. On a montré que l'adsorption de la molécule non-polaire d'éthylène correspond à un processus de physisorption et que, dans le cas d'adsorption sur la silicalite-1, il n'y a pas de sites privilégiés. Donc, les calculs devraient être effectués sur différentes orientations des molécules. Les modifications des spectres d'adsorbat/adsorbant et leur interprétation ont été aussi présentées. Les déplacements causés par l'interaction de la molécule avec la silicalite tendent pour la plupart des modes de vibration vers les fréquences plus basses. La silicalite-1 peut adsorber jusqu'à 11 molécules par cellule élémentaire. Par conséquent, à haute charge, les interactions entre molécules jouent un rôle important. Ceci signifie que l'on doit également simuler l'adsorption de deux ou plusieurs molécules d'éthylène.

En s'appuyant sur des calculs *ab initio*, on a pu prouver plusieurs hypothèses et justifier les approches théoriques concernant les structures des systèmes étudiés, leur spectre et les processus induits par l'interaction de la matière avec le rayonnement. Ces calculs fournissent un support important à la spectroscopie moléculaire, dont l'objet est l'étude du rayonnement émis ou absorbé par un système moléculaire, dans la mesure où la fréquence du rayonnement émis ou absorbé et les intensités de ces rayonnements sont liées aux propriétés de l'ensemble des molécules constituant la substance considérée. Les propriétés d'une molécule isolée, ou bien celles des complexes ou de cristaux moléculaires (quand les interactions entre molécules jouent un rôle important) peuvent être obtenues par les calculs *ab initio*. Cela donne une ouverture sur la modélisation des spectres et augmente la crédibilité de leur interprétation.

Grâce à des études de plus en plus détaillées et précises, il est possible d'inclure tous les domaines spectraux compris entre l'ultraviolet et les micro-ondes de la spectroscopie moléculaire. Il y a donc des possibilités d'impact sur de multiples domaines qui relèvent des sciences pures et appliquées. Il faut

s'attendre à ce que les systèmes à modéliser soient de plus en plus grands, si bien que les avancées vont être également conditionnées par le temps calcul, l'espace disque, et la convergence des calculs. Ces obstacles majeurs seront contournés par la «force brute», avec l'accroissement de la puissance des machines, mais également par le développement de méthodes spécifiques et l'application d'hypothèses adaptées à chaque application, ce qui nécessite de continuer les recherches !

9.2 Perspectives

Dans l'avenir, je me propose d'élargir le domaine de mes études sur l'interaction du rayonnement avec la matière et de me consacrer à la modélisation des systèmes complexes. Les complexes moléculaires (van der Waals et liaison hydrogène) sont de plus en plus souvent considérés comme des contributeurs à plusieurs processus importants, tant physiques que chimiques, dans des environnements très variés, comme les atmosphères planétaires ou le milieu interstellaire. Il existe ainsi un besoin croissant d'enquêtes systématiques théoriques et expérimentales. Les études sur les complexes d'interaction faible constituent un défi pour les calculs *ab initio* de haute précision. La clustérisation et le piégeage des molécules présentent un intérêt pour plusieurs applications, y compris astrophysiques. Les structures cristallines qui maintiennent dans leurs cages une ou plusieurs molécules hôtes comme les clathrates hydrates de méthane, par exemple, sont présents en abondance dans certains sédiments marins, dans le permafrost terrestre, dans le permafrost et les calottes polaires de Mars, dans les satellites de glace et dans certains noyaux cométaires. La modélisation des systèmes périodiques et de leurs spectres reste un domaine largement ouvert. Ceci ouvre de grands axes pour mes recherches :

- interactions molécule–molécule ;
- interactions molécule–surface ;
- interaction matière–rayonnement ;
- modélisation des systèmes complexes.

Dans l'immédiat, je compte poursuivre parallèlement, dans les deux grandes thématiques développées dans ce document :

- les calculs *ab initio* pour les complexes d'interêt atmosphériques et astrophysique, notamment, pour les complexes avec la molécule du méthane. Ce projet concerne l'étude du dimère CH_4-N_2 pour les applications atmosphériques et astrophysiques (Titan) et s'inscrit dans la logique de l'expérience sur les dimères et les calculs *ab initio*. Pour ce projet, nous avons obtenu une thèse en cotutelle franco-russe de l'Ambassade de France à Moscou depuis octobre 2007, que je codirige à Dijon, en collaboration avec V. Boudon, dans le cadre de l'ANR CH_4@Titan. Je m'intéresse à la construction d'une surface de potentiel dont la forme analytique décrit l'ensemble des configurations nucléaires (radiales et angulaires) qui peut servir aux applications variées : forme de la bandes rovibrationnelles, énergies de transition rovibrationnelles inter- et intra moléculaires, qui peuvent également justifier la précision de la surface de potentiel ;
- les calculs *ab initio* pour la spectroscopie de molécules piégées dans des solides (zéolithes, matrices,...), qui me semblent constituer un thème très porteur pour l'avenir, avec de nombreuses appplications potentielles telles que la dépollution. En ce qui concerne les silicalites, il y a encore bien des sites à étudier, y compris des cavités (intersections) ;
- les calculs *ab initio* pour le dimère C_2H_4 - C_2H_4, traités actuellement dans le cadre de thèse de Yulia Kalugina , qui présentent un interêt certain pour mieux comprendre le problème d'adsorption d'éthylène sur les zéolithes (le cas de deux molécules dans une cavité) ;
- les travaux sur les zéolithes peuvent aisément être étendus à l'étude du méthane ou d'autres molécules piégées dans des cristaux de glace, appelées clathrates. Les clathrates («hydrates de gaz») sont présents sur terre et seraient aussi à l'origine du méthane dans l'atmosphère de Titan. Cette étude fait partie des objectifs du Pôle de Sciences Planétaires de Bourgogne Franche-Comté.

Il s'agit bien entendu d'un travail considérable, qui ne peut s'envisager que sur de nombreuses années et dans le cadre de collaborations avec d'autres équipes, tant au niveau théorique qu'expérimental.

Chapitre 10
BIBLIOGRAPHIE

[1] J.-L. Rival. *Éléments de chimie quantique à lusage des chimistes*. InterEditions/Editions du CNRS, 1989.

[2] M. J. Frisch, G. W. Trucks, H. B. Schlegel, G. E. Scuseria, M. A. Robb, J. R. Cheeseman, J. A. Montgomery, Jr., T. Vreven, K. N. Kudin, J. C. Burant, J. M. Millam, S. S. Iyengar, J. Tomasi, V. Barone, B. Mennucci, M. Cossi, G. Scalmani, N. Rega, G. A. Petersson, H. Nakatsuji, M. Hada, M. Ehara, K. Toyota, R. Fukuda, J. Hasegawa, M. Ishida, T. Nakajima, Y. Honda, O. Kitao, H. Nakai, M. Klene, X. Li, J. E. Knox, H. P. Hratchian, J. B. Cross, V. Bakken, C. Adamo, J. Jaramillo, R. Gomperts, R. E. Stratmann, O. Yazyev, A. J. Austin, R. Cammi, C. Pomelli, J. W. Ochterski, P. Y. Ayala, K. Morokuma, G. A. Voth, P. Salvador, J. J. Dannenberg, V. G. Zakrzewski, S. Dapprich, A. D. Daniels, M. C. Strain, O. Farkas, D. K. Malick, A. D. Rabuck, K. Raghavachari, J. B. Foresman, J. V. Ortiz, Q. Cui, A. G. Baboul, S. Clifford, J. Cioslowski, B. B. Stefanov, G. Liu, A. Liashenko, P. Piskorz, I. Komaromi, R. L. Martin, D. J. Fox, T. Keith, M. A. Al-Laham, C. Y. Peng, A. Nanayakkara, M. Challacombe, P. M. W. Gill, B. Johnson, W. Chen, M. W. Wong, C. Gonzalez, and J. A. Pople. Gaussian 03, Revision C.02. Gaussian, Inc., Wallingford, CT, 2004.

[3] W. J. Hehre, W. A. Lathan, R. Ditchfield, M. D. Newton, and J. A. Pople. Gaussian 70, quantum Chemistry Program Exchange, program no. 237. Gaussian, Carnegie Mellon University,1970.

[4] H.-J. Werner, P. J. Knowles, R. Lindh, F. R. Manby, M. Schütz, P. Celani, T. Korona, A. Mitrushenkov, G. Rauhut, T. B. Adler, R. D. Amos, A. Bernhardsson, A. Berning, D. L. Cooper, M. J. O. Deegan, A. J. Dobbyn, F. Eckert, E. Goll, C. Hampel, G. Hetzer, T. Hrenar, G. Knizia, C. Köppl, Y. Liu, A. W. Lloyd, R. A. Mata, A. J. May, S. J. McNicholas, W. Meyer, M. E. Mura, A. Nicklass, P. Palmieri, K. Pflüger, R. Pitzer, M. Reiher, U. Schumann, H. Stoll, A. J. Stone, R. Tarroni, T. Thorsteinsson, M. Wang, and A. Wolf. Molpro, version 2008.3, a package of ab initio programs, 2008. see http ://www.molpro.net.

[5] M.W.Schmidt, K.K.Baldridge, J.A.Boatz, S.T.Elbert, M.S.Gordon, J.J.Jensen, S.Koseki, N.Matsunaga, K.A.Nguyen, S.Su, T.L.Windus, M.Dupuis, and J.A.Montgomery. Gamess, version 21. Gamess, J. Comput. Chem. 14, 1347-1363, 1993.

[6] T. Koopmans. The classification of wave functions and eigen-values to the single electrons of an atom. *Physica*, 1 :104, 1934.

[7] C. C. J. Roothaan. New development in molecular orbital theory. *Rev. Mod. Phys.*, 23 :69–89, 1951.

[8] J.A. Pople and R.K. Nesbet. Self consistent orbitals for radicals. *J. Chem. Phys.*, 22 :571, 1954.

[9] L. Zulike. *Quantum Chemistry*. Mir, 1976.

[10] C. Møller and M.S. Plesset. Note on an approximation treatment for many-electron systems. *Phys. Rev.*, 46 :618–622, 1933.

[11] P. Hohenberg and W. Kohn. Inhomogeneous electron gas. *Phys. Rev.*, 136 :B864–B871, 1964.

[12] W. Kohn and L.J. Sham. Self-consistent equations including exchange and correlation effects. *Phys. Rev.*, 140 :A1133–A1138, 1965.

[13] C. Adamo and V. Barone. Toward reliable adiabatic connection models free from adjustable parameters. *Chem. Phys. Lett.*, 274 :242–250, 1997.

[14] C. Adamo and V. Barone. Exchange functionals with improved long-range behavior and adiabatic connection methods without adjustable parameters : The MPW and MPW1PW models. *J. Chem. Phys.*, 108 :664–675, 1998.

[15] C. Adamo and V. Barone. Toward reliable density functional methods without adjustable parameters : The PBE0 model. *J. Chem. Phys.*, 110 :6158–6179, 1999.

[16] T.H. Dunning. Gaussian basis sets for use in correlated molecular calculations. i. the atoms boron through neon and hydrogen. *J. Chem. Phys.*, 90 :1007, 1989.

[17] D. Feller. Applications of systematic sequences of wave functions to the water dimer. *J. Chem. Phys.*, 96 :6104–6114, 1992.

[18] A. G. Császár, W. D. Allen, Yu.Yamaguchi, and H.F. Schaefer III. *Computational Molecular Spectroscopy ed. by P. Jensen and P.R. Bunker*. John Wiley & Sons Ltd, 2000.

[19] J.M.L. Martin. Ab initio total atomization energies of small molecules - towards the basis set limit. *Chem. Phys. Lett.*, 259 :669–678, 1996.

[20] T. Helgaker, W. Klopper, H. Koch, and J. Noga. Basis-set convergence of correlated calculations on water. *J. Chem. Phys.*, 106 :9639, 1997.

[21] D. Truhlar. Basis-set extrapolation. *Chem. Phys. Lett.*, 294 :45–48, 1998.

[22] V. Barone. Anharmonic vibrational properties by a fully automated second-order perturbative approach. *J. Chem. Phys.*, 122 :014108, 2005.

[23] J. M. Bowman. The self-consistent-field approach to polyatomic vibrations. *Acc. Chem. Res.*, 19 :202, 1986.

[24] M. A. Ratner and R. B. Gerber. Excited vibrational states of polyatomic molecules - the semiclassical self-consistent field approach. *J. Chem. Phys.*, 90 :20, 1986.

[25] J. O. Jung and R. B. Gerber. Vibrational wave functions and spectroscopy of $(H_2O)_n$, $n = 2,3,4,5$: Vibrational self-consistent field with correlation corrections. *J. Chem. Phys.*, 105 :10322, 1996.

[26] J. O. Jung and R. B. Gerber. Vibrational wave functions and energy levels of large anharmonic clusters : A vibrational scf study of Ar_{13}. *J. Chem. Phys.*, 105 :10682, 1996.

[27] S. K. Gregurick, E. Fredj, R. Elber, and R. B. Gerber. Vibrational spectroscopy of peptides and peptide-water complexes : Anharmonic coupled-mode calculations. *J.Phys.Chem. B*, 101 :8595, 1997.

[28] G.G. Gray and K.E. Gubbins. *Theory of molecular fluids. Volume 1 : Fundamentals*. Clarendon Press, 1984.

[29] J.O. Hirschfelder, C.F. Curtiss, and R. Byron Bird. *Molecular theory of liquids and gases*. John Wiley & Sons Ltd, 1964.

[30] T. Gabard. *Etude des effets collisionnels dans les molécules tétraedriques. Application au méthane perturbé par l'argon*. PhD thesis, Université de Bourgogne, 1996.

[31] P. R. Bunker. *Molecular Symmetry and Spectroscopy*. Academic Press, 1979.

[32] H. C. Longuet-Higgins. The symmetry groups of non-rigid molecules. *Mol. Phys.*, 6 :445, 1963.

[33] Ad van der Avoird, P. E. S. Wormer, and R. Moszynski. From intermolecular potentials to the spectra of van der waals molecules, and vice versa. *Chem.Rev.*, 6 :445, 1963.

[34] Y. Scribano. *Etude théorique du dimère de l'eau $(H_2O)_2$ et de son rôle dans l'atmosphère*. PhD thesis, Université de Montpellier II, 2006.

[35] C. Leforestier, L. Braly, K. Liu, M. Elrod, and R. Saykally. Fully coupled six-dimensional calculations of the water dimer vibration-totation-tunneling states with a split wigner pseudo spectral approach. *J. Chem. Phys.*, 106 :8527, 1997.

[36] H. L. Williams, K. Szalewicz, B. Jeziorski, R. Moszynski, and S. Rybak. Symmetry-adapted perturbation theory calculation of the Ar-H_2 intermolecular potential energy surface. *J. Chem. Phys.*, 98 :1279–2006, 1993.

[37] R. Moszynski, P. E. S. Wormer, B. Jeziorski, and Ad van der Avoird. Symmetry-adapted perturbation theory calculation of the He-HF intermolecular potential energy surface. *J. Chem. Phys.*, 101 :2811–2824, 1994.

[38] R. Moszynski, P. E. S. Wormer, B. Jeziorski, and Ad van der Avoird. Ab initio potential energy surface and near-infrared spectrum of the He-C_2H_2 complex. *J. Chem. Phys.*, 102 :8385–8397, 1995.

[39] B. Jeziorski, R. Moszynski, and K. Szalewicz. Perturbation theory approach to intermolecular potential energy surfaces of van der waals complexes. *Chem.Rev.*, 94 :1887–1930, 1994.

[40] S. F. Boys and F. Bernardi. The calculation of small molecular interactions by the differences of separate total energies. some procedures with reduced errors. *Mol. Phys.*, 19 :553–566, 1970.

[41] A. J. Stone. *The Theory of Intermolecular Forces, The Internal Series of Monographs on Chemistry*. Clarendon Press, 1996.

[42] P. R. Bunker and P. Jensen. *Molecular Symmetry and Spectroscopy*. NRC Research Press, 1998.

[43] M. J. Frisch, G. W. Trucks, H. B. Schlegel, G. E. Scuseria, M. A. Robb, J. R. Cheeseman, V. G. Zakrzewski, J. A. Montgomery, R. E. Stratmann Jr., J. C. Burant, S. Dapprich, J. M. Millam, A. D. Daniels, K. N. Kudin, M. C. Strain, O. Farkas, J. Tomasi, V. Barone, M. Cossi, R. Cammi, B. Mennucci, C. Pomelli, C. Adamo, S. Clifford, J. Ochterski, G. A. Petersson, P. Y. Ayala, Q. Cui, K. Morokuma, D. K. Malick, A. D. Rabuck, K. Raghavachari, J. B. Foresman, J. Cioslowski, J. V. Ortiz, A. G. Baboul, B. B. Stefanov, G. Liu, A. Liashenko, P. Piskorz, I. Komaromi, R. Gomperts, R. L. Martin, D. J. Fox, T. Keith, M. A. Al-Laham, C. Y. Peng, A. Nanayakkara C. Gonzalez, M. Challacombe, P. M. W. Gill, B. G. Johnson, W. Chenand M. W. Wong, J. L. Andres, M. Head-Gordon, E. S. Replogle, and J. A. Pople. Gaussian 98, Revision A.01. Gaussian, Inc., Pittsburgh, PA, 1998.

[44] D. Papousek andM. Aliev. *Non-specific and specific interactions of molecules of different electronic structures with solid surface*. Elsevier, 1982.

[45] J.M.L. Martin and A. Sundermann. Correlation consistent valence basis sets for use with the Stuttgart-Dresden-Bonn relativistic effective core potentials : The atoms Ga-Kr and In-Xe. *J. Chem. Phys.*, 114 :3408–3420, 2001.

[46] P.J. Robinson and K.A. Holbruk. *Unimolecular reactions*. Wiley, 1972.

[47] N. Zvereva. *Etude théorique des niveaux électroniques de basse énergie de certaines molécules du point de vue de leur dissociation*. PhD thesis, Tomsk University, 1994.

[48] M.J. Molina, Tai-Ly Tso, L.T. Molina, and F.C.Y. Wang. Antarctic stratospheric chemistry of chlorine nitrate, hydrogen chloride, and ice : release of active chlorine. *Science*, 238 :4831, 1987.

[49] D.C. Clary. Molecules on ice. *Science*, 271 :1509, 1996.

[50] F.M. Geiger, J.M. Hich, and A.C. Dios. *Ab initio* study of HOCl, HCL, H_2O and Cl_2 interacting with four water molecules mimicking a hexagonal ice surface. *J.Phys.Chem. A*, 102 :1514–1522, 1998.

[51] D.A. Estrin, J. Kohanoff, D.H. Laria, and R.O. Weht. Hybrid quantum and classical mechanical monte carlo simulations of the interaction of hydrogen chloride with solid water clusters. *Chem. Phys. Lett.*, 280 :280–286, 1997.

[52] Sh.Sh. Nabiev and Yu.N. Ponomarev. Spectrochemical aspects of laser remote control of the accidental releases at the sites of nuclear fuel cycle. *Atmos.Oceanic Opt.*, 94 :1931–1974, 1994.

[53] N.A. Zvereva, Sh.Sh. Nabiev, and Yu.N. Ponomarev. Energies of the $S_0 \rightarrow S_1$ vertical transitions of low electronic states of optically active hydrogen bonding complexes. *Atmos.Oceanic Opt.*, 12 :810–814, 1999.

[54] Sh.Sh. Nabiev. IR spectroscopy of the interhalogen XF_3 and XF_5 ($X = Cl, B$). *Atmos.Oceanic Opt.*, 13 :123–132, 2000.

[55] K. Nakamoto. *Infrared and Raman Spectra of Inorganic and Coordination Compounds*. John Wiley & Sons Ltd, 1986.

[56] Ch. Wanger, J.-P. Champion, and V. Boudon. The partition sum of methane at high temperature. *J. Quant. Spectrosc. Radiat. Transfer*, 109 :2967–2706, 2008.

[57] S. Albert, S. Bauerecker, V. Boudon, L.R. Brown, J.-P. Champion, M. LoŚte, A. Nikitin, and M. Quack. Global analysis of the high resolution infrared spectrum of methane $12^c h_4$ in the region from 0 to 4800 cm^{-1}. *J. Quant. Spectrosc. Radiat. Transfer*, 356 :131–146, 2009.

[58] L.S. Rothman, I.E. Gordon, A. Barbe, D.Chris Benner, P.F. Bernath, M. Birk, V. Boudon, L.R. Brown, A. Campargue, J.-P. Champion, K. Chance, L.H. Coudert, V. Dana, V.M. Devi, S. Fally, J.-M. Flaud, R.R. Gamache, A. Goldman, D. Jacquemart, I. Kleiner, N. Lacome, W.J. Lafferty, J.-Y. Mandin, S.T. Massie, S.N. Mikhailenko, C.E. Miller, N. Moazzen-Ahmadi, O.V. Naumenko, A.V. Nikitin, J. Orphal, V.I. Perevalov, A. Perrin, A. Predoi-Cross, C.P. Rinsland, M. Rotger, M. Simecková, M.A.H. Smith, K. Sung, S.A. Tashkun, J. Tennyson, R.A. Toth, A.C. Vandaele, and J. Vander Auwera. The hitran 2008 molecular spectroscopic database. *J. Quant. Spectrosc. Radiat. Transfer*, 110 :533–572, 2009.

[59] A.V. Kiselev. Non-specific and specific interactions of molecules of different electronic structures with solid surface. *Disc. Far. Soc. Intermolecular Forces*, 40 :205, 1965.

[60] L.W. Bruch, M.W. Cole, and E. Zaremba. *Physical adsorption : Forces and phenomena*. Clarendon Press, 1997.

[61] V. Staemmler. The cluster approach for the adsorption of small molecules on oxide surfaces. *Top. Organomet. Chem.*, 12 :219–256, 2005.

[62] W.M. Meier and D.H. Oslo. *Atlas of zeolites structure types, Third revised edition*. Butterworth-Heinemann, 1992.

[63] G.T. Kokotallo, S.L. Lawton, D.H. Olson, and W.M. Meier. Structure of synthetic zeolite ZSM-5. *Nature*, 272 :437, 1978.

[64] H. van Koningsveld., H. van Bekkum, and J.C. Jansen. The location of p-xylene in a single crystal of zeolite H-ZSM-5 with a new, sorbate-induced, orthorhombic framework symmetry. *Acta Cryst. B*, 45 :423, 1989.

[65] E.M. Flanigen and et al. Silicalite, a new hydrophobic crystalline silica molecular sieve. *Nature*, 271 :512, 1978.

[66] H. Thamm. Adsorption site heterogeneity in silicalite : a calorimetric study. *Zeolite*, 7 :341, 1987.

[67] B.F. Mentzen and P. Gelin. The silicalite/p-xylene system : Part I Fflexibility of the MFI framework and sorption mechanism observed during p-xylene pore-filling by X-ray powder diffraction at room temperature. *Materials Research Bulletin*, 30(3) :373, 1995.

[68] R. Wallas. The torsional energy levels of ethylene : A re-evolution. *Chem. Phys. Lett.*, 159 :35–36, 1989.

[69] Airliquide. http ://www.airliquide.com.

[70] F. Thibault-Starzyk and Collectif. *Les matériaux micro et mésoporeux. Caractérisation*. EDP Sciences, 2004.

Chapitre 11

Curriculum vitæ

Nom	:	ZVEREVA-LOËTE (KHAMOVITCH)
Prénoms	:	Natalia
Née le	:	18 mars 1962 à Novossibirsk - Russie
Nationalité	:	Russe, Française
Situation familiale	:	Mariée, 2 enfants (23, 21 ans)
Adresse personnelle	:	78, rue de Fontaine, 21121 Daix, France
Adresse électronique	:	natalia.loete@u-bourgogne.fr ; natalia_loete@yahoo.fr
Téléphone	:	0380582207(pers.) ; 0676054248(portable), 0380395967(lab.)
Situation actuelle	:	IR (ANR), Laboratoire ICB, Université de Bourgogne, Dijon, France

Formation - Emplois occupés

Thèse : 1994, Faculté de Physique à l'Université d"Etat de Tomsk, Russie.

Carrière scientifique :

- 1984-1991 - Assistant à la faculté de Physique Théorique - Université d'Etat de Tomsk.
- 1991-1994 - Doctorante à la faculté de Physique - Université d'Etat de Tomsk.
- 1994-1996 - Chercheur à l'Institut de Physique de Sibérie - Université d'Etat de Tomsk.
- 1996-1999 - Chercheur senior à l'Institut de Physique de Sibérie - Université d'Etat de Tomsk.
- 1999-2002 - Chercheur senior à la faculté de Physique - Université d'Etat de Tomsk.
- Depuis 2002 - Chercheur senior à l'Institut d'Optique Atmosphérique - Tomsk.
- Avril 2003 - Professeur invitée (1 mois) - LPUB - Université de Bourgogne (depuis 2007 - Institut Carnot de Bourgogne ICB).
- 2003-2009 - Chercheur libre - LPUB (ICB) - Université de Bourgogne.
- Qualifiée Maître de Conférences - 30e section - Février 2005.
- Juin-Juillet 2005 - Professeur invitée (2 mois) - PhLAM - Université de Lille I.
- Novembre 2005 - Professeur invitée (1 mois) - LCT - Université de Marne-la-Vallée.
- Avril 2007 - Professeur invitée (1 mois) - laboratoire de Chimie LRRS (ICB) - Université de Bourgogne.
- Qualifiée Maître de Conférences - 30e et 31e sections - Février 2009.
- Depuis avril 2009 - Ingénieur de Recherche - ANR CH_4@Titan - ICB - Université de Bourgogne.

Activités d'enseignement

- Cours et TD de mécanique quantique (1 année) aux étudiants de Physique (3e et 4e année) - Université de Tomsk.
- Cours et TD de chimie quantique (1 année) aux étudiants de Chimie (3e et 4e année) - Université de Tomsk.
- 27 h TP optique L1 Science Vie, Science et Techniques, Université de Bourgogne, S1 2008
- 18 h TP optique L1 Science Vie, Science et Techniques, Université de Bourgogne, S1 2009

Activités de recherche

- Spectroscopie moléculaire, photophysique et photochimie de molécules et de systémes molèculaires.
- Calculs *ab initio* : modélisation moléculaire - recherche des configurations les plus stables, étude d'états vibrationnels et électroniques de molécules et de systèmes complexes, étude des interactions faibles molécule-surface (molécule piégées) et molécule-molécule.
- Logiciels scientifiques : Gaussian, Gamess, Molpro, VASP
- programmation : FORTRAN, MAPLE

1. Faculté de Physique à l'Université d'État de Tomsk 1984–1994.

Pendant cette période, j'ai travaillé sur les niveaux électroniques de basse énergie de molécules telles que les aldéhydes et les alcools aliphatiques, l'objectif principal étant l'étude de leur photodissociation. Ceci a été réalisé à partir de calculs *ab initio*. J'ai notamment déterminé les constantes de vitesse de photodissociation et les barrières d'activation. J'ai également étudié le mécanisme de photo fragmentation en vue de la détection de molécules organiques par spectroscopie. Ces travaux ont fait l'objet de ma thèse et de plusieurs publications [P1-P3, P5-P7].

2. Institut de Physique de Sibérie à l'Université d'État de Tomsk 1994–1999.

Dans cet institut, j'ai continué un travail commencé pendant la période précédente concernant l'étude des états électroniques du dimère de l'eau $(H_2O)_2$ [4]. Je l'ai étendu à l'étude de la densité de charge des complexes $(H_2O)_n$ [P10] et l'effet spectroscopique de liaisons hydrogène pour clusters d'eau [P11]. Les résultats ont été obtenus par calculs *ab initio*. Dans le même temps, je me suis intéressée à un nouveau thème de recherche sur les processus photophysiques dans les molécules de TNT et de 3-4 benzopyrène [P8-P9]. J'ai proposé différentes approches pour leur détection en phase gazeuse.

3. Faculté de Physique à l'Université d'État de Tomsk et Institut d'Optique Atmosphérique - Tomsk 1999-2003.

Dans le prolongement des études précédentes sur les complexes, je me suis intéressée à l'étude des différents complexes de l'eau. J'ai déterminé leur structure, leurs fréquences de transition électroniques et vibrationnelles par calculs *ab initio*, afin d'interpréter les spectres existants. Ces travaux ont porté sur les complexes de l'eau elle-même [P12,P13] et les complexes de l'eau avec H-Cl [P14,P15,P17], HF [P12,P16,P18] et NH_3, PH_3, AsH_3 [P19]. Les résultats obtenus figurent dans une base de données pour les applications atmosphériques [P20]. L'ensemble de ces travaux sont également détaillés dans les livres [L1,L2,L3].

4. Université de Bourgogne - LPUB - ICB - 2003–2009.

Depuis mon arrivée à Dijon, j'ai travaillé dans le groupe de Spectroscopie Moléculaire et Applications (SMA) dirigé par V. Boudon et avec M. Rotger et M. Loëte. Dans un premier temps j'ai travaillé sur les molécules quasi-sphériques et par calculs *ab initio* (avec Gaussian), j'ai déterminé les constantes de distorsion centrifuge et le moment dipolaire de la molécule SO_2F_2 pour valider la théorie et interpréter le spectre [P21, P23]. J'ai également commencé le calculs des constantes d'anharmonicité de la molécule SF_5Cl afin de faciliter l'analyse des polyades vibrationnelles.
Par ailleurs je poursuis l'étude du spectre IR du dimère HF-H_2O enregistré à Moscou ("Institut de Physique Générale" : A. Nadezdinskii, D. Stavrovskii, S. Chernin). Les calculs *ab initio* que j'ai effectués ont permis d'identifier et d'interpreter des structures de bandes chaudes issues des niveaux d'interaction entre les monomères.
En parallèle je me suis engagée dans un travail à long terme concernant les molécules piègées. A ce titre je participe à l'étude de la molécule C_2H_4 piégée dans des zéolithes. Ce projet implique l'équipe SMA (Spectroscopie Moléculaire et Application) et l'équipe ASP (Adsorption sur solides Poreux) de l'ICB et est au centre du GDR COMOVI (GDR CNRS N^0 2997 Spectroscopies Vibrationnelles des Molécules Confinées dans des Solides) dirigé par J.-P. Bellat et M. Rotger de l'ICB . Il s'agit d'étudier par calculs *ab initio* les changements de structure de la molécule dans les canaux de la zéolithe et d'interpreter les déplacements en fréquences et les variations en intensité dans le spectre de la molécule piègée. Le première phase a consisté à élaborer un modèle réaliste pour un canal de zéolithe. Le modèle établi a été confirmé par comparaison avec le spectre IR expérimental. La deuxième phase concerne la molécule piègée dans cette structure. Les premiers résultats sont encourageants et vont également dans le sens des observations effectuées par spectroscopie infrarouge par l'équipe ASP. Pour répondre aux differents problèmes posés je collabore avec le professeur C. Adamo de l'ENSCP de Paris depuis octobre 2007. Ces calculs couteux en temps ont fait l'objet de plusieurs communications à des congrès et d'une publication [P24]. A noter que ces travaux peuvent être étendus á l'étude du méthane piégé dans des cristaux de glace, appelés clathrates. Les clathrates sont présents sur terre et seraient aussi á l'origine du méthane dans l'atmosphére de Titan. Cette étude fait partie des objectifs du Pôle de Sciences Planétaires de Bourgogne Franche-Compté.
Conjointement j'ai mis en place une collaboration entre le groupe de spectroscopie à Dijon et le département de physique de l'Université d'Etat de Tomsk. Ce projet concerne l'étude du dimère CH_4-N_2 pour les applications atmosphériques et astrophysiques (Titan) et s'inscrit dans la logique de l'expérience sur les dimères et les calculs *ab initio* de l' équipe de Tomsk. Pour ce projet, nous avons obtenu une thèse en cotutelle franco-russe de l'Ambassade de France à Moscou, que je codirige officieusement depuis octobre 2007 à Dijon sous couvert V. Boudon (HDR) et officiellement depuis octobre 2008. Ces calculs ont fait l'objet de plusieurs communications à des congrès et une publication vient d'être publiée [P25]. Ce travail s'inscrit dans le cadre de l'ANR CH_4@Titan, qui effectue une étude exhaustive de l'absorption du méthane dans l'atmosphére de Titan par le calcul et l'experimentation.

5. Université de Lille - Juin-Juillet 2005.

Au laboratoire PhLAM, en collaboration avec Jean Demaison, j'ai effectué des calculs *ab initio* pour déterminer le champ de force anharmonique et la structure à l'équilibre de la molécule C_2H_3Br. Par ailleurs, j'ai écrit un programme permettant de déterminer la géométrie à l'équilibre de cette molécule à partir des constantes rotationnelles obtenues par l'analyse des spectres. La comparaison entre les deux approches est satisfaisante et un article a été publié au "Journal of Molecular Spectroscopy" [P22].

6. Université de Marne-la-Vallée - Novembre 2005.

Le projet proposé par le professeur R. Marquardt du Laboratoire de Chimie Théorique (LCT) est intitulé "Surface d'énergie potentielle du complexe (H_2O)–(HF) pour l'étude des mouvements de large amplitude des noyaux". Il s'agit principalement d'étudier, par calculs *ab initio* (Molpro), la surface de potentiel de

différents niveaux électroniques, pour déterminer les structures des points stationnaires correspondant aux différentes configurations du complexe. Le projet se poursuit actuellement avec le professeur R. Marquardt depuis professeur à Strasbourg.

7. Diffusion des résultats

- 3 participations à des livres
- 25 articles dans les revues à comité de lecture
- 8 actes de colloques
- 46 communications à des congrès
- 4 séminaires

8. Collaborations Scientifiques

- Moscou, RRC “Institut de Physique Moléculaire” : Sh. Nabiev, L. Suchanov.
- Moscou, “Institut de Physique Générale” : A. Nadezdinskii, D. Stavrovskii, S. Chernin.
- Dijon, Université de Bourgogne, LPUB (ICB) : M. Rotger, V. Boudon, M. Loëte, T. Gabard
- Dijon, Université de Bourgogne, LRRS (ICB) : J.P. Bellat, G. Weber.
- Lille, Université de Lille I, PhLAM : J.Demaison.
- Champs-sur-Marne, Université de Marne-la-Vallée, LCT : R.Marquardt.
- Tomsk, "Faculté de Physique - Université d’Etat de Tomsk" : V. Cherepanov, M. Buldakov.
- Tomsk, "Institut d’Optique Atmosphérique" : Yu. Ponomarev.
- Paris, E.N.S.C.P., Lab. d’Electrochimie et Chimie Analytique, Equipe Modélisation des Systèmes Complexes (MSC), C. Adamo, L. Joubert.
- Besançon, Institut UTINAM, UMR CNRS 6213, équipe DREAM : Béatrice Honvault

9. Participation à l’organisation de colloques

- Participation à l’organisation du Workshop international “Atmospheric Spectroscopy Application, ASA” 25 - 28 Aug. 2002, Moscow.
- Comité Scientifique. Atelier francofone. Clathrates dans les environnements naturels : études thermodynamiques et méthodes d’analyse. Besançon. Janvier 2010.

10. Activités de rapporteur

- Int. Journal : Computational Materials Science - 2007.
- Expert ANR, programme blanc - 2008 et 2009.
- Int. Journal : Journal of Physical Chemistry -2009

11. Encadrement d’étudiants

- Gospodareva Yulia, “*Ab initio* study of the hydrogen bonding complexes” Niveau 3 à 5 - 2001 - 2003.
- Grebenshikova Svetlana, “Basis set effect on the structure, energy, charge density of the molecule” Niveau 3 - 2001 - 2002.
- Dikanov Maksim “ROHF method possibility for study electronic states of molecules” Niveau 3 - 2001 - 2002.

- Yulia Kalugina : Thèse en cotutelle franco-russe, co-direction avec V. Boudon (ICB), V. Cherepanov, M. Buldakov (Université d'Etat de Tomsk).
- Chanda-Malis Ouk : Thèse, co-direction avec Béatrice Honvault DR CNRS (Institut UTINAM, UMR CNRS 6213, équipe DREAM) :"Détermination *ab initio* d'hypersurfaces d'éneregie potentielle pour l'interaction atome [=O(^{1}D), N(^{2}D)] + CH_4] et techniques de representation en vue de l"étude de la dynamique collisionnelle de ces systèmes".

12. Autres activités scientifiques

- Participation aux "Journées de Spectroscopie Moléculaire", 2004, Dunkerque.
- Participation à l'Ecole d'Eté "Molecules Trapped in Solids", Septembre 2004, Dijon.
- Participation à la journée méthane, 4 Février 2005, Dijon.
- Participation à la journèe GDR "COMOVI", 13 Décembre 2007, Dijon
- Participation aux "Journées Ter@tec 2008", 3 - 4 Juin 2008, Evry.
- Participation à la journèe GDR "COMOVI" , 08 Décembre 2009, Dijon

Autres

Langues :

- russe - langue maternelle ;
- français - courant (certificat du Centre International d'Etudes Françaises (CIEF) Université de Bourgogne) ;
- anglais - courant.

Chapitre 12

Liste des Travaux

Thèse

22/09/1994 - Université d'Etat de Tomsk - Russie - Etude théorique des niveaux électroniques de basse énergie de certaines molécules du point de vue de leur dissociation.

Participations à des livres

L1 Zvereva N.A., *Ab initio* methods of calculations in the theory of many electron systems, edited by Cherepanov V.N. - Tomsk (Tomsk State University) - **2000** - 49 pp.

L2 Zvereva N.A., Optically active hydrogen bonding complexes in the atmosphere, Spectroscopy from Space, Kluwer Academic Publisher, Dodrecht, **2001**, pp. 341 – 350.

L3 Zvereva N.A., Sh. Sh. Nabiev, Ponomarev Yu.N., Structure and properties of water molecular complexes with minor gaseous constituents of the atmosphere - **2003** - Tomsk : Publishing House of the Institute of Atmospheric Optics. - 140 pp.

Articles dans des revues à comité de lecture

P1 Zvereva N.A., Ippolitov I.I., Terpugova A.F., Theoretical investigation of the aldehydes photofragmentation, Atmospheric optics, vol. 4, pp. 55 – 61, **1991**.

P2 Zvereva N.A., Ippolitov I.I., Terpugova A.F., Investigation of low-lying electronic states of molecules in connection with photodissociation problem, Izvestiya Vuzov. Fizika, vol. 35, pp. 86 – 98, **1992**.

P3 Zvereva N.A., Ippolitov I.I., Terpugova A.F., Photofragmentation of aldehydes with COH radical formation, Izvestiya Vuzov. Fizika, vol. 36, pp. 121 – 122, **1993**.

P4 Buldakov M.A., Zvereva N.A., Ippolitov I.I., Terpugova A.F., Stability of $(H_2O)_2$ dimer in the ground and low-lying excited electronic states, Izvestiya Vuzov. Fizika, vol. 36, pp. 11 – 15, **1993**.

P5 Zvereva N.A., Ippolitov I.I., Terpugova A.F., Laser-induced photofragmentation of molecules. A theoretical study of photochemistry and photophysics of organic molecules, Atmospheric and Oceanic Optics, vol. 6, pp. 411 – 415, **1993**.

P6 Artyukhov V.Ya., Zvereva N.A., Ippolitov I.I., Terpugova A.F., Formaldehyde and acetaldehyde photodissociation in the excited state S_2, Atmospheric and Oceanic Optics, vol. 7, pp. 658 – 705, **1994**.

P7 Buldakov M.A., Zvereva N.A., Ippolitov I.I., Terpugova A.F, Photodissociation of water vapor by UV laser radiation, Atmospheric and Oceanic Optics., vol. 8, pp. 927 – 930, **1995**.

P8 Bazyl'â O.K., Zvereva N.A., Ippolitov I.I., Terpugova A.F., About photodissociation of the TNT molecule, Khimiya vysokikh energii (High energy chemistry), vol. 30, pp. 19 – 24, **1996**.

P9 Artyukhov V.Ya., Bratashov V.A., Zavodskii A.G., Zvereva N.A., Ippolitov I.I., Study of photophysical processes in the molecule of 3,4-benzpyrene in connection with the problem of its detection in the environment, Atmospheric and Oceanic Optics, vol. 11, pp. 387 – 392, **1998**.

P10 Zvereva N.A., Ippolitov I.I., Theoretical study of electron density redistribution under S0 $\rightarrow$ S1 transition in $(H_2O)_n$ ($n = 2 \ldots 6$) complexes, Izvestiya Vuzov. Fizika, vol. 42, pp. 8 –11, **1999**.

P11 Zvereva N.A., Spectroscopy effects of Intermolecular hydrogen bond for water clusters, Izvestiya Vuzov. Fizika, vol. 42, pp. 87 – 91, **1999**.

P12 Zvereva N.A., Nabiev Sh.Sh., Ponomarev Yu.N., Energies of the $S_0 \rightarrow S_1$ vertical transitions of low electronic states of optically active hydrogen bonding complexes, Atmospheric and Oceanic Optics, vol. 12, pp. 810 – 814, **1999**.

P13 Zvereva N.A., Theoretical Description of the Photodossociation Spectrum of Monomer and Dimer Forms of Water, Optics and Spectroscopy, vol. 91, pp. 604 – 608, **2001**.

P14 Zvereva N.A., Ab initio study of (H_2O)–(HCl) (1 : 1, 1 : 2, 2 : 1) complexes, Journal of Structural Chemistry, vol. 42, pp. 730 – 738, **2001**.

P15 Zvereva N.A., Terpugova A.F., Theoretical description of $H_2O \ldots HCl$ complex photodissociation spectrum, Russian Physics Journal, vol. 44, pp. 358 – 364, **2001**.

P16 Zvereva N.A., Nabiev Sh.Sh., Nadezhdinskii A.I., Ponomarev Yu., Stavrovskii D.B., Chernin S.M., Shubenkina T.A., IR spectra of HF and its complexes with water under atmospheric conditions, Atmospheric and Oceanic Optics, vol. 14, pp. 1009 – 1011, **2001**.

P17 Zvereva N.A., Ponomarev Yu.N., Molecular complexes of water and hydrogen chloride in the atmosphere, Atmospheric and Oceanic Optics, vol. 15., pp. 316 – 320, **2002**.

P18 Zvereva N.A., Nabiev S.S., Ponomarev Y.N., Sukhanov L.P., Structurally nonrigid molecular complexes $(H_2O)_n(HF)_m$ ($n+m \geq 2$) and their spectroscopic features, Russiian Chemical Bulletin, International Edition, vol. 52, pp. 45 – 54, **2003**.

P19 Zvereva N.A., Complexes with inorganic hydrides (NH_3, PH_3, AsH_3), Atmospheric and Oceanic Optics, vol. 16, pp. 203 – 210, **2003**.

P20 Zvereva N.A., Gospodareva Yu.S., Ponomarev Yu.N., Data base on the spectral, structural and energy parameters of the $(H_2O)_n$Mn complexes in gas phase, Atmospheric and Oceanic Optics, vol. 17, pp. 832 – 836, **2004**.

P21 Boudon V., Rotger M., Zvereva-Loëte N., Loëte M., The SO_2F_2 quasi-spherical top : Correspondence between tensorial and Watson's formalisms, Journal of Molecular Structure, vol. 780 - 881, pp. 124 – 133, **2005**.

P22 Zvereva-Loëte N., Demaison J., Rudolph H.D., Ab initio anharmonic force field and equilibrium structure of vynil bromide, Journal of Molecular Spectroscopy, vol. 236, pp. 248 – 254, **2006**.

P23 Rotger M., Boudon V., Loëte M., Zvereva-Loëte N., Margulès L., Demaison J., Merke I., Hegelund F., Bürger H., The Bending Triad of the Quasi-Spherical Top Molecule SO_2F_2 in the 550 cm^{-1} Region, Journal of Molecular Spectroscopy, vol. 238, pp. 145 – 157, **2006**.

P24 Zvereva-Loëte N.A., Ballandras A., Weber G., Rotger M., Boudon V., J. - M. Simon - Experimental IR study and *ab initio* modelling of ethylene adsorption in a MFI zeolite-type host zeolite - Molecular Physics, vol. 107, pp. 2081–2093, **2009**.

P25 Kalugina Yu. N., Buldakov M. A., Cherepanov V. N., Zvereva-Loëte N., Boudon V., Theoretical investigation of the potential energy surface of the van der Waals complex CH_4 - N_2 - Journal of Chemical Physics, vol. 131, N15, pp. 134304 (9), **2009**.

P26 Buldakov M. A., Cherepanov V. N., Kalugina Yu. N., Zvereva-Loëte N., Boudon V., Static polarizability surface of the van der Waals complex CH_4 - N_2 - Journal of Chemical Physics, in press, **2010**

P27 Kalugina Yu. N., Buldakov M. A., Cherepanov V. N., Zvereva-Loëte N., Boudon V., Theoretical investigation of the dipole moment surface of the van der Waals complex CH_4 - N_2 - Journal of Chemical Physics, en redaction, **2010**.

Actes de colloques

A1 Zvereva N.A., Ippolitov I.I., Terpugova A.F., Theoretical investigation of the detection of aldehydes in the gas phase, PROCEEDINGS SPIE., vol. 2205, pp. 391 – 394, **1994**.

A2 Zvereva N.A., Ippolitov I.I., Ab initio calculations of low-lying excited states of water clusters $(H_2O)_n$, $n = 2 \ldots 6$. PROCEEDINGS SPIE, vol. 3090, pp. 88 – 90, **1997**.

A3 Zvereva N.A., Structural and vibrational features of $(H_2O)_7$ complex, PROCEEDINGS SPIE, vol. 3583, pp. 113 – 118, **1998**.

A4 Zvereva N.A., Nabiev Sh.Sh., Ponomarev Yu.N., Structural and spectral features of $(H_2O \ldots HF)_n$, $n = 1 \ldots 3$, complexes, PROCEEDINGS SPIE, vol. 3983, pp. 9 – 15, **1999**.

A5 Zvereva N.A., Ab initio study of the $(H_2O \ldots HF)_n$, $n = 1 \ldots 5$, complexes, PROCEEDINGS SPIE, vol. 4063, pp. 122 – 125, **2000**.

A6 Zvereva N.A., Theoretical study of H-bond complexes electronic spectra, PROCEEDINGS SPIE , vol. 4341, pp. 24 – 31, **2000**.

A7 Zvereva N.A., Nabiev Sh.Sh., Ponomarev Yu.N., Weak H-bond complexes, PROCEEDINGS SPIE, vol. 4341, pp. 31 – 49, **2000**.

A8 Dikanova Yu.S., Ponomarev Yu.N. and Zvereva N.A., Database of structure, energy, and spectral characteristics of molecular complexes in atmosphere, PROCEEDINGS SPIE, vol. 6522, pp. 652208 – 652215, **2006**.

Communications à des congrès

C1 Zvereva N.A., Ippolitov I.I.,Terpugova A.F., Laser induced fluorescence, theoretical study of photochemistry and photophysics of organic molecules, International conference “Pulsed lasers on the transitions of the atoms and molecules” - Tomsk - **1992**.

C2 Zvereva N.A., Ippolitov I.I., Estimation of mechanisms of water vapor absorption in UV-field, International conference “Pulsed lasers on the transitions of the atoms and molecules” - Tomsk - **1995**.

C3 Zvereva N.A., Ippolitov I.I., Ab initio calculations of the low-excited states of water clusters $(H_2O)_n$, $n = 1 \ldots 6$. XII Symposium Ð School High Resolution Molecular Spectroscopy. Petergof - **1996**.

C4 Zvereva N.A., Ippolitov I.I., UV-radiation influence on the hydrogen bonded complexes, IV International Symposium of the Optics of Atmosphere and Ocean - Tomsk - Abstracts - **1997**.

C5 Zvereva N.A., Ippolitov I.I., The spectroscopy of water molecule and water complexes, 29 EGAS. Berlin. 21C. Europhysics conference abstracts. **1997**.

C6 Zvereva N.A., Structural and vibrational features of $(H_2O)_7$ complex, 5th International Symposium “Optics of atmosphere and ocean” and International school “Physics of the environment” - Tomsk - **1998**.

C7 Zvereva N.A., Nabiev Sh.Sh., Ponomarev Yu.N., Stable configurations of complexes $(H_2O)_n(HF)_m$ in the atmosphere and vibrational frequencies, VI International Symposium of the Optics of Atmosphere and Ocean - Tomsk - **1999**.

C8 Zvereva N.A., Ab initio study of the $(H_2O\acute{E}HF)_n$, $n = 1 \ldots 5$, complexes, High Resolution Molecular Spectroscopy. XIII Symposium-School - Tomsk - **1999**.

C9 Zvereva N.A., Nabiev Sh.Sh., Ponomarev Yu.N., The stable configuration of $(H_2O)_n(HF)_m$ complexes in the atmosphere, XVI Colloquium on High Resolution Molecular Spectroscopy. Dijon - France - **1999**.

C10 Zvereva N.A., Photodissociation dynamics of water molecule and its hydrogen-bonded complexes in the first absorption band, XVI Colloquium on High Resolution Molecular Spectroscopy. Dijon - France - **1999**.

C11 Zvereva N.A., Theoretical study of the hydrogen bonded complexes electronic spectra, VII International Symposium of the Optics of Atmosphere and Ocean - Tomsk - **2000**.

C12 Zvereva N.A., Nabiev Sh.Sh., Ponomarev Yu.N., Weak hydrogen bond complexes, International Symposium of the Optics of Atmosphere and Ocean - Tomsk - **2000**.

C13 Zvereva N.A., Optically active hydrogen bonding complexes in the atmosphere, NATO Advanced Research Workshop, Spectroscopy from Space, Bratislava - **2000**.

C14 Zvereva N.A., Nabiev Sh.Sh., Ponomarev Yu.N, Spectrochemical aspects of remote laser monitoring of radioactive discharges in the atmosphere, NATO Advanced Research Workshop, Spectroscopy from Space, Bratislava, **2000**.

C15 Zvereva N.A., Nabiev Sh., Ponomarev Yu., Methodical features of the calculations of structural, energy and spectroscopic parameters of nonrigid complexes $(HHAL)_n \ldots (H_2O)_m$ (HAL=F,Cl) ($n+m \geq 2$), Atmospheric and ocean optics, Atmospheric Physics, VIII Joint International Symposium, Irkutsk - **2001**.

C16 Nabiev Sh., Zvereva N.A., Ignatov S. et al., Structurally nonrigid molecular complexes of water with atmospheric gases : problems, approaches, solution, Atmospheric and ocean optics, Atmospheric Physics, VIII Joint International Symposium, Irkutsk, **2001**.

C17 Zvereva N.A., Theoretical description of the photodissociation spectrum of monomer and dimer forms of water, Atmospheric and ocean optics, Atmospheric Physics, VIII Joint International Symposium, Irkutsk, **2001**.

C18 Zvereva N.A., Ponomarev Yu., Molecular complexes of water in the atmosphere, 17th Colloquium on High Resolution Spectroscopy, Nijmegen, The Netherlands - **2001**.

C19 Zvereva N.A., Theoretical description of photodissociation spectra of hydrogen bonding complexes, 17 Colloquium on High Resolution Spectroscopy, Nijmegen, The Netherlands - **2001**.

C20 Zvereva N.A., Hydrogen bonding effects on electronic transition energies : hydrated clusters of hydrogen chloride - XVII International Conference on High Resolution Molecular Spectroscopy, Prague - **2002**.

C21 Zvereva N.A., Nabiev Sh.Sh., Nadezhdinskii A.I., Ponomarev Yu., Stavrovskii D.B., Chernin S.M., Shubenkina T.A., Analysis of IR-spectra of hydrogen fluoride and water complexes - XVII International Conference on High Resolution Molecular Spectroscopy, Prague - **2002**.

C22 Zvereva N.A., Nabiev Sh.Sh., Nadezhdinskii A.I., Ponomarev Yu., Stavrovskii D.B., Chernin S.M., Shubenkina T.A., Analysis of IR spectra of hydrogen fluoride and water compexes - Moscow - ASA - **2002**.

C23 Zvereva N.A., Rotger M., Boudon V., Loëte M., Ab initio calculations of the SF_5Cl molecule - 18 Colloquium on HRMS - Dijon - **2003**.

C24 Zvereva N.A., Complexes with inorganic hydrides (NF_3, PH_3, AsH_3) - 18 Colloquium on HRMS - Dijon - **2003**.

C25 Rotger M., Boudon V., Loëte M., Zvereva-Loëte N., Symmetry-adapted tensorial formalism for the spectroscopy of the SO_2F_2 quasi-spherical top : application to the bending triad. - Colombus (USA) - **2004**.

C26 Rotger M., Boudon V., Loëte M., Zvereva-Loëte N., Rovibrational parameters for the ground state and the $\nu_3/\nu_7/\nu_9$ triad for the asymmetric SO_2F_2 molecule - Prague - **2004**.

C27 Rotger M., Boudon V., Loëte M., Zvereva-Loëte N., Symmetry-adapted tensorial formalism for the spectroscopy of SO_2F_2 quasi-spherical top : application to the bending triad - Prague - **2004**.

C28 Zvereva-Loëte N.A., Boudon V., Rotger M., *Ab initio* calculation of rovibrational constants for the SO_2F_2 and SF_5Cl molecules. XII International Symposium on Atmospherics Optics - Tomsk - **2005**.

C29 Zvereva-Loëte N.A., Boudon V., Rotger M., *Ab initio* study of ethylene trapped in an atomic cage. 19th Colloquium on High Resolution Molecular Spectroscopy - Salamanca - Espagne - **2005**.

C30 Zvereva-Loëte N.A., Boudon V., Rotger M., *Ab initio* study of ethylene trapped in an atomic cage, NATO advanced research workshop on Remote Sensing of the Atmosphere for Environmental Security. Rabat - Maroc - **2005**.

C31 Zvereva-Loëte N.A., Ponomarev Yu.N., Structurally non-rigid molecular complexes of HF with water under atmospheric conditions, NATO advanced research workshop on Remote Sensing of the Atmosphere for Environmental Security. Rabat - Maroc - **2005**.

C32 Zvereva N.A., Dikanova Yu.S, Ponomarev Yu.N., Database of structure, energy, and spectral characteristics of molecular complexes in atmosphere, - XII-th Joint International Symposium "Atmospheric and Ocean Optics, Atmospheric Physics". Tomsk - Russia - **2006**.

C33 Rotger M., Boudon V., Loëte M., Zvereva-Loëte N., Margules L., Demaison J., MerkeI., Hegelund F., Bürger H., La triade de pliage de la toupie quasi-sphérique SO_2F_2 dans la région des 550 cm^{-1}. - Dijon. - **2006**.

C34 Zvereva-Loëte N., Demaison Rudolph, H.D., Champ de force anharmonique ab initio et structure Ĺ équilibre du bromure de vynile, - Journés de Spectroscopie Moléculaire , - Université Claude Bernard Lyon 1. - **2006**.

C35 Rotger M., Boudon V., Loëte M., Zvereva-Loëte N., Margules L., Demaison J., MerkeI., Hegelund F., Bürger H., Analysis of the $\nu_3/\nu_7/\nu_9$ Bending Triad of the Quasi-Spherical Top Molecule SO_2F_2, - XV International Conference on High Resolution Molecular Spectroscopy N.-Novgorod. - Russie - **2006**.

C36 Zvereva-Loëte N., J.Demaison, H.D.Rudolph, Ab initio Anharmonic Force Field and Equilibrium Structure of Vinyl Bromide - XV International Conference on High Resolution Molecular Spectroscopy N.-Novgorod. - Russie - **2006**.

C37 Zvereva-Loëte N., Boudon V., Computational Approaches to the study Ethylene trapped in a Zeolite. - XV International Conference on High Resolution Molecular Spectroscopy N.-Novgorod. - Russie - **2006**.

C38 Zvereva-Loëte N., *Ab initio* calculations : the effect of zeolite framework on the properties of ethylene. - XIV-th International Symposium "Atmospheric and Oceanic Optics, Atmospheric Physics" - Buryatiya, Russie - **2007**.

C39 Zvereva-Loëte N., Boudon V., Computational modelling to study Si/O nanoporous structures. Molecules trapped in zeolite. *Ab initio* calculations and IR spectroscopy study. - IWCMM17 - Paris - France - **2007**.

C40 Zvereva-Loëte N.A., Ballandras A., Weber G., Rotger M., Boudon V. - Effect of zeolite framework on the spectroscopic properties of ethylene : FTIR measurements and quantum calculations - 20th Colloquium on High Resolution Molecular Spectroscopy - Dijon - France - **2007**.

C41 Zvereva-Loëte N.A. - Calculs *ab initio* pour des molécules piégées dans les zéolithes - PAMO - JSM - Lille - France - **2008**.

C42 Kalugina Yu. N, Zvereva-Loëte N.A., Boudon V. T - *Ab initio* calculations for the CH_4 - N_2 Van der Waals complexe. Polarizability and dipole moment functions : semiempirical approach - XV Intern. Joint Symposium "Atmoshperic and Oceanic Optics. Atmospheric Physics" - Krasnoyarsk - Russie - **2008**.

C43 Kalugina Yu. N, Zvereva-Loëte N.A., Boudon V. - Theoretical investigation of the energy surface and electrical properties of the Van der Waals complexes – HRMS - Prague - **2008**.

C44 Ballandras A., Zvereva-Loëte N.A., Rotger M., Weber G., Bellat J. - P., et Manceron L. - Infrared spectroscopy measurements and *ab initio* calculations of physisorption of ethylene in Silicalite-1 – 4th International FEZA conference - Paris - **2008**.

C45 Kalugina Yu. N., Buldakov M. A., Cherepanov V. N., Zvereva-Loëte N., Boudon V., Theoretical investigation of the potential energy surface of the van der Waals complex CH_4 - N_2 - HighRus - Irkutsk - Russie - **2009**.

C46 Kalugina Yu. N., Buldakov M. A., Cherepanov V. N., Zvereva-Loëte N., Boudon V., Theoretical investigation of the of the van der Waals complex CH_4 - N_2 properties - HRMS - Stabia - Italie - **2009**.

Séminaires

S1 Zvereva N.A. “Vibrational analysis with Gaussian” - LPUB - Université de Bourgogne - Dijon - France **2003**.

S2 Zvereva-Loëte N.A. “Calculs *ab initio* pour l’étude de molecules stables et de complexes non-rigides” - LCT - Université de Marne-la-Vallée - Champs-sur-Marne - France **2006**.

S3 Loëte M., Zvereva-Loëte N.A., Rotger M., Boudon V.,“Recent High-Resolution Molecular Spectroscopy Developements in the Dijon Group” - LAAS - Institut d’Optique Atmosphérique - Tomsk - Russie **2006**.

S4 Zvereva-Loëte N. "Modélisation *ab initio* de molécules et de systèmes complexes" - ICB - Université de Bourgogne - Dijon - France **2008**.